CALIFORNIA
ENERGY COMMISSION

Energy Research and Development Division

FINAL PROJECT REPORT

Air Quality Implications of Using Biogas to Replace Natural Gas in California

Gavin Newsom, Governor

May 2020 | CEC-500-2020-034

PREPARED BY:

Primary Author:
Dr. Michael J. Kleeman[1]
Dr. Thomas M. Young[1]
Dr. Peter G. Green[1]
Dr. Stefan Wuertz[1]
Dr. Ruihong Zhang[2]
Dr. Bryan Jenkins[2]
Dr. Norman Y. Kado[3]
Dr. Christopher F.A. Vogel[3]

[1]Department of Civil and Environmental Engineering
[2]Department of Biological and Agricultural Engineering
[3]Department of Environmental Toxicology
University of California, Davis
One Shields Avenue, Davis, CA, 95616
Phone: 530-752-8386
http://ucdavis.edu

Contract Number: PIR-13-001

PREPARED FOR:
California Energy Commission

Yu Hou
Project Manager

Jonah Steinbuck, Ph.D.
Office Manager
ENERGY GENERATION RESEARCH OFFICE

Laurie ten Hope
Deputy Director
ENERGY RESEARCH AND DEVELOPMENT DIVISION

Drew Bohan
Executive Director

ACKNOWLEDGEMENTS

The analysis described in this report was partially conducted by graduate students, postdoctoral scholars, and research scientists with guidance from their faculty mentors. In several cases these students and postdocs are the lead authors of individual chapters that will be submitted for publication in peer-reviewed journals. The student, postdoctoral scholar, and research scientist team consisted of the following individuals from the Department of Civil and Environmental Engineering at University of California, Davis:

- Christopher Alaimo – Staff Research Associate
- Minji Kim – Postdoctoral Scholar
- Yin Li – Graduate Student
- Joshua Peppers – Graduate Student
- Luann Wong – Junior Specialist
- Jian Xue – Postdoctoral Scholar

In addition to the major funding provided by the California Energy Commission, portions of this study were supported by California Air Resources Board (CARB) Project #13-418. CARB also supported this research through in-kind support, conducting mobile source testing of vehicles powered by compressed natural gas and biomethane at the Haagen-Smit Laboratory in El Monte, California. Special thanks are due to Mang Zhang, Richard Ling, Aiko Matsunaga, Hyun Ji Lee, and the dedicated staff in the Organic Analysis Section and Aerosol Analysis and Methods Evaluation Section. Special thanks are also due to Thomas Valencia, Wayne McMahon, Bruce Frodin, Henry Toutoundjian, Manuel Cruz, Gary Mikailian, Shishan Hu, and Tin Truong.

The authors thank the members of the technical advisory committee for their feedback and guidance during the project.

- Valentino Tiangco (Sacramento Municipal Utility District), Josh Rapport (CleanWorld), Greg Kester (California Association of Sanitation Agencies), Johannes Escudero (Renewable Natural Gas Coalition), Ken Kloc (Office of Environmental Health Hazard Assessment), Frank Mitloehner (UC Davis), John Shears (Center for Energy Efficiency and Renewable Technologies), Brian Helmowski (California Department of Resources Recycling and Recovery), and May Lew (Southern California Gas Company).

The authors thank all the biogas producers who collaborated during the project: CleanWorld, Kiefer Landfill, New Hope Dairy, and VanWarmerdam Dairy.

The authors thank Xiguang Chen and Helee LLC for their in-kind support in providing the membrane separation unit used to upgrade biogas to biomethane.

PREFACE

The California Energy Commission's (CEC) Energy Research and Development Division manages the Natural Gas Research and Development Program, which supports energy-related research, development, and demonstration not adequately provided by competitive and regulated markets. These natural gas research investments spur innovation in energy efficiency, renewable energy and advanced clean generation, energy-related environmental protection, energy transmission and distribution and transportation.

The Energy Research and Development Division conducts this public interest natural gas-related energy research by partnering with RD&D entities, including individuals, businesses, utilities and public and private research institutions. This program promotes greater natural gas reliability, lower costs and increases safety for Californians and is focused in these areas:

- Buildings End-Use Energy Efficiency.
- Industrial, Agriculture and Water Efficiency
- Renewable Energy and Advanced Generation
- Natural Gas Infrastructure Safety and Integrity.
- Energy-Related Environmental Research
- Natural Gas-Related Transportation.

Air Quality Implications of Using Biogas (AQIB) to Replace Natural Gas in California is the final report for the Air Quality Implications of Using Biogas to Replace Natural Gas in California (Contract Number PIR-13-001) conducted by the University of California at Davis. The information from this project contributes to Energy Research and Development Division's Natural Gas Research and Development Program.

For more information about the Energy Research and Development Division, please visit the CEC's research website (www.energy.ca.gov/research/) or contact the CEC at 916-327-1551.

ABSTRACT

Upgraded biogas or biomethane can be used as a renewable fuel in place of petroleum natural gas in California. Different feedstocks produce biogas and biomethane with different levels of trace impurities, affecting air pollution emissions. This project evaluated the air quality impacts of using biogas and biomethane fuels produced from different feedstocks in multiple end sectors, including commercial electricity generation (five locations), mobile sources (cargo van), and home appliances (stove and water heater). All combustion emissions were diluted to representative atmospheric concentrations under simulated day and night conditions before collection and analysis. The research team analyzed combustion exhaust samples for toxicity, chemical composition, and biological organisms.

The combustion exhaust from biomethane exhibited low levels of toxicity similar to natural gas exhaust. Toxicity differences were apparent between biomethane and natural gas in the first round of results from home appliances tests. DNA damage produced by exposure to combustion exhaust from a water heater and a cooking stove was slightly higher for biomethane than petroleum natural gas. Likewise, mutagenicity (the capacity to create mutations), related to possible carcinogenicity, produced by exposure to the exhaust from a cooking stove was slightly higher for biomethane than for petroleum natural gas. A second round of cooking stove tests with multiple samples confirmed the initial biomethane combustion results, but in that round, toxicity from natural gas emissions was measured at similarly high levels. The increased toxicity of the natural gas combustion exhaust may have been caused by changes in the natural gas composition between the first and second round of tests. The toxicity trends are related to the chemical composition of the combustion exhaust, but more thorough testing is needed to determine how the feedstock and production methods for biomethane should be enhanced to reduce toxicity. It may be possible to reduce toxicity by controlling more tightly the composition of both biogas and biomethane and natural gas.

Keywords: Biogas, biomethane, air quality, toxicity, mutagenicity, photochemical reaction, power-generation, mobile sources, home appliances

Please use the following citation for this report:

Kleeman, Michael J., Thomas M. Young, Peter G. Green, Stefan Wuertz, Ruihong Zhang, Bryan Jenkins, Norman Y. Kado, and Christopher F.A. Vogel. 2020. *Air Quality Implications of Using Biogas to Replace Natural Gas in California*. California Energy Commission. Publication Number: CEC-500-2020-034.

TABLE OF CONTENTS

LIST OF FIGURES

Page

LIST OF TABLES

Page

EXECUTIVE SUMMARY

Introduction

Renewable energy sources are essential to reducing greenhouse gas emissions in California. Biogas — a renewable fuel produced by converting organic waste materials into a gaseous mixture of carbon dioxide and methane — reduces greenhouse gas emissions in two ways. First, it replaces fossil natural gas. Second, biogas collection captures methane from landfills, waste treatment plants, and other activities that would otherwise be released into the atmosphere. Biogas can be used directly to produce electricity or it can be cleaned and upgraded to biomethane by removing carbon dioxide and other impurities so that it can be used in all applications that currently use natural gas.

Project Purpose

Any new fuel adopted in California must undergo careful air quality analysis, given the challenges to meet air quality standards designed to protect public health. This project evaluated the potential air quality impacts of using biogas and biomethane in commercial electricity generation, mobile sources, and home appliances.

Project Process

The research team analyzed biogas produced at five locations: two food waste digesters, two dairies, and one landfill. The team collected exhaust from electricity engine-generators operating on biogas at each site. The team then produced upgraded biomethane for further testing at three of the sites using a two-stage membrane separation system. This biomethane was used as fuel in a cargo van and in two home appliances (water heater and stove), as was compressed natural gas (CNG). The team diluted exhaust samples to low concentrations to allow chemical transformations to take place in the real atmosphere. Exhaust samples were also aged in simulated sunlight to study the formation of chemical reaction products.

The research team tested samples of diluted and aged exhaust for toxicity along four pathways for injury, including generation of reactive oxygen species, cellular inflammation, DNA damage, and mutagenicity (the capacity to cause mutations). To test for these pathways, the team used assays based on recommendations made by the California Air Resources Board when evaluating the potential health effects of new fuels. The macrophage reactive oxygen species assay measured the reactive oxygen species generating capacity of exhaust particulate matter using rat macrophage cells. Cellular in-vitro assays measured inflammatory and toxic potential using human macrophages in cell culture that can directly exhibit inflammatory responses. A genotoxicity assay measured DNA alteration (mutations) in several strains of bacterium, positively identifying 50 percent to 90 percent of known human carcinogens. The chemical and microbial content of the samples was also measured. The team performed statistical analyses to find relationships between toxicity and composition.

Project Results

The combustion exhaust from biomethane exhibited low-levels of toxicity similar to petroleum natural gas exhaust with mixed results, depending on the end point.

Generation of reactive oxygen species (which often cause cell damage) was higher for CNG than biomethane during vehicle tests. Generation of reactive oxygen species was similar for CNG and biomethane during appliance tests.

Markers of cellular inflammation were highest for CNG during vehicle tests but higher for biomethane during appliance tests.

DNA damage and mutagenicity were higher for biomethane than for CNG, with the strongest consistent effects apparent during tests of home appliances. Biomethane combustion exhaust from a cooking stove was 11-16 times more mutagenic than CNG combustion exhaust. A second round of cooking stove tests confirmed the results for biomethane combustion exhaust, but the mutagenicity for the petroleum natural gas combustion exhaust increased to similar levels. The CNG used in the second round of tests was obtained at a different time and location than the CNG used in the first round of testing. It is possible that changes in CNG composition caused the observed change in the mutagenicity of the CNG combustion exhaust. Future studies should investigate variability in natural gas composition and the resulting mutagenicity of combustion exhaust.

This increased CNG mutagenicity in the repeated tests could not be explained by changes in the concentrations of target chemical compounds between the two rounds of testing. Future gas standards can be set to protect public health if the chemical compounds responsible for toxicity can be identified and controlled. Acetaldehyde was correlated (greater than 95 percent certainty) with mutagenic activity in the original appliance tests and the stove retests; additional nontarget compounds were also correlated with mutagenicity in the original appliance tests ($C_6H_3NO_4$, dialdehyde) or in the stove retests (C_2H_5NO). Although these "nontarget" chemical compounds have known formulas, the exact structures of these compounds require more investigation so that they can be better monitored in biogas. Further analysis of non-target compounds may identify the cause of this increased mutagenicity, but these analyses were beyond the scope of this study.

Risk of exposure to bacteria, viruses, and fungi was not increased in the biomethane combustion exhaust compared to the natural gas combustion exhaust. None of the toxicity assay results was correlated with these microbiota results.

Ultrafine particle emissions from petroleum natural gas and biomethane were very similar when the siloxane and sulfur content of the biomethane was low. Up to 60 percent of the particles emitted by the combustion of natural gas or biomethane in home appliances evaporated when they were diluted in the atmosphere. However, the particles emitted from raw biogas combustion did not evaporate when they were diluted.

Technology/Knowledge Transfer

The technology developed in the current project has been transferred to stakeholders and to the public using multiple channels. All methods and results are documented in this final report. The authors have publicized the results through presentations at technical conferences hosted by the Air and Waste Management Association, the American Association for Aerosol Research, and Analytica. Finally, selected chapters of this final report have been published in peer-

reviewed journals, including *Environmental Science & Technology* and *Biomass & Bioenergy*. These publications can be found in the reference section of this final report.

Interest in the research results has been strong. Many of the stakeholders involved in the study requested copies of the final report, including producers, industry representatives, and regulatory agencies such as the California Air Resource Board and California Department of Resources Recycling and Recovery. Several producers requested analysis for additional biogas samples outside the original project scope. It is expected that the results of the current project will support future decisions about the adoption of biogas as an energy source in California.

Benefits to California

This research shows that biogas and biomethane combustion exhaust is similar to natural gas combustion exhaust, meaning that the renewable fuels can be safely used in California. The increased mutagenicity measured during some biogas combustion tests identifies a potential issue that can be researched and solved before widespread adoption of the new fuels. The finding that biogas, biomethane, and natural gas toxicity depends on chemical composition that changes over time provides a starting point for further studies that will better define safe standards for both fuels.

CHAPTER 1: Introduction

Motivation

Biogas and biomethane (scrubbed biogas) has great potential as a source of renewable energy for California, but care must be exercised before widespread adoption of biogas across the residential, commercial, and transportation sectors. Natural gas is predominantly methane with lesser amounts of larger alkanes, but biogas often contains many additional compounds with a composition that varies depending on the biogas feedstock and the degree of cleanup/purification. Biogas is typically produced on a small scale, which makes it difficult to apply sophisticated upgrading techniques. Even purification to pipeline-standard biomethane leaves residual compounds in the gas that are not found in traditional natural gas. Some of these additional compounds have the potential to adversely impact air quality either in the unburned state or after the associated combustion products age in the atmosphere.

California is committed to adopting renewable energy sources through the Renewables Portfolio Standard (RPS) and GHG legislation like Assembly Bill 32 (Núñez, Chapter 488 Statutes of 2006). Biogas already contributes on a small scale to the RPS at some wastewater treatment plants and is used for vehicle fuel at a few projects in California. The best expanded use of biogas and biomethane will depend, in part, on the air quality outcomes associated with each potential scenario. At one end of the potential use spectrum, biogas with moderate scrubbing to remove hydrogen sulfide (H2S) and siloxanes can be used by larger stationary turbines and reciprocating engines that can be sited to minimize public exposure to emissions. At the other end of the spectrum, extensive scrubbing of biogas and direct use of the resulting biomethane in mobile sources and home appliances could provide a flexible replacement for fossil fuel but also potentially increase public exposure to trace contaminants in the combustion products. All the strategies for biogas adoption involve different expensive infrastructure investments, and so they require careful analysis before adoption.

The research described in this proposal builds on past work to make new measurements and model predictions to determine the biogas and biomethane adoption strategy with the best outcomes for air quality and the biogas industry in California. The microorganisms (including infectious agents) that could be present in biogas were examined to determine if they pose a health threat. The research team conducted emissions tests to measure the detailed composition of biogas and biomethane combustion exhaust from multiple residential, commercial, and mobile sources under representative atmospheric conditions. The team used photochemical aging tests to determine if any of the biogas and biomethane emissions act as precursors for toxic chemical reaction products. Regional air quality models were then be used to estimate public exposure to biogas or biomethane through the entire life cycle (direct gas, fresh combustion emissions, photochemical reaction products).

The project results help establish a sound scientific foundation for informed strategies for biogas and biomethane adoption that optimize air quality outcomes and maximize use of this resource.

Research Objectives

The overall hypothesis that was tested in the current study is that biogas adoption can be configured so that it has negligible impacts on air quality relative to equivalent utilization of traditional natural gas. The next phase of biogas research must examine remaining biogas air quality questions over the entire life cycle of biogas production, clean up and upgrading, distribution, combustion, and atmospheric aging of emissions.

Project Tasks

The project was organized around the following major tasks:

Task 1a: Establish Project Advisory Group

This task established and conducted advisory group meetings and work with the group to identify candidate plants that were currently or nearly ready to produce biomethane/biogas in California. The final selection of gas streams was based on the recommendations of the advisory group. All candidate plants and gas streams that were selected for inclusion in the project were approved by Energy Commission to ensure that the selections met the project goals. The final membership of the advisory group is listed in Table 1:

Table 1: List of Advisory Group Members and Affiliation

Name	Affiliation	Contact Information
Valentino Tiangco	SMUD	Valentino.Tiangco@smud.org
Josh Rapport	CleanWorld	josh.rapport@cleanworld.com
Greg Kester	CASA	gkester@casaweb.org
Johannes Escudero	RNG Coalition	johannes@rngcoalition.com
Ken Kloc	OEHHA	Kenneth.Kloc@oehha.ca.gov
Frank Mitloehner	UC Davis	fmmitloehner@ucdavis.edu
John Shears	CEERT	shears@ceert.org
Brian Helmowski	CalRecycle	Brian.Helmowski@CalRecycle.ca.gov
May Lew	SoCalGas	MLew@semprautilities.com

Source: University of California, Davis

Task 1b: Obtain Upgrading Equipment

The original project plan specified upgrading biogas to biomethane using a transportable pressure swing adsorption (PSA) unit to be supplied by ATMI. Between the time that the proposal was submitted and the proposal was funded, the director of platform marketing at ATMI left for another position, and the replacement ATMI representatives were not able to provide a portable PSA unit without significant additional funding that could not be accommodated in the project budget.

In consultation with Energy Commission and the TAC, the UC Davis project team sought new industry partners and eventually identified Helee LLC, which could provide a transportable membrane separation unit to upgrade biogas to biomethane. The membranes were made from polyimide (Air Liquide). Input biogas was compressed to about10 bar to force carbon dioxide (CO2) and other contaminants such as O2, H2O, and H2S across the membrane during

separation. The membrane could not separate N2 from methane, making it impossible to purify gas streams with significant air entrainment. Liquid and gaseous water was removed prior to the membrane using a refrigeration dryer for bulk water removal and a solid desiccant dryer for trace water removal.

The upgrading unit had a maximum feed biogas capacity of 100 Nm3 hr-1 (2,500 standard L min-1) and a maximum biomethane production capacity of about 50 Nm3 hr-1 with methane content as high as 97%. As operated in the current study, the Helee LLC unit processed nearly 50 Nm3 hr-1 of feed biogas producing about 25 Nm3 hr-1 of biomethane. Typical power consumption was 16.8 kilowatts (kW) for a specific energy consumption of 0.336 kW/(m3 hr-1 raw gas). Figure 1shows the Helee LLC upgrading unit.

Figure 1: Helee LLC Upgrading Unit on Transportable Trailer Installed at UC Davis READ Biogas Plant

Source: University of California, Davis

Task 1b: Coordinate With Producers

The UC Davis project team, based on recommendations of the advisory group and approval of the selected sources by the Energy Commission, contacted and coordinated with the following producers to obtain permission to produce biomethane.

The research team made preliminary biogas characterization measurements for biogas produced at all sites under sponsorship from CARB Project #13-418. Significant quantities of nitrogen (N_2) were detected in biogas streams from the VanWarmerdam dairy and Kiefer landfill, reflecting active air injection (dairy) or air intrusion (landfill). The N_2 could not be removed from the upstream raw biogas, and the membrane separation unit provided by Helee LLC could not remove the N_2 from the downstream upgraded biomethane. This resulted in biomethane with unacceptably low concentrations of CH_4 that could not be used for home appliance or mobile source tests. Biomethane samples for testing in home appliance and mobile source tests were therefore obtained from the first three sources in Table 2.

Table 2: List of Producers Participating in Project

Name	Feedstock	Biogas Production	Contact Information
CleanWorld - READ	Food waste and other organic waste	Three-stage digester operating at a thermophilic temperature from 50-55^{o} Celsius © with ~21-day retention time. Biogas is combined with landfill gas.	Josh Rapport (josh.rapport@cleanworld.com)
CleanWorld - SATS	Food waste and other organic waste	Three-stage digester operating at a thermophilic temperature from 50-55^{o}C with ~21-day retention time.	Josh Rapport (josh.rapport@cleanworld.com)
New Hope Dairy	Scraped manure from 1200 cows	Heated, constantly stirred tank reactor (CSTR) digester operating at mesophilic temperature (35-40 ^{o}C) with a ~50-day retention time.	Ross Buckenham (rbuckenham@calbioenergy.com)
VanWarmerdam Dairy	Flushed manure from 1200 cows	Covered lagoon digester operating at ambient temperature and ~100-day retention time	Daryl Maas (daryl@maasenergy.com)
Kiefer Landfill	Mixed residential and commercial landfill material	1,084-acre landfill operated since 1967	Tim Israel (israelt@saccounty.net)

Source: University of California, Davis

Task 1c. Measure Emissions From On-Site Combustion Sources

Each of the biogas producers listed in **Error! Reference source not found.** has the capacity to combust the biogas on-site to generate electricity. The details of electricity generation at each location are summarized in Table 3.

Table 3: List of On-site Combustion Sources Tested

Name	Pre-cleaning Technology	Generator
CleanWorld - READ	Activated carbon scrubber for sulfur removal followed by cooling to remove moisture	Three 200 kW microturbines
CleanWorld - SATS	Activated carbon scrubber for sulfur removal followed by cooling to remove moisture	190 kW engine-generator (2G-Cenergy)
New Hope Dairy	Iron chloride injection into digester, air injection into digester	450 KW engine-generator (2G-Cenery)
VanWarmerdam Dairy	Air injection into covered lagoon	600 kW engine-generator (Guascor)
Kiefer Landfill	Cooling to remove moisture	3.05 MW generation capacity from five Caterpillar 3616 IC engines

Source: University of California, Davis

The research team measured emissions from each on-site generator using various methods. Initial samples for some tests were collected after cooling to ambient temperature to characterize the raw exhaust at the highest possible concentrations. Samples were also collected for all tests after cooling and dilution to realistic ambient concentrations. Finally, samples were also collected for all tests after dilution to realistic ambient concentrations and exposure to ultraviolet (UV) radiation to simulate photochemical aging in the atmosphere. These latter tests were accomplished using a transportable photochemical smog chamber with a volume of 5 cubic meters (m^3). The chamber was operated at each site to characterize the emissions under the most realistic conditions possible.

Figure 2: Transportable Photochemical Smog Chamber Housed in Trailer Operating at New Hope Dairy

Source: University of California, Davis

Task 1d. Measure Emissions From Biomethane Combusted in Home Appliances and Mobile Sources

Biomethane collected from the first three in Table 2 was combusted in two home appliances (water heater and cooking stove) and in a van configured to operate on compressed natural gas (CNG). The details of each source are shown below.

Table 4: List of Home Appliances and Mobile Sources Tested

Combustion Endpoint	CNG/Biomethane Source	Dilution Conditions	Comments
Rheem XG40T06EC36U1 40-gallon water heater (complies with 40ng NOx/J emissions)	(i) PG&E CNG (ii) READ (iii) SATS (iv) New Hope	(i) 50:1 dark (ii) 500:1 dark (iii) 500:1 UV light	50:1 representative of nighttime conditions. 500:1 representative of daytime conditions
General Electric JGBS60DEKWW 4.8 ft^3 Range (cooking stove)	(i) PG&E CNG (ii) READ (iii) SATS (iv) New Hope	(i) 100 cfm ventilation dark	Air exchange rate meets standards for commercial cooking. UV light not appropriate for indoor source.
CNG 2015 Chevrolet 2500 Express Van	(i) PG&E CNG (ii) 28%CNG +72%SATS (iii) 7.7%CNG +33.5%READ +34.4%SATS +24.4%New Hope	(i) 13:1 UC dark (ii) 13:1 UCH dark (iii) 50:1 UC dark (iv) 50:1 UC light	UC=Unified Cycle or UC-LA92 cold-start driving cycle. UCH=UC hot start.

Source: University of California, Davis

Sources that typically exhaust emissions to ambient air (water heater and van) were tested in the dark (nighttime conditions) and in the presence of UV light (daytime conditions). Dilution conditions were adjusted for dark/light test pairs with the goal to achieve 50-100 parts per billion (ppb) of oxides of nitrogen NO_x in the smog chamber. The van was equipped with a catalytic converter to reduce NO_x concentrations; therefore, the required dilution ratio was an order of magnitude lower than the dilution required for the water heater test.

The research team added a mixture of volatile organic compounds consisting of 55% ethylene, 35% n-hexane, and 10% xylenes to the smog chamber along with the diluted combustion exhaust to generate a realistic ambient mixture of photochemical oxidants. Target ozone concentrations in the mixture were 100 ppb representing conditions on a polluted summer day in California.

Task 1e. Chemical and Biological Analysis

Biogas and biomethane combustion samples were subjected to an extensive range of chemical and biological measurements. Full details are provided in Chapters 5, 6, and 7.

Task 1f. Assays

The authors used assays to directly monitor chemical and biological responses associated with key health-effects pathways. The suite of assays employed in the current study was based on recommendations made by the California Air Resources Board when evaluating the potential health effects of new fuels (Herner, 2013). The macrophage reactive oxygen species (ROS) assay measured the ROS generating capacity of exhaust particulate matter using rat macrophage cells. Cellular in-vitro assays measured inflammatory and toxic potential using human macrophages in cell culture that can directly exhibit inflammatory responses. The Ames genotoxicity assay measured DNA alteration (A.K.A. mutations) in several strains of bacterium, positively identifying 50-90% of known human carcinogens.

Task 1g. Reporting

The contractor submitted quarterly progress reports and a final report (this document) in fulfillment of the contract deliverables.

Report Structure

- Chapter 2 describes the performance of the membrane separation system for biomethane production. Dominant removal mechanisms and calculated removal efficiencies are presented for trace contaminants that may be important for air quality. The chapter presents cost projections to estimate the feasibility of upgrading and pipeline injection for small producers.
- Chapter 3 summarizes the exhaust testing methods for on-site engine-generators, home appliances, and mobile sources.
- Chapter 4 presents the results from health effects assays collected from all combustion tests. Three major types of assays are considered to characterize generation of reactive oxygen species, markers of inflammation, and mutagenicity.
- Chapter 5 summarizes results from microorganism characterization of all combustion samples. Results are divided into major categories studied including bacteria, viruses, and fungi.
- Chapter 6 summarizes measurements of target chemical compounds and elements carried out in all combustion exhaust tests. This analysis is beyond the scope of the original contract but is included as a quality control check on the nontarget analysis presented below. Concentrations of chemical compounds are regressed against assay results to identify potential drivers for toxicity.
- Chapter 7 summarizes measurements of nontarget chemical compounds automatically identified using peak retention time and mass spectra. This broad analysis of all the compounds in the combustion exhaust samples is regressed against assay results to identify potential drivers for toxicity.
- Chapter 8 compares emission rates for ultrafine particles from applications using biomethane vs. petroleum natural gas. Most of the airborne particulate matter emitted from the combustion of traditional petroleum natural gas falls into the ultrafine size

range. A clear understanding of the potential changes to these emissions due to biogas adoption is key for this emerging pollutant.

- Chapter 9 presents a preliminary modeling analysis of air quality impacts due to widespread adoption of landfill gas for electricity generation.
- Chapter 10 summarizes all the target chemical compounds that were analyzed in the current study. A larger number of nontarget chemical compounds were also measured and correlated with toxicity tests, where possible.

CHAPTER 2:
Performance of Membrane Separation Upgrading Unit

Introduction

The biomethane tested in the current study was produced using membrane separation to remove CO_2 and other minor and trace impurities from the raw biogas. Efficiency and economic feasibility are important considerations for membrane separation as an upgrading approach for biogas in California. Typical biogas production facilities are smaller than traditional facilities producing compressed natural gas. This makes it impractical to adopt expensive upgrading methods to these locations. Technologies such as membrane separation that can be economically scaled to smaller sizes will be required to make biomethane adoption practical across California.

The most common use for biogas is on-site heat and power production (Makaruk et al., 2010). This application requires only limited gas purification with no need for expensive removal of carbon dioxide. This is often a good choice when heat consumers are nearby. However, biogas upgraded to natural gas quality allows additional uses that may bring in more revenue and provide an increase in overall energy efficiency. The upgraded gas, known as biomethane, can be injected into the natural gas grid or used as a vehicle fuel and sold for a higher price. In addition, injection into the grid ideally allows for 100% utilization of the biogas because the grid can act as a storage vessel (Ong et al., 2014).

Traditionally, only large plants with high biomass throughputs have had the capital to inject biogas in the pipeline. However, as air quality standards become stricter, small-scale facilities, such as dairy farms with digesters and food waste processing plants, have pipeline injection as a possible alternative. In addition, economic incentives are helping drive biomethane production (Ong et al., 2014) (Patterson et al., 2011). Currently, there are no dairy digesters in the California injecting biomethane into the natural gas grid (Black, 2015).

There are several traditional treatment methods available to upgrade biogas, including water scrubbing, amine scrubbing, and pressure swing adsorption. These methods have long been used to process crude natural gas and have been successful for treating biogas. However, the upgrading process has not been standardized for small-scale biogas producers in the United States, and lack of performance and cost data has been a barrier for implementation (Ong et al., 2014) (GTI, 2009). Membrane separation is an up-and-coming technology for biogas upgrading due to simplicity, small footprint, and low cost, especially at small scales (Thran, 2014) (Chen et al., 2015) (Shimekit, 2012) (Perry, 2008).

Recently, California legislation such as AB 32 has driven an increase in biogas production and the number of plants that produce biogas (2006). Many of these plants are designated food and organic waste processing plants that receive materials that have been diverted from landfills. Others are dairy farms that previously did not manage methane emissions but now

desire to take advantage of biogas as a resource and revenue stream. Food waste processing plants and dairy farms tend to be relatively small biogas producers compared to wastewater treatment plants and landfills. Since these producers work at smaller scales, the biogas management options must be evaluated differently. For upgrading to pipeline quality, the optimal choice from several technology options may not be obvious to the biogas producer. While there are many studies on the traditional biogas treatment methods at industrial scale (water absorption, amine absorption, pressure swing adsorption), there are relatively few studies on membrane separation of biogas at the industrial scale (Chen et al., 2015) (Ryckebosch et al., 2011). The intent of this study is to assess the performance of a biogas membrane upgrading unit relative to natural gas quality and environmental standards to evaluate the efficacy of using this technology for the small-scale biogas producer. An economic analysis is also included so that policy makers and small-scale biogas producers may make informed decisions regarding the fate of the biogas.

This study evaluates the technology and economics of a dual-stage membrane system with a capacity of 100 Nm^3/h biogas to provide useful information to biogas project developers in California. As the quality of the upgraded gas is critical for efficacy in the pipeline, this study investigates the effect of the membrane on most of the major compounds in biogas: nitrogen, oxygen, carbon dioxide, and methane. Water removal was not measured. Membrane effect on categories of trace components (<0.1% by volume) in the biogas is also investigated to provide information for later air quality studies.

Background

Hollow-fiber membranes allow some gases to permeate quickly, while other gases are mostly retained or permeate very slowly. ransport of each compound through the membrane is a function of the partial pressure over the membrane and the permeability of the component in the membrane material. Significant differences in permeability must exist to separate two compounds completely using hollow-fiber membranes. In application to biogas, the function of the membrane is primarily to remove carbon dioxide (CO_2) from methane (CH_4) but it can also remove limited amounts of other contaminants in biogas, including hydrogen sulfide, oxygen, and water (Hagen, 2001). Figure 3 shows the relative permeabilities of major compounds through a membrane used in biogas separation.

Figure 3: Relative Membrane Permeation Rates for Various Compounds

Source: Adapted from (Milieutechniek, 2014)

Air entrainment causes separation difficulties in membrane systems, especially with nitrogen and methane, since polyimide membranes are nearly as impermeable for nitrogen (N_2) as they are for methane (Harasimowicz et al., 2007; Lin, 2000).

Membranes are typically part of a larger process for biogas processing because either they have limited ability to separate the full spectrum of components in the gas, or certain

components can be harmful to the membrane and must be removed upstream. Contaminants that could harm the membrane include hydrogen sulfide (H_2S), siloxanes, water (H_2O), ammonia (NH_3), VOCs, particles, and oil vapor. These components should be limited in the gas feeding the membrane as they compete with CO_2 for adsorption into the membrane. This competition will reduce CO_2 permeability in the near term, and in the long term, itcan lead to plasticization of the membrane (Scholes, 2011) (Scholes, 2009). Depending on the operating conditions, membranes must be replaced after 2 to 10 years of use (Ong et al., 2014).

Major natural gas transmission and distribution companies in California such as Pacific Gas and Electric (PG&E) and Southern California Gas Company (SoCalGas) specify numerous trace compounds that must be removed, if present, in the biogas. These compounds include alkanes, alkenes, ammonia, halogenated hydrocarbons, hydrogen, particulate matter, siloxanes, and sulfur compounds. Typically, these compounds constitute less than 1% of total biogas volume but can have significant impacts on equipment and human health if they are not controlled. Siloxanes are considered the most adverse component in biogas because they can poison catalysts in engines and erode seals and moving parts of end use equipment (GTI, 2009). Siloxanes are typically present in landfill gas and other sources of biogas that process cosmetics, soaps, and detergents. Sulfur compounds may form corrosive solutions when dissolved in water or oil, emit SO_2 (an air toxin) when combusted, and may poison air-pollution control catalysts. Generally, some pretreatment of sulfur is required for membrane separation to limit the degradation of the membrane material and for meeting the pipeline requirements (Rasi et al., 2011). Aldehydes and ketones may degrade the quality of gas odorization. The major natural gas utility providers in California, PG&E and SoCal Gas, do not provide a maximum limit for aldehydes and ketones, but these compounds may be subject to certain requirements depending on the users of the gas (GTI, 2012). Halogenated hydrocarbons are corrosive when dissolved in water and can lead to emissions of air toxins polycyclic aromatic hydrocarbons, hydrogen chloride, and hydrogen fluoride during combustion.

Trace compounds are typically removed by adsorption onto solid media such as activated carbon, aluminum oxide, or various forms of zeolite (Scholz et al., 2013) (Ryckebosch et al., 2011). Absorption into liquid media may also be used for hydrogen sulfide and siloxane abatement (GTI, 2014). The authors could not find any reports that describe the trace component levels in upgraded biogas from membrane separation in California.

The energetic standard for pipeline gas is achieved by increasing the methane purity of biogas. Operating commercial-scale membrane systems produce biomethane with a variety of methane purities depending on the level of upgrading technology applied. A survey of the published literature indicates 88%-99% biomethane purity can be achieved at flow rates between 25 $Nm^3\ h^{-1}$ to 2,600 $Nm^3\ h^{-1}$ using membrane separation alone or in conjunction with other upgrading technologies (Yang et al., 2014; Scholz et al., 2013; Makaruk et al., 2010; Patterson et al., 2011; Shimekit, 2012; Sun et al., 2015; Ong et al., 2014).

While technically feasible, upgrading biogas at small scales for injection into the natural gas pipeline is economically challenging. Project developers in California face even higher costs than those in other states due to high pipeline interconnection costs and stringent gas quality standards (Ong et al., 2014). As seen in Figure 4, the specific production costs for biomethane

increases nonlinearly at flows less than 200 $Nm^3\ h^{-1}$, which places small-scale biogas producers at a disadvantage. Some have suggested using a centralized upgrading plant for multiple producers to lower the unit cost of upgrading (Ong et al., 2014; Jaffe, 2016).

Figure 4: Specific Cost of Upgrading and Injecting Biogas as a Function of Capacity

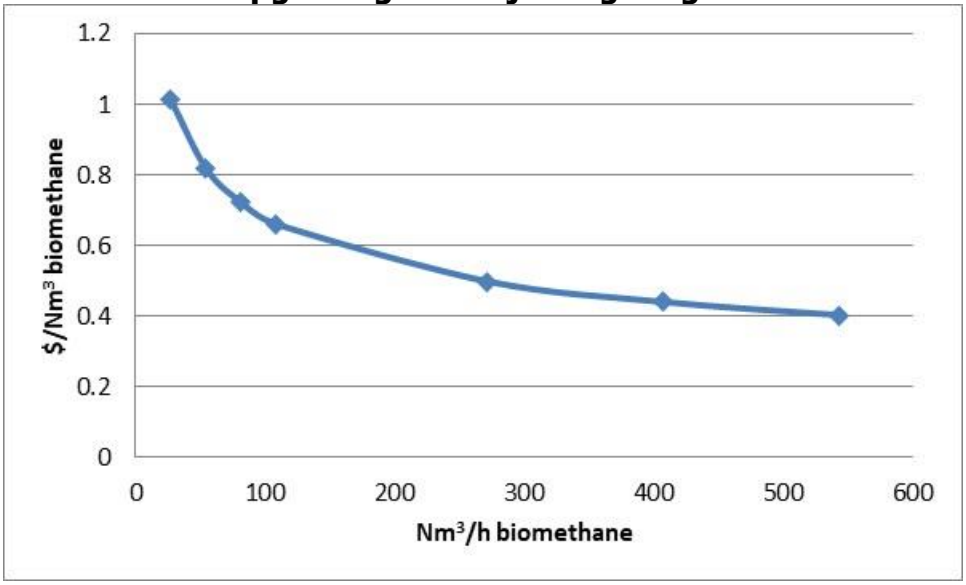

Source: Adapted from (Kosusko et al., 2016)

Methods

Biogas Plants

The research team collected and upgraded biogas at three facilities: a food waste digester (Food Waste 1) operated by Clean World, Inc. in Davis (Yolo County) that processes 45.5 metric tons per day of mixed organic wastes; a food waste digester (Food Waste 2) operated by Clean World, Inc. in Sacramento that processes 22.7 metric tons per day of food waste; and a dairy digester operated by California BioEnergy, LLC in Galt (Sacramento County) that processes waste from 1,200 cows. Food Waste 1 was colocated alongside a landfill, and the gas streams were mixed. Some of the composition analysis for the raw gas obtained from Food Waste 1 reflects the composition of mixed landfill gas.

Figure 5 shows the process to produce and upgrade gas at both food waste plants, and Figure 6 shows the processes used to produce and upgrade gas at the dairy digester. The mobile upgrading process used in this study is highlighted in both figures by a dashed line. Food Waste 2 produced primarily biomethane that was blended with pipeline natural gas for use in vehicles. This facility had a dedicated single-state membrane unit that was not operating at the time that biomethane was collected for the current project. Food Waste 1 and the dairy digester generated revenue with renewable electricity production using the direct biogas produced at these facilities. An iron oxide scrubber was used for sulfur removal at Food Waste 1 and Food Waste 2, while an activated carbon bed was used to remove sulfur at the dairy digester.

Figure 5: Food Waste Digester Process Flow

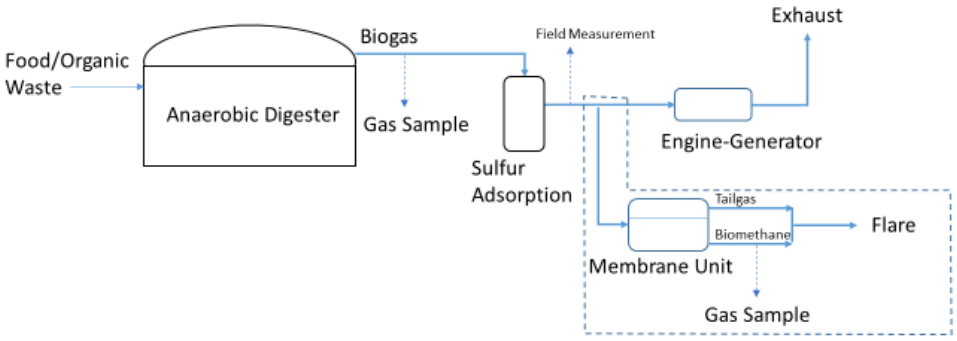

Anaerobic digester actually consists of three stages (not shown).

Source: University of California, Davis

Ferric chloride was injected into the anaerobic digester at the dairy to reduce hydrogen sulfide. Small quantities of air injection were also used at this facility, and residual traces of nitrogen and oxygen were apparent in the biogas as a result. Other pretreatment steps prior to use of the biogas in an engine were chilling of the gas to remove water and a bed of activated carbon for removing trace compounds.

Figure 6: Dairy Manure Digester Process Flow

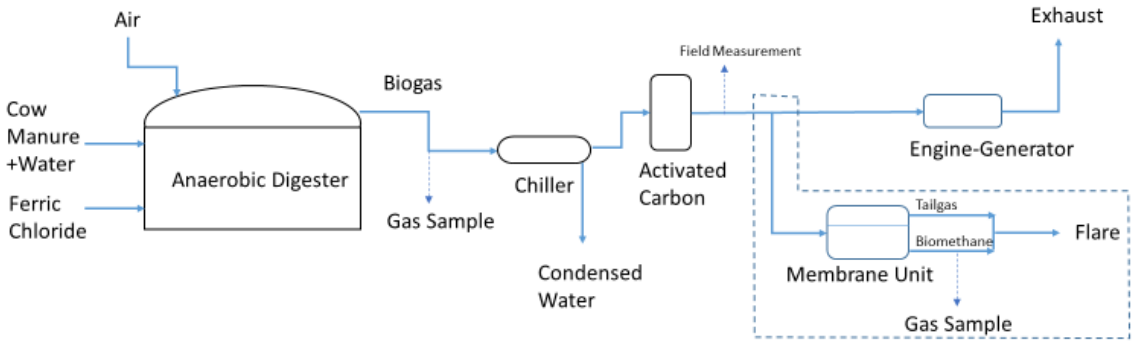

Source: University of California, Davis

Pipeline natural gas from a CNG refueling station in Los Angeles served as the control variable in the experiment and was sampled and analyzed in a similar manner as the biogas.

Biogas Upgrading

A slipstream, or current, of biogas from each of these three facilities was fed to the membrane unit for upgrading to pipeline quality. The raw biogas was conditioned using a skid-mounted system consisting of various filters, dryers, compressor, and membrane modules. The unit was designed and built by Helee Inc. (Hayward, Alameda County) and was placed on a trailer for transport to each biogas site. The specifications of the Helee unit state that it can process 100 $Nm^3\ h^{-1}$ raw biogas to produce a high-value methane gas with less than 3% carbon dioxide. Required pretreatment included liquid water removal and reduction of hydrogen sulfide to

reduce corrosion damage to the membrane and associated equipment. Figure 7 shows the unit operations onboard the Helee upgrading unit.

Figure 7: Membrane Upgrading Unit Process Flow

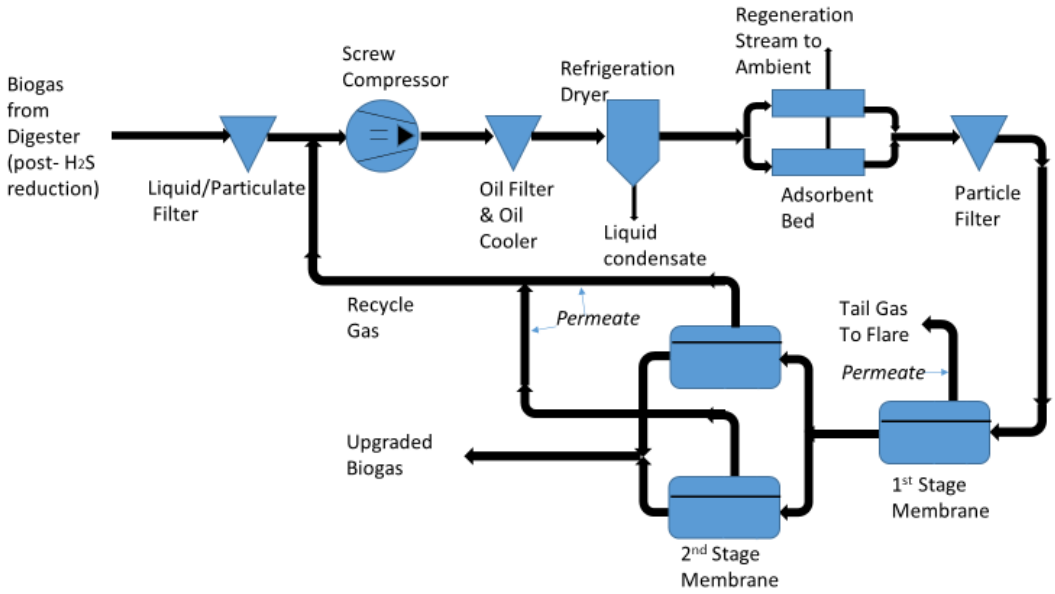

Source: University of California, Davis

In this study, water-saturated, H_2S-treated biogas at 50-70 $Nm^3\ h^{-1}$ entered the Helee unit under a slight vacuum (typically 0-5 kPa [0-20 inches H_2O], negative gauge), where condensed water was removed by a coalescing filter before gas compression to 0.90 to 1.1 MPa (160-175 psia). The compressor was oil-flooded for lubrication and sealing; hence, the biogas came into contact with the petroleum-based oil during processing. The oil was removed from the biogas in a coalescing filter, cooled by heat exchange with air, and returned to the compressor. Gas then entered a refrigeration dryer, where it was chilled to 5 ^{0}C (40 ^{0}F) for moisture reduction. Additional particle and aerosol filters downstream removed any remaining oil to less than 0.003 parts per million (ppm), according to the design specifications. The gas then went through an aluminum oxide adsorbent bed to remove water vapor and other polar compounds. The moisture content of the upgraded gas was not measured in this study, but other studies using similar processes have measured the dew point of the gas to be -30 to -60 ^{0}C (Hagen, 2001). The aluminum oxide beds were regenerated by flowing a small portion of the dry biogas through the offline bed counter-currently and exhausting the resulting gas to the ambient air.

The Helee unit used polyimide hollow fibers membranes (Medal brand by Air Liquide) arranged in a cylindrical shell with an approximate diameter of 6" and an approximate length of 35". The number of fibers in each shell was not measured. A two-stage system was used, where feed gas flows through one module in the first stage and then flows through two parallel modules in the second stage. Carbon dioxide permeated the membrane more quickly than methane, resulting in a "tail gas" stream of mostly carbon dioxide. The tail gas from the first stage exited the system to a flare. Permeate pressure was close to ambient, and the tail gas

flow was typically close to one-half of the feed rate. Other components also permeated the membrane, such as methane, hydrogen sulfide, oxygen, and water vapor; these became part of the tail gas. Permeate from the second stage membranes was recycled back to the compressor and was estimated at 50% of the feed flow using a model supplied by Air Liquide.

Biogas Measurement and Data Analysis

The research team measured the volumetric mixing ratio of CH_4, CO_2, O_2, and H_2S in biogas and upgraded biomethane at the time of production using a portable gas analyzer (Landtec Biogas 5000, Colton, San Bernardino County). The gas balance was assumed to be N_2 for upgraded gas measurements and a combination of N_2 and H_2O for raw gas measurements. The research team later subjected the biogas and biomethane samples to multiple analytical techniques to quantify hundreds of trace compounds, including aldehydes, ketones, extended hydrocarbons, halocarbons, siloxanes, volatile and semivolatile compounds, and sulfur.

For laboratory analysis, the research team sampled the biogas three times at each facility. The sampling point was immediately downstream of the digester and before any treatment steps. Table 5 shows the methods and instruments used in analyzing the biogas.

Upgraded gas was collected from the Helee membrane unit in 61-liter compressed natural gas (CNG) cylinders (CNG Cylinders International, Oxnard, Ventura County). To obtain enough gas for emission testing of a motor vehicle and various household appliances, the gas was compressed to 248 bar (3,600 psi) using a compressor designed for residential CNG vehicle use (PHILL Compressor, BRC Fuel Maker Corporation; Cherasco, Italy). The compressor required about 10 hours to fill each of the three CNG tanks per facility. Gas was generally collected on three consecutive days and did not coincide with sampling of raw biogas. The research team then sampled and analyzed the collected biomethane in a similar manner as raw gas as described below.

The separate performance of the membrane for each compound was assessed by the removal efficiency (RE) calculated as:

$$RE = \left[1 - \frac{C_{i,u}}{C_{i,r}}\right] * 100 \qquad (2\text{-}1)$$

where $C_{i,u}$ is the fraction of compound i in the upgraded gas and $C_{i,r}$ is the concentration of compound i in the raw gas. A positive removal efficiency indicates the concentration in product gas has decreased compared to the raw gas. A negative removal efficiency indicates the concentration has been enhanced in the product gas relative to the feed gas. Negative removal efficiency can occur when the compound does not cross the membrane, while permeable gases like CO_2 do cross the membrane. This leads to enhanced concentrations of the remaining compounds due to a reduction in the total volume of product gas. Spurious negative removal efficiency can also occur in later tests when compounds are released that had physically adsorbed onto components of the upgrading system during earlier tests.

The variability in removal efficiency was characterized by the standard deviation and calculated by equation (2-2):

$$standard\ deviation = RE * \sqrt{\left[\left(\frac{\sigma_{Cf}}{C_f}\right)^2 + \left(\frac{\sigma_{Cp}}{C_p}\right)^2\right]} \quad (2\text{-}2)$$

where C_f is the concentration in the feed gas, C_p is the concentration in the product gas, σ_{Cf} is the standard deviation of the concentration in the feed gas, and σ_{Cp} is the standard deviation of the concentration in the product gas.

Table 5: Methods and Instruments Used to Analyze Biogas and Biomethane

Analyte	Collection	Instrument	Method
H_2S	Tedlar Bag	GC-FPD	6850 GC, HP-1 column, 30m long 0.32mm inner diameter, 5um film, 1mL min^{-1} He
Other Sulfur Compounds	Tedlar Bag	GC-FPD	
CO_2	Tedlar Bag	GC-TCD	6850 GC, CP-Sil 5CB column, 60m long, 0.32mm inner diameter, 8um film, -20C to 260C, 1mL min^{-1} He
N_2	Tedlar Bag	GC-TCD	
CH_4	Tedlar Bag	GC-TCD	
NH_3	Tedlar Bag	TD-GC-MS	6890 GC, 5973N MS, Markes inlet, DB-VRX column, 60m long, 0.32mm inner diameter, 1.4um film, 1 mL min^{-1} He
VOCs (semivolatiles)	XAD Sorbent Tube	GC-QTOF-MS	7890 GC, 7200 Q-TOF MS, HP-2 (DB-5) column, 30m long 0.25mm inner diameter, 0.25um film, 1mL min^{-1} He
Halocarbons	Tedlar Bag	TD-GC-MS	
C_2+ (volatiles)	Tedlar Bag	TD-GC-MS	
Aldehydes & Ketones	DNPH Sorbent Tube	LC-QTOF-MS	1200LC with 6530 Q-TOF-MS, Ascentis C18 column, 25cm long, 4.6mm inner diameter, 5um particles, water-ACN gradient, 1mL min^{-1}
Mercury & All Metals/ Semimetals	Acid traps/impingers	ICP-MS	7500 quadrupole, 1300W Ar plasma, 0.4mL min^{-1}, tuned for 1.5% Ce+2/Ce+ and <0.5% CeO+/Ce+
Siloxanes	Charcoal Sorbent Tube	GC-QTOF-MS	

TD= Thermal Desorption; GC= Gas Chromatography; LC= Liquid Chromatography; MS= Mass Spectrometry; TCD= Thermal Conductivity Detector; FPD= Flame Photometric Detector; QTOF= Quadrupole Time-of-Flight; ICP= Inductively Coupled Plasma

Source: University of California, Davis

Economic Analysis

The research team constructed a financial model to evaluate the economic viability of using a membrane separation unit to upgrade gas at small-scale plants (100 $Nm^3\ h^{-1}$ biogas) for pipeline injection in California. The model used inputs from primary sources or literature specific to California, where possible. Prices were adjusted to 2017 dollars using the U.S. Department Bureau of Labor CPI inflation calculator.[1]

The scope of the financial analysis included all capital, installation, operating, and maintenance expenses of upgrading biogas to pipeline quality using the Helee membrane separation system. The scope also included the capital expenses to install a pipeline connection to the natural gas grid for a single digester. The scope did not include the digester, upstream gas pretreatment equipment, or waste gas flare. The scope for the single digester analysis assumed the pipeline was able to accept additional gas of 20-60 $Nm^3\ h^{-1}$ (the approximate flow rates used in the current study). To simplify the model, the product gas leaving the membrane upgrading unit was assumed to contain 95% methane that was then enriched with propane to reach the typical requirement of 38,854 GJ Nm^{-3} (990 BTU SCF^{-1}) in California.

The research team developed a second financial model to evaluate a cluster of five digesters each producing 100 $Nm^3\ h^{-1}$ raw biogas and upgrading to pipeline quality at a centralized facility with a capacity of 250 $Nm^3\ h^{-1}$ biomethane. The five digesters were assumed to pretreat the biogas for sulfur and water before transferring the gas via pipeline to the central plant no more than 2 kilometers (km) away. The team assumed that the cost of pipeline connection from each digester to the upgrading plant would not be subsidized. The upgrading plant processes 500 $Nm^3\ h^{-1}$ biogas from all five producers to produce 250 $Nm^3\ h^{-1}$ biomethane that is enriched with propane to meet the energetic requirement of the pipeline. The upgrading plant uses a membrane separation unit similar to the configuration described for the single digester scenario but with increased capacity to accommodate the larger flow rates. The upgrading plant compresses the gas for injection into the distribution pipeline, with costs calculated for various distances between the facility and the injection point.

One of the main factors for profitability of a gas project is the value of the gas. There are three variables that influence this value: wholesale natural gas price, environmental credits from California's Low Carbon Fuel Standard (LCFS), and federal Renewable Identification Numbers (RINs). Prices for natural gas over the last three years have varied between \$1.90 and \$4.74 GJ^{-1} (\$2.00 and \$5.00 per MMBtu),[2] yet the other sources of revenue have been more volatile. The LCFS credit is based on the carbon intensity of the process used to produce the renewable fuel. For manure-based biomethane, the LCFS credit was \$47.73 GJ^{-1} (\$50.35 $MMBtu^{-1}$) in February 2018, with yearly averages of \$23.06 to \$37.56 GJ^{-1} during 2015 and 2017, respectively (Coker, 2018). The largest source of revenue from biomethane is through the RIN program, which valued 1 GJ of gas between \$21.80 and \$33.18 in 2016[4]. Both the LCFS credit and RIN value have uncertain futures and are contracted on a short-term basis,

[1] https://data.bls.gov/cgi-bin/cpicalc.pl.

[2] https://www.eia.gov/electricity/wholesale/index.php#history.

making project financing difficult (Black, 2015; Olson, 2017). Because of this variability and uncertainty, a range of gas values from \$5 to \$30 GJ^{-1} were considered in the current economic analysis.

Distance to the pipeline was also a significant variable in the analysis. Construction labor and material costs for natural gas pipe in California are estimated to be roughly \$1 million per 1.6 km (1 mile), though the cost can vary depending on the geography and zoning classification of the terrain. For project developers, the closest pipeline may not necessarily be the point of injection; the location must have the capacity for the additional gas. Project owners, however, may not have to bear the full cost of the pipeline. The California Public Utilities Commission established the Biomethane Interconnector Monetary Incentive Program, which provides a 50% rebate up to \$1.5 million for producers to connect to a California pipeline. Additional costs with pipeline connection include meter charges, engineering, feasibility study, and gas testing and monitoring equipment (Jaffe, 2016). Distances from 0.8 to 3.2 km are considered in the present analysis.

Project costs were divided into capital and operating costs. Maintenance costs were included in the operating costs. Costs were further broken down into upgrading plant costs and pipeline injection costs.

Major capital expenses include pipeline material and labor, pipeline interconnection fee, engineering for pipeline installation, gas conditioning, compression equipment, gas monitoring instrument, membrane upgrading unit, and site work for installation. Although the scope did not include pretreatment equipment exclusive of the membrane separation unit, results from this study showed a need for additional gas conditioning. Major operating expenses include general plant maintenance, electricity, propane, replacement of disposable media, membrane replacement, laboratory gas analysis, and insurance. Table 6 provides the capital costs included in the analysis.

Siloxane removal equipment cost is based on a regression analysis from GTI (2014), who surveyed gas treatment vendors with equipment capacities of 340-1,700 $Nm^3\ h^{-1}$ biogas. A 50 $Nm^3\ h^{-1}$ capacity reciprocating compressor was included at \$30,000 installed cost to boost the product gas pressure from 0.82 to 3.55 MPa (120 psig to 500 psig) for pipeline injection. The research team estimated the labor to install the upgrading plant at 10% of the plant capital cost, while utility installation and preparation of the site of the upgrading plant were estimated at 15% of plant capital cost.

The analysis assumed gas would be monitored by an online instrument at \$250,000 capital cost. Typical monitoring requirements for pipeline gas include the major components and H_2S, but testing of trace contaminants specific to California would likely be performed by grab samples and analyzed by a third-party laboratory. Charges of \$10,000 are included in the annual operating and maintenance costs for this expense. Annual testing of biomethane trace compounds is in compliance with the standards set by PG&E and SoCalGas for compounds below the trigger level. Any compound detected above the trigger level will be subject to quarterly testing.

Table 6: Capital Costs of Upgrading and Pipeline Injection

Activity	Value	Reference
Pipeline Injection		
Pipeline Material and Labor ($ km^{-1})	625,000	Jaffe et al. 2016
Interconnection Capacity Study ($)	5,000	SoCal Gas 2017
Engineering ($)	200,000	
Interconnection Fee	560,000	Ong et al. 2014
Rebates & Incentives ($)	one-half of pipeline connection costs up to $1.5 million	California Public Utility Commission 2017
Gas Monitoring Equipment ($)	250,000	Ong et al. 2014
Biogas Upgrading (100 Nm^3 biogas h^{-1} capacity)		
Piping and Controls for Propane Addition ($)	30,000	Clean World, Inc. 2016
Upgrading Unit—Membrane ($)	350,000	Helee, Inc. 2017
Siloxane Removal Equipment[a] ($)	162,000	GTI, 2014
Compression Boost to Pipeline ($)	30,000	Roloson et al. 2006
Plant Site Work ($)	10% of upgrading costs	
Plant Site Preparation ($)	15% of upgrading costs	
Contingency- 10% total capital costs ($)	variable	

[a]from regression equation, p. 34 of GTI report 2014: equipment cost ($) = 35,064*(SCFM biogas flow)$^{0.375}$

Source: University of California, Davis

Table 7 and Table 8 show the plant operating and maintenance costs for a production rate of 50 Nm^3 h^{-1} biomethane.

The net present value (NPV) is used in this study to determine economic feasibility and is defined as:

$$NPV = \sum_{i=1}^{i=T} \frac{ACF_i}{(1+r)^i} \quad (3)$$

where ACF_i is the annual cash flow for year *i*, T is the project lifetime in years, and r is the annual interest rate (Rapport, 2008). Projects with positive NPV are considered feasible economic investments. For this analysis the project lifetime was 15 years, and the interest rate was 6%. Expenses were escalated over the project lifetime at 2.57%. The revenue stream was not escalated but rather was an independent variable. The research team assumed the plant ran 360 days per year.

Table 7: Assumptions and Operating Costs in the Economic Model

Assumptions	Value	Reference
Gas Facility		
Plant Maintenance- 2.3% of capital ($ yr^{-1})	9,430	(Deng, 2010 #47)
Siloxane Removal Equipment ($ yr^{-1})	10,395	GTI (2014)
Utilities		
Electricity Use (kWh Nm^{-3} raw gas)	0.35	Measured
Electricity Cost ($ kWh^{-1})	0.11	(Deng, 2010 #47
Meter Charge ($ day^{-1})	4.599	PG&E Cal P.U.C. Sheet No. 40011-E
A-10 Demand Charge ($ kW^{-1})	11.23	PG&E Cal P.U.C. Sheet No. 40011-E
Gas Testing and Monitoring ($ yr^{-1})	10,000	(Lucas, 2016 #70)
Propane ($ MJ^{-1})	0.0179	(Rapport, 2016 #74)
Economic Parameters		
Interest rate on debt (% yr^{-1})	6	(Rapport, 2016 #74)
Economic Life (y)	15	(Rapport, 2016 #74)
Price Escalation (% yr^{-1})	0.0257	(Rapport, 2008 #75)
Additional Costs		
Insurance- 2% of capital ($ yr^{-1})	11,500	(Deng, 2010 #47)

Source: University of California, Davis

Table 8: Operating Costs in the Economic Model

Item	Value	Reference
Upgrading Plant		
Maintenance ($ yr^{-1})	2.3% of capital costs	Deng et al. 2010
Siloxane Removal Media[a] ($ yr^{-1})	10,400	GTI, 2014
Gas Testing and Monitoring ($ yr^{-1})	10,000	Lucas, 2016
Membrane Replacement[b] ($ yr^{-1})	4,000	Helee 2017
Propane[c] ($ yr^{-1})	13,900	Rapport, 2016
Utilities		
Electricity Use-Upgrade (kWh Nm^{-3} raw gas)	0.35	Measured
Electricity Use-Pipeline (kWh Nm^{-3} product gas)	0.14	Calculated
Electricity Cost ($ kWh^{-1})	0.13	(Krich, 2005)
Additional Costs		
Insurance ($ yr^{-1})	2% of capital costs	Deng et al. 2010

[a] Based on regression equation of GTI report (p. 34): O&M ($)= 306.1* (SCFM biogas)$^{0.952}$

[b] Assumes a five-year membrane life and $20,000 replacement cost.

[c] Based on upgrading product gas with 95% methane to pipeline specification of 38,854 kJ/Nm^3 (990 BTU SCF^{-1}). Propane material and delivery costs are estimated at $1.79x10^{-5}$ kJ^{-1}.

Source: University of California, Davis

Results and Discussion

Membrane Removal Efficiency for Major Compounds

Mean raw biogas concentrations are shown in Figure 8. Air intrusion or active air injection or both resulted in elevated concentrations of air in the upgraded gas at all three facilities. Gas at all three facilities had mean values in excess of 6% nitrogen (N_2) and 7% oxygen (O_2). Previous studies have found less than 5% N_2 and 2% O_2 in digester biogas (Scholz et al. 2013; Yang et al. 2014). Haider et al. (Haider, 2016) reported trace amounts of N_2 and O_2 in farm plant biogas. In addition, large variations in the raw gas concentrations were encountered at each facility, showing that the gas composition changed greatly depending on the feedstock and season. The dairy digester, for example, had coefficients of variation (standard deviation divided by mean) of 0.79, 0.58, 0.29, and 0.48 for N_2, O_2, methane (CH_4), and carbon dioxide (CO_2), respectively.

Figure 8: Raw Gas Composition on a Dry Basis

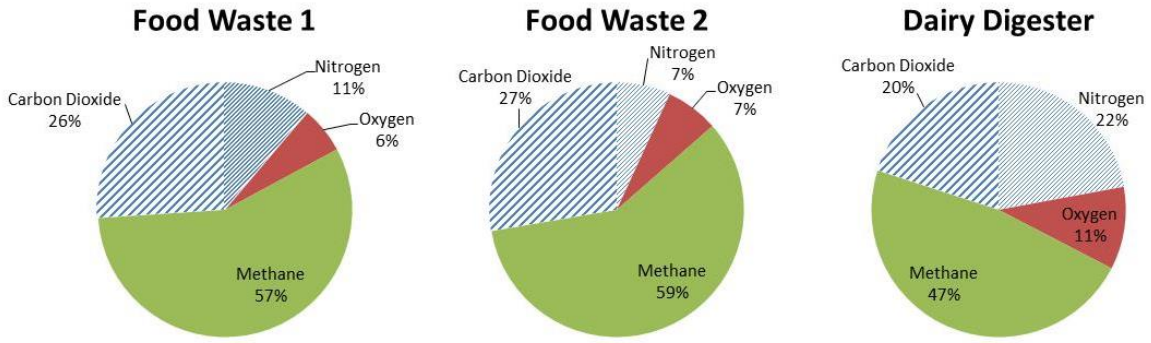

Source: University of California, Davis

As mentioned above, the authors used air injection to reduce H_2S formation at the dairy digester. Air was also injected in the H_2S mitigation step at the Food Waste 2 facility to reduce H_2S emissions. Additional air may have entered the inlet gas stream to the upgrading unit through the connections of the temporary piping assembled at each facility. Air intrusion would not be expected at a commercial upgrading facility using permanent piping since this would lower methane purity and potentially lead to a hazardous situation when the O_2 to CH_4 content reaches critical levels. Air mixed with 5%-15% CH_4 by volume forms an explosive mixture (NFPA, 2014). Biogas containing 5% CH_4 forms an explosive mixture when O_2 exceeds roughly 11%. The CH_4 content in most digester biogas is nearly 50%, raising the critical O_2 concentration to 35% for a combustible mixture (Holtappels, 2011).

Despite the high levels of N_2 in the feed gas, the upgraded gas at each location was relatively free of N_2 (Figure 9). This result is surprising, given the expected retention of N_2 with CH_4 in the upgraded gas through the membrane process. O_2 and CO_2 were also significantly reduced in the upgraded gas, but the CO_2 concentration was still higher in the upgraded gas than predicted. For commercial upgrading applications, methane purity would have to be increased to meet pipeline specifications.

Figure 10 shows the concentration reduction in the product biomethane relative to the raw biogas for N_2, O_2, and CO_2. N_2 removal was unexpected, as the permeability of N_2 is similar to that of CH_4 which should have caused N_2 to be retained in the product gas (Harasimowicz et al. 2007; Scholz et al. 2013). The high degree of variation in the N_2 removal efficiency suggests that some other process besides the membrane removal may influence the apparent removal efficiency of this component from the gas stream. The consistently high O_2 removal rates were also greater than the 30% value predicted based on a membrane performance model supplied by Air Liquide. The removal efficiency of CO_2 was greater than 60% at all three sites.

Figure 9: Major Compound Concentration in Upgraded Gas

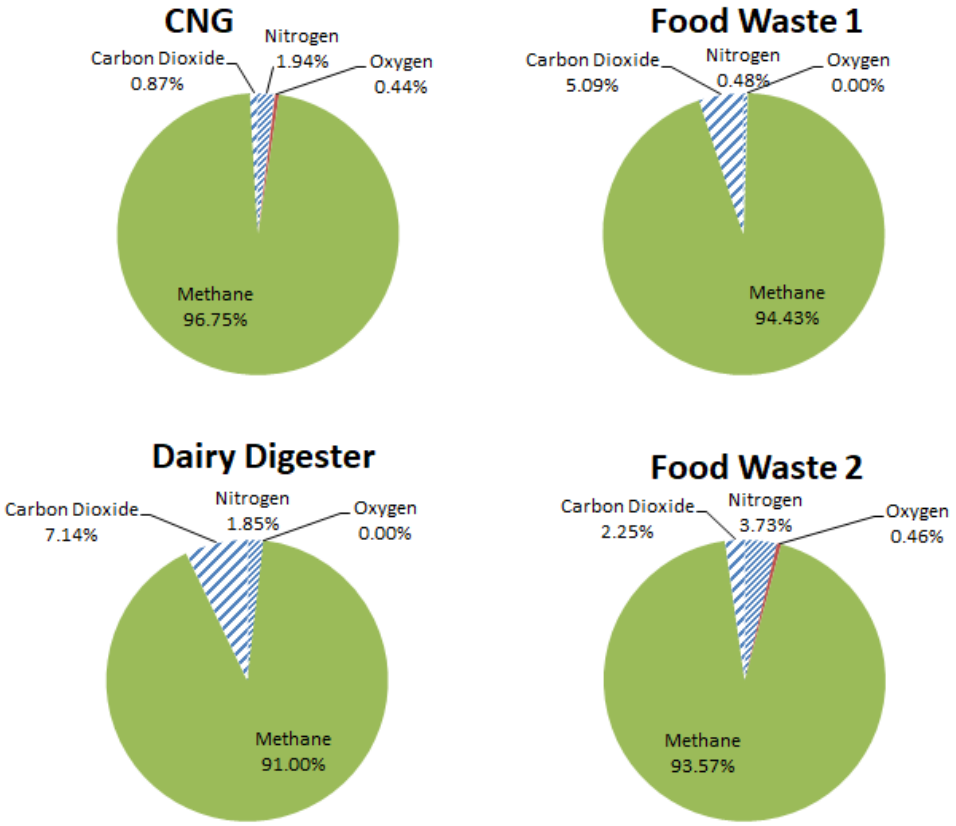

Source: University of California, Davis

Figure 10: Removal Efficiency of Major Compounds

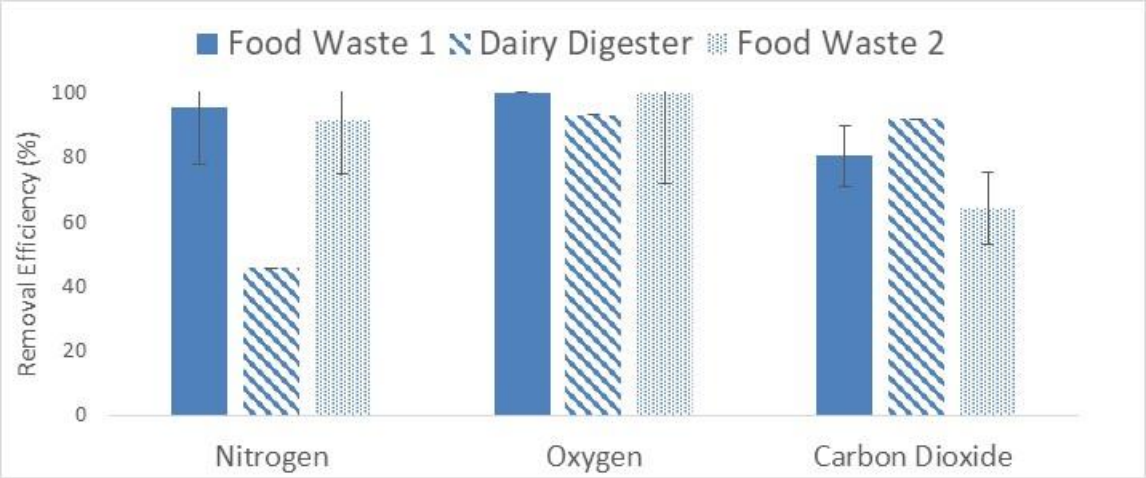

Source: University of California, Davis

Upgrading at all three facilities produced gas with an average CH_4 content of 93% despite the fact that average N_2 concentrations in raw biogas were measured from 7% to 22% (Figure 8). The membrane model by Air Liquide predicted a mean CH_4 concentration of 78% in biomethane under these conditions. One possible explanation for this discrepancy is that air may have leaked into the sample train (at negative pressure) during collection of raw biogas for chemical analysis. This theory is supported by measurements made with a portable gas analyzer (Landtec model 5000) during operation of the upgrading unit. The portable gas analyzer measured lower N_2 and O_2 concentrations (Table 9) that were closer to biogas values reported in the published literature and more closely matched the raw gas composition predicted by the model from Air Liquide.

Table 9: Raw Gas Composition

Element	Food Waste 1	Food Waste 2	Dairy Digester
Nitrogen	2.15±0.52	7.9±6.0	5.83±1.74
Oxygen	0.4±0.05	0.1±0.1	0.45±0.13
Methane	50.71±3.95	56.1±10.8	51.3±2.5
Carbon Dioxide	46.86±3.80	35.9±9.7	42.3±1.5

% Volume, Dry Basis) With Standard Deviation as Measured by a Portable Gas Analyzer (n⩾3)

Source: University of California, Davis

Figure 11 shows that the mean CH_4 content in the upgraded gas declined slightly with a rise in ambient temperature. The upgrading unit used an air heat exchanger to cool the oil and gas from the discharge of the compressor. The temperature of the gas through the membrane was thus affected by ambient temperature. The trends observed in the current study are consistent with previous observations that a rise in gas temperature through the membrane decreases the selectivity between CO_2 and CH_4 (Lin;Makaruk et al.).

Figure 11: Methane Content of Upgraded Gas With Ambient Temperature (n=3)

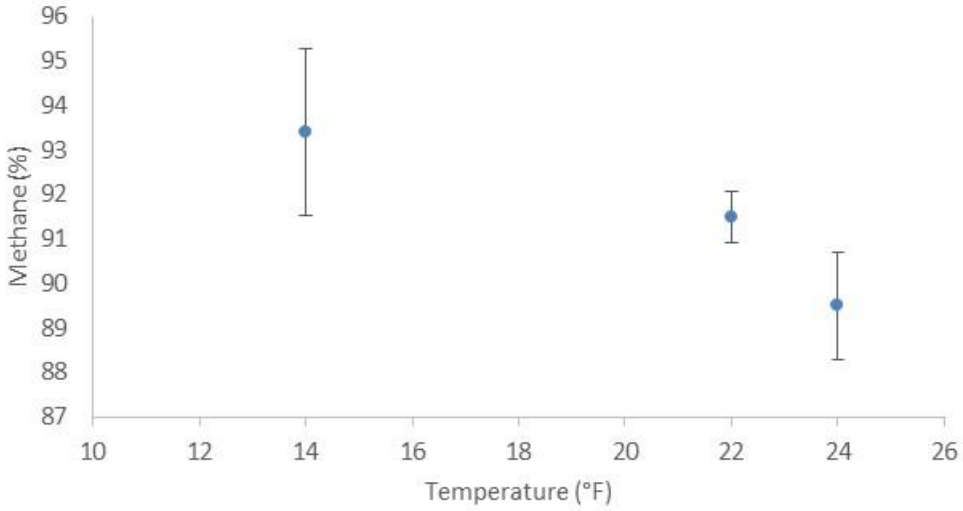

Source: University of California, Davis

Membrane Removal Efficiency for Trace Compounds

The average concentrations of trace compounds in the biogas entering the upgrading system are shown in Table 10. The dairy digester had lower concentrations of aldehydes, ketones, siloxanes, and higher hydrocarbons (C_2+) than the food waste plants. There was substantial variability in the concentrations of trace compounds between the food waste digesters and the dairy digester. Siloxane, halocarbon, and C_2+ concentrations were higher-than-expected values at Food Waste 1, possibly due to inadvertent mixing with biogas from the neighboring landfill when the raw gas sample was collected. Food Waste 1 digester shared a gas-conditioning skid with a nearby landfill with a pipeline connection between the systems. The measures taken to isolate Food Waste 1 biogas from the landfill gas may not have been successful. Previous studies have found no detectable siloxanes in biogas produced from animal waste, whereas landfill gas was found to contain 0.1 to 3.5 ppm siloxanes (GTI, 2014). Siloxane content in organic food waste digester gas typically falls between these extreme values.

Sulfur compounds were substantially elevated in the raw biogas at the dairy digester despite the preliminary sulfur mitigation efforts carried out directly in the digester (air injection and ferric chloride addition). These sulfur concentrations were further reduced by passing the gas through the activated carbon bed at the dairy before upgrading with the membrane separation unit.

Table 10: Mean Trace Compound Concentration of Raw Gas at Each Facility (n=3)

Constituent (ppb)	Food Waste 1	Dairy Digester	Food Waste 2
Aldehydes	362	40	349
Ketones	224	37	251
Siloxanes	1,600	0.17	55.9
C2+	6,800	958	1925
Sulfur	14,900	48,300	13,500
Halocarbon	800	238	74

Source: University of California, Davis

The result of gas processing by the membrane system was the removal of trace contaminants in all categories for the food waste facilities but enhancement of most contaminants at the dairy digester (Figure 12).

Figure 12: Trace Compound Removal Efficiency at Each Facility

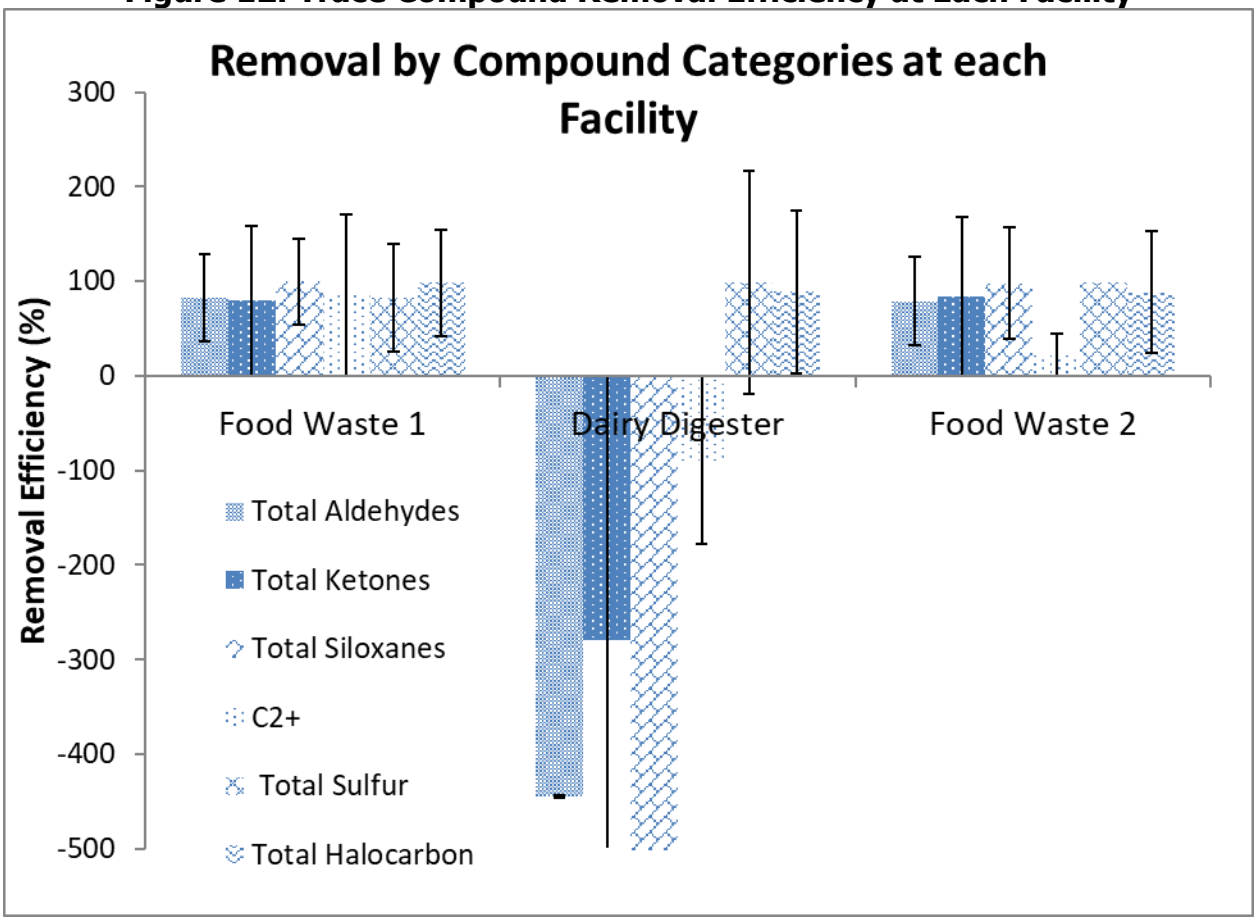

Source: University of California, Davis

The results reflect the multistage upgrading process and the potential for carryover between locations. Previous studies have reported pretreatment for trace compounds is required for upgrading biogas with membrane systems (Abatzoglou and Boivin, 2009;GTI, 2014; Ryckebosch et al., 2011). Pretreatment in this study was carried out using equipment at each facility or equipment on the membrane separation skid itself or both. It is likely that aldehydes,

ketones, siloxanes, and extended hydrocarbons were adsorbed onto these pretreatment systems. The adsorbed compounds continued to propagate through the adsorption bed, consistent with numerous observations of physical adsorption (Giraudet, 2017; Zhang, 2017). Food Waste 1 was the first plant to be tested, and all contaminants were removed at this site. The dairy digester was the second plant tested, but trace contaminants concentrations in the product biomethane were substantially higher than concentrations in the upstream biogas. This result likely occurred because compounds adsorbed at the previous site were flushed out of the system at the dairy digester. Food Waste 2 was the final plant tested, with removal of all trace contaminants observed at this location. Given the scaling times apparent from the previous tests, the trace compound concentrations measured at this location likely reflect the composition of the biogas at the previous site.

Sulfur compounds and halocarbon compounds did not exhibit the breakthrough behavior described above. These compounds were consistently removed from the biogas at all three locations, suggesting that they are permeable through the membrane or the associated migration velocity through the adsorbent bed was sufficiently slow that breakthrough did not occur during the current measurement campaign.

The fact that the adsorbent beds can retain and then release compounds important to gas quality reinforces the concept that all membrane upgrading plants need to be equipped with appropriately sized pretreatment steps to remove trace contaminants of concern from the biogas. Siloxanes, halocarbons, and sulfur compounds, at a minimum, should be reduced during biogas purification and upgrading. Alternatively, care can be taken to prevent inorganic wastes from entering the digester to lower the concentrations of these undesirable compounds in the raw biogas. Other compounds, such as larger hydrocarbons, aldehydes, and ketones, may not have to be removed if present in the biogas, since they will burn like other hydrocarbons; this depends upon the owner of the pipeline receiving the gas (GTI, 2014).

Biomethane Composition vs. Standards

Specific guidelines for trace contaminants in upgraded biogas have been established by the California Air Resources Board (CARB) and the California Office of Environmental Health Hazard Assessment (OEHHA) as part of California Assembly Bill 1900 (Gatto, Chapter 602, Statutes of 2012). AB 1900 identified 12 contaminants of concern in biogas and established threshold values to protect human health and pipeline integrity. A risk management strategy was also developed that includes a *trigger level, lower action level*, and an *upper action level*. Monitoring these constituents in the upgraded biomethane is required at a frequency that increases as concentrations approach levels of concern. Tests are conducted annually for compounds below the trigger level and quarterly for compounds that exceed the trigger level. Biomethane that tests above the lower action level three times in one year or biomethane that tests once above the upper action level cannot be injected into the pipeline. If the compound is then tested to be below the trigger level for four consecutive quarters, pipeline injection can resume, and the compound will be tested annually (Ong et al. 2014; SoCalGas Rule 30).

Mean concentrations of the 12 constituents of concern in the upgraded biomethane were below the trigger level in this study (Table 11).

Table 11: Constituents of Concern in Upgraded Biomethane Compared to the Risk Management Level From OEHHA

	LOQ	Food Waste 1	Food Waste 2	Dairy Digester	OEHHA Risk Management Trigger Level [a]
Arsenic (µg m^{-3})0	0.005	0.0	0.0	0.022	18.4
p-Dichlorobenzene (ppb)	1.5	<LOQ	<LOQ	4.37	950
Ethylbenzene (ppb)	3.4	17	94.8	43.2	6,000
n-Nitroso-di-n-propylamine (ppb)	0.029	<LOQ	<LOQ	<LOQ	6
Vinyl Chloride (ppb)	2.4	<LOQ	0.0	8.0	330
Antimony (µg m^{-3})	0.005	0.0	0.0	0.028	597
Hydrogen Sulfide (ppm)	0.298	0.0	0.0	0.0	22
Copper (µg m^{-3})	0.005	0.0	0.0	0.006	52
Lead (µg m^{-3})	0.1	0.0	0.0	0.0	76
Methacrolein (ppb)	0.053	<LOQ	<LOQ	0.086	9
Sulfur Mercaptans (ppb)	52	1080	716	0.0	12,000
Toluene (ppb)	4.1	206	180	409	240,000

[a]From (OEHHA, 2013)

Source: University of California, Davis

Upgrading Biomethane to Pipeline Quality

The biomethane produced from membrane upgrading used in this study did not meet several major requirements for California pipeline quality gas, including N_2, O_2, CO_2, and higher heating value (Table 12). Since other operating plants have achieved greater than 95% methane gas with similar membrane systems, it is likely that gross air entrainment into the biogas overwhelmed the ability of the membrane to separate the major contaminants from methane. At Food Waste 1, it is apparent that the neighboring landfill gas mixed with the digester gas through the connected piping. It is likely that air leakage will not be an issue for permanent upgrading systems, which would alleviate the N_2 and O_2 concerns apparent in Table 12.

Figure 13 shows that the energy content of the biomethane generated in this study was 5.4% below the higher heating value specified by Pacific Gas and Electric and 2.5% below the higher heating value specified by most other states (Ong et al. 2014). In comparison, the higher heating value for the petroleum CNG tested in this study was 3% above the California pipeline standard. The CH_4 content of biomethane and petroleum CNG was similar in this study (Table 12), but the petroleum CNG contained 5.6% ethane, which substantially enhanced the heating value.

Table 12: Biomethane Quality Comparison to Pipeline Gas

	Biomethane Average	Pipeline Natural Gas (CNG from Los Angeles, CA)	Pacific Gas and Electric Standard[a]
Nitrogen (%)	2.0	1.83	$(N_2+CO_2) < 4\%$
Oxygen (%)	0.1	0.42	<0.4
Methane (%)	93.0	91.2	No Requirement
Carbon Dioxide (%)	5.3	0.82	<1
H_2S (ppm)	ND	ND	<4
Halocarbons (ppb)	15.2	ND	<100
Siloxanes (mg Si m^{-3})	0.01	ND	<0.1[c]
HHV (kJ Nm^{-3})	36,739	40,031[b]	(38,854-41,208)[d]
HHV (BTU SCF^{-1})	936	1020	(990-1050)

ND= not detected [a]from Ong et al. 2014 [b]CNG contains 5.4% ethane and 0.33% propane [c]trigger level is 0.01 mg Si m^{-3} [d]varies with receipt point.

Source: University of California, Davis

Figure 13: Heating Value Comparison of Upgraded Biogas and Pipeline Natural Gas

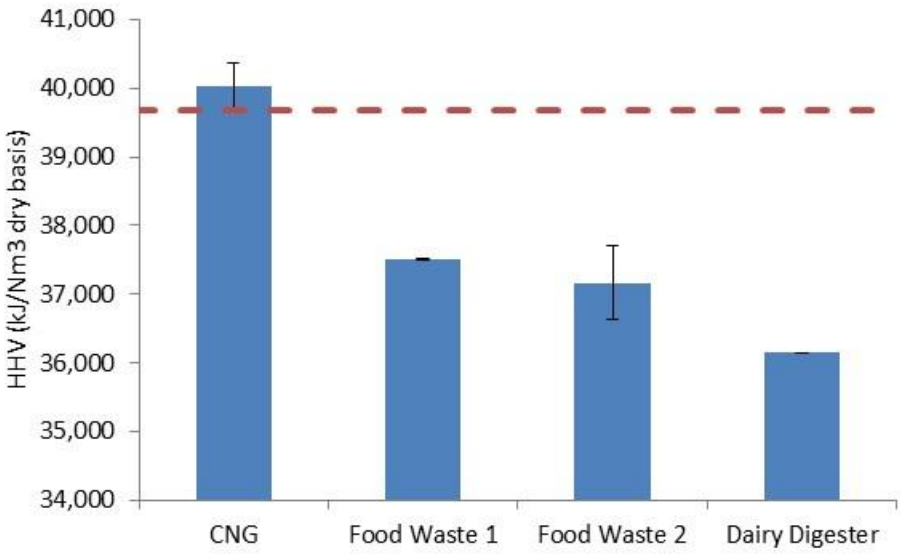

Dashed line shows heating value of 100% methane.

Source: University of California, Davis

Meeting energetic standards using CH_4 alone requires a CH_4 concentration of 98% in California or 95% in most other states. While upgrading to 98% CH_4 is technically feasible, it adds significant cost and complexity to the upgrading operation. Advocates from the biogas industry in California have proposed adopting energetic standards of 960-980 British thermal units (Btu) SCF^{-1} (similar to other states) for pipeline injection of biomethane, which would lower the threshold CH_4 concentration to 95%. This level of purity can be achieved using standard upgrading technologies.

Some gas distribution companies allow blending of low quantities of biomethane with pipeline gas if the resulting mixture still meets desired quality requirements. If the Wobbe index of the

natural gas is higher than the minimum limit, the mixture of natural gas and biomethane can meet the requirement even if the biomethane is lower than the limit (Hagen et al. 2001). Alternatively, up to 5% propane can be added to achieve the proper heating value (AGA, 2001). For an upgraded gas stream of 50 $Nm^3\ h^{-1}$ with 95% methane, about 0.75 $Nm^3\ h^{-1}$ of propane would be injected to increase the heating value from 37,676 to 38,854 kJ Nm^{-3} (960 to 990 Btu SCF^{-1}). In this study, the research team assumes that the propane injection of 1.83% by volume in the biomethane does not negate the ability to obtain environmental credits.

The research team advises a pretreatment step for siloxanes, halocarbons, and sulfur compounds to remove these contaminants from the biomethane before pipeline injection. A bed of activated carbon located after water removal but upstream of the membrane can serve this purpose. This configuration will reduce competition for adsorption between water and trace contaminants. Since the activated carbon media is fairly inexpensive, about $8.05 per kg, the bed could be replaced just before contaminant breakthrough rather than undergo an expensive regeneration step using heated purge gas (Cooper, 2002). Using the peak siloxane concentration of 1,600 ppb measured in this study and a capacity factor of 0.5, a bed of 74 kg activated carbon would need to be replaced every 90 days. The activated carbon will also remove most of the volatile organic compounds, although PG&E and SoCalGas do not state maximum limits on aldehydes, ketones, and extended hydrocarbons. These hydrocarbons will contribute to the heating value of the gas and are not known to pose pipeline safety concerns or produce adverse combustion products. Testing for aldehydes, ketones, and extended hydrocarbons is not standard but may be required by local pipeline owners (GTI, 2012).

Economics of Upgrading and Injecting Biogas Into the Natural Gas Pipeline

Both the single digester and digester cluster scenarios had specific production costs of $16 GJ^{-1} or more. This specific cost increased with distance to the pipeline and lower production rates mainly due to the capital cost for each scenario. Figure 14 shows the decrease in specific production costs with a decrease in pipeline distance for both digester scenarios. For the single digester case, an increase in capacity caused the specific production cost to decrease although not linearly. An increase of capacity from 20 to 40 $Nm^3\ h^{-1}$ decreased the specific production cost by 43%, while an increase of capacity from 40 to 60 $Nm^3\ h^{-1}$ resulted in a cost reduction of 26%.

Figure 14: Production Costs of Single Digester and Digester Cluster

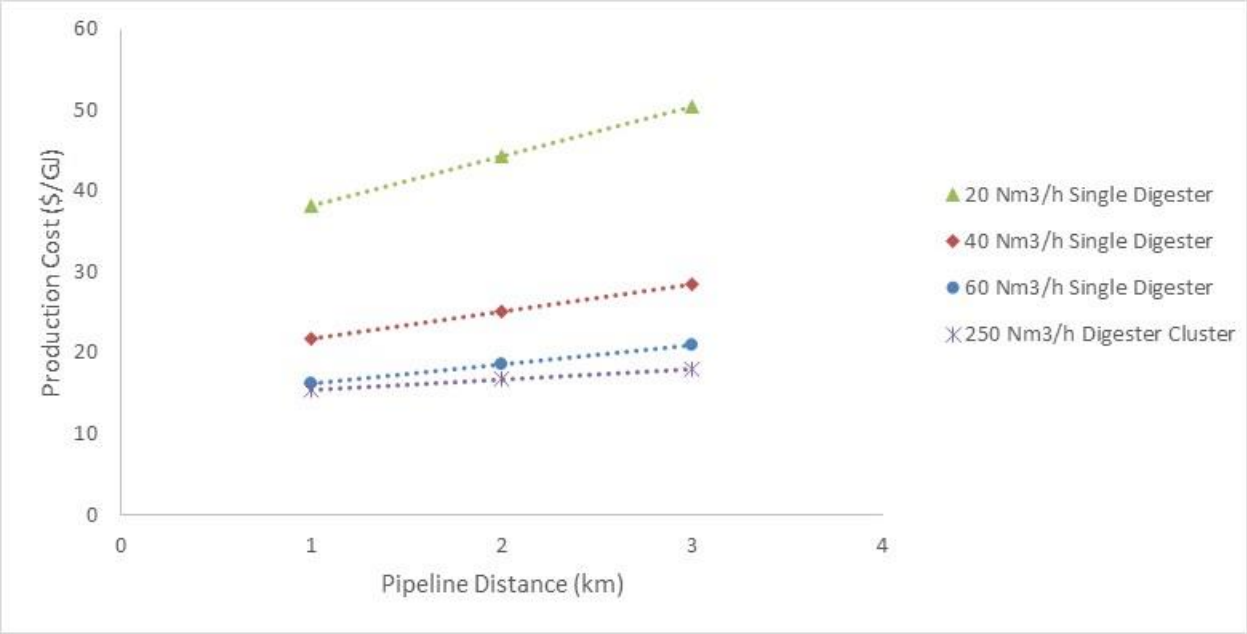

Costs represent average over 15 years.

Source: University of California, Davis

At \$16 GJ^{-1} production cost for a single digester and \$14 GJ^{-1} for a digester cluster, none of the scenarios evaluated using historical natural gas prices are economically feasible without incentives (Figure 15). The 20-year average natural gas price is about \$4 GJ^{-1}, which means single digester biogas project contracting would need \$12 GJ^{-1} in incentives. As mentioned, RIN values in 2017 varied between \$31.63 and \$37.54 GJ^{-1} for renewable natural gas, suggesting incentives may be able create financial feasibility for some biogas projects.

Figure 15: Historical Natural Gas Prices From Henry Hub

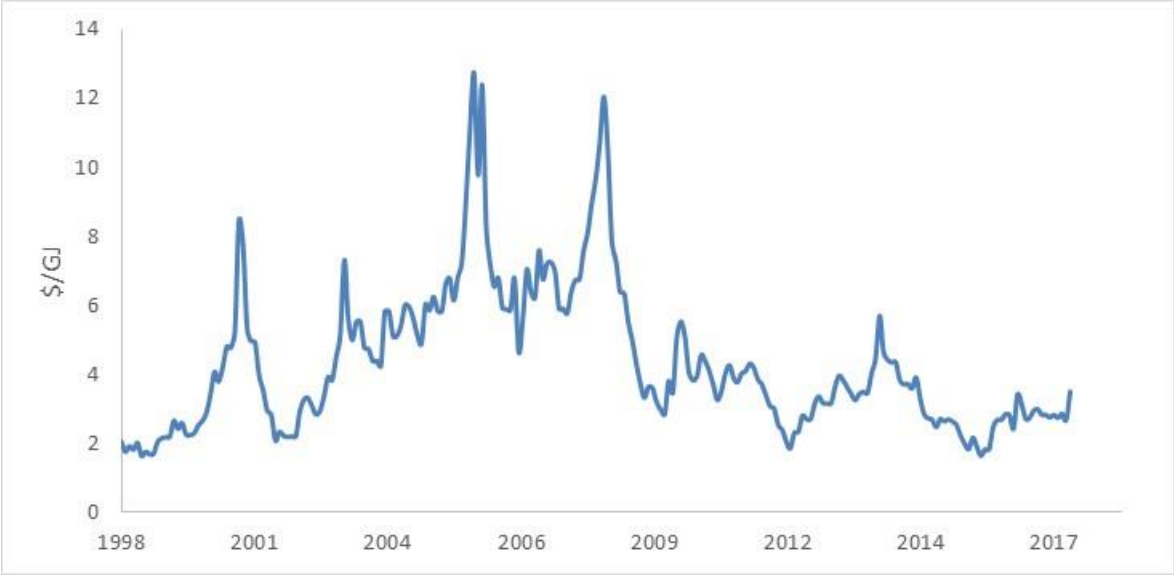

Source: Adapted from (Administration, 2017)

Figure 16 shows the NPV of single digester biogas projects over a range of gas capacities with a 1-km transport distance to the pipeline. The NPV increases as capacity and gas value increase with breakeven costs (NPV=0) of \$16 GJ^{-1}, \$22 GJ^{-1}, and \$38 GJ^{-1} for 60 Nm^3 h^{-1}, 40 Nm^3 h^{-1}, and 20 Nm^3 h^{-1} capacities, respectively. Thus, for a moderate gas contracting price of \$22 GJ^{-1}, only capacities greater than 40 Nm^3 h^{-1} would result in a profitable plant.

The change in slope of the NPV line was proportional to the change in plant capacity, showing that maximizing production throughput is essential for leveraging the value of the gas. A plant averaging 40 Nm^3 h^{-1} biomethane production over a 15-year period at a gas value of \$20 GJ^{-1} will not be profitable, while a plant that produces an average of 60 Nm^3 h^{-1} of biomethane over one year at the same gas value will profit more than \$500,000.

Figure 16: Single Digester NPV for 1 Km Pipeline Distance

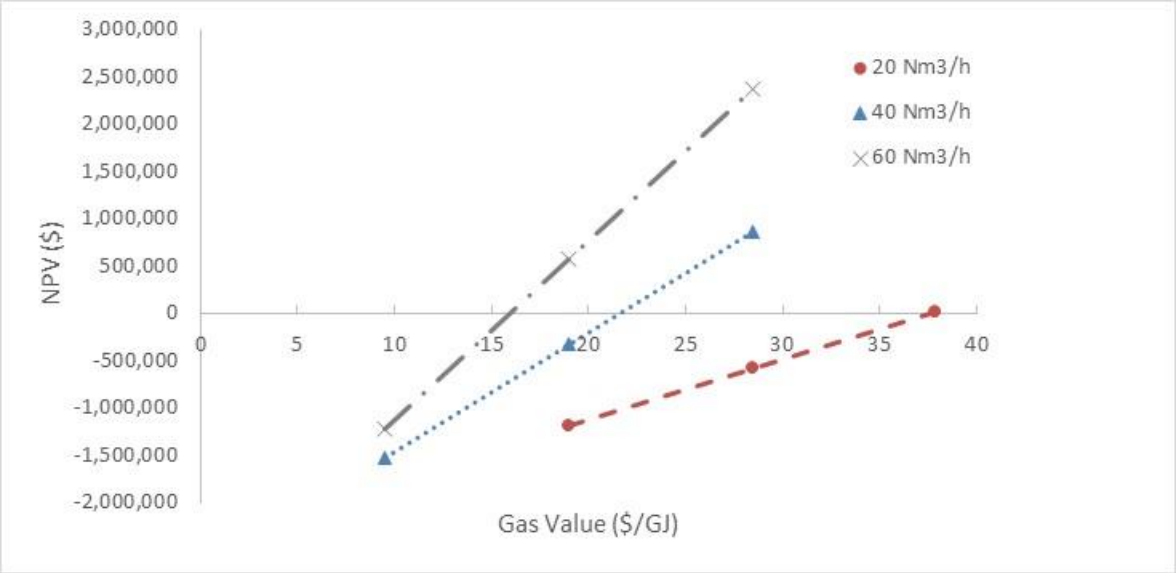

Lines show a linear fit to the data.

Source: University of California, Davis

The digester cluster had breakeven costs of \$15.6 GJ^{-1}, \$16.8 GJ^{-1}, and \$18.0 GJ^{-1} for 1-km, 2-km, and 3-km pipeline distances, respectively (Figure 17). Thus, contracting at a moderate gas value of \$20 GJ^{-1} results in a positive NPV for the digester cluster scenarios, with significant value added with incremental increases in gas value.

Plant capacity and pipeline distance had significant but opposite effects on the cost of production. Increasing distance to the point of injection increased the specific cost of production, while increasing plant capacity decreased the specific cost of production for a single digester (Figure 17).

Figure 17: Digester Cluster NPV Against Gas Value and Pipeline Distance

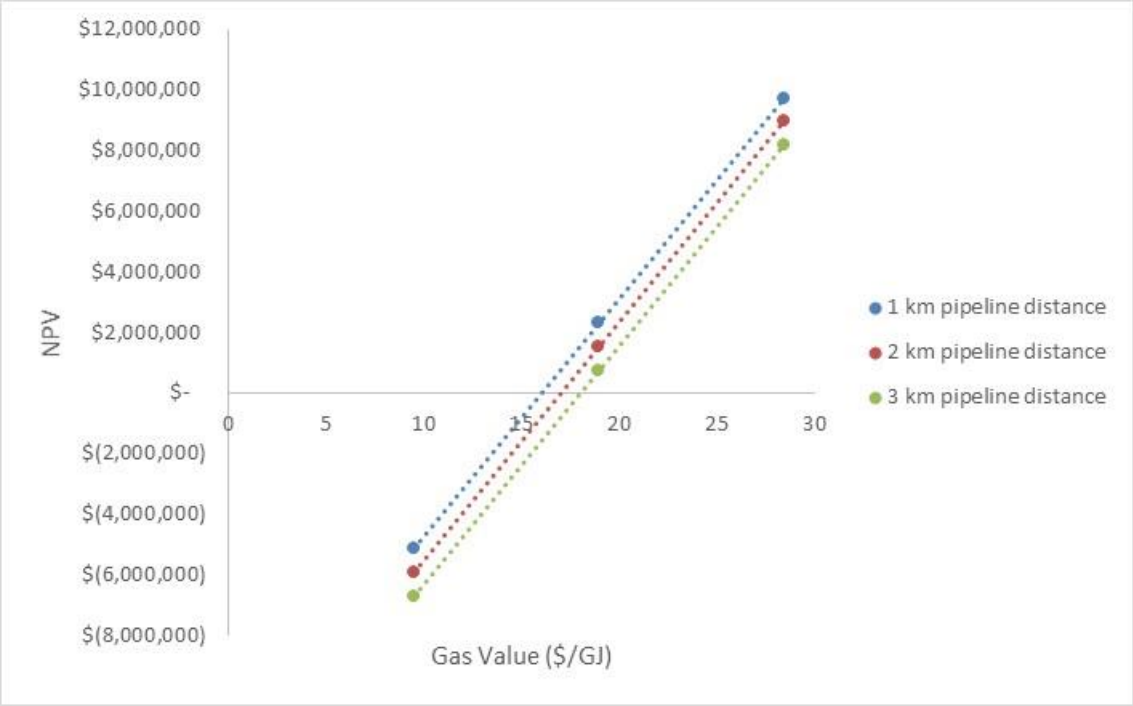

Source: University of California, Davis

There were significant economies of scale for the single digester scenario across all pipeline distances (Figure 18). Sensitivity of the specific cost was greatest at low capacities. An increase of capacity from 20 to 40 $Nm^3\ h^{-1}$ decreased the specific production cost by 43%, while an increase of capacity from 40 to 60 $Nm^3\ h^{-1}$ resulted in a cost reduction of 26%.

Figure 18: Single Digester-Specific Production Cost Versus Plant Capacity and Pipeline Distance

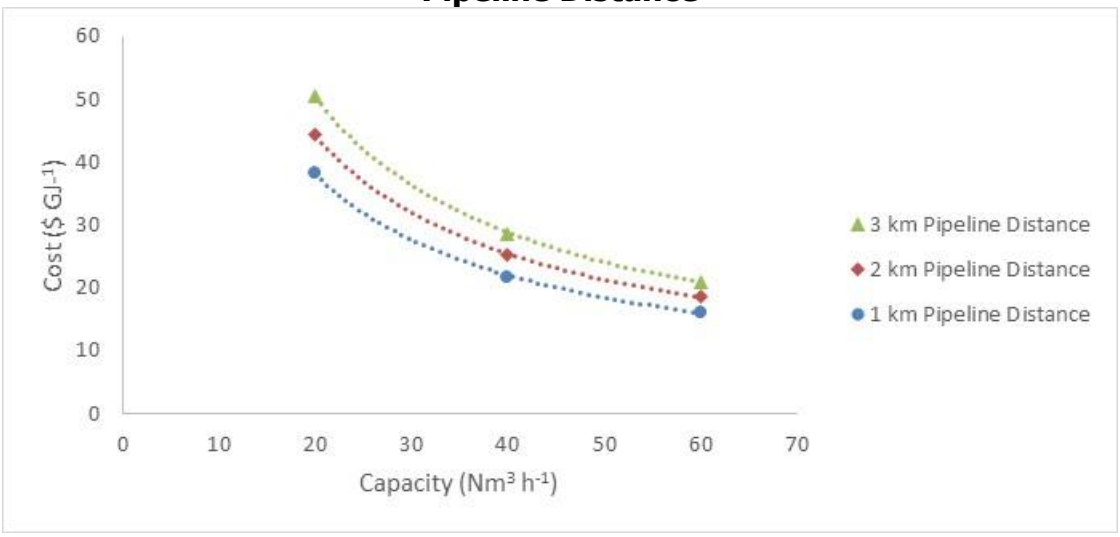

Source: University of California, Davis

Single digester production costs for 1-km pipeline distance in Figure 18 are similar to the costs from Kosusko et al. (Kosusko et al., 2016) in Figure 4, building confidence in the model. For 1-

km pipeline distance, the variation between the model and Kosusko was 11% to 33%, depending on capacity. For 3-km pipeline distance, the variation was 5% to 45%.

O&M costs were 35%-40% of the total production costs for a single digester with plant capacity of 40 $Nm^3\ h^{-1}$. Specific capital costs increased at a greater rate than specific O&M costs, with pipeline distance (Figure 19) showing pipeline costs become a greater part of the production costs as the distance to pipeline injection increases. Pipeline distance had little effect on O&M costs.

Figure 19: Capital and O&M Costs Relative to Pipeline Distance (for a Single Digester With Plant Capacity of 40 $Nm^3\ h^{-1}$)

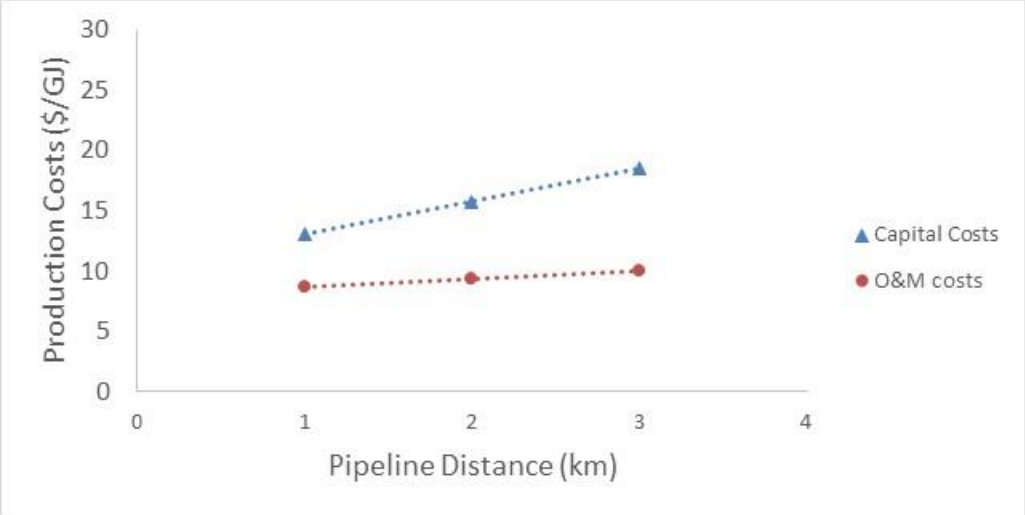

Source: University of California, Davis

The economic results show incentives are required to make viable upgrading and injecting biogas on a small scale in California. Production costs and NPV were highly sensitive to plant capacity. Clustering of digesters can reduce production costs, depending on additional costs incurred relative to the single digester.

Conclusions

The authors tested a small-scale membrane upgrading system with a capacity of 100 $Nm^3\ h^{-1}$ at two food waste digesters and one dairy digester in California. The membrane removed most of the carbon dioxide and part of the oxygen from the biogas matching performance predicted by the manufacturer. The membrane also appeared to remove nitrogen at a higher rate than the performance predicted by the manufacturer. The mechanisms for this nitrogen removal are not known at this time.

Despite the unexpectedly high removal rate, the total concentration of nitrogen and other inert gases diluted the methane content of the biomethane such that it did not meet pipeline specifications. Air injection or air intrusion or both would be minimized in permanent upgrading plants, which should allow the methane content of the product gas to reach 95% or higher. Additional injection of propane would be required to meet current pipeline requirements for higher heating value in California, but new standards consistent with other

states may be adopted in the future that would not require additional measures to increase the heating value of the biomethane.

The average composition of upgraded biomethane satisfied the trace contaminant requirements for pipeline injection in California, mainly because the precleaning steps upstream of the membranes removed these contaminants from the gas stream. Many of the trace contaminants were removed by physical adsorption in packed beds. The results indicate that contaminants are mobile in the beds, and breakthrough can occur if they are not sized properly. This finding was especially evident for siloxanes but also apparent for ketones, aldehydes, and extended hydrocarbons. Other trace contaminants including sulfur and halocarbons were consistently removed from the biogas by the membrane upgrading unit, possibly because they are permeable through the membrane or because the related migration velocity through the packed adsorption beds was sufficiently slow that breakthrough did not occur.

An economic model developed for a single digester and a cluster of five digesters predicted that pipeline quality gas production costs would be \$16 GJ^{-1} or more. The single digester had breakeven costs (NPV=0) of \$16, \$22, and \$38 GJ^{-1} for 60, 40, and 20 $Nm^3\ h^{-1}$ capacities, respectively. The digester cluster had breakeven costs of \$15.6, \$16.8, and \$18.0 GJ^{-1} for 1-, 2-, and 3-km pipeline distances, respectively. Given the current price of CNG at \$3.79 GJ^{-1}, it is clear that environmental incentives are required to make small-scale biogas projects viable. Production costs rose at an increasing rate with decreasing plant capacity. As plant capacity decreased, production costs were increasingly sensitive to pipeline distance. The production cost for the digester cluster scenario was less sensitive to pipeline distance compared to the single digester scenarios.

Future Work

Additional characterization of the membrane system, including a full mass balance, would help elucidate the fate of trace compounds important to air quality such as halogenated hydrocarbons, siloxanes and sulfur. Composition of the permeate gas and liquid condensate from the membrane system could be analyzed to understand the potential impacts of these major discharge streams. In addition, water in the biogas could be characterized to validate that the product gas meets the pipeline quality standard of 147 ppm H_2O. Additional modeling could evaluate the clustering of digesters in more detail. Gas conditioning and transport configurations could be optimized for life-cycle costs.

CHAPTER 3:
Exhaust Testing Method

Introduction

The research team sampled and analyzed exhaust from common biogas, biomethane, andCNG end-use applications, including electricity generators (biogas only), a residential water heater (biomethane and CNG), a cooking stove (biomethane and CNG), and a CNG vehicle (biomethane and CNG). Sources that emit exhaust directly into the atmosphere (generators, water heater, and vehicle) were tested by injecting the emissions into a Teflon photochemical reaction chamber. The products were collected after a three-hour aging period under atmospherically relevant conditions. The authors also sampled and analyzed vehicle exhaust after rapid dilution to ambient temperature (dilution factor ~13) in a constant volume sampling tunnel. Exhaust from the cooking stove was collected in the breathing zone immediately above the cooking zone with the ventilation system operating at 100 cfm. The cooking stove exhaust was not aged in the photochemical reaction chamber since the primary exposure route for this exhaust is the indoor environment. Figure 20 shows the schematic of all the exhaust testing methods.

Figure 20: Schematic of Exhaust Testing Methods

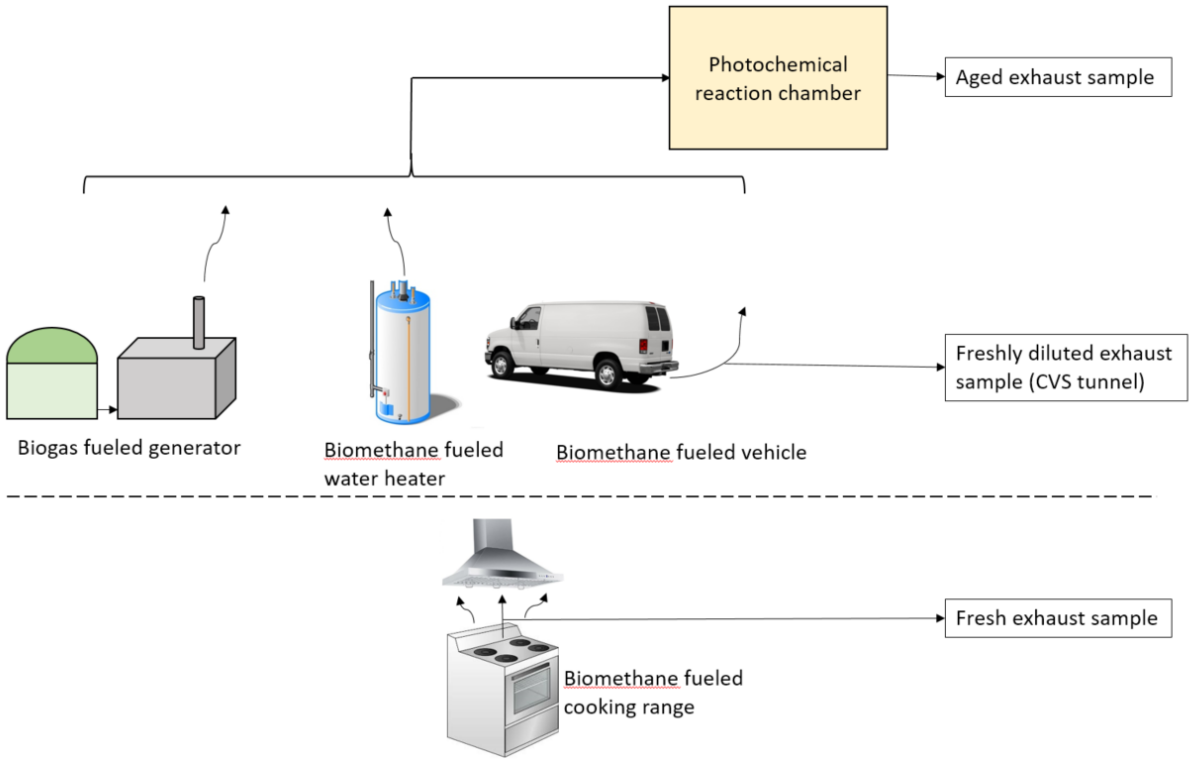

Source: University of California, Davis

Photochemical Reaction Chamber

The photochemical reaction chamber consisted of a 5.5 cubic meter (m^3) Teflon bag (5 m x 1 m x 1.1m), top and bottom UV lights emitting at wavelengths between 280 and 400 nanometers (nm), and polished aluminum side panels that have 95% reflectivity. Figure 21 shows the interior of the reaction chamber. The photochemical chamber system was assembled in the laboratory for appliance testing. The photochemical chamber system was placed in a 24-ft. trailer and taken directly to testing centers for mobile sources and stationary generator sources.

Figure 21: Photochemical Chamber Used in This Study

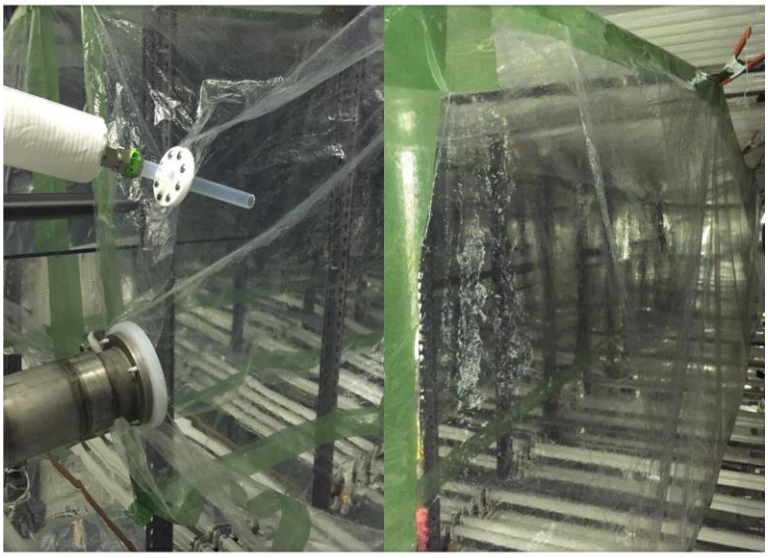

Source: University of California, Davis

The operating procedures for the photochemical chamber tests were designed to reproduce the atmospheric chemical system so that the reaction products could be studied under controlled conditions. Each test began by filling the Teflon bag to 50% capacity using dilution air that passed through the 4-inch diameter * 5-foot long stainless steel port shown in Figure 21. Dilution air was pre-cleaned using granulated activated carbon to remove background gas-phase species followed by a high efficiency particulate arrestance (HEPA) filter to remove background particles. Hot exhaust (50~55℃) collected before dilution in the CVS was then introduced into the reaction chamber through the 1-inch Teflon port. The amount of exhaust injected into the chamber was chosen so that NO+NO2(=NOx) concentrations would remain in realistic ranges to represent (i) a stagnant atmosphere during the night and (ii) a well-mixed atmosphere during the day. Immediately after exhaust injection, 100 liters of VOC surrogate gas (1.125±0.022 ppmv m-xylene and 3.29±0.07 ppmv n-hexane in air, Scott Marrin, Inc.) was injected into the reaction chamber over five minutes, creating a final VOC concentration of 90 ppb C (calculated based on calibrated flow rates). The remainder of the chamber was then filled with dilution air, ensuring that the exhaust and surrogate background VOC were well mixed.

The surrogate background VOC was to react with the NOx from the combustion source to produce oxidant concentrations representative of typical urban conditions in California. Atmospheric aging started when the bag was filled and lasted for three hours, at which time sample collection started. Daytime aging tests were conducted with UV lights turned on, creating a measured 50 watts m^{-2} UV intensity that represents a typical late summer day in California. Ozone concentrations during these tests reached nearly 100 ppb. Nighttime aging tests were conducted with the UV lights turned off and the chamber completely covered by aluminum reflective sheets.

Vehicle Exhaust Sampling

The research team conducted the motor vehicle tests at California Air Resource Board's (CARB) Haagen-Smit Laboratory (HSL) lab in El Monte (Los Angeles County). The lab is equipped with a 48-inch single-roll electric chassis dynamometer for light-duty vehicles, a constant volume sampler (CVS), and sampling systems that fully meets certification requirements defined by the Code of Federal Regulations (Agency, 1995) and partially meets more recent standards for measurements of lower-emission vehicles (Agency, 2014). The CVS was operated at a constant flow of 22.3 m^3 min^{-1}. A compressed natural gas (CNG) fueled van was used for this test. The research team made no modifications for use of the vehicle with biomethane. The specification of the vehicle are given in Table 13. Three kinds of fuel were tested in the vehicle. The first test used commercial CNG from nearby filling station (3528 E Foothill Blvd, Pasadena, California, 91107). The second test used a mixture of 27.8% CNG and 72.2% SATS biomethane because the vehicle tank could not be drained lower than 1,000 psi before reading empty. For this same reason, the third test contained residual amounts of CNG and SATS biomethane plus additional biomethane from other sources. The exact composition of the fuel in the third test was 7.7% CNG, 24.4% NH biomethane, 33.5% READ biomethane, and 34.4% SATS biomethane. Chapter 2 lists the composition of all fuels used in this study.

Each vehicle test used the California Unified Cycle (UC) that contains three phases, including a "cold start" phase, a "stabilized phase," a "hot soak," and a "hot start" phase. A speed time trace for the UC cycle is presented in Figure 22. Tests were conducted using cold start conditions and hot start conditions (applied to the same driving trace). Cold start tests preconditioned the vehicle on the prior day and stored the vehicle in a temperature-controlled environment overnight before pushing it onto the dynamometer and starting the engine when the test begins. Hot start tests repeated the driving trace after the vehicle had already been drive and reached operating temperature.

Table 13: Specification of the SULEVII Testing Vehicle

Manu-facturer	Model	Year	Engine Family	GVWR(lb)	ODOM (mi)	After-treatment	Fuel
IMPCO Technologies. Inc	Chevrolet Express 2500	2015	FZ9XT06.0CDA	8.500	6640	SFI/HO2S/TWC	CNG/ biomethane

Source: University of California, Davis

Figure 22: Speed Time Trace of California Unified Cycle

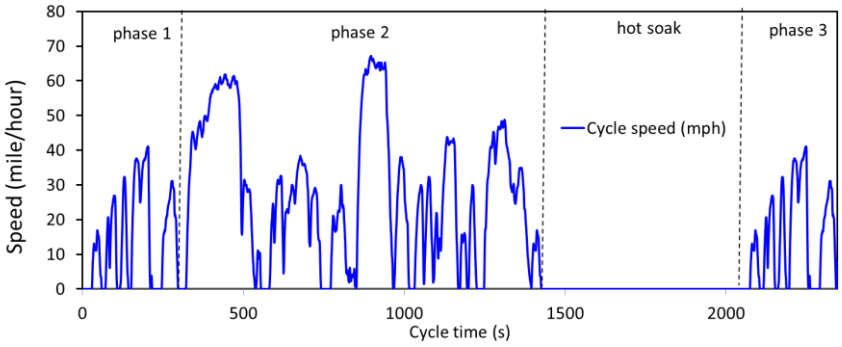

Source: University of California, Davis

The research team used a Fourier-transform infrared spectroscopy (FTIR) (AVL, SESAM 4) to measure a variety of gaseous species (CO_2, CO, NO_x, NH_3, SO_2, small hydrocarbons, and etc.) in undiluted tail pipe exhaust. The team measured and recorded concentrations of the regulated gaseous species (i.e CO_2, NMHCs, CH_4, CO and NO_x) in the CVS tunnel during the tests. The authors used the resulting concentrations to estimate the dilution factor (*DF*) in the tunnel with Eq. (3-1) (Agency, 2014).

$$DF = \frac{1}{(1+\frac{\alpha}{2}+3.76\times(1+\frac{\alpha}{4}-\frac{\beta}{2}))\times(X_{CO2}+X_{NMHC}+X_{CH4}+X_{CO})} \quad \text{(Eq. 3-1)}$$

where X_{CO2}, X_{NMHC}, X_{CH4}, and X_{CO} are flow-weighted concentration of CO_2, C_1-equivalent nonmethane hydrocarbon (NMHC), CH_4, and CO measured over UC cycle, respectively; α and β are the ratio of atomic hydrogen-to-carbon and atomic oxygen-to-carbon in the test fuel, which were set to be 4 and 0, respectively, for the CH_4 fuel used in this study.

Freshly diluted exhaust in the CVS was drawn into photochemical smog chamber through an insulated, ½-inch stainless steel transfer line at a constant flow rate of 61 liters (L) min^{-1} over the entire cycle (not including the "hot soak" period during which the vehicle was not running). The emissions measured from chamber therefore represent the cycle averaged value since they were collected over all phases of the UC driving cycle. Both the diluted exhaust from CVS tunnel and the further diluted and aged exhaust from photochemical chamber were collected on different media to support a range of chemical, biological, toxicological, and metal analysis. Figure 23 shows the vehicle and test setup.

Figure 23: Vehicle Exhaust Sampling Setup

Showing Tested Vehicle, Tailpipe Exhaust Transfer Line, CVS Dilution Tunnel, and the Photochemical Reaction Chamber

Source: University of California, Davis

Home Appliances Exhaust Sampling

Two types of natural gas appliances were tested in this study – a cooking stove and a water heater. Both appliances were tested inside a Teflon film-sealed chamber (6-ft. long x 2.6-ft. wide x 5.5-ft. high) with a stainless steel venting hood on top. Precleaned dilution air was supplied from the front bottom left of the chamber so that the background did not contribute contaminant gases or particles to the chamber exhaust. The research team controlled the total flow rate through the chamber at 100 SCF min^{-1}. Fuels tested in home appliances included pipeline CNG, SATS biomethane, READ biomethane and New Hope biomethane.

The team measured concentrations of CO_2 alongside the sampling port using a portable CO_2 sensor (TSI Model 8550 Q-Trak IAQ monitor) to estimate the DF for each test using Eq. 3-1. The DF estimated using only CO_2 was up to ~10% higher than the value estimated using the full set of gaseous species in Eq. 3-1. Temperature and RH were also recorded at the sampling port to ensure that water vapor did not condense in sampling tubes. Appliances were operated for 15 minutes (until the CO_2 concentration was stable) before collecting samples for chemical analysis.

Cooking Stove

The stove (GE, Model # JGBS10DEKWW) had four 9,100 Btu hr^{-1} (2.67 kW) burners and a 4.8 cu. ft. oven. Four stainless steel pots filled with Milli-Q® water (18.2 MΩ cm, TOC<50 ppb) were used to simulate cooking. The water was changed frequently to avoid boiling.

Researchers set the burner controls to 67% of maximum, and the same amount of water was heated during each test. The oven was set at 350° F. Samples were drawn from the center of the hood, 3 feet above the stove top. The ventilation rate of 100 SCF min^{-1} through the test chamber was typical of ventilation rates in a home kitchen. The team performed no further aging tests in the photochemical chamber for cooking stove exhaust because the greatest exposure typically occurs in the immediate vicinity of the stove. The team collected particle and gaseous samples for different chemical, biological, toxicological, and metal analysis.

Figure 24: Cooking Stove Exhaust Sampling Setup

Source: University of California, Davis

Water Heater

The water heater (Rheem, Model # XG40T06EC36U1) used in this study was designed to meet the South Coast Air Quality Management District ultra-low NO_x requirements typical of newer generations of home appliances. Hot water was continuously drawn from the water heater, while cold water was continuously supplied so that the burner was active throughout the testing period. Undiluted exhaust was drawn from 10 inches beneath the top of the water heater exhaust vent and injected into the photochemical reaction chamber through a ½-inch insulated stainless steel transfer line. The research team diluted the exhaust to represent nighttime and daytime concentrations in the reaction chamber, and VOC surrogate gas was added to trigger the photochemical aging. The team collected particle and gaseous samples after a three-hour aging period and used them for different chemical, biological, toxicological, and metal analysis.

Figure 25: Water Heater Exhaust Sampling Setup

Source: University of California, Davis

Generator Exhaust Sampling

The team collected exhaust samples from five biogas-fueled electricity generators in this study. The biogas source and generator information are listed in Table 3. Exhaust was drawn from the top of the stack through a ½-inch insulated stainless steel transfer line and pumped into the photochemical reaction chamber at a flow rate of 26 L min^{-1} (50~55℃). Atmospheric aging was then performed in the reaction chamber under either dark or light conditions at different exhaust dilution ratios. Figure 26 shows the exhaust sampling setup at Van Warmerdam Dairy.

Figure 26: Engine Exhaust Sampling Setup at Van Warmerdam Dairy

Source: University of California, Davis

CHAPTER 4:
Health Effects Assay Results

Introduction

The research team used assays to directly monitor chemical and biological responses associated with key health-effects pathways. Airborne particles emitted from fuel burning enhance oxidation reactions, leading to inflammation in the human body (Ghio et al., 2012), which causes short-term health effects (some of which are very serious, including potential death). Oxidative capacity and inflammatory response are, therefore, critical short-term pathways that must be monitored in this study. Air pollution exposure can also damage DNA (Somers et al., 2002), leading to increased cancer risk over longer periods. The effects of the damage can manifest in the exposed generation, (Masiol et al., 2012) or defects can be passed to later generations (Somers et al., 2002), leading to even longer-term health effects. An approach to monitor the complex emissions from biogas and biomethane combustion is available through the use of short-term tests for genotoxicity. For example, the mutagenicity and DNA damaging effects of gas stoves burning methane have been reported (Monarca et al., 1998). The mutagenic potential of samples must be evaluated to quantify these potential chronic health effects associated with widespread biogas and biomethane adoption.

Methods

The suite of assays employed in this study was based on recommendations made by the California Air Resources Board when evaluating the potential health effects of new fuels (Herner, 2013). CARB has adopted this standardized suite of assays so that results across multiple research tests can be intercompared to develop a relative risk ranking for different fuels (Yoon et al., 2013). Table 14 summarizes the standard assays that were used in this project and the health endpoints that they detect. ll assays were conducted on biogas and biomethane (direct gas or combustion products) samples collected on Teflon filters followed by adsorbent cartridges (XAD-PUF-XAD) to capture particle-phase and gas-phase emissions.

Table 14: Chemical and Biological Assays Used to Quantify Potential Health Effects

Type	Name	Laboratory		Toxicological Effect Measured
Cellular in vitro Assays	Macrophage ROS	Schauer/Schafer	U. Wisconsin	Oxidative Activity
	Inflammatory and Oxidative markers mRNA	Vogel	UC Davis	Inflammatory and Oxidative Activity
Genotoxicity Assays	Comet Assay	Vogel/Kado	UC Davis	DNA damage
	Ames Assay	Kado	UC Davis	Mutagenicity

Source: University of California, Davis

Macrophage ROS Assay

The macrophage reactive oxygen species (ROS) assay listed in Table 14 measure the ROS generating capacity of water extracts of particulate matter in exhaust samples. The reagent DCFH-DA (2′,7′-Dichlorofluorescin diacetate) is a cell-permeable ROS indicator that is modified by the ubiquitous esterases in the cell cytoplasm and then by the ROS species to generate a fluorescent product DCF (dichlorofluorescein), which is detected using a fluorometer. Rat alveolar macrophage cells were exposed to filter water extract at three dilutions for a 2.5-hour incubation, together with untreated controls and zymosan controls. Linear regression of fluorescence units vs. zymosan concentration was performed so that final ROS concentrations could be expressed in units of equivalent µg Zymosan.

Inflammatory and Oxidative Markers Assay

The cellular in vitro assays listed in Table 14 measure oxidative potential using living cells in culture as a biologically relevant marker that can also directly exhibit inflammatory responses. The mRNA assay used human U937 macrophages that are the first line of defense in the human lung. Chemical components of the sample interacted with the macrophage cells though the toll like receptors (TLR), aryl hydrocarbon receptor (AhR) and the NF-KappaB protein complex. Biomarkers were monitored inside the cells to detect action along these pathways, including cytochrome P450 monooxygenase (CYP1A1: marker for PAHs), interleukin 8 (IL-8: marker for inflammation), and cyclooxygense (COX-2: a key enzyme for inflammation; upregulated in cancer cells).

DNA Damage Comet Assay

The comet assay, also called the single cell electrophoresis test, is a technique that detects DNA damage to cells (Singh et al., 1988;Ostling and Johanson, 1984). The name is derived from the developed image that resembles a comet. The comet "head" is the intact DNA, while the comet "tail" is the fragmented pieces of DNA reflecting the degree of damage. Monocytic human U937 cells (monocytes) were used throughout. Typically, the PM extracts in DMSO were added to cells, and the culture incubated at 37° C for 4 hrs. The research team then harvested and prepared cells for analysis using the Trevigen (Gaithersburg, MD) Cometassay® system under alkaline buffer conditions (Trevigen, 2012). Briefly, about 1 x 10^3 cells in 0.05 ml phosphate buffered saline (PBS) were mixed with 0.5 ml Low-Melting Ararose (at 37° C), and 0.05 ml of this mix was added to the comet slides (Trevigen, Inc., Gaithersburg, MD.) The cells were then dried, lysed, and had electrophoresis performed. The slides were stained with SYBR Gold, and researchers analyzed comet images using a Leitz Laborlux fluorescence microscope and scored them using the Comet Assay IV (Perspectives Instruments, UK) scoring system. DNA damage was based on the intensity of the comet tail. The team counted at least 100 cells per exposure, and determinations were conducted blind and decoded after scoring. The DNA damage values reported are based on the relative intensity of stain in the comet tail vs. the head of the comet.

Mutagenicity Assay

The genotoxicity assays listed in Table 14 measure the potential for the biogas or biomethane sample to alter DNA in bacteria (Ames). The Ames assay measures mutations in several strains of the bacterium *Salmonella typhimurium* that require histidine (an amino acid) to grow. Chemicals within the tested sample may cause mutations in the bacteria that enable them to grow independently, making their own histidine. These mutated cells are call "revertants" since they have reverted to the ability to survive without histidine. Assay results are therefore reported as the number of observed revertants in each sample.

The Ames assay is the most tested mutagenicity assay for carcinogen screening for more than 30 years and positively identifies 50%-90% of known carcinogens as mutagenic (McCann et al., 1975). The modified "microsuspension" version of the Ames assay (Kado et al., 1986) was used to increase sensitivity by ~10x. Tester strain TA98 was used to measure frame-shift substitutions mutations. Liver homogenate (S-9) from male Spraque Dawley rats (Mol Tox, Boone, NC) was added to the assay to provide metabolic activation of the sample.

Filter Samples

Filters for the chamber studies and the direct exhaust from biogas plants were 47 mm Teflon filters and for the vehicle emission tests were 90 mm Teflon filters (Zefluor, 2 µm pore size) (Pall Life Sciences, Ann Arbor, MI). All filters were precleaned in methanol (3x), followed by dichloromethane (3x) with shaking. Filters were air dried in a HEPA-fitted bio hood. Filters were placed in stainless steel or anodized aluminum 47 mm filter holders and fitted onto the sampling manifold previously described. Sampling rates were nominally 20 l min^{-1} for chamber or direct exhaust samples and 200 l min^{-1} for the vehicle emission tests. Filter samples were stored at -20° C until extraction.

Vehicle exhaust sampling tapped into the CVS tunnel at the California Air Resources Board Light-Duty Vehicle testing center in El Monte. The details of the CVS are provided in Sec. 3.3 of this report. Filter samples for the mutagenicity and molecular markers for inflammation were collected separately. The research team drew samples from the dilution tunnel using stainless steel probes positioned in the same plane as the PM probes used for Code of Federal Regulations (CFR) PM measurements. Briefly, a 1.0 " O.D. stainless steel probe was positioned in parallel to the CVS PM probe and connected to a 90 mm stainless steel filter holder. The team stored filter samples at -20° C until shipment to University of California, Davis, investigators. Filters were extracted using pressurized solvent extraction at 2,000 psi, 100° C using a Dionex ASE 200 extraction unit with dichloromethane (Burdick and Jackson GC grade). he extracts obtained were dried and redissolved in dimethylsulfoxide (DMSO) for testing.

Results

Macrophage ROS Assay Results

Averaged ROS levels (µg Zymosan $filter^{-1}$) in different exhaust samples are listed in Table 15. In both cold and hot start vehicle tests, exhaust ROS levels from CNG tests were a factor of 10 higher than ROS levels in SATS biomethane or mixed biomethane tests. In water heater tests, CNG exhaust showed A slightly higher level of ROS than biomethane exhaust, while in stove

tests, exhaust generated from the biomethane mixture had higher ROS levels than exhaust from CNG.

Table 15: Average ROS Levels Reported for Exhaust Samples

Test	Fuel	Average ROS (µg Zymosan filter^{-1})	Standard deviation (µg Zymosan filter^{-1})
Vehicle cold start	CNG	186.05	33.75
	SATS	13.18	11.74
	Biomethane mixture	8.29	16.01
Vehicle hot start	CNG	113.39	8.44
	SATS	8.14	3.69
	Biomethane mixture	7.62	18.39
Water heater	CNG	23.02	11.46
	SATS	14.57	7.42
	READ	10.17	7.06
	New Hope	10.15	4.29
Cooking stove	CNG	19.86	4.51
	Biomethane mixture	27.31	1.04

Source: University of California, Davis

To normalize for the effects of different rates of fuel consumption, exhaust dilution, and sampling time between tests, all the ROS values were normalized to units of "µg Zymosan MJ^{-1}". This can be interpreted as the amount of ROS associated with each MJ of heat generated by the tested fuel in the tested application, allowing a cross comparison of ROS values among different types of exhaust samples. Normalized ROS values are listed in Table 16. Consistent trends are observed in Table 15 and Table 16 within each test category because test conditions (fuel consumption, dilution ratios, collection duration) were similar within each category. More interestingly, cold-start CNG vehicle tests had the highest ROS level per MJ of energy across all applications.

Table 16: Average ROS Levels Normalized to Unit of MJ Fuel Burnt

Test	Fuel	Average ROS (µg Zymosan MJ^{-1})	Standard deviation (µg Zymosan MJ^{-1})
Vehicle cold start	CNG	223.25	40.50
	SATS	16.69	14.86
	Biomethane mixture	10.42	20.12
Vehicle hot start	CNG	44.66	3.33
	SATS	2.56	1.16
	Biomethane mixture	3.12	7.53
Water heater	CNG	6.36	4.11
	SATS	4.34	2.87
	READ	3.10	2.79
	New Hope	3.16	1.73
Cooking stove	CNG	29.23	8.63
	Biomethane mixture	43.98	2.19

Source: University of California, Davis

Inflammatory and Oxidative Markers mRNA Assay Results

Effect of Biogas Samples on CYP1a1 mRNA Expression

Biogas samples with a significant effect on the mRNA expression of CYP1A1 concentrations are shown in Table 17. The READ Raw samples led to a 2.7-fold increase of CYP1A1 compared to READ Blank sample. There was no significant increase of CYP1a1 expression level after treatment with exhaust samples collected from the turbine-generator at READ with or without aging (light vs. dark). The VW Dark or VW Light samples had no significant effect on CYP1A1 expression compared to the chamber blank. The NH Dark sample had no significant effect, whereas NH Light led to 1.7-fold increase of CYP1A1 compared to chamber blank.

Kiefer Light and Kiefer Dark samples had no increasing effect on CYP1A1 concentrations, but Kiefer Direct Exhaust induced CYP1A1 expression in macrophages by about 180-fold compared to the chamber blank. The Kiefer Raw sample induced CYP1A1 fourfold above blank control.

SATS Dark and SATS Light samples had no significant effect on CYP1A1 concentrations expression in macrophages, whereas SATS Direct Exhaust induced CYP1A1 expression by fifteenfold compared to chamber blank.

The CNG Vehicle sample (Tunnel Cold) induced CYP1A1 concentrations 5.8-fold above blank control. The SATS Tunnel Cold and Mix Tunnel Cold induced CYP1A1 expression fourfold and threefold, respectively, above blank control. Biogas Hi Vol samples with significant effects on the mRNA expression of CYP1A1 are shown in Table 18. These results are consistent with the ROS findings where CNG was highest, followed by the SATS biomethane. The emissions are also presented on a per-mile basis, illustrated in Figure 27. The CNG resulted in the highest emissions per mile, followed by SATS and Mixed fuels.

Cooking stove samples from all fuels (SATS, READ, New Hope, and CNG) induced CYP1A1 expression significantly by 92.4-fold, 225.3-fold, 101.3-fold, and 52.7-fold, respectively, per cubic meter of exhaust sample. Biogas cooking stove exhaust samples with significant effects on the mRNA expression of CYP1A1 are shown in Table 19 and are illustrated in Figure 28.

Water heater samples from CNG Dark, SATS Dark, NH Dark, and READ Dark significantly induced expression of CYP1A1 38.3-fold, 30.8-fold, 86.2-fold, and 34-fold, respectively, above control. Biogas water heater exhaust samples with significant effects on the mRNA expression of CYP1A1 are shown in Table 20 and illustrated in Figure 29.

Effect of Biogas Samples on mRNA Expression of Inflammatory Markers IL-8 and COX-2

No significant change of IL-8 or COX-2 expression was found in macrophages treated with READ Dark or READ Light samples at the concentration used in this study. Biogas samples with a significant effect on the mRNA expression of IL-8 and COX-2 are shown in Table 17. The READ Raw samples led to a 3.5-fold increase of IL-8 and threefold increase of COX-2 compared to the READ Blank sample. The VW Dark or VW Light samples had no significant effect on IL-8 or COX-2 expression compared to the chamber blank. The NH Dark sample had no significant effect on IL-8 or COX-2, whereas NH Light led to a 1.7-fold increase of IL-8 compared to chamber blank. Kiefer Light and Kiefer Dark samples had no increasing effect on

IL-8 or COX-2 mRNA levels, but Kiefer Direct Exhaust induced IL-8 and COX-2 expression in macrophages by 18.9-fold and 12.9-fold compared to chamber blank. The Kiefer Raw sample induced IL-8 and COX-2 by threefold above blank control. SATS Dark and SATS Light samples had no significant on IL-8 or COX-2 expression in macrophages, whereas SATS Direct Exhaust induced IL-8 and COX-2 expression by 18.8-fold compared to chamber blank.

The CNG Motor Vehicle sample (Tunnel Cold) induced IL-8 and COX-2 by 3.2-fold and 1.9-fold, respectively, above blank control. The SATS Tunnel Cold and Mix Tunnel Cold induced IL-8 expression 2.6-fold and 1.6-fold, respectively, above blank control. The effects of the Biogas Hi Vol samples on the mRNA expression of IL-8 and COX-2 are shown in Table 18. COX-2 expression was increased by 1.6-fold and 1.5-fold after treatment with SATS Tunnel Cold and Mix Tunnel Cold, respectively. The results based on emission increases per mile are illustrated in Figure 27. The CNG-powered vehicle resulted in the highest emission rate per mile.

Cooking stove samples from all plants SATS, READ, New Hope, and CNG-induced IL-8 expression significantly by 33.2-fold, 46.7-fold, 25.9-fold, and 20.7-fold, respectively, per cubic meter sample. The expression of COX-2 was significantly increased by 24.9-fold, 26.8-fold, 20.7-fold, and 23.0-fold after exposure to cooking stove samples from SATS, READ, New Hope, and CNG, respectively. Biogas cooking stove exhaust samples with effects on the mRNA expression of IL-8 and COX-2 are shown in Table 19 and are illustrated in Figure 28.

Water heater samples from CNG Dark, SATS Dark, NH Dark, and READ Dark significantly induced expression of IL-8 by 13.1-fold, 10.9-fold, 20.7-fold, and 13.3-fold, respectively, above control. The expression of COX-2 was significantly increased by 11.9-fold, 11.5-fold, 17.8-fold, and 14.1-fold after exposure to water heater samples from CNG Dark, SATS Dark, NH Dark, and READ Dark, respectively. Biogas water heater exhaust samples with effects on the mRNA expression of IL-8 and COX-2 are shown in Table 20 and are illustrated in Figure 29.

Table 17: Engine-Generator Samples With a Significant Effect on the mRNA Expression of CYP1A1, IL-8 and COX-2 Concentrations

Sample name	Gene target		
	CYP1A1	IL-8	COX-2
Blank	33	12.6	12.6
READ Raw	87.2	43.6	37.8
Kiefer Direct exhaust	5913	238	163.3
SATS Direct Exhaust	498.9	38.2	38.2
Kiefer Raw	135.8	39.3	39.3

Averages of molecular markers are shown as fold increase per $m^{3.}$

Source: University of California, Davis

Table 18: Mobile Source Samples With a Significant Effect on the mRNA Expression of CYP1A1, IL-8 and COX-2 Concentrations

Sample name	Gene target		
	CYP1A1	IL-8	COX-2
Blank	14.3	3.0	3.8
CNG	81	9.9	7.2
SATS	57.8	7.9	6.0
MIXED	42.5	4.4	5.6

Averages of molecular markers are shown as fold increase per m^3.

Source: University of California, Davis

Table 19: Cooking Stove Samples With a Significant Effect on the mRNA Expression of CYP1A1, IL-8 and COX-2 Concentrations

Sample name	Gene target		
	CYP1A1	IL-8	COX-2
SATS	92.4	33.2	24.9
READ	225.3	46.7	26.8
New Hope	101.3	25.9	20.7
CNG	52.7	21.6	23.0

Averages of molecular are shown as fold increase per m^3. Values are shown as fold increase above control (=1).

Source: University of California, Davis

Table 20: Water Heater Samples With a Significant Effect on the mRNA Expression of CYP1A1, IL-8 and COX-2

Sample name	Gene target		
	CYP1A1	IL-8	COX-2
CNG	38.2	13.1	11.9
SATS	30.8	10.9	11.5
New Hope	86.2	20.7	17.8
READ	34.0	13.3	14.1

Averages of molecular are shown as fold increase per m^3. Values are shown as fold increase above control (=1).

Source: University of California, Davis

Figure 27: Motor Vehicle Emissions per Mile for Molecular Expression of CyP1A1, IL-8, and COX-2 Molecular Markers

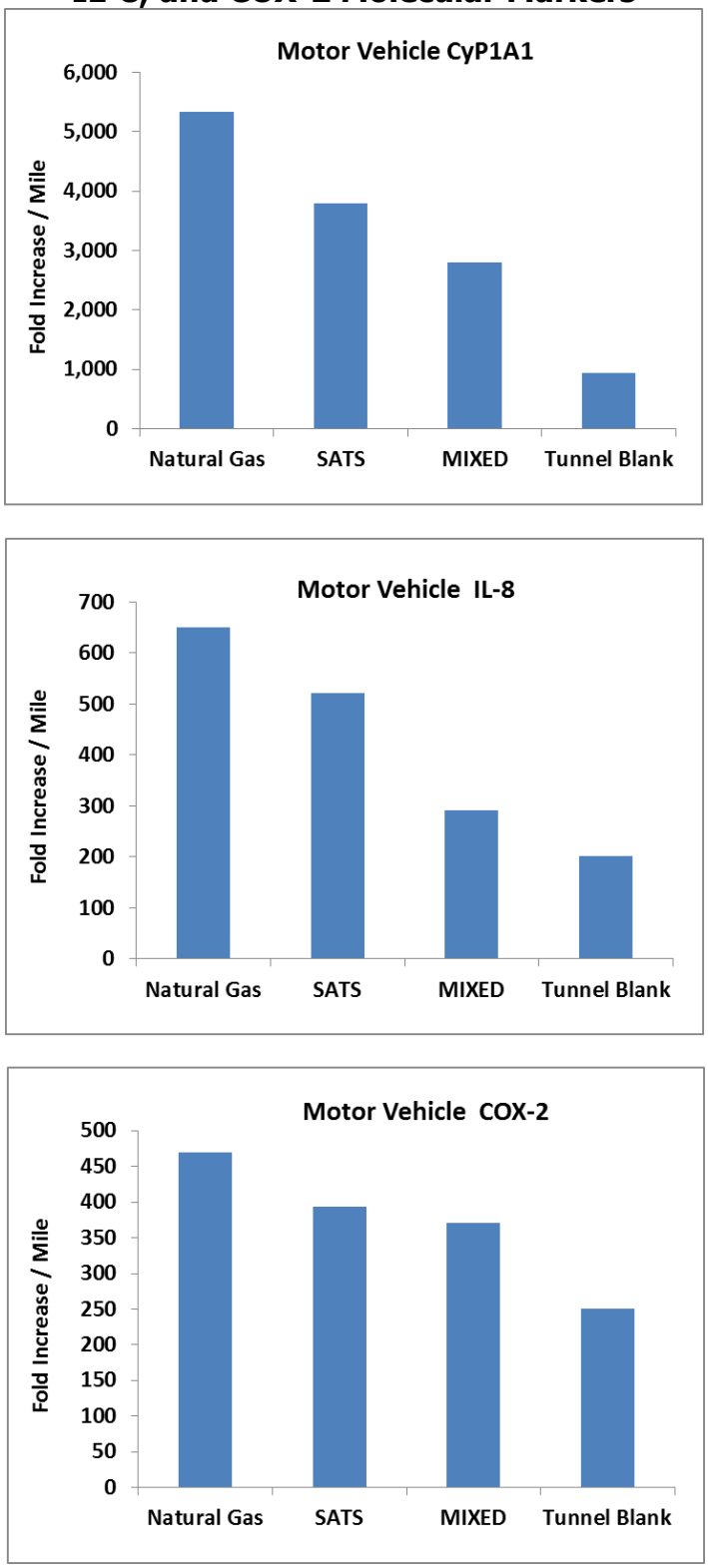

Source: University of California, Davis

Figure 28: Cooking Stove Fold Increases of CYP1A1, IL-8, and COX-2 Concentrations

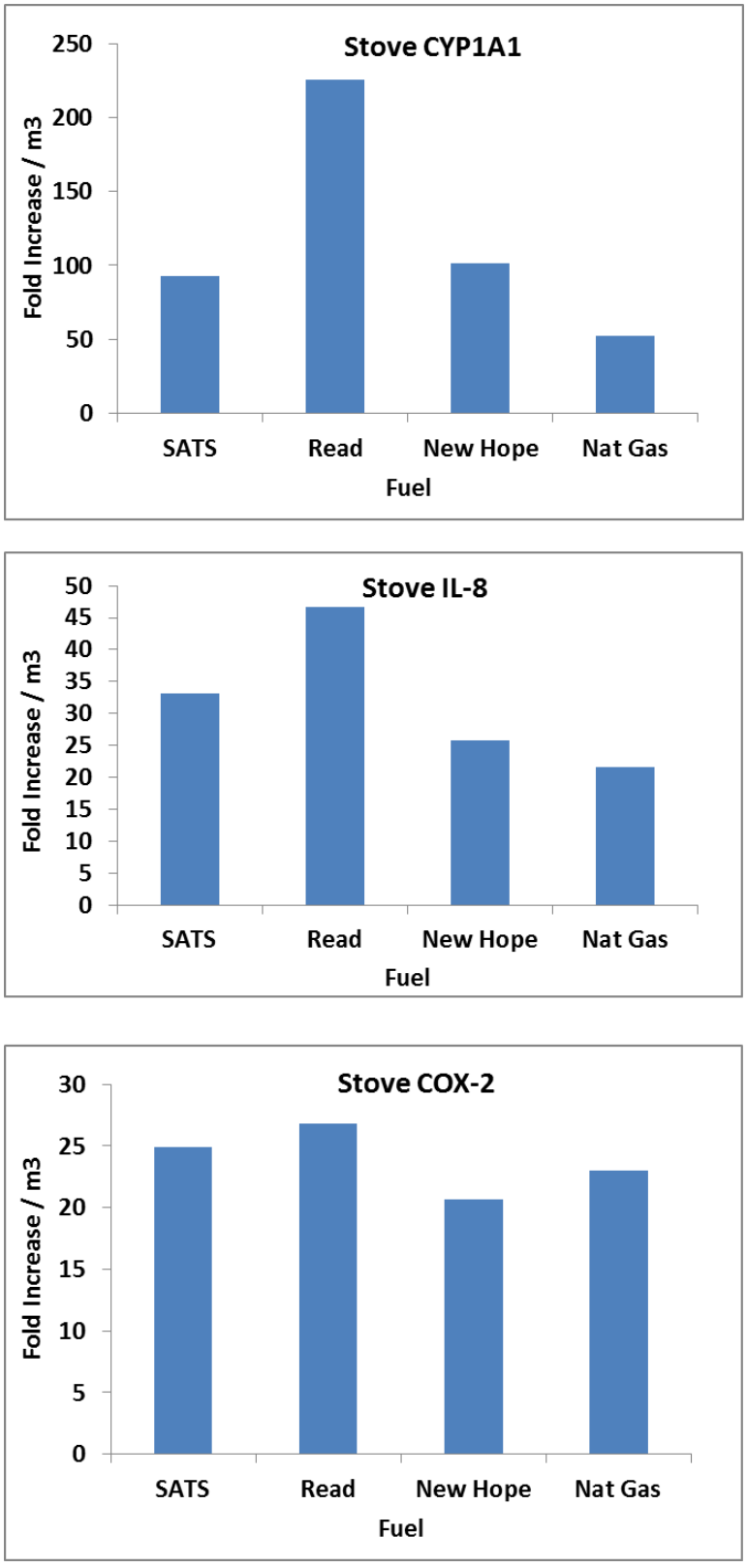

Source: University of California, Davis

Figure 29: Water Heater Fold Increases of CYP1A1, IL-8, and COX-2 Concentrations

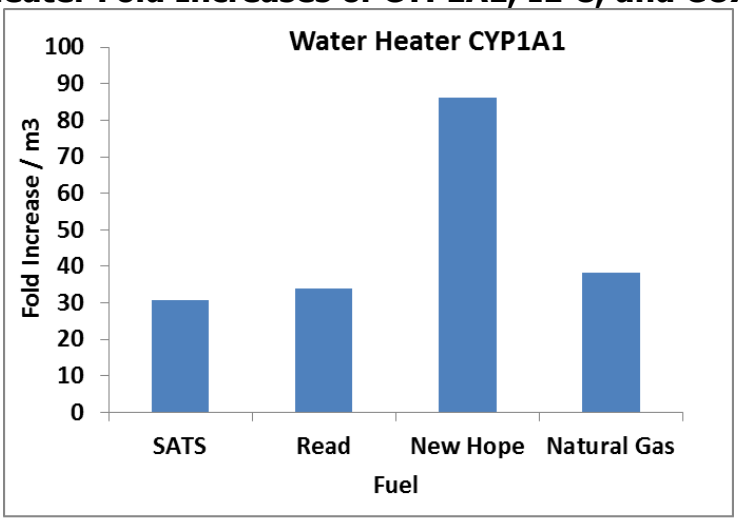

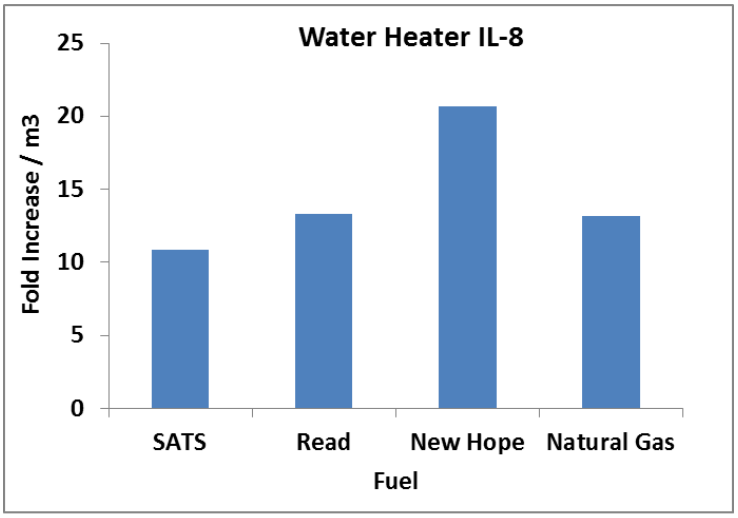

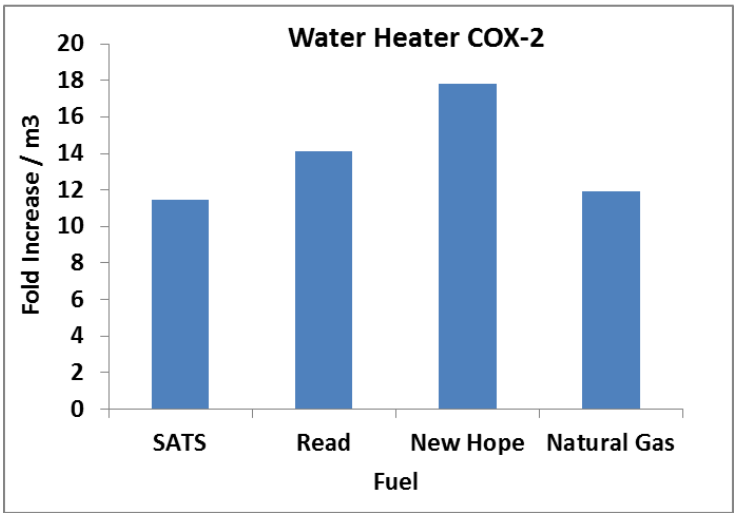

Source: University of California, Davis

DNA Damage Assay Results

Mobile Sources

DNA damage caused by exposure to exhaust from motor vehicles ranged from 640 # $mile^{-1}$ to 923 # $mile^{-1}$. DNA damage was lowest for the tests using natural gas and highest for the tests using biomethane from SATS. The research team did not conduct replicate analysis because of resource limitations, so it is not possible to comment on the statistical significance of the differences in apparent DNA damage induced by these samples.

Figure 30: DNA Damage Emissions per Mile Caused by Exposure to Motor Vehicle Exhaust

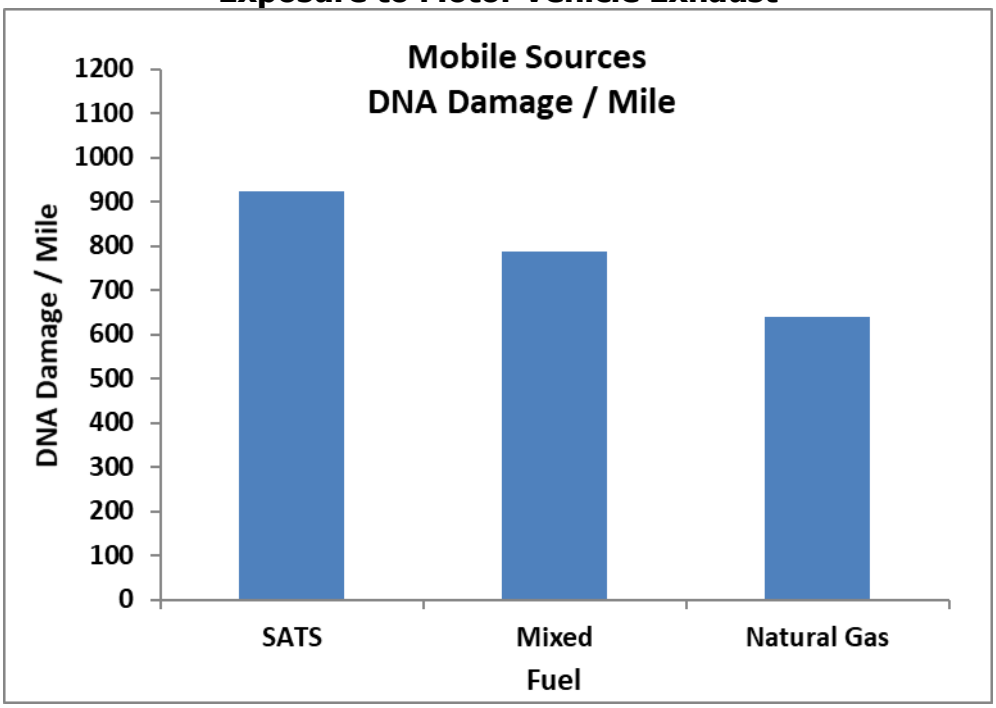

Source: University of California, Davis

Home Appliances

DNA damage caused by exposure to exhaust from the residential water heater ranged from 34 # m^{-3} to 67.1 # m^{-3}. DNA damage was lowest for the biomethane produced at the READ facility, followed by natural gas, followed by biomethane produced at the New Hope and SATS facilities. These results are completely consistent with the trends illustrated in Figure 30, given the mixed fuel composition used in motor vehicle testing was 7% CNG, 24% New Hope biomethane, 34% READ biomethane, and 34% SATS biomethane. Weighting the results shown in Figure 31 with these fractions would produce an estimated DNA damage for a "mixed fuel" equal to 52 # m^{-3}, which falls between the low value for natural gas and the high value for SATS biomethane. Replicate analysis was not conducted due to resource limitations, so it is not possible to comment on the statistical significance of the differences in apparent DNA damage induced by these samples.

Figure 31: DNA Damage Caused by Exposure to Water Heater Exhaust

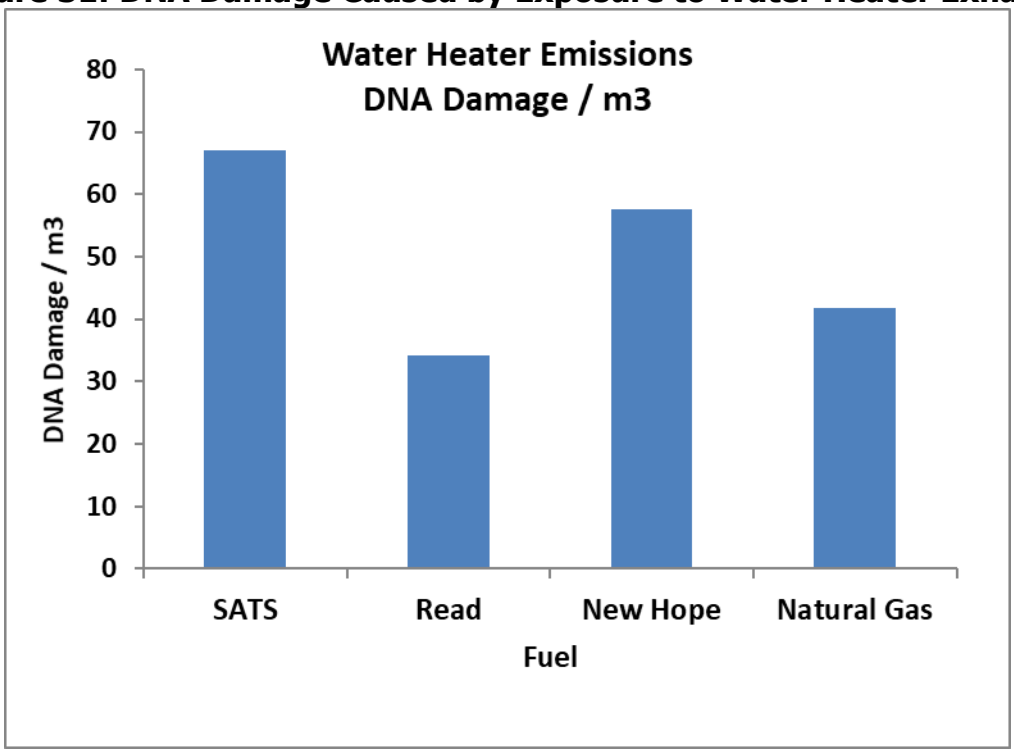

Source: University of California, Davis

DNA damage caused by exposure to exhaust from the cooking stove ranged from 41 # m^{-3} to 88.1 # m^{-3}. Once again, the natural gas tests generally had the lowest measured DNA damage, while the biomethane tests produced the highest DNA damage. The READ biomethane had the highest DNA damage in the stove tests (Figure 32) but the lowest DNA damage in the water heater tests (Figure 31). These results suggest the potential for variability in the results. The research team did not conduct replicate analysis because of resource limitations, so it is not possible to comment on the statistical significance of the differences in apparent DNA damage induced by these samples.

Figure 32: DNA Damage Caused by Exposure to Stove Exhaust

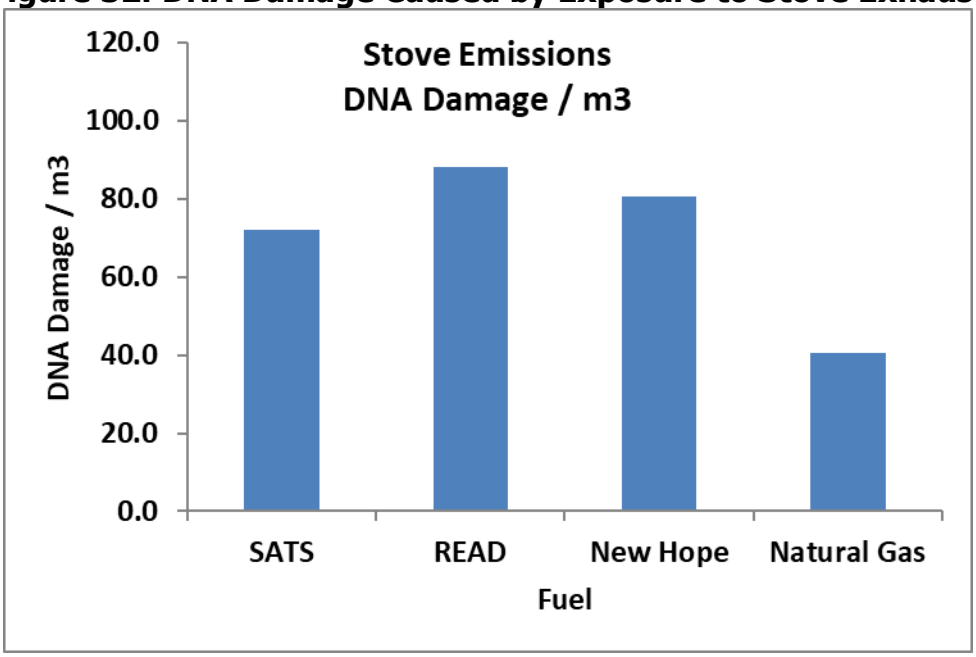

Source: University of California, Davis

The appliance data summarized in Figure 31 and Figure 32 were pooled to enable a statistical comparison between DNA damage caused by exposure to biomethane combustion exhaust vs. DNA damage caused by exposure to CNG combustion exhaust. The null hypothesis was taken to be equal DNA damage for both types of fuel, while the alternative hypothesis was taken to be higher DNA damage for biomethane (one-sided test). P-values for SATS, READ, and New Hope biomethane were 0.03, 0.30, and 0.12, respectively. These values indicate the potential for higher DNA damage caused by exposure to some types of biomethane exhaust compared to CNG exhaust. The sample sizes of 2 data points for this analysis is extremely small and so these results must be considered preliminary.

Ames Assay Results

On-Site Engine-Generators

Mutagenic activity from biogas combustion exhaust was highest from the engine-generator at Kiefer Landfill with readings of 5,600 revertants m^{-3}. Mutagenic activity was also somewhat high in the exhaust from the SATS engine-generator at 206 revertants m^{-3}. These results are consistent with the mRNA expression of CYP1A1 (a marker of PAH exposure), where the Kiefer and SATS combustion exhaust readings were 5,913-fold m^{-3} and 499-fold m^{-3}, respectively. These readings suggest that the landfill biogas may contain compounds that produce mutagenic PAHs when combusted.

Mutagenic activity was under 100 revertants m^{-3} for most of the samples collected in the photochemical reaction chamber at atmospherically relevant dilution rates for daytime conditions. The largest number of mutations were observed in the aged exhaust from the engine-generator at Van Warmerdam dairy, which were roughly twofold higher than other photochemically aged samples. These results suggest that photochemical aging does not strongly enhance the mutagenicity of the biogas combustion exhaust.

Mobile Sources

Mobile source combustion exhaust from SATS biomethane was near 1,000 revertants mile^{-1}, with the next most mutagenic sample found to be petroleum natural gas (CNG) at 600 revertants mile^{-1}. Previous tests of a light-duty CNG-powered vehicle (2007 Honda Civic) under similar conditions measured mutagenic activity at 108 revertants mile^{-1}. The difference in the CNG results may be due to the vehicle engine size (4.8L in the current test vs. 1.8L in the previous test). It is also possible that the previous measurements underestimated the mutagenicity of the CNG exhaust because more than 10 cold-start UC test cycles were required to obtain sufficient mass for the assay, and the large amount of sample gas passing over the filter may have caused some of the trapped particulate matter to evaporate. In comparison, the current study used two cold-start UC test cycles, which greatly reduced the potential losses.

The mutagenicity of mixed biomethane vehicle exhaust was measured as roughly 100 revertants mile^{-1}, which is similar to previous measurements from the Honda Civic. As discussed in Chapter 3, the mixed biomethane contained 7.7% CNG, 24.4% NH biomethane, 33.5% READ biomethane, and 34.4% SATS biomethane. In contrast, the SATS biomethane fuel contained 27.8% CNG and 72.2% SATS biomethane. The correlation between fuels and mutagenicity is difficult to interpret based on fuel mixtures, but these associations will be explored in the statistical analysis presented in Chapters 6 and 7.

Figure 33: Motor Vehicle Mutagenic Activity Measured in the Dark (TA98 With the Addition of S-9 Metabolic Enzymes)

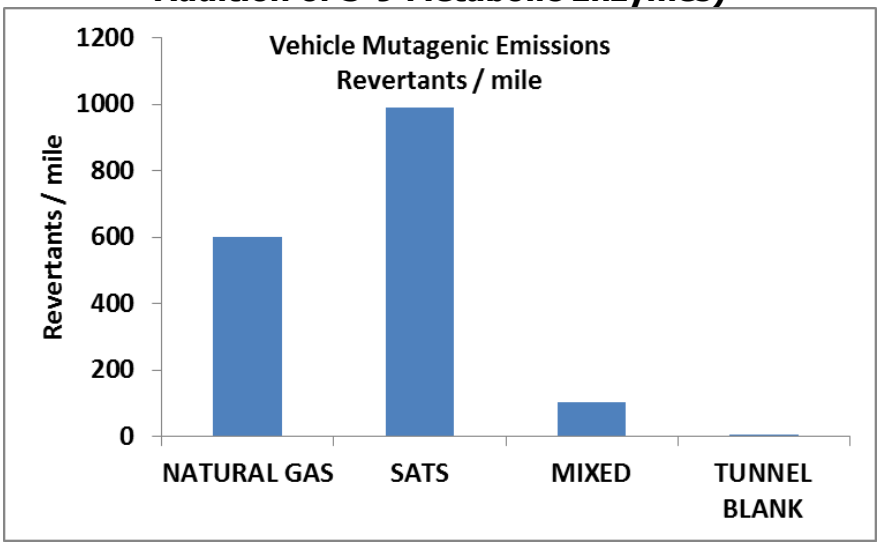

Source: University of California, Davis

Home Appliances

Mutagenic activity was higher in the water heater exhaust powered by READ and New Hope biomethane than petroleum natural gas. Even stronger trends were observed in the first round of the stove tests. Mutagenic activity in the emissions for New Hope biomethane was nearly three times higher than CNG, while READ biomethane was about two times higher than CNG.

Figure 34: Water Heater Mutagenic Activity Concentrations Measured in the Dark (TA98 With the Addition of S-9 Metabolic Enzymes)

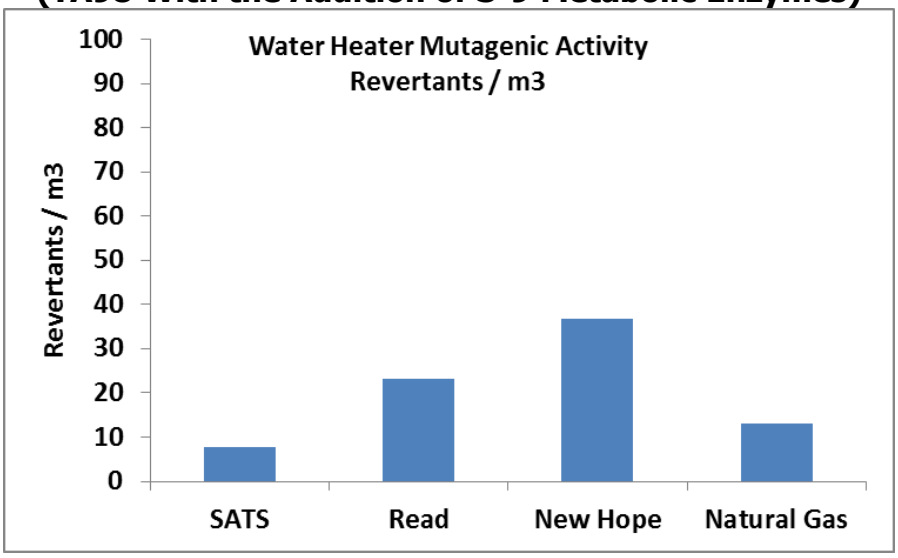

Source: University of California, Davis

Figure 35: Cooking Stove Mutagenic Activity Concentrations Measured Immediately Above the Cooking Surface (TA98 With the Addition of S-9 Metabolic Enzymes)

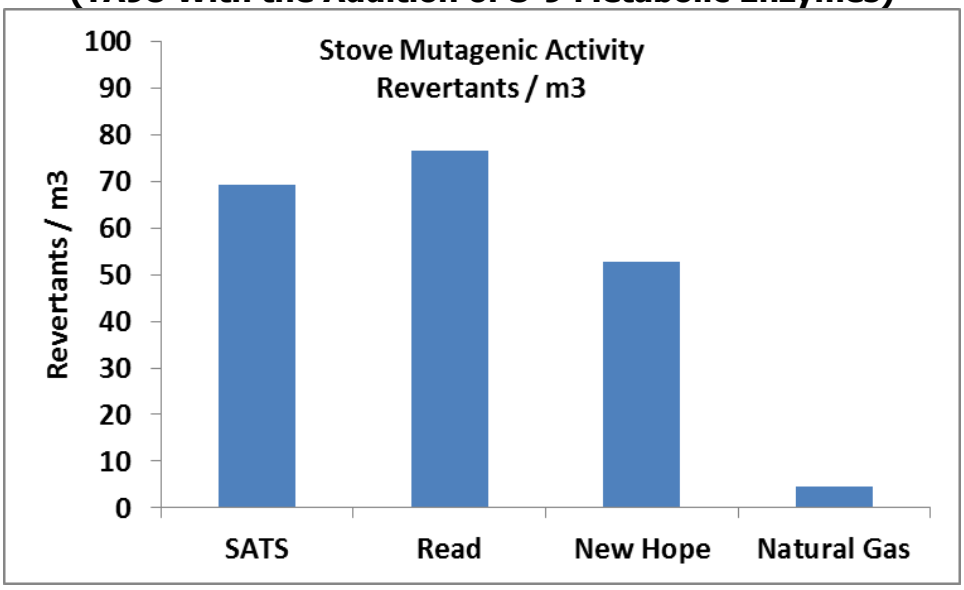

Source: University of California, Davis

These measurements summarized in Figure 34 and Figure 35 strongly suggest that biomethane combustion exhaust from home appliances has higher mutagenic activity than petroleum natural gas combustion exhaust, but these tests were based on single measurements. The research team performed a further round of testing with the cooking stove using three replicates and a blank measurement to better quantify the uncertainty in this analysis. The results summarized in Figure 36 show that the biomethane combustion exhaust results are consistent with the first round of testing (55-72 revertants m^{-3}), but the natural gas combustion exhaust results are considerably higher in the second round of testing (51±5.8

revertants m^{-3}). The original natural gas combustion exhaust measurement of 4.6 revertants m^{-3} is 8 standard deviations away from the mean measured in the second round of testing. The cause for this extreme change in results is not known but a new sample of natural gas fuel was used to supply the second round of testing. It is possible that variability in the composition of the natural gas caused the observed change in mutagenicity.

Figure 36: Replicate Cooking Stove Mutagenic Activity Concentrations Measured Immediately Above the Cooking Surface (TA98 With the Addition of S-9 Metabolic Enzymes)

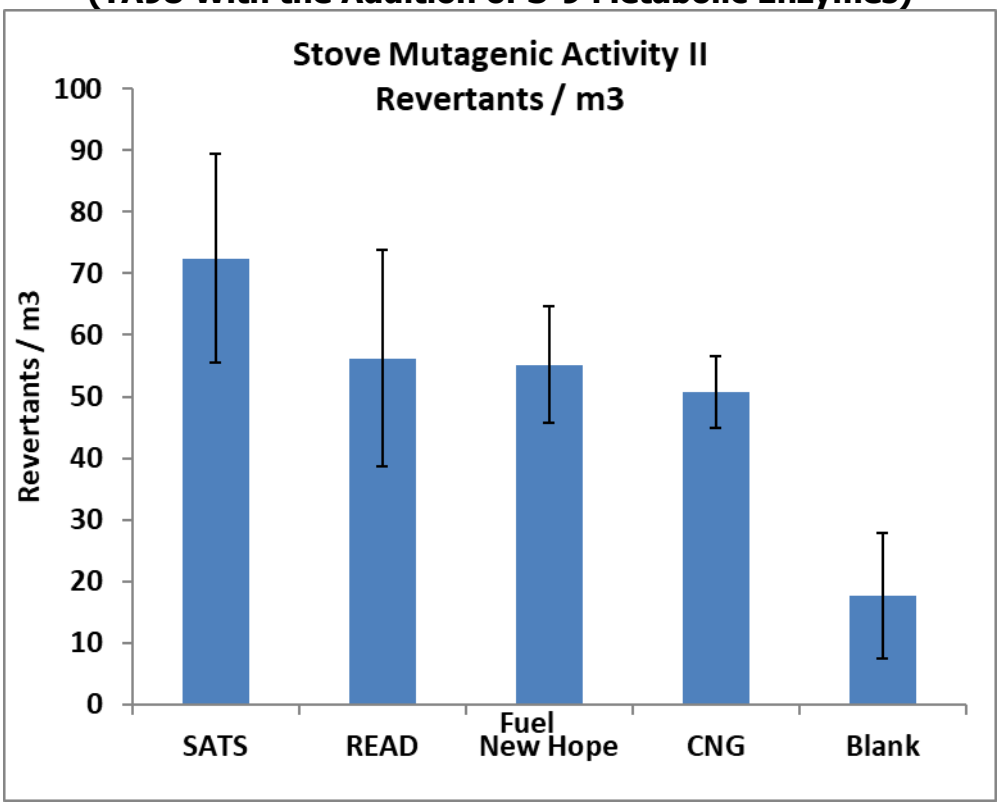

Source: University of California, Davis

Conclusions

All the assays (macrophage ROS, molecular proinflammatory markers, genotoxicity) had detections above background levels and showed variability among the fuels and combustion applications despite the fact that samples were collected at atmospherically relevant (that is, low) concentrations. The assays are sensitive to different mechanisms of injury that may be driven by different chemical and biological agents.

The macrophage reactive oxygen species (ROS) generation results indicate that mobile sources powered by CNG had higher macrophage ROS generation than mobile sources powered by biomethane. Macrophage ROS generation from consumer appliances operating on CNG and biomethane were similar at the 95% confidence level.

Molecular proinflammatory markers were enhanced above background levels across several fuels and combustion applications. The CYP1A1 response was elevated above background levels in all mobile source tests, with comparable results for all fuels (including CNG).

Unburned motor oil or motor oil combustion products present in the vehicle exhaust may be relatively uniform across tests, which could explain the consistency of these results. In other applications, CYP1A1 and IL-8 were higher for READ biomethane than CNG in cooking stove tests. CYP1A1, IL-8, and COX-2 were higher in New Hope biomethane than CNG for water heater tests. CYP1A1 response was elevated in engine-generator tests operating on raw biogas at Kiefer Landfill. The CYP1A1 responses indicate compounds that activate critical cellular receptors for toxic compounds such as PAHs or related compounds.

Increased levels of DNA damage were detected in samples exposed to biomethane combustion exhaust than natural gas combustion exhaust from mobile sources and home appliances. Pooled data from home appliances suggest that these results are statistically significant at the 95% confidence level for the SATS biomethane.

Elevated mutagenicity above background levels was detected in mobile source tests fueled by SATS biomethane. Elevated mutagenicity above background levels was also detected in cooking stove tests fueled by SATS and READ biomethane and water heater tests fueled by New Hope biomethane. Mutagenicity was elevated in engine-generator tests operating on raw biogas at Kiefer Landfill. Repeated tests using the stove produced consistent biomethane results, but these tests also produced elevated CNG mutagenicity above background levels in this study. The cause of the inconsistent stove CNG result is not known at this time.

Photochemical reaction under typical summer conditions did not increase any toxicity measured by the health effects assays considered in this analysis.

Future Work

The results of the bioassays considered in the current study suggest that all petroleum natural gas and biomethane fuels combusted in a mobile source promote inflammatory responses. Future tests should verify that this outcome is driven by the reaction products of the motor oil in these tests, and should consider whether synthetic vs. traditional motor oil has similar properties.

The increased mutagenicity of biomethane combustion products compared to petroleum natural gas combustion products burned in the same device requires further study, especially for sources with high exposure potential, such as cooking stoves. Further tests should be performed to verify this finding, fully identify the chemical or biological agents responsible for the increased mutagenicity, and suggest methods to remove these agents from the biomethane production stream.

CHAPTER 5:
Microorganism Characterization Results

Introduction

Microbial analysis focused on a subset of agents with the highest likelihood to impact health in the indoor or near-indoor environment. Biological agents that were monitored include members of the following categories: bacteria – *Staphylococcus aureus, Mycobacterium tuberculosis,* and *Streptococcus pneumoniae* (all commonly found human pathogens in indoor air); *Propionibacterium acnes* (preferentially aerosolizes from digesters); *Legionella pneumophila* (ubiquitous pathogen of concern), (2) human viruses – Adenoviruses (found in a variety of environments and known to cause disease by inhalation), and (3) fungi.

Methods

Exhaust samples with minimum dilution were collected for microorganism analysis to optimize detection limits in cultivation and molecular analysis. Microorganisms were collected from gas-phase combustion exhaust using 47 mm, 0.4-µm pore-size polycarbonate membrane filters. Depending on sample type, the total sample gas volume ranged from 38–540 liter per filter. Two filters were collected during sampling events. After sample collection, the research team removed the filters from the filter folders using forceps and then separately submerged them in 50-ml Falcon tubes containing 15 ml of sterile phosphate buffered saline (PBS) to prevent filter dehydration. One of the Falcon tubes was placed in a GasPak anaerobic pouch system to minimize inactivation of potential anaerobic bacteria by oxygen contact. Samples were stored at 4º C until analysis. For cultivation and molecular tests, biological material on filters stored in PBS was eluted by vortexing for 5 seconds and manually shaking for 2 minutes. The eluted microorganisms from the two Falcon tubes were pooled (about 30 ml) and placed into aliquots for cultivation and molecular analyses.

Cultivable heterotrophic and spore-forming bacteria were quantified with the most probable number (MPN) test using thioglycolate (TG) and tryptic soybroth (TSB) media, respectively. For spore-forming bacteria enumeration, an aliquot of eluted microorganisms was heated for 15 min at 80º C to inactivate nonspore-forming bacteria before inoculation into TSB. Cultivable fungi were tested by spreading the aliquot of eluted microorganisms on Sabouraud dextrose agar. Samples were incubated under aerobic or anaerobic conditions at 37º C for seven days (cultivable bacteria); for three days at 32º C (spore-forming bacteria); or for three days at 25º C followed by incubation for two days at 37º C (cultivable fungi). Cultivable bacteria were further characterized using DNA sequencing by conducting polymerase chain reaction (PCR) analysis of cultivation positive samples with the universal bacteria assay targeting the 16S rRNA gene (Nadkarni et al., 2002).

For molecular analysis, each aliquot of sample was concentrated by centrifugation at 3,500 revolutions per minute (rpm) for 10 min. Nucleic acids were extracted using the Fast DNA® SPIN KIT for Soil (MP Biomedicals, Irvine, CA) following the manufacturer's protocol. Eight qPCR assays targeting total bacteria (Nadkarni et al., 2002), M. tuberculosis (Chen and Li,

2005), S. pneumoniae (Abdeldaim et al., 2008), S. aureus (Fang and Hedin, 2003), P. acnes (Eishi et al., 2002), L. pneumophila (Yáñez et al., 2005), human adenoviruses (Heim et al., 2003) and total fungi (Zhou et al., 2000) were selected from the literature. The research team carried out reactions for qPCR in analytical duplicate with serial dilutions. The qPCR products amplified with target pathogen assays were recovered from the qPCR plates and sequenced for further confirmation. The authors compared the sequence results with publicly available databases for taxonomic identification.

Biological entities measured in the exhaust samples were converted to the level of target microorganisms found per kg of fuel used for combustion by calculating the fuel-to-combustion exhaust ratios for each test (Table 21). For the vehicle and home appliance tests where CO2 concentrations were measured, biological entities in the exhaust samples were converted to the level of target microorganisms that can be found by burning of per kg fuels, using the equation shown below,

$$ER_{Bio} = \frac{Bio}{\Delta CO_2} f_{carbon} \quad \text{(Eq. 5-1)}$$

where ER_{Bio} is the emission rate of the target microorganism, in microbial unit per kg-fuel; *Bio* is the target microorganism concentration in the exhaust, in microbial unit cm^{-3}; ΔCO_2 represents the background corrected CO_2 concentration, in g-carbon cm^{-3}; f_{carbon} represents the carbon fraction of the fuels, in g-carbon/kg-fuel calculated based on the composition listed in Table 35, respectively.

For the engine-generator tests during where CO_2 concentration was not measured, ER_{Bio} was estimated as,

$$ER_{Bio} = \frac{Bio \times DF \times (R_{air/fuel}+1)}{d_{fuel}} \times 1000 \quad \text{(Eq. 5-2)}$$

where ER_{Bio} is the emission rate of the target microorganism, in microbial unit per kg-fuel; *Bio* is the target microorganism concentration in the exhaust, in microbial unit cm^{-3}; DF is the dilution factor that was determined by the volume ratio of the dilution air and the exhaust that were injected into the chamber, which was 1 in the biological samples because exhaust samples were analyzed without further chamber dilution; $R_{air/fuel}$ is air-to-fuel ratio; d_{fuel} is the density of the fuel at 21° C and 1 atm, in g cm^{-3} calculated based on the composition listed in Table 35.

Results

Vehicle Exhaust

The concentrations of biologicals measured in cultivation tests and molecular analysis are summarized in Table 22 and Table 23, respectively.

No cultivable bacteria and fungi were found in the vehicle exhaust samples. In the molecular analysis, the universal bacteria DNA concentrations were lower than the quantifiable level in all samples. The sample limits of detection (SLODs) of the universal bacteria assay ranged from 2 x 10^3 – 2 x 10^4 gene copies per sample volume collected, which were equivalent to 1 x 10^4 – 2 x 10^5 gene copies m^{-3} of exhaust. Since the universal bacteria assay targets 16S rRNA of total

bacteria, false positives from endogenous contamination of qPCR reagents with *E. coli* and/or another bacterial DNA could hinder the qPCR application. To estimate reliable concentrations, only target gene concentrations that were significantly higher than qPCR negative template controls and nucleic acid extraction negative controls prepared in the laminar flow hoods were reported as quantifiable values in the universal bacteria assay. *Propionibacterium acnes* DNA was estimated to be near the detection limit for one of the mixed biomethane exhausts in the cold start experiment. While fungal DNA was detected in mixed biomethane exhaust in the hot start experiment, the research team did not find cultivable fungi in the same sample.

Home Appliances

Cooking Stove Exhaust

During the first cooking stove test, the research team found cultivable aerobic spore-forming bacteria in the READ exhaust at a level close to the detection limit of the cultivation assay (Table 22). Further taxonomic identification of the bacteria by DNA sequencing was not successful due to the lack of amplification of the 16S rRNA gene. In the second stove test with replicates, the team found aerobic cultivable (spore-forming) bacteria in one of the New Hope exhausts (Table 24). Sequencing results showed that *Micrococcus* and *Bacillus* species are most closely related to the cultivable heterotrophic bacteria and spore-forming bacteria, respectively. Cultivable bacteria were also found in the chamber air blank, and the identity was determined as *Micrococcus* species that are found in soil, dust, water, and air, as well as mammalian skin.

The research team detected *Mycobacterium tuberculosis* DNA in New Hope exhaust by qPCR analysis in the first cooking stove test (Table 23), but at a very low concentration (four gene copies m^{-3}-exhaust). Further DNA sequencing of the qPCR amplicon revealed that the DNA sequence was 100% identical to *Mycobacterium microti* and *Mycobacterium canetti* instead of *M. tuberculosis*. *M. microti* is a pathogen of wild rodents, while *M. tuberculosis* and *M. canetti* can cause human infection. No *M. tuberculosis* DNA was detected in the second stove test (Table 25).

Staphylococcus aureus DNA was found in the SATS and New Hope exhausts in the first stove test (Table 23). *S. aereus* nucleic acid was not detected in any biomethane exhaust, while it was found in one of the CNG exhausts in the second stove test. Given that no cultivable bacteria were found in the corresponding samples, the detected levels might have come from dead cells or extracellular DNA that cannot cause infection.

P. acnes DNA was detected in SATS and New Hope exhausts in the first stove test, while it was below detection limits in all samples in the second test. Preferential aerosolization of *P. acnes* from anaerobic digesters has been reported (Moletta-Denat et al., 2010); hence, the presence of *P. acnes* is not surprising.

Legionella pneumophila DNA was found in New Hope exhaust in the first test and one of the New Hope, READ, and CNG exhaust samples in the second test. Interestingly, the research team detected no target pathogenic bacterial DNA in the upgraded biomethane before combustion. Neither the clean air control collected in the home appliance test chamber nor the

negative control of DNA extraction and qPCR was positive for these pathogens; thus, the origins of these pathogens remain unclear.

DNA representing human adenovirus (HAdV) was frequently detected in the exhaust from the second cooking stove test, but the related concentrations were not significantly different between exhausts from biomethane and CNG. QPCR products targeting the human adenovirus gene (*hexon*) were sequenced for further confirmation. Sequencing results showed that the adenovirus DNA detected in qPCR was most closely related (99%) to HAdV-2, -5 and -6 of the human adenoviruses group C that are more common in the respiratory tract. Given that the target DNA was also detected in one of the chamber blank replicate, measured HAdV values might be considered at background level.

Water Heater Exhaust

During water heater testing, the research team detected universal bacteria DNA in CNG exhaust, but in biomethane exhausts it was below detection limits (Table 23). The human adenovirus target gene was found in SATS exhaust, but the concentration was comparable to that of CNG exhaust. Cultivable (spore-forming) bacteria or fungi were not isolated (Table 22).

Engine/Turbine Generators

In on-site generator tests, the research team found cultivable bacteria and fungi in New Hope, Van Warmerdam, and Kiefer generator exhaust (Table 22). DNA sequencing of cultivable bacteria revealed that viable bacteria detected in the exhausts were most closely related to *Paenibacillus* species or *Bacillus* species or both, relatively ubiquitous bacteria in the environment. Nucleic acids of target pathogens were all below detection limits (Table 23). Since there was no CNG control from on-site generators, a comparison with CNG was not possible.

Table 21: Conversion Factor for Biologicals[a]

Test	Parameter Sources	CO_2 in the exhaust (ppm)	ΔCO_2 (g-carbon/cm^3)	f_{carbon} (g-carbon/kg-fuel)
Vehicle test[b]	SATS	7266	3.416×10^{-6}	679
	Mixed	7513	3.538×10^{-6}	647
	CNG	7185	3.375×10^{-6}	709
Home appliances test	SATS	4150	1.865×10^{-6}	668
	READ	4000	1.791×10^{-6}	644
	New Hope	4000	1.791×10^{-6}	622
	CNG	4130	1.855×10^{-6}	750
		$R_{air/fuel}$	d_{fuel} (g/cm^3)	
Generator test[c]	SATS	7.5	1.12×10^{-3}	
	New Hope	7.5	1.13×10^{-3}	
	Van Warmerdam	29	0.96×10^{-3}	
	Kiefer	29	1.19×10^{-3}	

[a] Conversion factors were estimated to convert the concentrations of microbiota found per m^3 of exhaust into per kg of fuel.

[b] For the vehicle and home appliance tests in which CO_2 was measured, biological entity per m^3 of exhaust was converted to the level of target microorganisms per kg fuel burned using the background corrected CO_2 concentration and the carbon fraction of the fuel.

[c] For the generator test in which CO_2 wasn't measured, the concentration of biologicals found per m^3 of exhaust was converted to that of microbiota per kg-fuel using the air-to-fuel ratio and the density of the fuel at 21° C and 1 atm.

Source: University of California, Davis

Table 22: Microbiota Found in Sources Using Cultivation Analysis Under Aerobic and Anaerobic Conditions

Test	Sample type	Parameter	Aerobic incubation (MPN[h] or CFU[i]/kg-fuel)			Anaerobic incubation (MPN or CFU/kg-fuel)		
		Source	Heterotrophic bacteria	Spore-forming bacteria	Fungi	Heterotrophic bacteria	Spore-forming bacteria	Fungi
Fuel used for exhausting test[a]	Upgraded biomethane	SATS	<SLOD[g]	<SLOD	<SLOD	<SLOD	<SLOD	<SLOD
		READ	<SLOD	<SLOD	<SLOD	<SLOD	<SLOD	<SLOD
		New Hope 1	<SLOD	<SLOD	<SLOD	<SLOD	<SLOD	<SLOD
		New Hope 2	<SLOD	<SLOD	<SLOD	<SLOD	<SLOD	<SLOD
		New Hope 3	<SLOD	<SLOD	<SLOD	<SLOD	<SLOD	<SLOD
	CNG[b]	CNG-Southern 1	<SLOD	<SLOD	<SLOD	<SLOD	<SLOD	<SLOD
		CNG-Southern 2	<SLOD	<SLOD	<SLOD	<SLOD	<SLOD	<SLOD
		CNG-Southern 3	<SLOD	<SLOD	<SLOD	<SLOD	<SLOD	<SLOD
		CNG-Northern	<SLOD	**1.0×10^2**	<SLOD	<SLOD	<SLOD	<SLOD
Vehicle exhaust test	Blank[c]	Tunnel air blank 1	<SLOD	<SLOD	<SLOD	<SLOD	<SLOD	<SLOD
		Tunnel air blank 2	<SLOD	<SLOD	<SLOD	<SLOD	<SLOD	<SLOD
	Cold start exhaust	SATS[e]	<SLOD	<SLOD	<SLOD	<SLOD	<SLOD	<SLOD
		Mixed 1[f]	<SLOD	<SLOD	<SLOD	<SLOD	<SLOD	<SLOD
		Mixed 2	<SLOD	<SLOD	<SLOD	<SLOD	<SLOD	<SLOD
		CNG 1	<SLOD	<SLOD	<SLOD	<SLOD	<SLOD	<SLOD
		CNG 2	<SLOD	<SLOD	<SLOD	<SLOD	<SLOD	<SLOD
	Hot start exhaust	SATS	<SLOD	<SLOD	<SLOD	<SLOD	<SLOD	<SLOD
		Mixed	<SLOD	<SLOD	<SLOD	<SLOD	<SLOD	<SLOD
		CNG	<SLOD	<SLOD	<SLOD	<SLOD	<SLOD	<SLOD
Home appliances exhaust test	Blank[d]	Chamber air blank	<SLOD	<SLOD	<SLOD	<SLOD	<SLOD	<SLOD
	Cooking stove exhaust	SATS	<SLOD	<SLOD	<SLOD	<SLOD	<SLOD	<SLOD
		READ	<SLOD	**1.4×10^4**	<SLOD	<SLOD	<SLOD	<SLOD

Test	Sample type	Parameter	Aerobic incubation (MPN[h] or CFU[i]/kg-fuel)			Anaerobic incubation (MPN or CFU/kg-fuel)		
		Source	Heterotrophic bacteria	Spore-forming bacteria	Fungi	Heterotrophic bacteria	Spore-forming bacteria	Fungi
		New Hope	<SLOD	<SLOD	<SLOD	<SLOD	<SLOD	<SLOD
		CNG	<SLOD	<SLOD	**3.4×10^4**	<SLOD	<SLOD	<SLOD
	Water heater exhaust	SATS	<SLOD	<SLOD	<SLOD	<SLOD	<SLOD	<SLOD
		READ	<SLOD	<SLOD	<SLOD	<SLOD	<SLOD	<SLOD
		New Hope 1	<SLOD	<SLOD	<SLOD	<SLOD	<SLOD	<SLOD
		New Hope 2	<SLOD	<SLOD	<SLOD	<SLOD	<SLOD	<SLOD
		CNG	<SLOD	<SLOD	<SLOD	<SLOD	<SLOD	<SLOD
Generator exhaust test	On-site engine combustion exhaust	SATS	<SLOD	<SLOD	<SLOD	<SLOD	<SLOD	<SLOD
		New Hope	**4.0×10^2**	NA[j]	**2.1×10^2**	<SLOD	NA	<SLOD
		Van Warmerdam	**6.6×10^2**	NA	<SLOD	<SLOD	NA	<SLOD
		Kiefer	<SLOD	**1.8×10^3**	**3.8×10^3**	<SLOD	<SLOD	<SLOD

[a] Biologicals in upgraded biomethane and CNG used for the exhaust tests were analyzed.

[b] CNG samples collected in southern and northern California were used for the vehicle test and the home appliances tests, respectively.

[c] Air in the sampling tunnel was collected as a field blank in the vehicle test.

[d] Pre-cleaned dilution air in the Teflon film sealed chamber was collected as a field blank in the home appliances test.

[e] SATS biomethane in the vehicle test was composed of 27.8% CNG and 72.2% SATS biomethane.

[f] Mixed biomethane in the vehicle test was a mixture of 7.7% CNG, 24.4% New Hope, 33.5% READ and 34.4% SATS biomethane.

[g] SLOD, sample limit of detection

[h] MPN, most probable number

[i] CFU, colony forming unit. Unit for fungi test was CFU/kg-fuel.

[j] NA, not analyzed

Source: University of California, Davis

Table 23: Microbiota Found in Sources Using Molecular Analysis

Test	Sample type	Parameter Source	qPCR (gene copies or genome/kg-fuel)[j]							
			Universal bacteria	***Mycobacterium tuberculosis***	***Streptococcus pneumoniae***	***Staphylococcus aureus***	***Propioni-bacterium acnes***	***Legionella pneumophila***	**Human adenoviruses**	**Fungi**
Fuels used for exhausting tests[a]	Upgraded biomethane	SATS	<SLOD[h]	<SLOD	<SLOD	<SLOD	<SLOD	<SLOD	<SLOD	<SLOD
		READ	<SLOD	<SLOD	<SLOD	<SLOD	<SLOD	<SLOD	<SLOD	<SLOD
		New Hope 1	<SLOD	NA[i]	NA	NA	NA	NA	NA	NA
		New Hope 2	<SLOD	<SLOD	<SLOD	<SLOD	<SLOD	<SLOD	<SLOD	<SLOD
		New Hope 3	<SLOD	NA	NA	NA	NA	NA	NA	NA
	CNG[b]	CNG-Southern 1	<SLOD	NA	NA	NA	NA	NA	NA	NA
		CNG-Southern 2	<SLOD	**1.0 x10^{0}**	<SLOD	<SLOD	<SLOD	<SLOD	<SLOD	<SLOD
		CNG-Southern 3	<SLOD	NA	NA	NA	NA	NA	NA	NA
		CNG-Northern	<SLOD	<SLOD	<SLOD	<SLOD	<SLOD	<SLOD	<SLOD	<SLOD
Vehicle exhaust test	Blank[c]	Tunnel air blank 1	<SLOD	<SLOD	<SLOD	<SLOD	<SLOD	<SLOD	<SLOD	<SLOD
		Tunnel air blank 2	<SLOD	<SLOD	<SLOD	<SLOD	<SLOD	<SLOD	<SLOD	<SLOD
	Cold start exhaust	SATS[f]	<SLOD	<SLOD	<SLOD	<SLOD	<SLOD	<SLOD	<SLOD	<SLOD
		Mixed 1[g]	<SLOD	<SLOD	<SLOD	<SLOD	**2.0 x10^{6}**	<SLOD	<SLOD	<SLOD
		Mixed 2	<SLOD	<SLOD	<SLOD	<SLOD	<SLOD	<SLOD	<SLOD	<SLOD
		CNG 1	<SLOD	<SLOD	<SLOD	<SLOD	<SLOD	<SLOD	<SLOD	<SLOD
		CNG 2	<SLOD	<SLOD	<SLOD	<SLOD	<SLOD	<SLOD	<SLOD	<SLOD
		SATS	<SLOD	<SLOD	<SLOD	<SLOD	<SLOD	<SLOD	<SLOD	<SLOD

Test	Sample type	Parameter Source	qPCR (gene copies or genome/kg-fuel)[j]							
			Universal bacteria	***Mycobacterium tuberculosis***	***Streptococcus pneumoniae***	***Staphylococcus aureus***	***Propioni-bacterium acnes***	***Legionella pneumophila***	**Human adenoviruses**	**Fungi**
	Hot start exhaust	Mixed	<SLOD	<SLOD	<SLOD	<SLOD	<SLOD	<SLOD	<SLOD	**2.0×10^5**
		CNG	<SLOD	<SLOD	<SLOD	<SLOD	<SLOD	<SLOD	<SLOD	<SLOD
	Biomethane from truck[d]	SATS	<SLOD	<SLOD	<SLOD	<SLOD	<SLOD	<SLOD	<SLOD	<SLOD
Home appliances exhaust test	Blank[e]	Chamber air blank	<SLOD	<SLOD	<SLOD	<SLOD	<SLOD	<SLOD	<SLOD	<SLOD
	Cooking stove exhaust	SATS	<SLOD	<SLOD	<SLOD	**7.1×10^4**	**1.0×10^7**	<SLOD	<SLOD	<SLOD
		READ	<SLOD	<SLOD	<SLOD	<SLOD	<SLOD	<SLOD	<SLOD	<SLOD
		New Hope	<SLOD	**1.4×10^3**	<SLOD	**8.0×10^5**	**7.6×10^6**	**2.3×10^6**	<SLOD	<SLOD
		CNG	<SLOD	<SLOD	<SLOD	<SLOD	<SLOD	<SLOD	<SLOD	<SLOD
	Water heater exhaust	SATS	<SLOD	<SLOD	<SLOD	<SLOD	**4.5×10^5**	<SLOD	**3.8×10^6**	<SLOD
		READ	<SLOD	<SLOD	<SLOD	<SLOD	<SLOD	<SLOD	<SLOD	<SLOD
		NH-1	<SLOD	<SLOD	<SLOD	<SLOD	<SLOD	<SLOD	<SLOD	<SLOD
		NH-2	<SLOD	<SLOD	<SLOD	<SLOD	<SLOD	<SLOD	<SLOD	<SLOD
		CNG	**2.8×10^7**	<SLOD	<SLOD	<SLOD	<SLOD	<SLOD	**2.9×10^6**	<SLOD
Generator exhaust test	On-site engine combustion exhaust	SATS	<SLOD	<SLOD	<SLOD	<SLOD	<SLOD	<SLOD	<SLOD	<SLOD
		NH	<SLOD	<SLOD	<SLOD	<SLOD	<SLOD	<SLOD	<SLOD	<SLOD
		VW	<SLOD	<SLOD	<SLOD	<SLOD	<SLOD	<SLOD	<SLOD	<SLOD
		Kiefer	<SLOD	<SLOD	<SLOD	<SLOD	<SLOD	<SLOD	<SLOD	<SLOD

[a] Biologicals in upgraded biomethane and CNG used for the exhaust tests were analyzed.

[b] CNG collected in southern and northern California were used for the vehicle test and the home appliances tests, respectively.

[c] Air in the sampling tunnel was collected as a field blank in the vehicle test.

[d] Remaining SATS biomethane in the truck tank after the vehicle tests was recovered and analyzed by qPCR.

[e] Pre-cleaned dilution air in the Teflon film sealed chamber was collected as a field blank in the home appliances test.

[f] SATS biomethane in the vehicle test was composed of 27.8% CNG and 72.2% SATS biomethane.

[g] Mixed biomethane in the vehicle test was a mixture of 7.7% CNG, 24.4% New Hope, 33.5% READ and 34.4% SATS biomethane.

[h] SLOD, sample limit of detection

[i] NA, not analyzed

[j] Unit for human adenoviruses assay was genome/kg-fuel

Source: University of California, Davis

Table 24: Microbiota Found in the Second Cooking Stove Experiment Using Cultivation Analysis Under Aerobic and Anaerobic Conditions

Test	Sample type	Parameter	Aerobic incubation (MPN[c] or CFU[d]/kg-fuel)			Anaerobic incubation (MPN or CFU/kg-fuel)		
		Source	Heterotrophic bacteria	Spore-forming bacteria	Fungi	Heterotrophic bacteria	Spore-forming bacteria	Fungi
Home appliances exhaust test	Blank[a]	Chamber air blank 1	**2.3×10^1**	<SLOD[b]	<SLOD	<SLOD	<SLOD	<SLOD
		Chamber air blank 2	<SLOD	<SLOD	<SLOD	<SLOD	<SLOD	<SLOD
	Cooking stove exhaust	SATS 1	<SLOD	<SLOD	<SLOD	<SLOD	<SLOD	<SLOD
		SATS 2	<SLOD	<SLOD	<SLOD	<SLOD	<SLOD	<SLOD
		SATS 3	<SLOD	<SLOD	<SLOD	<SLOD	<SLOD	<SLOD
		READ 1	<SLOD	<SLOD	<SLOD	<SLOD	<SLOD	<SLOD
		READ 2	<SLOD	<SLOD	<SLOD	<SLOD	<SLOD	<SLOD
		READ 3	<SLOD	<SLOD	<SLOD	<SLOD	<SLOD	<SLOD
		New Hope 1	<SLOD	<SLOD	<SLOD	<SLOD	<SLOD	<SLOD
		New Hope 2	**9.6×10^3**	**9.6×10^3**	<SLOD	<SLOD	<SLOD	<SLOD
		CNG 1	<SLOD	<SLOD	<SLOD	<SLOD	<SLOD	<SLOD
		CNG 2	<SLOD	<SLOD	<SLOD	<SLOD	<SLOD	<SLOD
		CNG 3	<SLOD	<SLOD	<SLOD	<SLOD	<SLOD	<SLOD

[a] Precleaned dilution air in the Teflon film sealed chamber was collected as a field blank in the home appliances test.

[b] SLOD, sample limit of detection

[c] MPN, most probable number

[c] CFU, colony forming unit. Unit for fungi test was CFU/kg-fuel.

Source: University of California, Davis

Table 25: Microbiota Found in the Second Cooking Stove Testing Using Molecular Analysis

Test	Sample type	Parameter	qPCR (gene copies or genome/kg-fuel)[c]							
		Source	Universal bacteria	*Mycobacterium tuberculosis*	*Streptococcus pneumoniae*	*Staphylococcus aureus*	*Propioni-bacterium acnes*	*Legionella pneumophila*	Human adenoviruses	Fungi
Home appliances exhaust test	Blank[a]	Chamber air blank 1	<SLOD[b]	<SLOD	<SLOD	<SLOD	<SLOD	<SLOD	<SLOD	<SLOD
		Chamber air blank 2	<SLOD	<SLOD	<SLOD	<SLOD	<SLOD	<SLOD	**3.7 x10^{3}**	<SLOD
	Cooking stove exhaust	SATS 1	<SLOD	<SLOD	<SLOD	<SLOD	<SLOD	<SLOD	**1.8 x10^{6}**	<SLOD
		SATS 2	<SLOD	<SLOD	<SLOD	<SLOD	<SLOD	<SLOD	**1.2 x10^{6}**	<SLOD
		SATS 3	<SLOD	<SLOD	<SLOD	<SLOD	<SLOD	<SLOD	<SLOD	<SLOD
		READ 1	<SLOD	<SLOD	<SLOD	<SLOD	<SLOD	<SLOD	<SLOD	<SLOD
		READ 2	<SLOD	<SLOD	<SLOD	<SLOD	<SLOD	<SLOD	**6.4 x10^{5}**	<SLOD
		READ 3	<SLOD	<SLOD	<SLOD	<SLOD	<SLOD	**1.4 x10^{6}**	**1.3 x10^{6}**	<SLOD
		New Hope 1	<SLOD	<SLOD	<SLOD	<SLOD	<SLOD	<SLOD	<SLOD	<SLOD
		New Hope 2	<SLOD	<SLOD	<SLOD	<SLOD	<SLOD	**6.8 x10^{5}**	**3.2 x10^{6}**	<SLOD
		CNG 1	<SLOD	<SLOD	<SLOD	<SLOD	<SLOD	<SLOD	<SLOD	<SLOD
		CNG 2	<SLOD	<SLOD	<SLOD	**2.4 x10^{5}**	<SLOD	<SLOD	**8.2 x10^{5}**	<SLOD
		CNG 3	<SLOD	<SLOD	<SLOD	<SLOD	<SLOD	**1.3 x10^{6}**	**2.2 x10^{6}**	<SLOD

[a] Precleaned dilution air in the Teflon film sealed chamber was collected as a field blank in the home appliances test.

[b] SLOD, sample limit of detection

[c] Unit for human adenoviruses assay was genome/kg-fuel

Source: University of California, Davis

Conclusions

The research team characterized microbiota using cultivation methods and molecular analyses in the combustion exhaust from a motor vehicle, home appliances including cooking stove/water heater, and on-site turbine/engine generators.

No significant differences were found between the DNA concentrations in vehicle combustion exhaust using either biomethane or CNG. These results suggest that there is no additional microbial risk associated with the use of biomethane as an alternative fuel source in motor vehicles.

The research team measured target pathogenic bacterial DNA in the biomethane exhausts in the cooking stove test. Given that these organisms were not cultivable, the bacterial DNA may have originated from dead cells or represented extracellular DNA. Human adenovirus DNA concentrations of biomethane and CNG exhausts were similar and comparable to background levels. The team found no target pathogenic bacterial DNA or cultivable microorganisms in biomethane exhausts in the water heater test. The results indicate that the likelihood of increased microbial emissions in the indoor environment by using biomethane in home appliances compared to the use of natural gas is low.

The authors detected no target pathogens in the on-site engine-generator exhaust tests. Based on the cultivation and molecular analysis results, the microbial risks of target pathogens from on-site engine/turbine generator usage appear low.

Future Work

In this study, the research team evaluated various pathogens of concern to estimate biological characteristics in the sources related to human health risk. The application of high-throughput sequencing technologies such as amplicon sequencing would provide insight into the microbial communities of biomethane and corresponding exhaust samples and enable further identification of other potential pathogenic species.

CHAPTER 6:
Target Chemical Analysis Results

Introduction

Constituents of potential human health concern in the emissions from biomethane combustion are expected to include both compounds quantified by established analytical methods (target compounds) and those not captured by those methods (nontarget compounds). The concentrations of target compounds can be quantified against reference standards of known concentration, and this chapter describes the results of these analyses. Nontarget compounds can be estimated (at least initially) only by chromatographic peak area, and these results are discussed in the next chapter. The research team conducted target compound measurements for the combustion exhaust tests as an extra effort (beyond the contract scope of work), in part because the tests provided a useful comparison with results already reported for raw biogas and upgraded biomethane under CARB Project #13-418. Target compounds quantified in this study included alkanes, polycyclic aromatic hydrocarbons and other semivolatile organic compounds, halocarbons and other volatile organic compounds, aldehydes and ketones, organic sulfur compounds, organic silicon compounds, polychlorinated biphenyls, pesticides, mercury, and metals. The results of these tests are summarized in the following sections.

Methods

Volatile Organic Compound Analysis

The research team collected gas samples for the measurement of volatile organic compounds, including halocarbons, hydrocarbons, and organic sulfur species, in Tedlar sample bags (SKC Inc.) using system pressure or a "Vac-U-Chamber" (SKC Inc.) sampling apparatus, to avoid sampling pump contamination of the sample. The authors flushed the Tedlar bags three times before use, and they were not reused.

The team analyzed volatile sulfur species are using a modified version of ASTM D6228. The authors analyzed volatile organic compounds (VOCs) and volatile halocarbons using a modified version of US EPA method TO-15 (USEPA, 1999b). Custom TO-15 and volatile sulfur gas standard mixtures (Air Liquide) were used to quantify these compounds. The team optimized these methods for its sampling techniques, analytical equipment, and target compounds.

The volatile organic compound analytical method used an Agilent 6890/5973N GC-MS system fitted with a Markes "Unity 2" gas sampling/thermal desorption system. The research team performed periodic multipoint calibrations to confirm instrument linearity. Prior to analysis, the authors analyzed a system blank to evaluate the cleanliness of the system. A one-point calibration was then performed using the calibration standard mixture(s) to confirm consistency in instrument response. A sulfur-specific trap material (Markes U-T6SUL-2S), which is also effective for nonsulfur-containing compounds, was used to collect the analytes. The trap was maintained at 25° C during a 2.0 min sampling time with a sample flow rate of 50 mL min^{-1}. Analytes were desorbed at 300° C held for 3.0 min. The transfer line temperature

was maintained at 140° C. The research team operated the GC is in constant pressure mode (32 bar) with helium (He) carrier gas. Separation was achieved using an Agilent J&W DB-VRX column (60 m x 0.25 mm x 1.40 µm). The temperature program was as follows: hold at 45 °C for 3 min, ramp from 45 °C to 190 °C at 10 °C min^{-1}, ramp from 190 °C to 250 °C at 20 °C min^{-1}, hold for 8 min.

Aldehyde and Ketone Analysis

The research team determined carbonyl compound concentrations in gas samples using a modified version of EPA method TO-11 (USEPA, 1999a). The team optimized the method for its analytical equipment and target compounds. The team drew biogas or biomethane samples through a pair of 8 x 115 mm 2,4-dinitrophenyl hydrazine (DNPH)-treated silica gel sorbent tubes (SKC, Inc.) for 58 to 225 min at a flow rate of 1 L min^{-1}. Sorbent tubes were not unsealed until just before sampling, and the flow rate was controlled with a calibrated 1-5 L min^{-1} adjustable flow meter (Dwyer Instruments, Inc.). Negative pressure was created at the back end of the sampling apparatus through the use of an explosion-proof Teflon diaphragm pump. At the conclusion of the specified sampling period, the research team immediately capped, labeled, and placed the sorbent tube into a cooler. Once transported back to the lab, the sorbent tube was stored in a 0°C freezer prior to extraction. Sorbent tubes may be held at 0°C for up to 30 days before being extracted. To extract the sorbent material, tubes were broken open, and each section of sorbent material was transferred to a labeled glass vial. One ml acetonitrile was added to each vial, which was then capped and allowed to sit for 30 minutes. The supernatant liquid was transferred to a labeled amber glass autosampler vial.

The research team analyzed the samples on an Agilent 1200 liquid chromatograph coupled with an Agilent 6530 quadrupole time-of-flight mass spectrometer (LC-qTOF-MS). Separation was accomplished using a Restek Ultra C_{18} Column (5 µm, 250 x 4.6 mm). The injection volume was 10 µl and the LC gradient wa: 40% A (deionized H_2O with 1 mM CH_3COONH_4) and 60% B (ACN/H_2O, 95/5 v/v with 1 mM CH_3COONH_4) for 7 minutes, followed by a linear increase to 100% B at 20 min, hold at 100% B for 0.5 min. Each sample run included a system blank, two sample blanks (1 set of sorbent tube extracts), calibration standards, and the samples. The authors used a multipoint calibration curve generated from the calibration standards (Sigma 47285-U TO-11 Standard Mix) to quantify the target compounds.

Semivolatile Organic Compound Analysis

The research team determined semivolatile organic compound (SVOC) concentrations in gas samples using a modified version of EPA method 8270D, "semivolatile organic compounds by gas chromatography/mass spectrometry (GC/MS)." The team enhanced the method for its analytical equipment and target compounds. Compounds quantified using this method included extended hydrocarbons, polycyclic aromatic hydrocarbons (PAHs), organic silicon compounds, semivolatile organic sulfur compounds, pesticides, and polychlorinated biphenyls (PCBs).

The research team drew the samples through an 8 x 110 mm 400 mg/200 mg XAD-2 sorbent tube (SKC, Inc.) for 58 to 225 minutes at a flow rate of 1 L min^{-1}. The authors unsealed the sorbent tubes immediately before sampling and controlled the flow rate with a calibrated 1-5 L min^{-1} adjustable flow meter (Dwyer Instruments, Inc.). Negative pressure was created at the

back end of the sampling apparatus using an explosion-proof Teflon diaphragm pump. At the conclusion of the sampling period, the sorbent tube was immediately capped, labeled, and placed into a cooler. Once transported back to the lab, it was stored in a 0°C freezer until extraction. Sorbent tubes may be held at 0°C for up to 30 days before being extracted. The research team extracted the sorbent tubes by breaking open each section and separately transferring the sorbent material to labeled glass vials. The team added ethyl acetate (1 ml) is to each vial, which was then capped and sonicated for 30 minutes. The supernatant liquid was transferred to a labeled amber glass autosampler vial.

The authors carried out the analysis is on an Agilent 6890 gas chromatograph coupled with an Agilent 5973 mass spectrometer (GC-MS). Each sample run included a system blank, two sample blanks (one set of sorbent tube extracts), calibration standards, and the samples. The team used a multipoint calibration curve generated from the calibration standards (Restek 31850 8270 Megamix) to quantify the target compounds. Separation was accomplished using an Agilent J&W HP5-MS UI column (30 m x 0.25 mm x 0.25 µm) with an injection volume of 1.0 µl and a flow rate of 0.8 mL min^{-1} in helium. The injector temperature was 250°C, and the temperature program was 35°C for 3 min, ramp to 325°C at 4°C min^{-1}, hold at 325°C for 3 minutes.

Analytical standards used to quantify extended hydrocarbons were Sigma 8S61394-U TPH Mix 3, Sigma 29680-10ML cyclopentane, Sigma 66490-10ML methylcyclopentane, Sigma 442630 isopropylbenzene, Sigma E49401-5G 2-ethyltoluene, Sigma 47324 1,2,4-trimethylbenzene, Sigma 442430 1-methylnaphthalene, and Sigma 36943-250MG 1,2-dimethylnaphthalene. The research team quantified organic silicon concentrations using the following external standards: 1,1,3,3-tetramethyldisiloxane (Sigma 235733-25G), pentamethyldisiloxane (Sigma 76840-5ML), hexamethyldisilane (Sigma 217069-5G), hexamethyldisiloxane (Sigma 205389-5ML), octamethyltrisiloxane (Sigma 235709-5ML), octamethylcyclotetrasiloxane (Sigma 43883-100MG), decamethyltetrasiloxane (Sigma 235679-25G), decamethylcyclopentasiloxane (Sigma 43217-250MG), dodecamethylpentasiloxane (Sigma 447269-10ML), and dodecamethylcyclohexasiloxane (Sigma 43216-25MG). The team also quantified pesticide concentrations using a pesticide standard mix (Sigma CRM46845 EPA 8081) and quantified PCBs using a PCB standard mix (Supelco 47330-U PCB Congener Mix 1).

Metals and Mercury Analysis

Metals (including mercury) were determined via EPA Method 29 (modified) "Determination of Metals Emissions from Stationary Sources." Briefly, gas samples flowed through aqueous acid impingers followed by analysis using ICP-MS, inductively coupled plasma mass spectrometry.

During the spring of 2016, continuing through the summer, the research team analyzed about 20 samples for a related project for mercury (Hg) by two methods: the traditional gold-coated trap method and the metals impinger series used for all elements. Results, including detection limit performance, were comparable. Confidence in the ability to exclude incidental signal from outside the sampled gas flow was more reliable with the impinger series. For those two reasons, the team reported results from the ICP-MS method.

Results

Target Chemical Compounds in Vehicle Exhaust

Table 26 summarizes the concentrations of target compounds that were detected at levels above the limit of quantification and above levels in the relevant blank samples. "Cold start" and "hot start" refer to measurements from freshly diluted tailpipe exhaust from the CVS dilution tunnel. Table 27 reports concentrations of these constituents following "dark" or "light" aging of the exhaust in the photochemical chamber. Background measurements from blank tests are also reported in these tables. A large number of target compounds were below detection limits in all experiments; these are not discussed further here.

Table 27 summarizes concentrations for carbonyls and hydrocarbons under dark aging and light aging conditions in the photochemical reaction chamber. Carbonyl emissions are relatively low compared to hydrocarbon emissions, but carbonyl concentrations in the light-aged tests are generally higher than carbonyl concentrations in the dark-aged tests. The research team expected this outcome since carbonyls are produced by the photochemically induced oxidation reactions occurring in the reaction chamber. The hydrocarbon concentrations in the light-aged were generally lower than concentrations in the dark-aged tests, indicating that photochemical reactions partially consumed these compounds during the three-hour aging time.

ND in Table 26 and Table 27 indicates that the compound was not detected, while <LOQ means the compound was detected at low concentrations but could not be quantified reliably above the background levels.

Blank levels shown in Table 26, Table 27, and Figure 37 were measured using the dilution air in the CVS, but no vehicle exhaust in the sampling system.

Table 26: Chemical Concentrations in Different Freshly Diluted Vehicle Exhaust From Tunnel (Ppb)

Chemical compound	LOQ (ppb)	Cold start			Hot start			Blank
		CNG	SATS	MIX	CNG	SATS	MIX	Blank
Formaldehyde	0.25	0.77	NM	2.15	0.33	NM	NM	0.53
Acetaldehyde	0.10	0.40	NM	0.29	0.24	NM	NM	0.30
Acetone	0.25	8.37	NM	2.22	1.12	NM	NM	2.43
m,p-Xylene	5.00	ND	ND	ND	ND	ND	ND	ND
n-Hexane	5.00	ND	ND	ND	ND	ND	ND	ND
Octane	5.00	ND	<LOQ	ND	ND	<LOQ	ND	ND
Phenol	5.00	ND	ND	ND	ND	ND	ND	<LOQ

NM = not measured, ND = not detected, LOQ = limit of quantification

Source: University of California, Davis

Table 27: Chemical Concentrations in Different Chamber-Aged Vehicle Exhaust (Ppb)

Chemical compound	LOQ (ppb)	Dark-aged			Light-aged			Blank
		CNG	SATS	MIX	CNG	SATS	MIX	
Formaldehyde	0.25	<LOQ	<LOQ	0.36	1.11	1.03	1.36	<LOQ
Acetaldehyde	0.10	0.13	<LOQ	0.15	0.27	0.73	0.55	<LOQ
Acetone	0.25	1.32	0.59	0.82	1.23	0.80	1.40	1.37
m,p-Xylene	5.00	14.70	15.16	26.84	<LOQ	ND	6.77	10.96
n-Hexane	5.00	53.57	51.14	67.08	20.54	29.75	46.69	35.22
Octane	5.00	8.70	13.51	51.82	<LOQ	6.62	39.60	5.76
Phenol	5.00	5.06	ND	ND	ND	ND	ND	ND

Note that m-xylene and n-hexane were added to the chamber as VOC-surrogate.

NM = not measured, ND = not detected, LOQ = limit of quantification

Source: University of California, Davis

Figure 37: Chemical Concentrations in Different Chamber-Aged Vehicle Exhaust (Ppb)

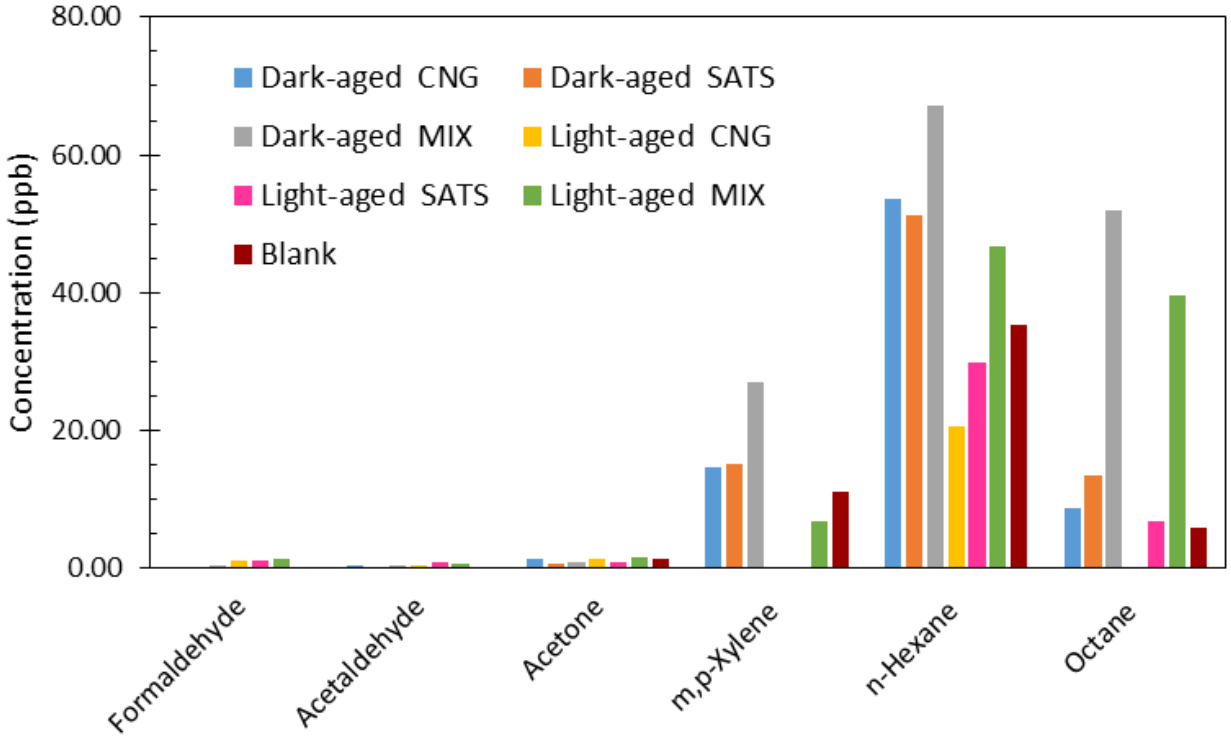

Note that m-xylene and n-hexane were added to the chamber as VOC-surrogate.

Source: University of California, Davis

Target Chemical Compounds in Home Appliances Exhaust

Table 28 summarizes carbonyl and hydrocarbon concentrations from cooking stove tests using different methane sources. The effect of aging on the exhaust composition over time can be visualized by comparing Figure 38, which summarizes constituent concentrations immediately post cooking stove combustion, with Figure 39, which summarizes the concentrations in water heater exhaust after aging under dark or light conditions.

Table 28: Chemical Concentrations in Different Cooking Stove Exhaust (Ppb)

Chemical compounds	LOQ	CNG	SATS	READ	New Hope
Formaldehyde	0.25	0.96	1.08	2.26	1.63
Acetaldehyde	0.10	0.13	0.12	0.21	0.15
Acetone	0.25	3.01	1.03	0.90	1.55
m,p-Xylene	5.00	ND	ND	ND	ND
n-Hexane	5.00	ND	ND	ND	ND
Octane	5.00	20.44	20.12	13.41	21.44
Phenol	5.00	5.39	ND	ND	ND

NM = not measured, ND = not detected, LOQ = limit of quantification

Source: University of California, Davis

Figure 38: Chemical Concentrations in Different Freshly Emitted Cooking Stove Exhaust Measured in the Dark (Ppb)

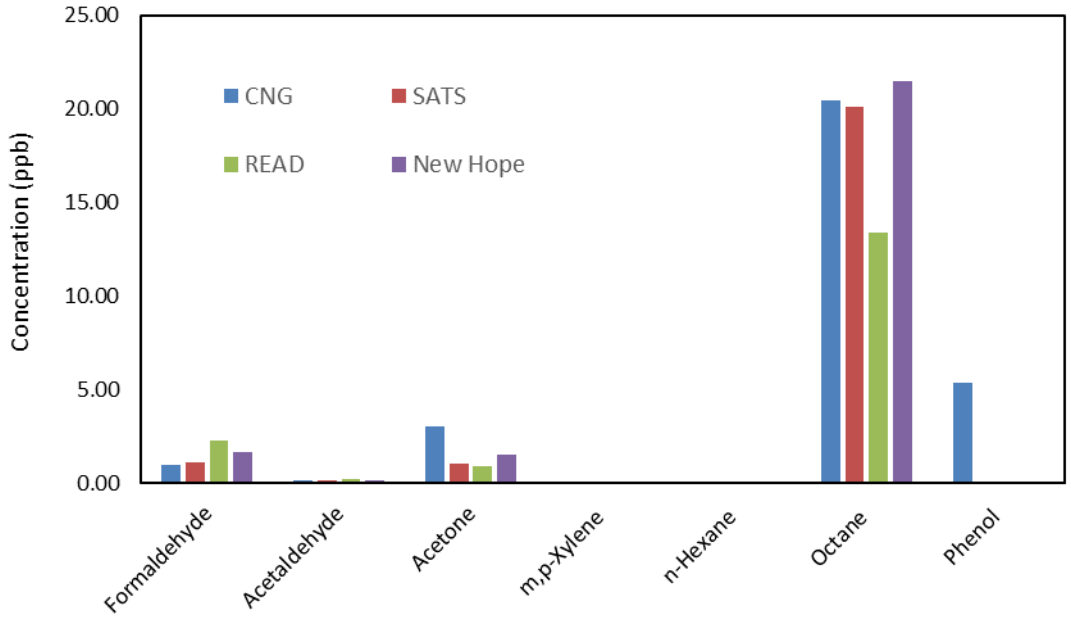

Source: University of California, Davis

Figure 39: Chemical Concentrations in Different Diluted (850:1) Chamber-Aged Water Heater Exhaust (Ppb)

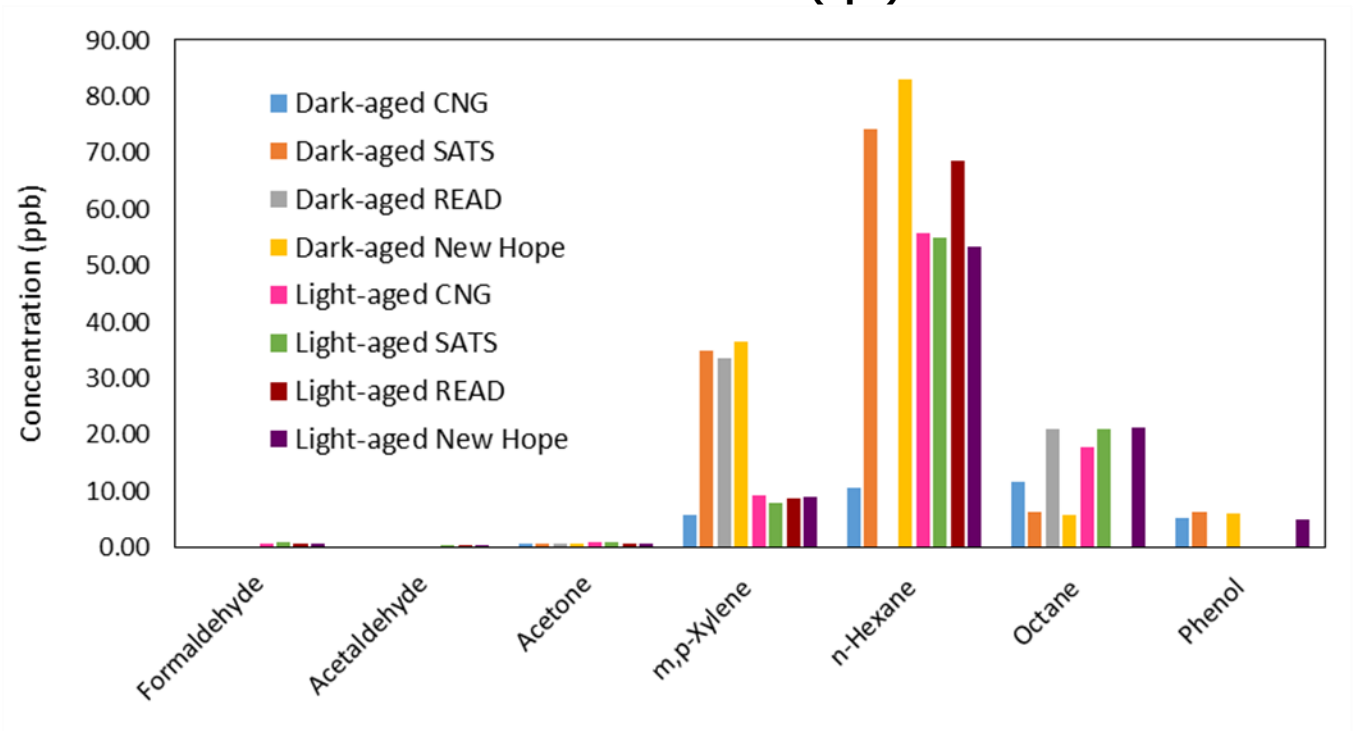

Source: University of California, Davis

Table 29: Chemical Concentrations in Different Water Heater Exhaust (Ppb)

Chemical compounds	LOQ	CNG	SATS	READ	New Hope
Water heater exhaust dark aged 25:1 diluted					
Formaldehyde	0.25	<LOQ	<LOQ	<LOQ	<LOQ
Acetaldehyde	0.10	<LOQ	<LOQ	<LOQ	<LOQ
Acetone	0.25	0.69	0.79	0.90	0.59
m,p-Xylene	5.00	ND	ND	ND	ND
n-Hexane	5.00	<LOQ	ND	ND	ND
Octane	5.00	12.18	8.57	53.80	ND
Phenol	5.00	5.70	7.34	ND	5.38
Water heater exhaust dark aged 850:1 diluted					
Formaldehyde	0.25	<LOQ	<LOQ	<LOQ	<LOQ
Acetaldehyde	0.10	<LOQ	<LOQ	<LOQ	<LOQ
Acetone	0.25	0.81	0.72	0.78	0.60
m,p-Xylene	5.00	5.70	34.97	33.47	36.47
n-Hexane	5.00	10.75	74.26	ND	83.03
Octane	5.00	11.73	6.45	20.95	5.85
Phenol	5.00	5.20	6.35	ND	6.12
Water heater exhaust light aged 850:1 diluted					
Formaldehyde	0.25	0.75	0.94	0.79	0.81
Acetaldehyde	0.10	0.32	0.51	0.37	0.39
Acetone	0.25	0.89	0.89	0.83	0.68
m,p-Xylene	5.00	9.25	7.85	8.83	9.02
n-Hexane	5.00	55.78	54.93	68.57	53.48
Octane	5.00	17.93	21.17	ND	21.43
Phenol	5.00	ND	ND	ND	5.03

ND = not detected, LOQ = limit of quantification

Source: University of California, Davis

As noted, the initial round of tests with cooking stove exhaust showed that the three biomethane samples had higher mutagenic activity than the CNG sample. These tests were repeated in triplicate with accompanying chemical analysis. Table 30 provides the results for the aldehyde and ketone concentrations in these replicate tests. These concentrations are generally higher than those in the original tests, especially for acetone, but the pattern of these results does not explain the higher mutagenicity in the CNG replicates than in the original test, while the mutagenicity of biomethane samples remained similar to the original test. Other volatile and semivolatile compound concentrations in the replicate tests were not significantly higher than the respective blank test concentrations or below limits of quantification. Overall, there was nothing in the **target** organic chemical concentration results that can explain the apparent increase in the mutagenic activity of the CNG samples during the replicate testing. Nontarget results are discussed in Chapter 7.

Table 30: Chemical Concentrations in Replicate Cooking Stove Exhaust Tests (Average±Standard Deviation, Ppb)

Chemical compounds	LOQ	CNG	SATS	READ	New Hope
Formaldehyde	0.25	4.05±0.14	2.16±0.77	4.15±0.04	1.07±0.26
Acetaldehyde	0.10	4.00±0.99	4.49±0.91	4.47±0.29	3.70±0.18
Acetone	0.25	119.28±51.4	154.48±24.7	105.27±8.44	97.26±27.7
m,p-Tolualdehyde	5.00	0.65±0.01	0.65±0.01	0.48±0.23	0.60±0.01

LOQ = limit of quantification

Source: University of California, Davis

Correlations Between Bioassay Results and Target Organic Compounds

The research team calculated linear correlation coefficients (Pearson's) between sample volume normalized bioassay activity measurements for each sample group (e.g., home appliance, onsite engine or vehicle tests) and the concentrations of varied target compound concentrations. Table 31 reports only compounds with statistically significant correlation coefficients. Correlations were calculated within experimental groups because some tests, especially the vehicle tests, have different dilution and sampling procedures, making comparability between, for example, home appliance and vehicle tests uncertain. Several aldehydes, ketones, and aromatic compounds were found to be correlated with bioactivity. The next chapter expands the search for compounds responsible for observed bioactivity results by employing nontarget chemical methods.

Table 31: List of Correlations (p<0.05) Between Target Compounds and Bioassay Results

Experimental Group	Bioassay	Significant correlation (p<0.05)
Appliance	CYP1A1	Acetaldehyde Propionaldehyde Crotonaldehyde 2-Butanone
	IL-8	Crotonaldehyde 1,3,5-Trimethylbenzene 2-Butanone Acetaldehyde Propionaldehyde Dodecane Benzaldehyde
	TA98	1,3,5-Trimethylbenzene Decane Acetaldehyde Undecane Crotonaldehyde 2-Butanone Propionaldehyde Methacrolein
Stove retest	TA98	Acetaldehyde
Engine	IL-8	Valeraldehyde
	COX-2	Valeraldehyde Hexaldehyde p-Xylene Tetradecane
Vehicle	ROS	m,p-Cresol 2-Methylnaphthalene p-Xylene Methyl naphthalene Acetaldehyde Acetone

Source: University of California, Davis

Metal Analysis

Table 32 reports the concentrations of metals measured in this study. Only four metals were detectable at statistically significant levels above zero. Notably, two elements known to produce volatile forms under reducing conditions, such as those found in the research team's biofuel sources, arsenic and antimony, produced some detections in the combustion chamber samples. The other two detectable elements, copper and lead, were associated with diverse manufactured products involved in these combustion studies. (In the table, "0" denotes <LOD for those samples.)

Figure 40 panels (a-c) below illustrate box and whisker plots of measured metals concentrations. The measured concentrations do not follow a Gaussian profile but rather appear to be sporadic detections at the lower tails of the method detection limit.

Figure 40: Box and Whisker Plots of Measured Metal Concentrations

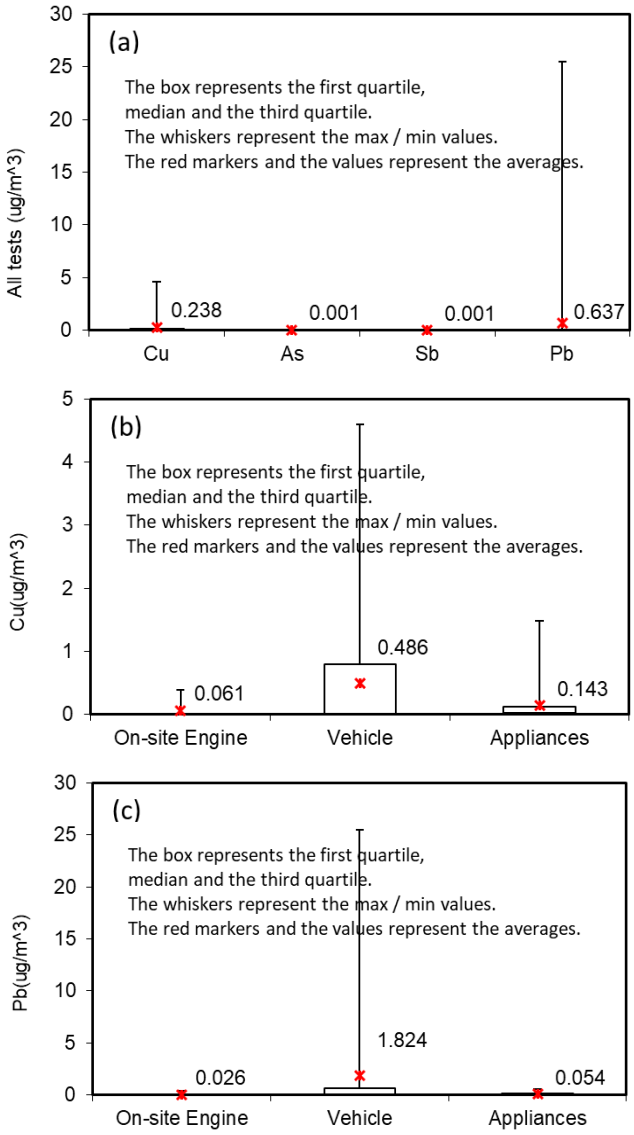

Panel (a) all metals across all tests. Panel (b) Cu across all tests. Panel (c) Pb across all tests.

Source: University of California, Davis

Table 32: Results of Metals Analysis
(All results in µg m^{-3})

Element:	Be	Cr	Mn	Co	Ni	Cu	Zn	As	Se	Sr	Mo	Cd	Ba	Sb	Hg	Tl	Pb
LOD (µg m^{-3})	0.005	0.005	0.005	0.005	0.02	0.02	0.2	0.01	0.2	0.01	0.005	0.01	0.02	0.002	0.005	0.005	0.005
On-Site Engine: 1						0.32											
2						0.32											0.40
3								0.02									
4														0.004			
5																	
6						0.39								0.004			
7																	0.045
8																	
9														0.003			
10														0.003			
11																	
12								0.03									
13																	
14																	
15																	
16																	
17																	
Vehicle Test: 1																	
2						0.79								0.045			25.5
3						0.86											6.6
4																	
5																	0.063
6																	0.030
7						0.03											0.082
8																	1.55
9						0.03											0.65
10																	0.024

Element:	Be	Cr	Mn	Co	Ni	Cu	Zn	As	Se	Sr	Mo	Cd	Ba	Sb	Hg	Tl	Pb
11						1.55											1.72
12																	
13						0.29											0.53
14																	
15																	
16						1.17											1.25
17						4.6								0.028			0.22
18																	0.014
19						0.88											0.088
20																	0.017
21																	
Cooking Stove: 1						1.48											
2						0.03											
3																	
4						0.05											
5																	0.046
Water Heater Test: 1						0.10											0.26
2																	0.52
3						0.41											0.083
4																	
5						0.57											
6																	
7						0.12											0.13
8																	0.16
9						0.08											0.016
10						0.05											0.010
11																	
12						0.29											0.029
13						0.16											0.053
14						0.05											0.053

Element:	Be	Cr	Mn	Co	Ni	Cu	Zn	As	Se	Sr	Mo	Cd	Ba	Sb	Hg	Tl	Pb
15																	0.008
16																	
17						0.01											
18						0.31											0.010
19																	0.021
20																	

Source: University of California, Davis

Conclusions

The concentration of standard analytes including hydrocarbons and aldehydes was similar in combustion exhaust generated using petroleum natural gas and biomethane. Although some of the target compound concentrations were linearly correlated with bioassay activities on a per-liter basis, it is not clear that they can completely explain the bioactivity differences observed between, samples. The next chapter expands the search for compounds responsible for elevated activity levels.

CHAPTER 7:
Nontarget Chemical Analysis Results

Introduction

The central research question underlying this project is whether chemical constituents of human health concern are generated when the compounds initially produced from diverse organic feedstocks, production processes, and upgrading technologies are transformed by combustion and subsequent atmospheric reactions. Given the complex composition of the starting feedstock and the wide variety of biotic and abiotic reactions that can occur during production and environmental transport, many, if not most, of the compounds produced may not be subject to monitoring with established methods, even when the list of target compounds is extensive, as in the preceding chapter. Complete chemical characterization of combustion emissions is an elusive goal, however, because the enormous range of chemical properties of these compounds makes finding a limited number of methods and instrumental techniques to collect, concentrate, detect, and identify them extremely challenging. In this work, the focus is on two groups of analytes, those with carbonyl functional groups and those that are soluble in basic aqueous solutions, to determine the related abundance relative to target constituents and the strength of the relationship of these analytes to bioassay results.

A wide range of organic compounds are produced during anaerobic digestion, with aldehydes and ketones prominent among them. Combustion of organic materials, including biogas fuels, also results in generation of similar compounds. Methods applied here allowed the collection, identification, and estimation of abundance of numerous carbonyl-containing substances beyond the 13 aldehydes and ketones quantified using TO-11 target method described in Chapter 6. Another group of compounds of interest resulting from biogas combustion are acidic gases, particularly those containing oxidized sulfur species. Reduced sulfur compounds were shown to be important components of raw biogas from various sources. During combustion, these materials may be incompletely oxidized, producing organic sulfates or sulfonates that may be important in subsequent photochemical processes.

Methods

Aldehyde and Ketone Analysis

The research team collected unknown carbonyl compounds in gas samples at the same time and using the same procedures as the target carbonyl compounds; details are provided in Chapter 6. Briefly, these samples were collected at a flow rate of 1 L min^{-1} on a pair of 8 x 115 mm sorbent tubes containing silica gel (SKC, Inc.) treated with 2,4-dinitrophenylhydrazine (DNPH). Compounds with aldehyde and ketone functionality react with the DNPH to form a hydrazone derivative, as shown by the reaction scheme below (Figure 41). Compounds containing more than one aldehyde or ketone group or with double bonds may react with more than one DNPH molecule following similar pathways. This reaction preserves the R_1-C-R_2 substructure of the parent carbonyl, forming a derivative with a molecular formula larger than that of the original compound by $+C_6H_4N_4O_3$ for compounds with a single carbonyl structure,

by + $C_{12}H_8N_8O_6$ for a dicarbonyl compound, and so on for compounds with three or more aldehyde groups.

Figure 41: Reaction Scheme Showing the Formation of a Hydrazone Derivative From a Carbonyl Compound and 2,4-Dinitrophenylhydrazine

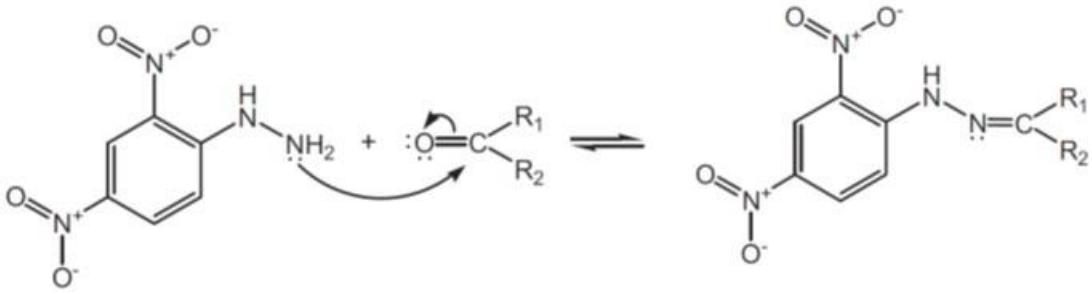

Source: University of California, Davis

The research team reanalyzed samples for the nontarget carbonyl analysis on an Agilent 1200 liquid chromatograph coupled with an Agilent 6530 quadrupole time-of-flight mass spectrometer (LC-qTOF-MS) in a single full scan run with a random sample order using the same chromatographic separation conditions outlined in Chapter 5. The use of the qTOF-MS provided sufficient mass accuracy (typically ±5 ppm mass error) and mass resolution (>10,000 at m/z 118) to assign molecular formulas solely based on ion mass-to-charge ratios and isotope patterns.

The experimental data analyzed for aldehydes and ketones included all chamber samples, solvent blanks, chamber blanks, and target compound standards. Data acquired during the LC-qTOF-MS run were processed using Profinder (Agilent Technologies, Inc., v. B08) to recursively group ions with retention times and mass-to-charge ratios within user-selectable tolerance ranges. In this iterative process, all related isotopes (e.g., $M+H^+$ or $M-H^-$ $M-2H^{-2}$ and ^{13}C or other isotopic analogs) and adducts (e.g., $M+Na^+$ or $M+F^-$) were grouped together to form a "molecular feature" representing a putative organic compound of unknown structure. The median retention times and molecular masses of the aligned molecular features were exported to the statistical analysis package Mass Profiler Professional (Agilent Technologies, Inc., v. 14.9), and molecular formulas were generated from the mass spectra using IDBrowser (Agilent Technologies, Inc. v. B08), forcing the formulas to have a minimum of 6 C, 4 N, 4 H, 4 O, and allowing the presence of S and P in addition to CHON.

Soluble Acidic Gases

The research team collected soluble acidic gases were impingers containing 20 mL of a pH 10 solution prepared by adding 880 µL of 0.15 N NaOH to 200 mL of deionized water (Milli-Q). The gas flow rate was between 0.3 L min^{-1} in all cases except for four preliminary tests conducted on the on-site microturbines at READ, where flow rates were 0.18-0.275 L min^{-1}. Following collection, impinger solutions were transferred to glass bottles and refrigerated at 4°C. Just before analysis, a 10 mL subsample was evaporated to 1 mL under a stream of nitrogen gas (Turbovap), and all samples were analyzed at both 1x and 10x concentration levels.

The research team analyzed impinger samples on an Agilent 1200 liquid chromatograph coupled with an Agilent 6530 LC-qTOF-MS in a full scan run with a randomized block sample order in which the randomly placed 1x samples were analyzed first and the 10x samples were analyzed second. The run was conducted in negative electrospray ionization mode using the following chromatographic separation conditions: Solvent A: 1 nM NH_4F in H_2O, Solvent B: acetonitrile, gradient: 2% B for 1.5 min (First min goes to waste), linear ramp to 100% B at 16.5 mins, hold at 100% B for 4 mins. (Total run time 20.5 mins). The injection volume was 20 µL.

The experimental data analyzed for soluble acidic gases included all chamber samples, solvent blanks, chamber blanks, and target compound standards. The research team processed the data acquired during the LC-qTOF-MS run using Profinder (Agilent Technologies, Inc., v. B08) to recursively group detected molecular features as described further above. The team exported the median retention times and molecular masses of the aligned molecular features to the statistical analysis package Mass Profiler Professional (Agilent Technologies, Inc., v. 14.9), and molecular formulas were generated from the mass spectra using IDBrowser (Agilent Technologies, Inc. v. B08), allowing for the presence of C, O, H, N, S, P, and Cl.

Results

Aldehyde and Ketone Analysis

Nontarget analysis of the DNPH data following the process described above yielded 3419 molecular features using the selected parameters. Of these, 2,894 could be assigned molecular formulas using the specified constraints. An example of the alignment process to extract features with similar masses and retention times, group them with the associated isotopes and adducts, and display the associated mass spectra is shown in Figure 42. Continuing the example, the molecular feature with a median retention time of 1.832 min and a neutral mass of 241.0451 was detected in 44/48 of the samples analyzed; this analysis was limited to only the front DNPH cartridge. The molecular formula generated for this feature ($C_7H_7N_5O_5$) had a monoisotopic exact mass of 241.0447, differing from the measured neutral mass by -1.39 ppm (-0.34 mDa). Based on the mass error, the isotope spacing and the relative isotope abundance, this formula had a match score of 99.45 (Figure 43). After subtracting the portion of the hydrazone attributable to the DNPH derivatizing reagent, this yielded an original molecular formula of CH_3NO_2. This relatively simple molecule has only a limited number of structures that might be successfully collected on a DNPH cartridge. Possible structures include a carboxylic acid (carbamic acid), an alkyl nitrate (nitromethane), or an alkyl nitrite (methyl nitrite). ecause carboxylic acids are generally nonreactive with DNPH, NO_2^- does react with DNPH, and nitrites are more reactive than nitrates, it seemed most likely that the detected compound was methyl nitrite rather than a carbonyl containing compound. This shows that the nontarget "carbonyls" method can provide additional information beyond the CHO-containing compounds that are the focus of the TO-11 target method. This example and all subsequent formula assignments and structural speculation require further confirmation through the acquisition of authentic standards, proof of reactivity toward DNPH, and verification of the retention time and mass spectra of the resulting hydrazone derivative.

Figure 42: Example of Feature Alignment Across a Subset of the 48 Combustion By-Product Samples Showing the Extraction of Compounds With Relatively Consistent Retention Times and Isotope Patterns

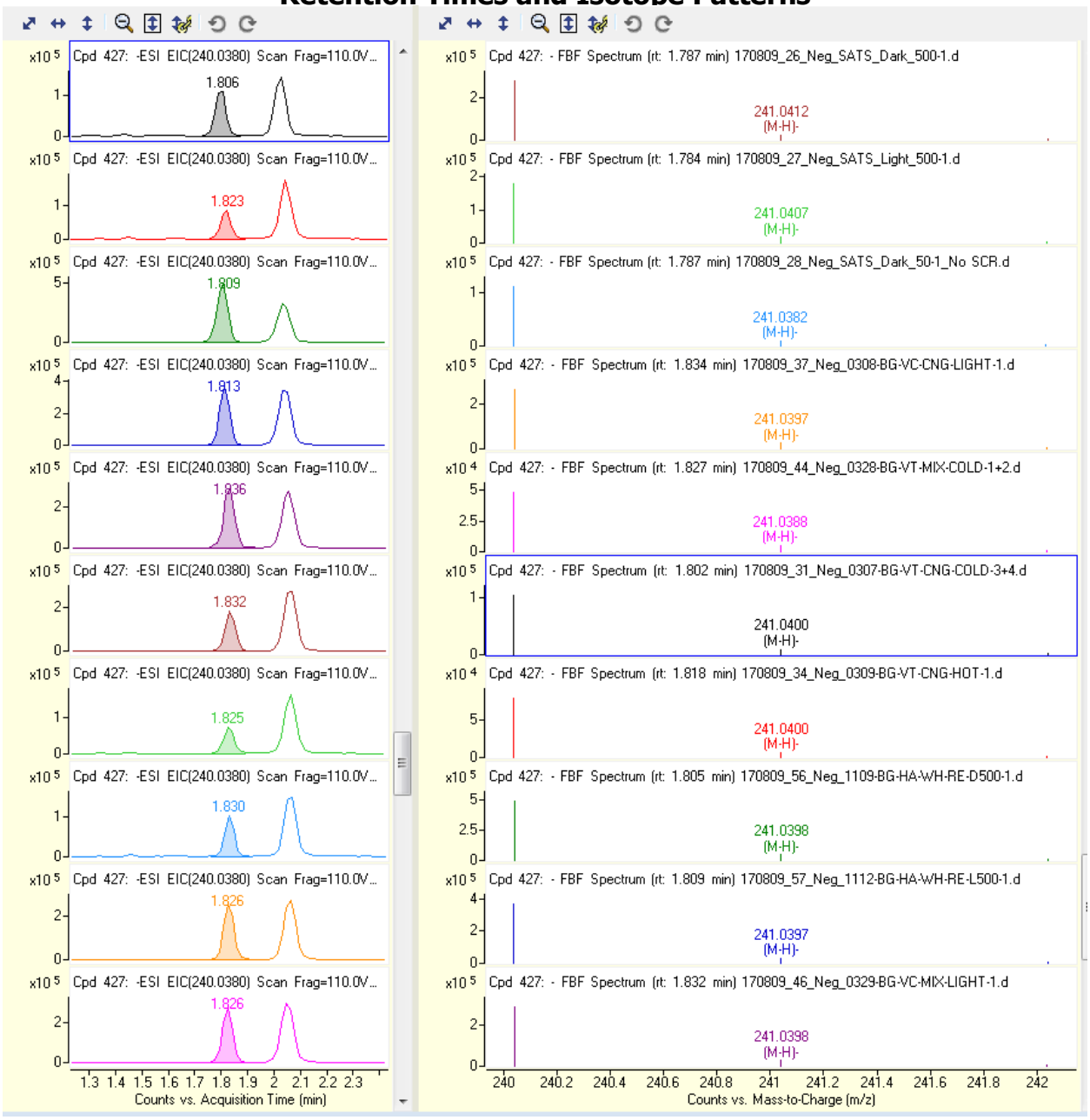

Source: University of California, Davis

Figure 43: Example of the Agreement Between Measured Isotope Spacing and Relative Abundance (Black Lines) and the Predicted Isotope Spacing and Abundance (Red Boxes) for the Best-Fit Molecular Formula Hydrazone Derivative of $C_7H_7N_5O_5$

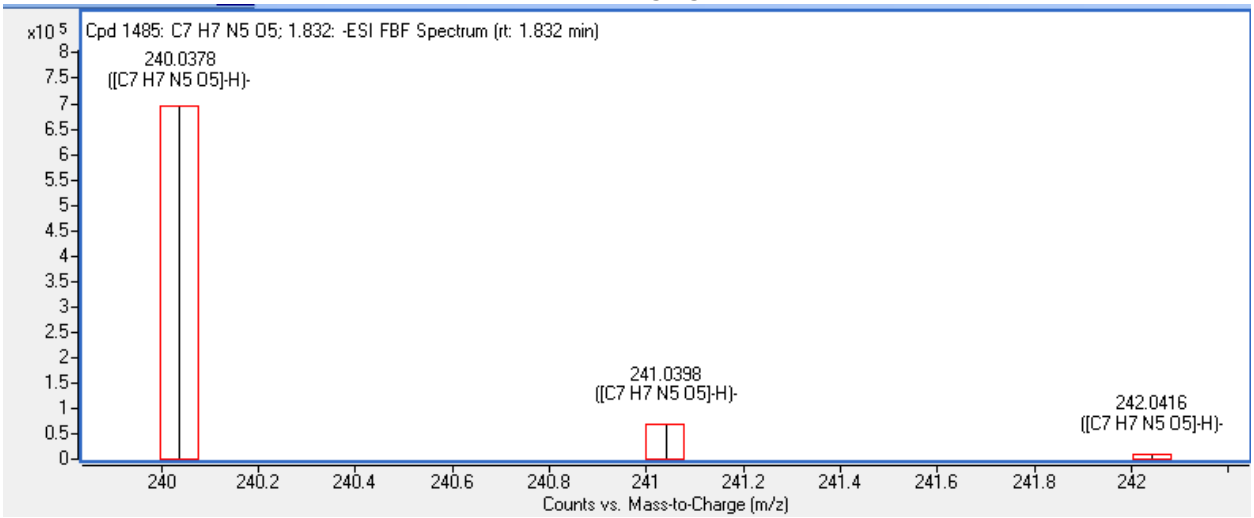

Source: University of California, Davis

A second example of formula assignment was the feature detected at retention time of 1.777 min (median) and a neutral mass of 434.0574 (median). This compound was detected in 42/48 of the samples analyzed. The molecular formula generated for this feature ($C_{14}H_{10}N_8O_9$) had a monoisotopic exact mass of 434.0571, differing from the measured neutral mass by −0.84 ppm (−0.36 mDa). Based on the mass error, the isotope spacing, and the relative isotope abundance, this formula had a match score of 99.06 (Figure 44). This molecular formula was also observed in 29/48 samples with a retention time of 2.844 min (median) and a measured neutral mass of 434.0570 (median). This feature had a mass error of +0.12 ppm (+0.05 mDa) and a match score of 97.04 (Figure 45). These formulas could be consistent with either a mono-carbonyl with a formula of $C_8H_6N_4O_6$ or a dicarbonyl compound with a formula of $C_2H_2O_3$. It is difficult to imagine a structural isomer for the first formula that contains only one DNPH reactive site since most possibilities include multiple $–NO_2$ and/or –CHO functional groups. The second possibility leads to a simpler molecular structure such as formic anhydride, a simple dialdehyde.

Figure 44: Example of Feature Alignment Across a Subset of the 48 Combustion By-Product Samples Showing the Extraction of Compounds With Relatively Consistent Retention Times and Isotope Patterns

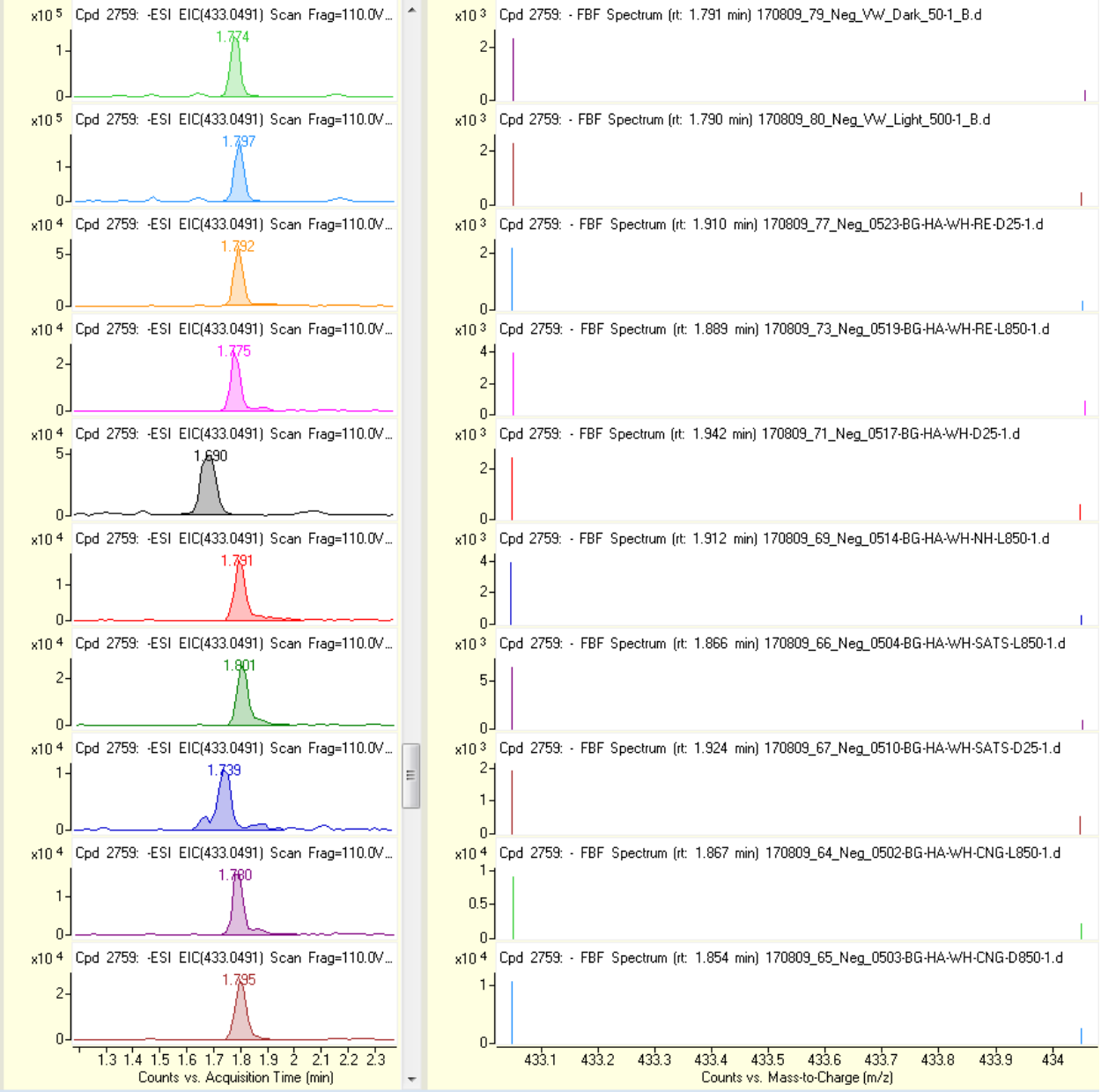

Source: University of California, Davis

Figure 45: Example of Agreement Between Measured Isotope Spacing and Relative Abundance (Black Lines) and Predicted Isotope Spacing and Abundance (Red Boxes) for Best-Fit Molecular Formula Hydrazone Derivative (or Dihydrazone Derivative) of $C_{14}H_{10}N_8O_9$

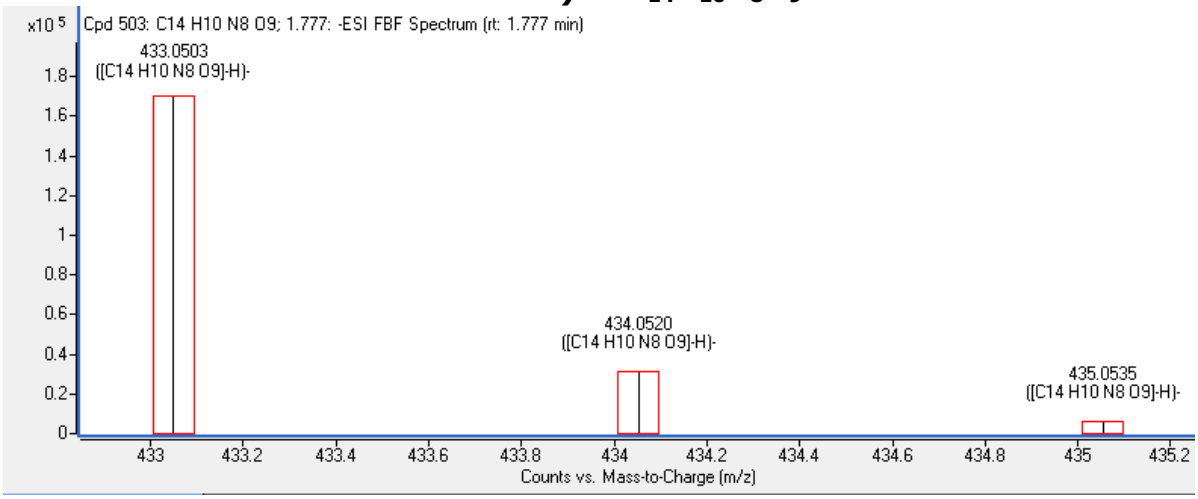

Source: University of California, Davis

It is not practical to assign molecular structures for each of the thousands of molecules isolated by the DNPH sorbent tube collection method following the procedures outlined in the examples above. Instead, the hope is to use the abundances and detection frequencies of unknown features to prioritize identification of compounds that are common, abundant, or correlated with high activity in bioassay tests. This approach assumes that nontarget abundance measurements are proportional to concentrations measured using established target methods. The research team tested this hypothesis by comparing the peak heights of aligned nontarget features with the same retention time and mass-to-charge ratio as the standard compounds with the known concentration of those standards. For every aldehyde and ketone quantified in Chapter 6, there was a very strong relationship (R^2>0.995) between the known target compound concentration and the peak height of the associated nontarget feature. (See example for acetaldehyde in Figure 46.) This provides support for comparing the abundance of different unknown nontarget features across tests as a measure of relative abundance. Comparing abundances across different compounds is more difficult; although there is similarity in MS response factors among the nontarget compounds because they all contain at least one dinitrohydrazone structure, without analytical standards, it is impossible to tell whether a compound with a higher peak height has a higher concentration.

To assess the relative importance of nontarget features and the distribution of carbonyl structures within and between samples, each aligned molecular feature was identified as either a target compound (based on retention times and mass-to-charge ratios) or a nontarget feature. Nontarget features were further subdivided by the number of carbons in the assigned molecular formula minus the six carbons associated with the DNPH derivatizing agent (assuming that a single DNPH-reactive site is present). Figure 47 through Figure 52 present the results from this analysis. Less than 1/3 of the total nontarget abundances can be accounted for by target carbonyls. Stated another way, 66%-98% of the estimated quantity of DNPH-reactive material is not accounted for by the target compounds and, therefore, is quantified for the first time in the present analysis.

Figure 46: Example of Close Correspondence Between Measured Concentration of Target Carbonyl-Containing Compound (acetaldehyde) and Peak Height of Nontarget Feature With Same Retention Time (6.255 min) and Neutral Mass (223.0473) as Target Compound

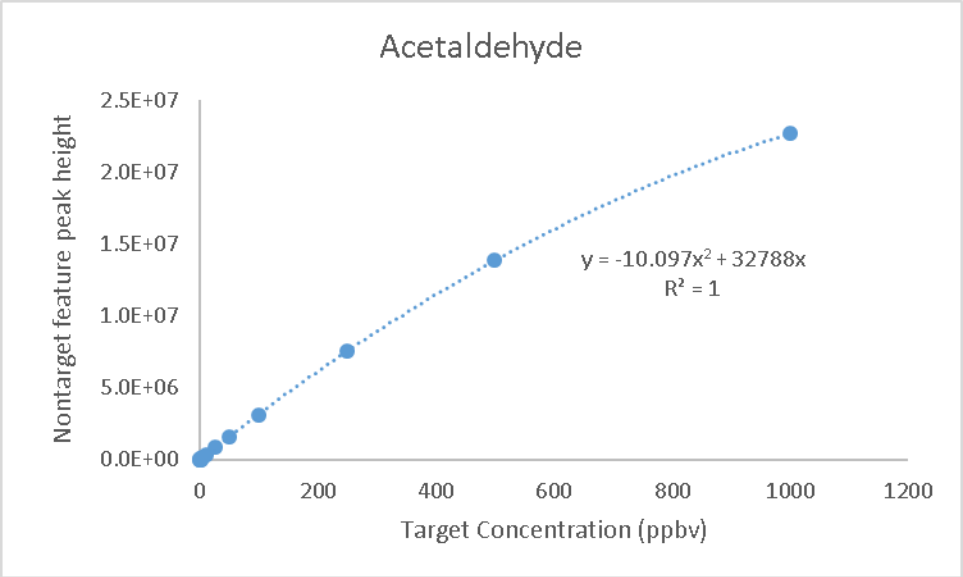

Source: University of California, Davis

Figure 47: Distribution of Nontarget Carbonyl Compounds in Stove Tests Burning Biomethane From Food Waste

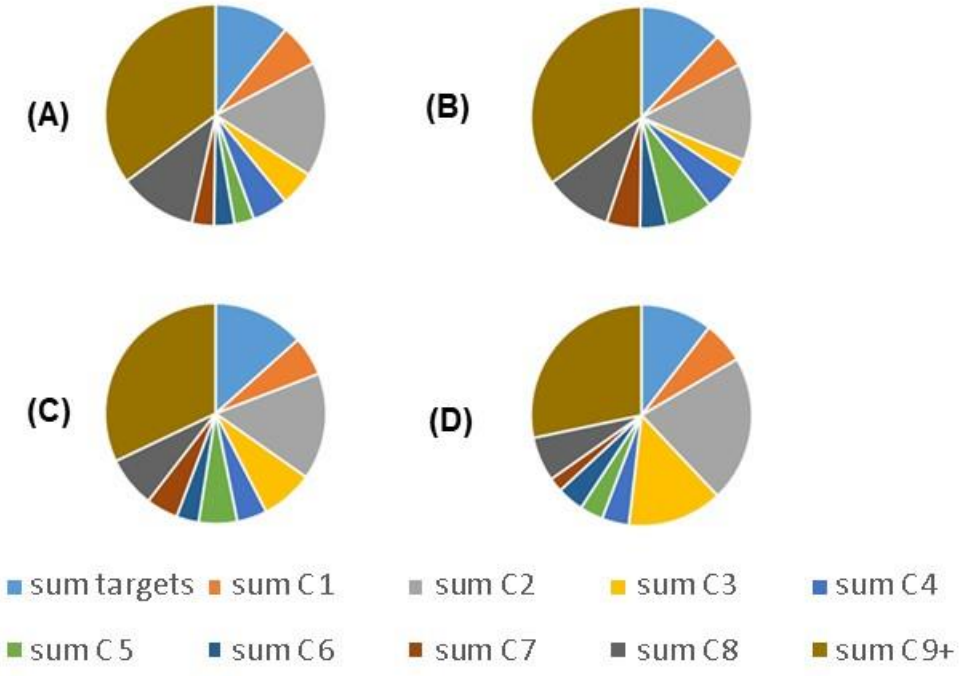

SATS: A, READ: B, dairy (NH: C) or compressed natural gas (D)

Source: University of California, Davis

Figure 48: Distribution of Nontarget Carbonyl Compounds in Water Heater Tests Burning Biomethane From Food Waste (READ) and Compressed Natural Gas (CNG) at Selected Dilutions and Lighting Conditions

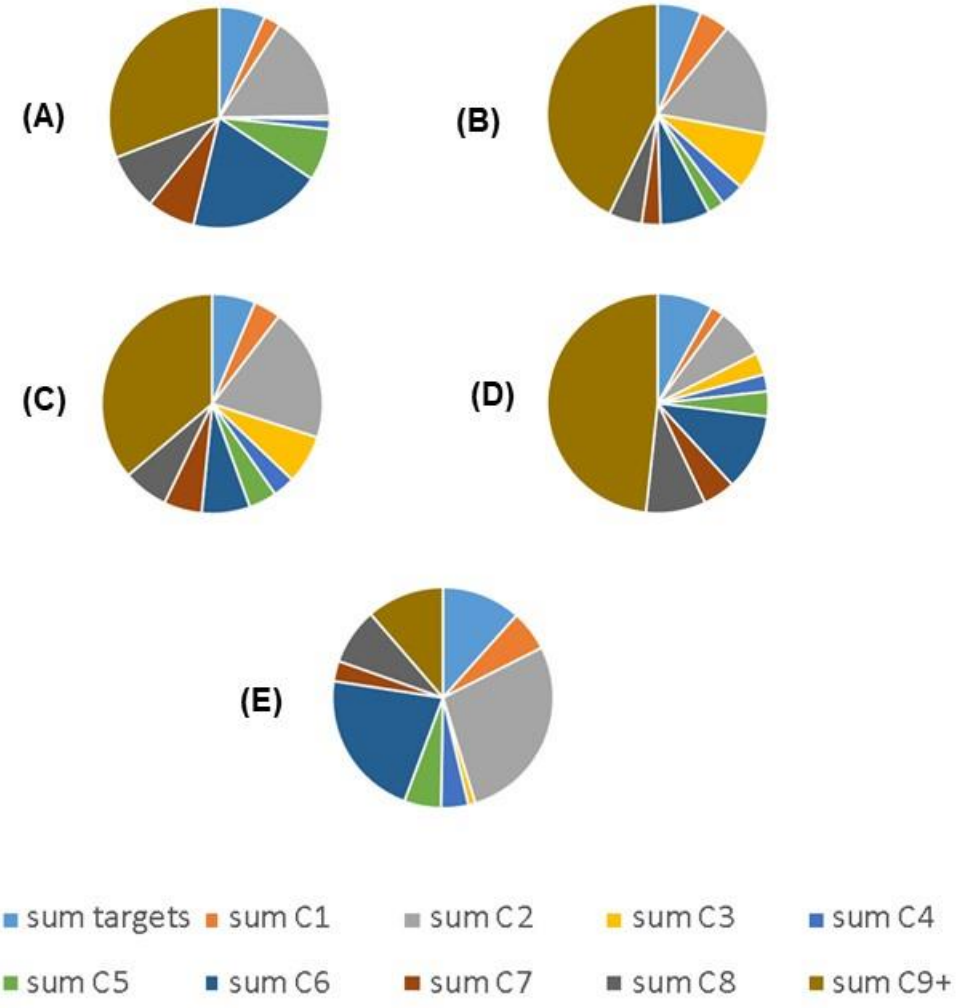

Dark tests shown for biomethane were conducted at 10:1 (A), 50:1 (C), and 500:1 (B) and a light test was conducted at 500:1 (D). The CNG test was a dark test at 50:1 dilution (E)

Source: University of California, Davis

Figure 49: Distribution of Nontarget Carbonyl Compounds in On-Site Engine Tests Burning Biom ing

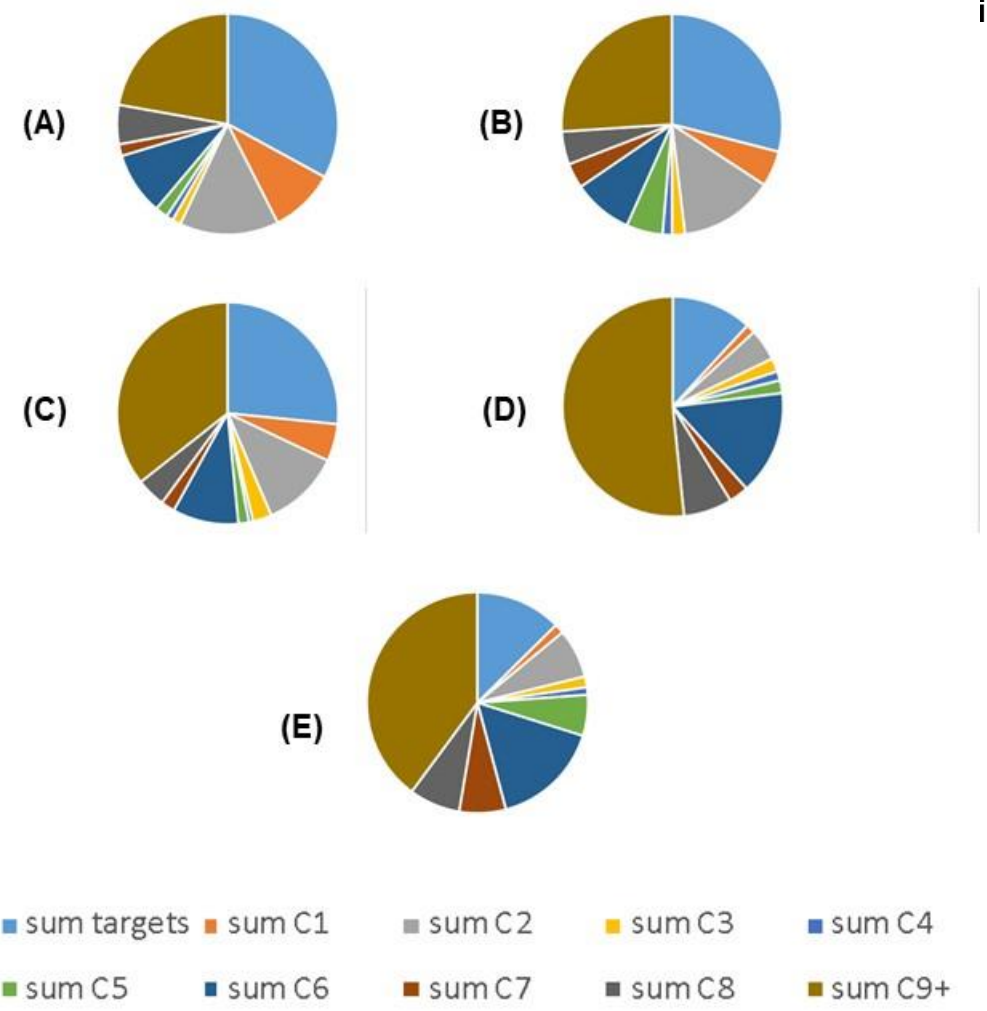

Conditions

Dark tests were conducted at 50:1 for both sources (A: VW, B: NH), and 500:1 for NH (C). The DNPH cartridge from the 500:1 dark test at VW was not usable because of condensation. Light tests for both sources were conducted at 500:1 (D: VW and E: NH).

Source: University of California, Davis

Figure 50: Distribution of Nontarget Carbonyl Compounds in On-Site Engine Tests Burning Biomethane From Landfill (KF) and Food Waste Digester (SATS) at

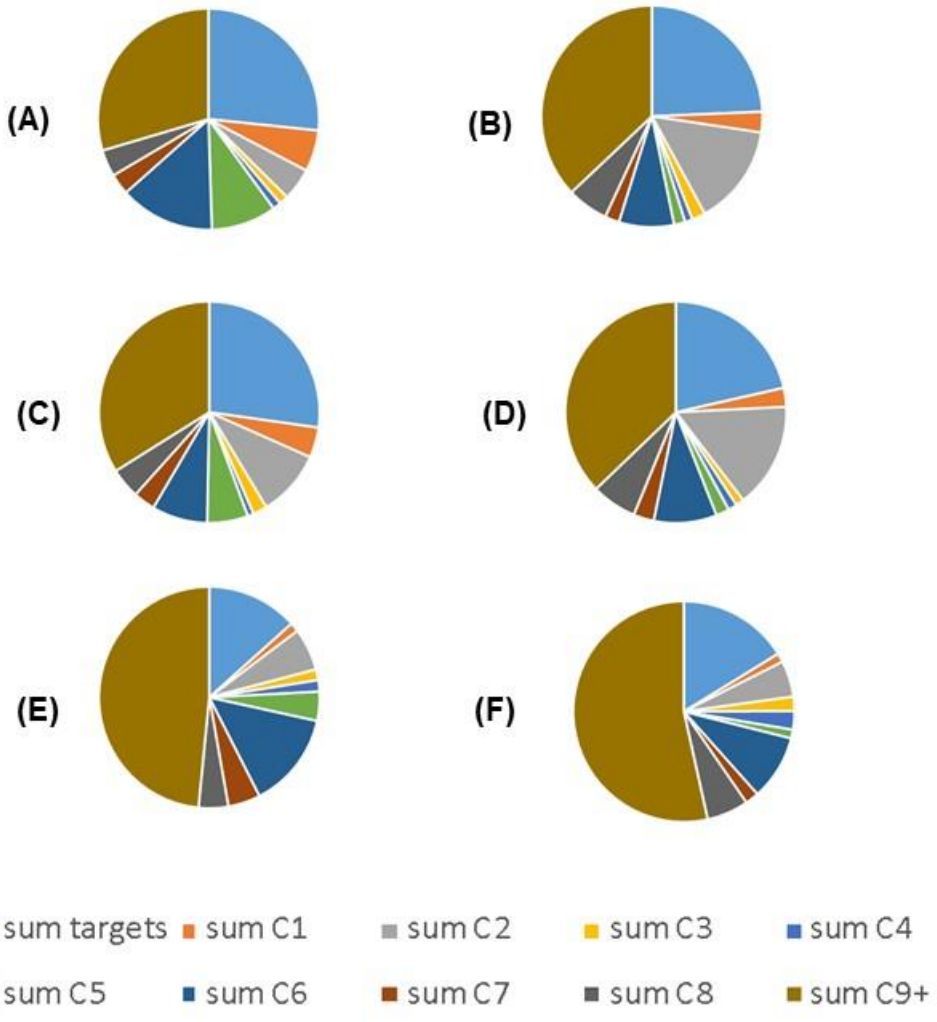

Dark tests were conducted at 50:1 (A: KF, B: SATS), and 500:1 (C: KF, D: SATS) for both sources. Light tests for both sources were conducted at 500:1 (E: KF and F: SATS).

Source: University of California, Davis

Figure 51: Distribution of Nontarget Carbonyl Compounds in Vehicle Tests Burning Compressed Natural Gas (CNG) at Different Dilutions and Lighting Conditions

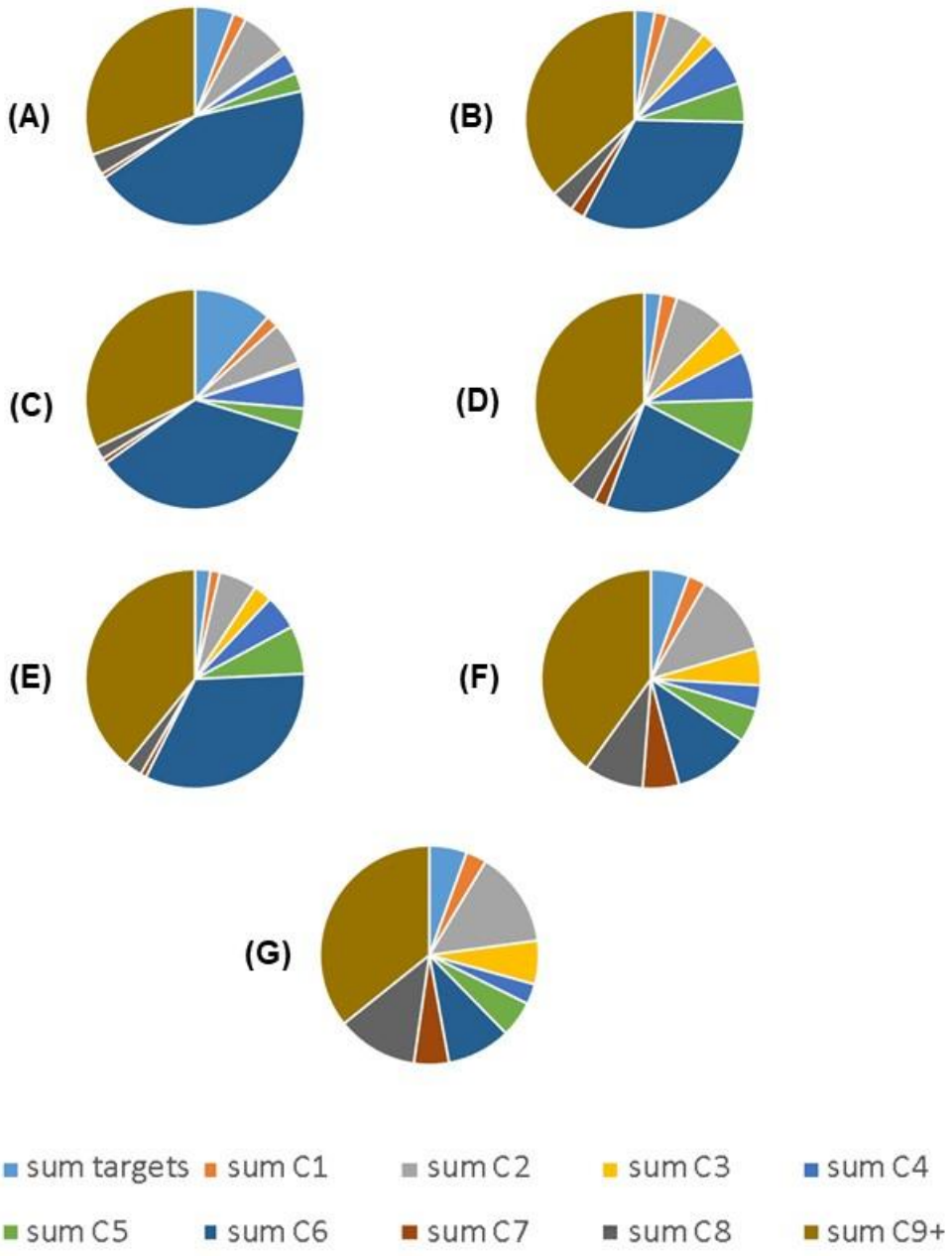

Samples were taken directly from the tunnel during Cold 1&2 (A), Cold 3&4 (C) and Hot (E) conditions. Tunnel samples were aged in the chamber with additional dilution under dark (B, D) or light (F, G) conditions.

Source: University of California, Davis

Figure 52: Distribution of Nontarget Carbonyl Compounds in Vehicle Tests Burning Biomethane From Food Waste (SATS) and a Biomethane/CNG Mix (MIX) at

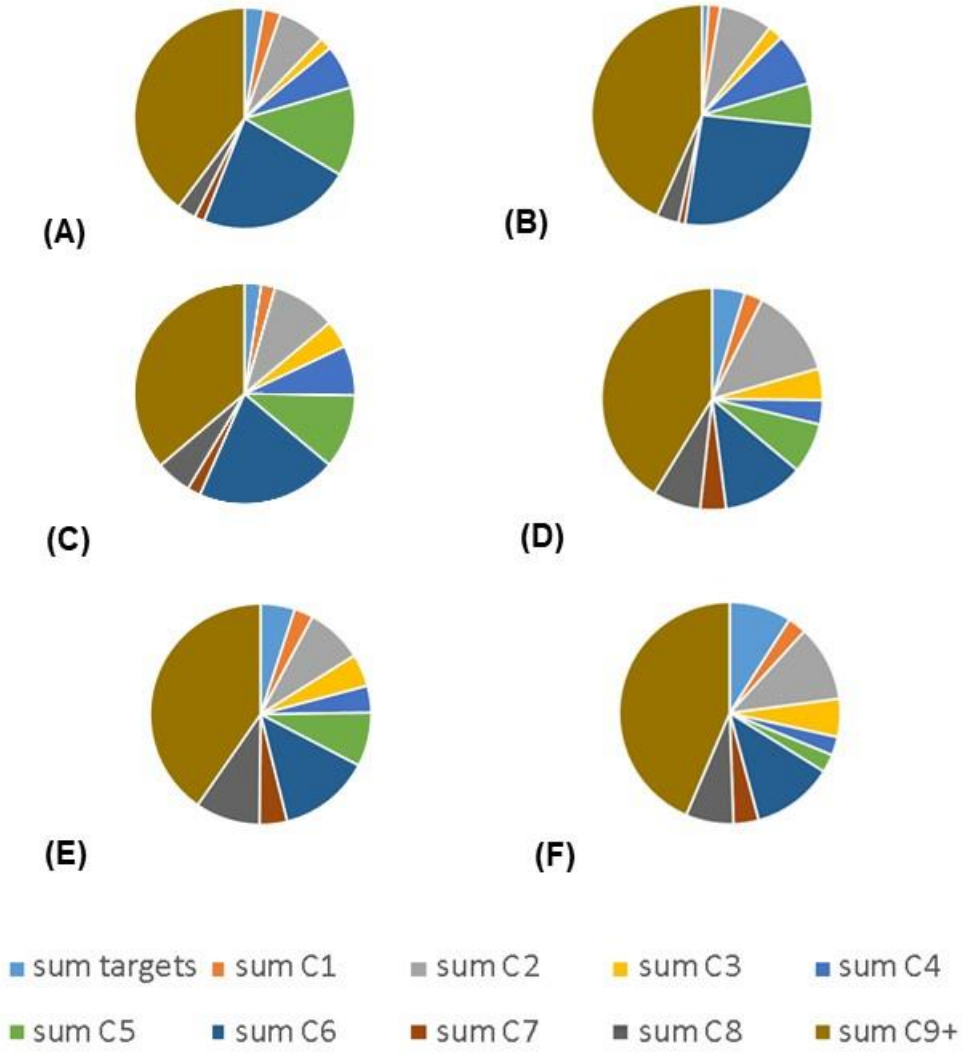

Samples were taken directly from the tunnel during MIX Cold 1&2 (A). Tunnel samples were aged in the chamber with additional dilution under dark (B: SATS, C: MIX) or light (D: SATS, E, F: MIX) conditions.

Source: University of California, Davis

Although the broad classification of the potential molecular sizes of DNPH-reactive structures across tests in Figure 47 to Figure 52 is useful in establishing the relative importance of nontarget carbonyls relative to those typically included in target methods, it does not provide any compound-specific information. To identify similarities and differences in specific molecules found in combustion emissions from the various source types, Figure 53 compares the two food waste derived samples (READ and SATS), the landfill sample (KF) and CNG. For each source, the entity (compound) list is limited to compounds found in 10% of the front DNPH cartridges for that sample group. The number of entities is therefore lower than the 3,419 complete entity list, in some cases significantly (e.g., KF). Compounds found in all four sample types (1189) comprise between 39% and 75% of the total in each group. The number of compounds unique to each of these groups (18-166) is a small fraction of the total for any of the sources. A similar comparison is provided in Figure 54 for the two dairy biomethane samples (VW and NH) and CNG. Although there is again a significant overlap in composition across sources, a much larger fraction of unique features were found in this sample comparison.

Figure 53: Comparison of DNPH-Reactive Features (e.g., Carbonyl Compounds) Detected in Combustion Emissions From Biomethane From Two Food Waste Digesters (READ and SATS), a Landfill (KF), and CNG

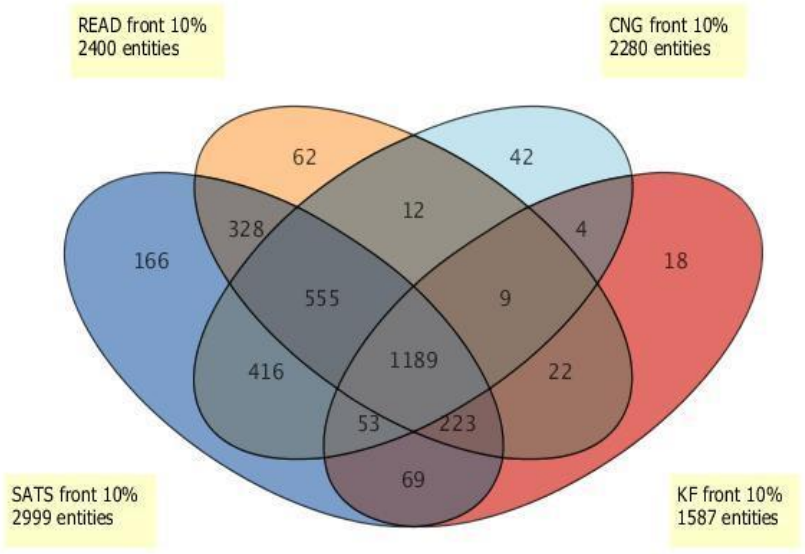

Source: University of California, Davis

Figure 54: Comparison of DNPH-Reactive Features (e.g., Carbonyl Compounds) Detected in Combustion Emissions From Biomethane From Two Dairies (NH and VW) and CNG

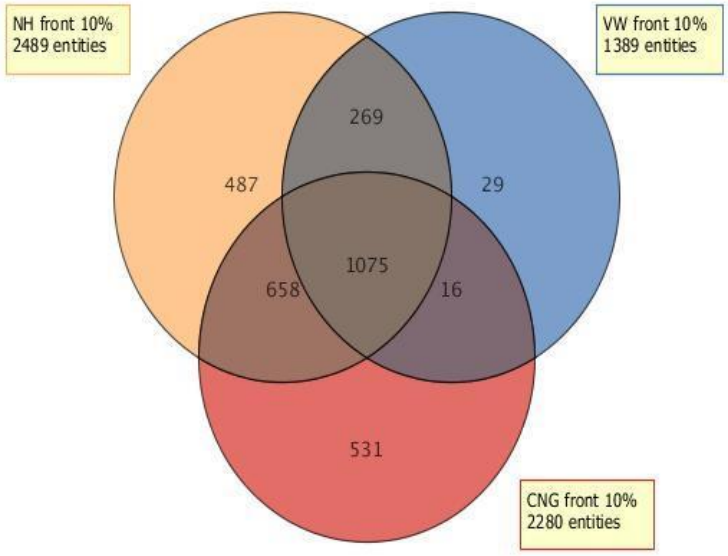

Source: University of California, Davis

Soluble Acidic Gases

Alignment of the data from the basic impingers yielded a set of 746 full-scan features across all samples, including quality control spikes and laboratory and chamber blanks. Features that were detected routinely (more than 75% of the time) in the quality control or either type of blank sample were removed from the list, leaving a set of 663 features present in at least 5% of experimental samples.

To identify similarities and differences in combustion emissions across methane source types, the research team combined features associated with each source type across emission tests, and Venn diagrams were prepared to differentiate between ubiquitous features and those that might serve as source or category-specific combustion markers. In Figure 55 and Figure 56, features common to all the sources represent the majority of detected compounds, and very few features are unique to any of the source classes.

Figure 55: Comparison of Features Collected in Basic Impingers Used to Sample Combustion Emissions From Biomethane From Two Food Waste Digesters (READ and SATS), a Landfill (KF), and CNG

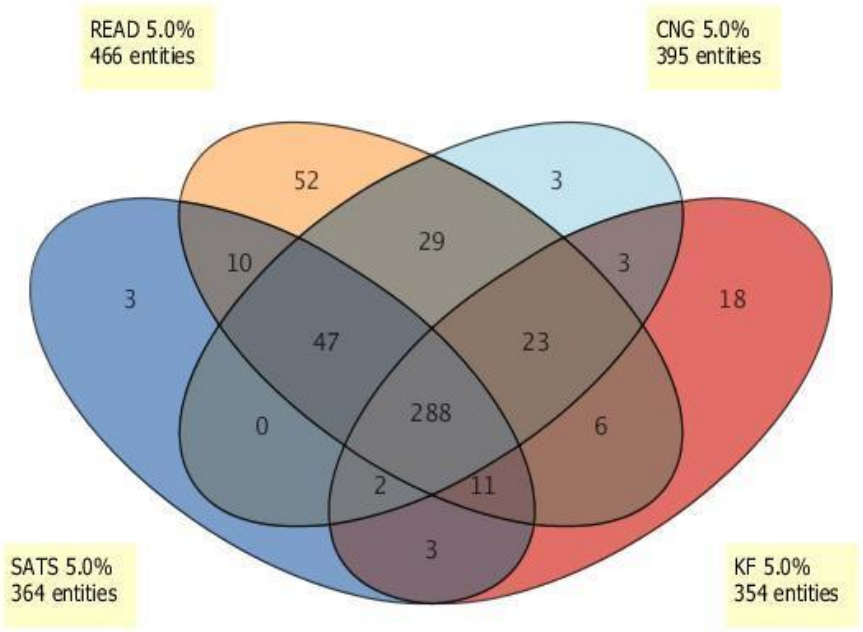

Source: University of California, Davis

Figure 56: Comparison of Features Collected in Basic Impingers Used to Sample Combustion Emissions From Biomethane From Two Dairies (NH and VW) and CNG

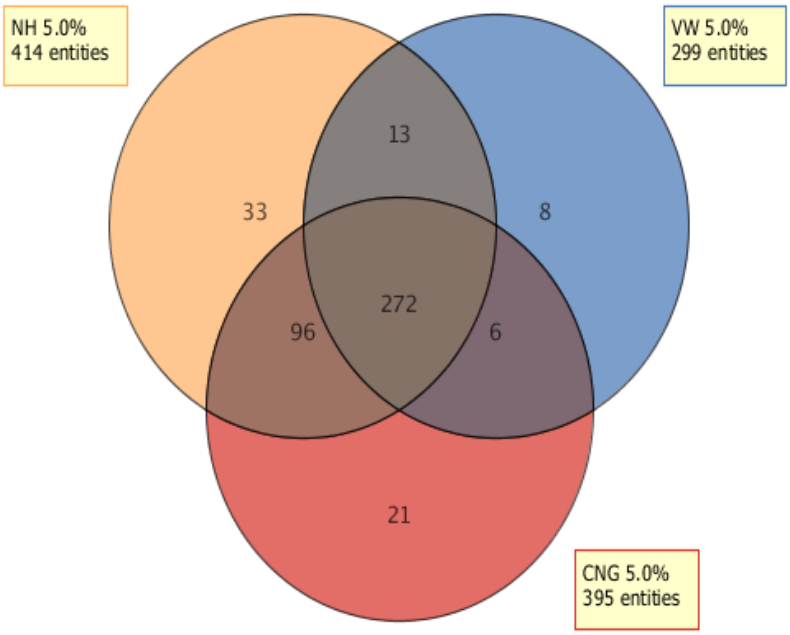

Source: University of California, Davis

Correlations of Nontarget Data With Bioassay Results

The correlation between nontarget abundance (i.e., peak height) and quantified target compound concentrations shown in Figure 46 suggests that correlations would be expected between bioassay activities and nontarget ion abundances for bioactive compounds. Differences in the volume of gas sampled and the degree of dilution across tests and analyses complicate efforts to identify these relationships, however. Gas volumes sampled during each type of test were used as normalization factors.

$$\frac{bioassay\_activity}{bioassay\_sample\_volume} = \alpha_i \frac{nontarget\_ion\_abundance}{nontarget\_sample\_volume}$$

Where α_i represents the constant of proportionality between specific bioactivity and specific nontarget abundance for nontarget feature i. Within the Mass Profiler Professional program used to perform the statistical evaluations nontarget abundances cannot be readily normalized as indicated in the equation above, so a modified version was used:

$$\left(\frac{nontarget\_sample\_volume}{bioassay\_sample\_volume}\right) \cdot bioassay_{activity} = \alpha_i \cdot nontarget\_ion\_abundance$$

Pearson linear correlation coefficients (ρ) were used to indicate the strength of the relationship in the above equation, and features with coefficients that were statistically significant ($p<0.05$) were identified. These correlations were determined for subgroups of experiments (e.g., on-site engine tests and home appliance tests) that were expected to have the greatest similarities in dilution and sampling conditions.

Table 33 and Table 34 summarize the correlation results for nontarget impinger and DNPH tests, respectively. For the impinger tests, the identification consists of a molecular formula that is the best match to the accurate mass, isotope spacing, and isotope abundance of the molecular feature with an isotopic abundance that was correlated with the bioassay result. In the case of the DNPH data, the formula reported is for the compound presumed to react with the DNPH to make the hydrazone derivative with the observed formula. In some cases, these compounds have more than one aldehyde/ketone functional group, and this is indicated in the table. The retention time, mass, and formula scores in Table 34 are for the hydrazone derivatives of the formulas in the table (+$C_6H_4N_4O_3$ for each aldehyde group).

Table 33: Nontarget Features From Impinger Tests With Statistically Significant Correlation (p<0.05) With Bioassay Results in Home Appliance Or On-Site Engine Tests

Compound	Retention Time	Mass	Score	source	assay
> limit	17.74	1145.93		appliance	ROS
C_3H_7NOS	7.66	105.0252	79.77	engine	IL-8
$C_5H_7Cl_3O_2S$	17.08	235.9269	68.07	appliance	ROS
$C_6H_{21}N_6O$	6.22	193.1745	73.16	engine	COX2
$C_7H_6NO_6S$	7.94	231.9933	66.2	appliance	COX2
$C_8H_{12}O_4$	2.06	172.0729	86.22	appliance	TA98
$C_8H_{16}O_2$	10.35	144.1144	98.75	appliance	TA98
$C_8H_{16}O_2$	10.35	144.1146	99.93	appliance	TA98
$C_8H_{16}O_3$	5.03	160.1094	87.3	appliance	TA98
C_8H_6NS	7.66	148.0231	83.12	engine	COX2,IL-8
$C_9H_{18}O_3$	6.31	174.1248	86.34	appliance	COX2
$C_9H_{18}O_3$	7.68	174.125	86.36	appliance	ROS
$C_9H_{20}ClO_4S$	7.54	259.0777	95.7	engine	IL-8
$C_9H_6N_4O_9S$	8.77	345.9852	83.46	appliance	COX2
$C_{11}H_{22}O_2$	12.88	186.1615	82.53	appliance	COX2
$C_{12}H_{20}O_3$	11.95	212.1408	99.24	appliance	IL-8
$C_{12}H_{22}O_2$	13.14	198.1616	85.01	appliance	ROS,
$C_{13}H_{10}O_3$	8.15	214.063	84.36	appliance	COX2, TA98
$C_{13}H_{12}N_6O_4S_4$	14.05	443.978	92.04	appliance	ROS
$C_{13}H_{20}O_4$	7.83	240.1365	98.73	appliance	TA98
$C_{13}H_{22}O_3$	12.46	226.1565	85.07	appliance	ROS
$C_{13}H_{26}O_2$	14.64	214.1926	83.22	appliance	COX2
$C_{14}H_7Cl_3NO_4$	13.13	357.9457	92.51	engine	COX2, IL-8
$C_{15}H_{28}O_2$	16.03	240.207	86.03	appliance	ROS
$C_{16}H_{26}O_3S$	11.307	298.1597	99.41	appliance	ROS
$C_{16}H_{28}O_3$	14.49	268.2036	84.21	appliance	ROS
$C_{17}H_{12}N_2O_{20}S$	11.59	595.9683	61.39	appliance	COX2
$C_{18}H_{30}O_3S$	12.28	326.1912	98.33	appliance	ROS
$C_{18}H_{36}N_{10}O_4$	19.10	456.2934	90.16	appliance	ROS, TA98
$C_{18}H_{40}N_2OS$	16.55	332.29	69.57	engine	TA98
$C_{20}H_8N_3O_{14}S$	11.09	545.9721	63.4	appliance	COX2
$C_{22}H_{24}N_{11}$	8.97	442.2207	82.2	appliance	ROS
$C_{23}H_{42}N_3OS_2$	16.32	440.2782	78.31	appliance	ROS
$C_{24}H_{10}N_3O_{25}$	9.29	739.9516	71	appliance	ROS

Source: University of California, Davis

Table 34: Nontarget Features From DNPH Tests With Statistically Significant Correlation (p<0.05) With Bioassay Results in Home Appliance or On-Site Engine Tests

Compound	Retention Time	Mass	Score	Test	Result
C_2H_5NO	2.66	239.0656	97.51	Engine	COX2
	1.81	239.0659	99.74	Stove retest	TA98 (mutagenicity)
$C_6H_3NO_4$ (dialdehyde)	14.64	513.0618	96.92	Appliance	CYP1A1, IL-8, TA98 (mutagenicity)
$C_7H_{14}O$	18.35	294.1353	97.43	Engine	COX2, IL-8
$C_8H_{16}O$	20.00	308.1488	95.61	Engine	COX2, IL-8
$C_{10}H_{10}O_2$ (dialdehyde)	19.37	522.1265	93.7	Engine	COX2
$C_{10}H_{18}O_2$	15.82	366.1545	97.79	Engine	CYP1A1
$C_{10}H_{18}O_3$ (dialdehyde)	17.74	546.1822	96.02	Engine	COX2
$C_{13}H_8O$	20.17	360.0862	98.75	Engine	TA98 (mutagenicity)
$C_{14}H_{20}O_2$	15.66	400.175	98.11	Engine	COX2

Source: University of California, Davis

Conclusions

The presence of bioassay activity above background levels, and in excess of that observed in CNG samples for at least some of the biomethane combustion samples, and the failure of the target analytes to explain the majority of that activity place additional emphasis on the nontarget investigation to understand the sources of the bioactivity. More than 40 compounds displaying a correlation with the observed bioactivity have been highlighted by the research to this point. Some of these molecular formulas of interest have structural isomers that could be responsible for the observed bioactivity in a concentration-dependent manner. Two examples of such compounds are C_2H_5NO (possible DNPH-reactive isomers include nitrosoethane or acetamide) and $C_{10}H_{10}O_2$ (possible isomers include 1-phenyl-1,3-butanedione). Each of these formulas has numerous possible isomers, several of which are likely to be DNPH-reactive, so these structures have not been confirmed. Because bioactivity has been measured for these particular isomers in other bioassay tests, they might be responsible for the response of the bioassays used in this study.

Correlations between nontarget analytes and the mutagenicity of appliance combustion samples have special significance in this study given the results described in Chapter 4. This analysis identified the nontarget analyte C6H3NO4 (dialdehyde) associated with increased mutagenicity in the original appliance tests and the nontarget analyte C2H5NO associated with increased mutagenicity in the stove retests.

Future Work

The high priority list of molecular features in Table 33 and Table 34 require further structural elucidation to determine whether they are possible causes of the observed bioactivity or if they are simply correlated with whatever the causative agent(s) turn out to be. argeted MS/MS experiments need to be performed to generate structural hypotheses so that authentic standards can be obtained to verify chromatographic retention times. Compounds that cannot be purchased will need to be assessed using retention index predictions of expected retention time for plausible isomers combined with in silico prediction of MS/MS fragmentation using Molecular Structure Correlator (Agilent, Inc.) and/or open source platforms such as CFM-ID (http://cfmid.wishartlab.com/) or MetFrag (http://c-ruttkies.github.io/MetFrag/). In cases where authentic standards can be obtained, add-back experiments can be conducted to prove that the chemicals obtained display the appropriate level and type of activity in the relevant bioassays. If ion signals are too small to obtain high quality MS/MS spectra, further concentration of samples would be required, followed by reanalysis.

CHAPTER 8:
Ultrafine Particle Analysis

Introduction

Ultrafine particles (UFPs) with aerodynamic diameter smaller than 0.1 µm ($PM_{0.1}$) are a subset of the fine (PM2.5) and coarse (PM10) airborne size fractions. Previous studies have linked UFPs with multiple human toxicity effects, possibly because these particles have a large surface area to volume ratio, which makes them very reactive. UFPs can also cross cell membranes, circulate in the blood, and translocate to different regions of the body (Brauner et al., 2007; Elder and Oberdorster, 2006). Previous studies have determined that natural gas and biogas combustion mainly emits particles in the UFP size range (Minutolo et al., 2010;Ozgen et al., 2017;Wallace et al., 2008). The changes in UFP emission rates and the health implications of switching from petroleum natural gas to biomethane are still unknown.

Here the research team studied UFP emissions from combustion sources fueled by petroleum natural gas, biomethane or biogas across the residential, commercial, and transportation sectors in California. Particle evaporation was studied under a range of dilution conditions to develop representative source specific emissions profiles that can be used in regional air quality models. The primary emissions from each source were characterized in a "photochemical chamber" so that they could be aged by UV radiation equivalent to roughly one summer daily cycle in California. The team also measured secondary organic aerosol formation in the exhaust of all outdoor sources. This research sought to determine if UFP concentrations are likely to change in response to the widespread adoption of biomethane and/or biogas as a renewable fuel in California.

Methods

Emission Tests

A description of the emission testing methods was presented in Section 3, so only methods specific UFP measurements are discussed here. An engine exhaust particle sizer (EEPS, TSI Model 3090) directly measured UFP number and size distributions with one-second resolution in the CVS used to dilute exhaust from the CNG-fueled van. The EEPS measured particles with mobility diameter varying from 5.6 to 560 nm for spherical particles with uniform density, or ~8 to ~150 nm aerodynamic diameter for fractal soot particles with density that changes with size. A SMPS system, consisting of a 85Kr diffusion charger, a differential mobility analyzer (TSI, Model 3080) and butanol-based condensation particle counter (CPC, TSI Model 3010 or 3775) were used to measure UFP number and size distributions from tests conducted using commercial power generators and home appliances (water heater and cooking stove). The SMPS was configured with aerosol and sheath flows equal to 1 and 7 L min^{-1}, respectively. The scan rate was set at two minutes (up scan of 90 seconds and down scan of 30 seconds), covering 99 size bins between 10.2 and 346 nm for spherical particles with uniform density, or ~13 to ~110 nm aerodynamic diameter for fractal soot particles. The TSI Aerosol Instrument

Manager, Version 8.0.0, was used to process the data and correct the diffusion loss and multiple changing. At least three size distribution scans were made during each test.

UFP Volatility

The research team used a range of dilution factors (DFs) to determine if semivolatile UFPs present in combustion exhaust near the emissions source will evaporate further downwind. DFs varying from 30 to 50 were explored to represent near-source conditions, while DFs between 500 and 8,000 were explored to represent far-downwind conditions. ear-source dilution conditions were achieved by mixing combustion exhaust with different amounts of primary dilution air. Far-downwind dilution conditions were achieved using a rotating disk thermodiluter (TSI, Model, 379020A) (Hueglin et al., 1997;TSI, 2018). Previous studies have shown that the rotating disk thermodiluter provides uniform dilution ratios for particles with diameter between 10 and 700 nm (Hueglin et al., 1997). The SMPS system with the 3775 CPC was used to measure particle-size distributions during all volatility tests.

Secondary UFPs Formation in Photochemical Chambers

Water heater, automobile, and engine generator exhaust was diluted and injected into the photochemical smog chamber to study likely atmospheric chemical reaction products. A surrogate VOC mixture designed to represent a typical urban atmosphere was injected alongside the combustion exhaust to promote realistic aging. The surrogate VOC consisted of 1.13 ppmv m-xylene and 3.29 ppmv n-hexane. These compounds have been used in previous studies to simulate urban atmospheres (Carter et al., 1995). The VOC surrogate mixed with the NO_x in the combustion exhaust to form a representative atmospheric mixture. The emissions were aged for three hours at 50 W m^{-2} of UV radiation, which is roughly equivalent to one photochemical daily cycle in California during the summer (Auguest-September). The final ozone concentration at the end of the chamber tests ranged between 76 ppb to 177 ppb, depending on the initial NO_x concentration. Only the tests with final ozone concentration measured between 110 ppb to 125 ppb was used for comparisons discussed in the current study. A SMPS system was used to measure the particle size distribution in every 30-60 minutes. Particle-wall loss was not included into the calculation because the research team assumed that the effects of wall losses would be similar for the CNG and biomethane tests, so they would not bias the comparison between the fuels.

ER_{PN} and ER_{PM}

UFPs emissions are reported as fuel-based emission rates of particle number (*ER_{PN}*, # kg^{-1}-fuel) and particle mass (*ER_{PM}*, g kg^{-1}-fuel). For the vehicle and home appliance tests that measured CO_2 concentrations, *ER_{PN}* and *ER_{PM}* were calculated based on mass balance of carbon content in the fuels (May et al., 2013c), as

$$ER_{PN} = \frac{PN}{\Delta CO_2} f_{carbon} \quad \text{(Eq.2)} \qquad ER_{PM} = \frac{PM}{\Delta CO_2} f_{carbon} \quad \text{(Eq.3)}$$

where *ΔCO_2* represents the background corrected CO_2 concentration, in g-carbon cm^{-3}; *f_{carbon}* represents the carbon fraction of the fuels, in g-carbon kg^{-1}-fuel; *PN* and *PM* are total particle number and mass concentration in the exhaust, in # cm^{-3} and g cm^{-3}, respectively. *PM* was

obtained by multiplying the particle volume concentration measured by the SMPS with the size-dependent particle-effective densities using the equation as below,

$$M_{ipsd} = \sum_i \rho_{eff,i} \cdot \left(\frac{\pi D_{p,i}^3}{6} \right) \cdot n_i \quad \text{(Eq. 4)}$$

where $D_{p,i}$, n_i and $\rho_{eff,i}$ are the particle mobility diameter (cm), particle number concentration (# cm^{-3}) and the effective density of the particles in size bin i (g cm^{-3}), respectively. In this study, a constant effective density of 1.46 g cm^{-3} was used for particles with mobility diameters ≤30 nm, which is the density of hydrated sulfuric acid at room temperature (Zheng et al., 2012). For particles larger than 30 nm, the effective density profile reported by Maricq and Xu was applied (Maricq and Xu, 2004). The research team used EEPS measurements to calculate ER_{PN} and ER_{PM} for mobile source particles with mobility diameter between 10.8 and 340 nm, while SMPS measurements were used to calculate ER_{PN} and ER_{PM} for particles emitted from other sources with mobility diameter between 10.2 and 346 nm.

For the engine-generator tests during which CO_2 wasn't measured, ER_{PN} and ER_{PM} were calculated as,

$$ER_{PN}(orER_{PM}) = \frac{PN(orPM) \times DF}{(R_{air-fuel)} + 1) * D_{fuel}} * 1000 \quad \text{(Eq.5)}$$

where $R_{air\text{-}fuel}$ is air-to-fuel ratio and D_{fuel} is the density of the fuel at 25°C and 1 atm, in g cm^{-3}. A summary of the fuel density calculation is presented in Table 35.

Table 35: Major Composition of the CNG, Biogas and Biomethane

Fuel	Supply/Source	N_2/CO (%)	O_2/Argon (%)	Methane (%)	CO_2 (%)	Sulfur compounds (ppm)	Density (g L^{-1}, 25C 1atm)
CNG	Commercial CNG	1.8	0.4	91.5	0.8	1.1	0.656[2]
CNG	Pipeline CNG					0.5	0.656
Biogas	Van Warmerdam	7.9	5.8	70.5	15.8	0.8	0.96
	New Hope	22.1	10.5	47.4	20	44.6	1.13
	Kiefer	37.6	8.8	35.4	18.2	5.6(core) 2.4(Perimeter)	1.19
	SATS	6.9	6.7	58.8	27.7	135.3	1.12
Biomethane	New Hope	4.1	3.0	89.5	3.4	0.6	0.656
	READ	2.1	2.9	91.5	3.5	2.6	0.656
	SATs	3.8	0.7	93.4	2.1	1.8	0.656

Source: University of California, Davis

Measurements of apparent ER_{PN} and ER_{PM} during blank tests were subtracted from all profiles measured during actual tests. The blank measurements followed the standard experimental protocol but did not include emissions from the combustion source. The measurement detection limit (MDL) is defined as average±2 times standard deviation of the measurement with blanks. Values lower than MDL were set to zero.

Results

Near-Source UFP Emissions

Figure 57 shows the fuel-based particle size distributions (PSDs) emitted from various applications under typical source test dilutions (i.e. *DFs*=13-50). The overall UFPs emission rates (ER_{PN} and ER_{PM}) are compared in Figure 58 and detailed in Table 35. For the automobile tests, the vertical error bars represent two standard deviations (confidence level of ~95%) of averaged PSD measurement over two or three UC cycles. For the cooking stove tests, the error bars represent two standard deviations of averaged PSD measurement during over two or three tests. For the water heater tests, the error bars represent two standard deviations of PSDs measured during the first tests of the day. For tests with engine-generators, the error bars represent two standard deviations of measurement during three SMPS scans over a single test.

Vehicle Exhaust

The CNG-powered van was tested with three fuels: (i) commercial CNG, (ii) a mixture of 27.8% CNG and 72.2% SATS biomethane (denoted as SATS in Figure 57a), and (iii) a mixture of 7.7% CNG, 34.4% SATS biomethane, 33.5% READ biomethane, and 24.4% New Hope biomethane (denoted as "mixed" in Figure 57a). Figure 57a shows PSDs from the vehicle exhaust exhibited trimodal size distributions for all fuels, including a wide accumulation mode with a geometric mean diameter (GMD) near 20 nm, a larger nucleation mode with a GMD of ~10 nm, and a smaller nucleation mode with GMD below 5.6 nm. The smaller nucleation mode particles were previously identified by Minutolo et al. (Minutolo et al., 2008; Minutolo et al., 2010) and D'Anan (D'Anna, 2009), who described them as *molecular particle precursors*. The larger nucleation mode particles are likely *soot particles* formed through the physical coagulation of the smaller particles (D'Anna, 2009; Wallace et al., 2008). The nucleation mode particles dominated the overall particle number concentration, while the accumulation mode particles accounted for ≥95% of the UFP mass. Concentrations of accumulation mode particles > 20nm were significantly higher in the vehicle tests than in other sources. Previous studies have shown that accumulation mode particles from vehicles are a combination of motor oil and soot agglomerates formed through incomplete combustion of fuel hydrocarbons (Vaaraslahti et al., 2004). CNG and biomethane are simple fuels composed mostly of methane that are not expected to contribute significantly to accumulation mode particles (D'Anna, 2009; Wagner et al., 2010). It is likely that the accumulation mode particles measured in the CNG/biomethane vehicle exhaust tests originated from motor oil. The *molecular particle precursors* were not detected during the tests of other sources because the instrument (SMPS with long DMA) did not cover the smaller size bins.

The research team found no significant variation among three tested fuels for either PSDs or ER_{PN}/ER_{PM} at a confidential level of 95%, as shown by the overlapping error bars in Figure 57a and Figure 58. This finding suggests that biomethane use by automobiles will not statistically alter primary UFPs emission relative to equivalent utilization of natural gas.

Home Appliances

The research team tested home appliances separately with commercial CNG, SATS biomethane, READ biomethane, and New Hope biomethane. Figure 57b, and Figure 57c show

that UFP emissions from the home appliances generally had a unimodal PSD irrespective of fuel type, with a nucleation mode at particle diameter <10 nm. These measurements are consistent with the PSDs reported by Wallace et al. (Wallace et al., 2008), who showed UFPs emitted from natural gas stove peaked at ~5.3 nm using a nano-DMA (TSI Model 3085).

Previous emission tests have shown that the nucleation mode particles emitted from home appliances using CNG contain mainly carbonaceous compounds, such as PAHs and oxygenated-PAHs (D'Anna, 2009;Rogge et al., 1993;Wagner et al., 2010). The presence of the sulfur in the fuel has the potential to increase or decrease net particle emission, depending on competing effects for different chemical components in the particles (Wagner et al., 2010; Glarborg, 2007). Most of the sulfur in the fuel oxidized to form gas-phase SO_2, with a small fraction forming sulfuric acid that increased particle emissions. SO_2 in the flame can oxidize soot particles, leading to a reduction in particle emissions (Lawton, 1989; Wagner et al., 2010; Gulder, 1993). UFP emissions rates in the current appliance tests summarized in Figure 57b and c, and Figure 58 generally follow a pattern with higher ER_{PN} and ER_{PM} associated with higher fuel sulfur content. Generally speaking, appliance ER_{PN} and ER_{PM} are higher for READ biomethane (sulfur content=2.8 ppm) and SATS biomethane (sulfur content=2.4 ppm) and lower for pipeline CNG (sulfur content=0.5 ppm) and NH Dairy biomethane (sulfur content=0.8 ppm). For the cooking stove tests, READ biomethane ER_{PN} and ER_{PM} were significantly higher than emissions rates corresponding to other fuels (confidence level of 95%; $p<0.05$). For the water heater tests, READ biomethane ER_{PN} and SATS biomethane ER_{PN} were significantly higher than pipeline CNG ER_{PN} ($p<0.05$). For other pairs of comparison, the differences were not significant at confidence level of 95%.

Residential exposure to UFPs can be very important since the average American spends 87% of his or her life indoors (Minutolo et al., 2010;Bhangar et al., 2011). ENREF 23 Previous studies have identified cooking as the largest UFP source in the indoor environment (Dennekamp et al., 2001; Long et al., 2001; Wallace et al., 2004). A survey by U.S. Census Bureau indicated 40% of U.S. homes are equipped with gas stoves (AHS, 2005). For the test conditions used in this study (fuel consumption rate = ~9 L min^{-1}, *DF*=31-37), *PN* and *PM* measured in the cooking stove exhaust fueled with READ biomethane were $1.54\pm0.15\times10^5$ # cm^{-3} and 0.31 ± 0.08 µg m^{-3}. These PN and PM emissions rates are 83 and 24 times higher ($p<0.05$) than *PN* and *PM* measured during comparable CNG tests. SATS and New Hope biomethane did not have higher stove emissions rates than pipeline CNG ($p>0.05$). These results suggest sulfur pretreatment should be used to remove sulfur from biomethane to avoid increasing UFP emissions from natural gas home appliances.

Previous studies found that the indoor nanoparticle concentrations produced by a domestic gas cooker varied from 10^3 to 10^6 # cm^{-3} based on the type of fuels, fuel consumption rates and the primary air addition (Wagner et al., 2010). The raw particle concentration measured in the current study using the cooking stove and water heater (10^3 to 10^5 # cm^{-3}) falls into this range.

Engine-Generators

The research team tested engine-generators at each biogas combustion site directly with locally produced biogas since it was impractical to retune the engines to operate using other

fuels. Test results therefore represent differences in the composition of the local biogas and the technology employed by the engine-generators.

Figure 57(d) and Figure 58 indicate that UFPs measured with four engine-generators can be divided into a high emissions category and a low emissions category. The *PN* measured in the exhaust of the Kiefer and the Van Warmerdam Dairy engine-generator were 210 and 331 times higher than the PN that measured in ambient air. UFPs from the higher emission sources exhibited a strong nucleation mode with a GMD of 22 or 27 nm. In contrast, the *PN* measured in the exhaust from the SATS and the NH Dairy engine-generators were at or below the *PN* measured in ambient air. Nucleation mode particles emitted from engine-generators had a larger GMD than nucleation mode particles emitted from automobile and home appliance tests, possibly due to coagulation of the smaller particles in the transfer lines. The overall retention time was 1-3 minutes.

To the team's best knowledge, this study is the first to report UFP particle emissions from engine-generators fueled with biogas. Similar variability had been reported in previous studies of UFP emissions from generators fueled by natural gas. For example, Brewer et al. measured UFP emission from a natural gas turbine and showed that overall PN in the exhaust were ~690 higher than those in the ambient air (Brewer et al., 2016). In contrast, Klippel et al. reported particles emitted from a modern natural gas turbine that was designed for "low emission levels" could be one order of magnitude lower than particles in the ambient air, which made the turbine a particle sink rather than a particle source (Klippel et al., 2002; Klippel et al., 2004).

Similar to mobile source tests, ER_{PN} and ER_{PM} trends from engine-generator exhaust did not follow the pattern of fuel sulfur content. It is likely that the observed variability was related to the technology used in the combustion systems rather than the composition of the fuel. Both of the lower-emitting generators were produced by Motoren-Werke Mannheim® and modified by 2G®. These systems were not equipped with particle filtration devices, so it appears that the engine design and engine tuning achieved the low emission rates observed.

No measurements were made for emissions from engines-generators powered by natural gas in this study. However, Table 36 to Table 38 show that ER_{PN} and ER_{PM} from the higher-emitting generators were one order of magnitude higher than ER_{PN} and ER_{PM} of the tested vehicle powered by CNG ($p<0.05$), while ER_{PN} and ER_{PM} of the lower engines-generator sources were two orders of magnitude lower than ER_{PN} and ER_{PM} of the tested vehicle powered by CNG ($p<0.05$). This wide range of results indicates that lightly upgraded biogas used directly on-site for electricity generation has the potential to emit very few UFPs. The NO_x and SO_x emissions from these sources may still contribute to nitrate and sulfate formation in the PM2.5 size fraction, however. Detailed modeling of scenarios is needed to understand how and where biogas can be appropriately used for electricity production.

Figure 57: Particle Size Distribution (PSDs) Measured From Different Emission Sources Burning CNG, Biogas or Biomethane

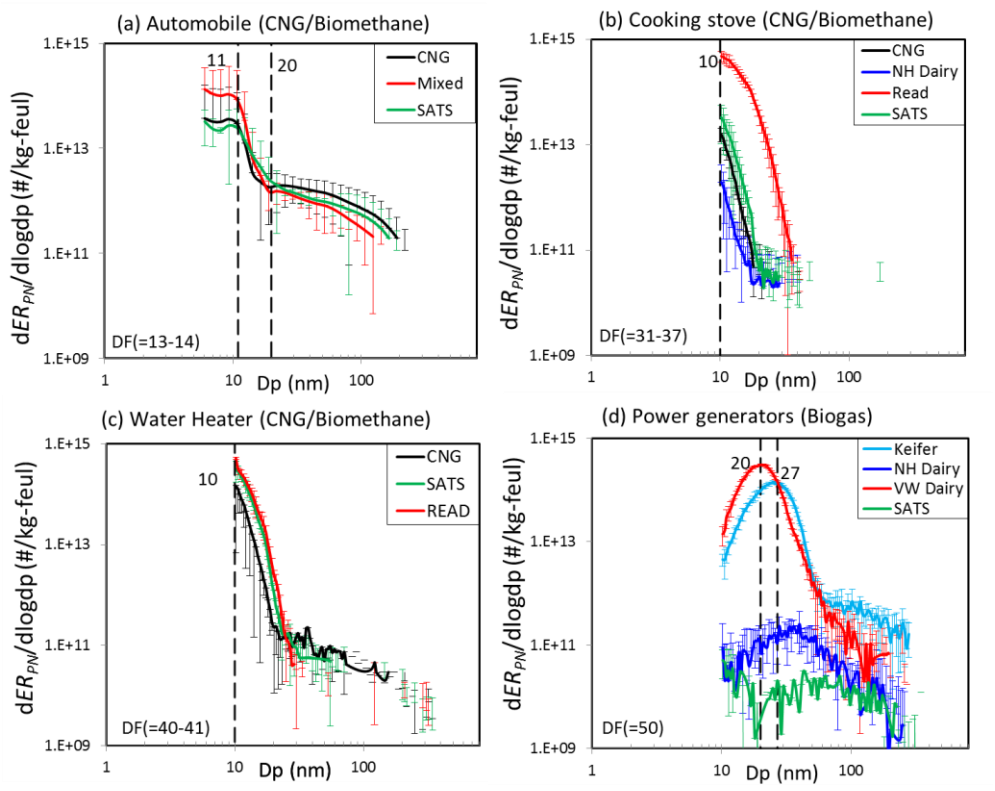

The emissions were corrected for background. Error bars represent two times standard deviation.

Source: University of California, Davis

Figure 58: Particle Number and Mass Emission Rates (ER_{PN} and ER_{PM}) Measured at Typical Source Tests *DF* (=13-50) Using CNG, Biomethane or Biogas

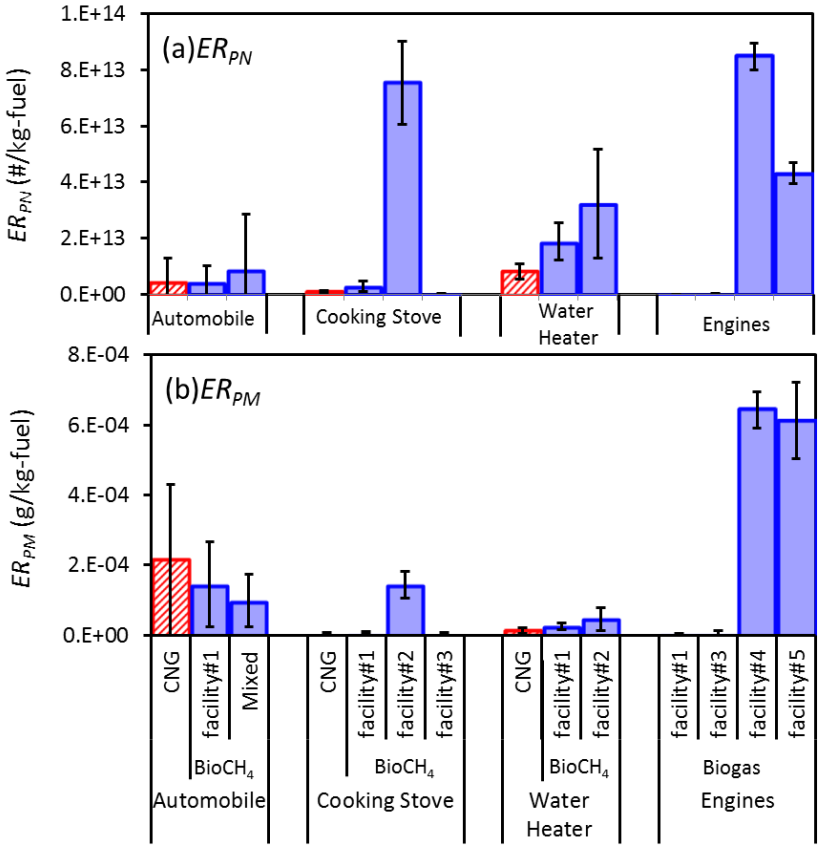

Data were corrected for background. Error bars represent two times standard deviation. Facility 1=SATS, facility 2=READ, facility 3=NH Dairy, facility 4=VW Dairy, facility 5=Kiefer.

Source: University of California, Davis

Table 36: PN and PM Measured From Different Sources Using Natural Gas, Biogas, or Biomethane: Section 1

Section 1: Exhaust rates at typical source test *DF*			*DF*	ER_{PN}(#/kg-fuel)	ER_{PM}(g/kg-fuel)
Automobile	commercial CNG		13-14	4.3E+12 ± 8.7E+12	2.2E-04 ± 2.2E-04
	Biomethane	SATS		4.3E+12 ± 6.0E+12	1.5E-04 ± 1.2E-04
		Mixed		8.7E+12 ± 2.0E+13	1.0E-04 ± 7.7E-05
Cooking Stove	pipeline CNG		31-37	1.0E+12 ± 3.5E+11	0.0E+00 ± 8.5E-06
	Biomethane	SATS		2.9E+12 ± 1.9E+12	7.8E-06 ± 3.3E-06
		READ		7.5E+13 ± 1.5E+13	2.2E-04 ± 5.6E-05
		NH Dairy		1.3E+11 ± 1.5E+11	0.0E+00 ± 6.5E-06
Water Heater	pipeline CNG		40-41	8.1E+12 ± 2.9E+12	2.0E-05 ± 1.1E-05
	Biomethane	SATS		1.9E+13 ± 6.7E+12	3.9E-05 ± 1.6E-05
		READ		3.2E+13 ± 1.9E+13	7.2E-05 ± 5.1E-05
Engines/turbine	Biogas	SATS	50	2.0E+10 ± 2.3E+10	2.2E-06 ± 3.9E-06
		NH Dairy		9.3E+10 ± 8.6E+10	5.3E-06 ± 8.5E-06
		VW Dairy		8.5E+13 ± 4.7E+12	9.5E-04 ± 6.5E-05
		Keifer		4.3E+13 ± 3.6E+12	7.9E-04 ± 1.2E-04

Uncertainty represents two times standard deviation

Source: University of California, Davis

Table 37: PN and PM Measured From Different Sources Using Natural Gas, Biogas, or Biomethane: Section 2

Section 2: Volatility			*DF*	ER_{PN}(#/kg-fuel)	ER_{PM}(g/kg-fuel)
Cooking Stove	pipeline CNG		56	1.3E+12 ± 1.6E+11	3.1E-06 ± 5.4E-07
			6972	5.4E+11 ± 3.7E+11	1.3E-06 ± 1.0E-06
	Biomethane	SATS	63	1.2E+13 ± 7.2E+12	2.6E-05 ± 2.0E-06
			7844	4.5E+12 ± 2.6E+12	1.0E-05 ± 6.6E-06
Water Heater	pipeline CNG		26	9.5E+12 ± 1.9E+12	3.1E-05 ± 6.8E-06
			3237	2.8E+12 ± 6.4E+11	1.9E-05 ± 2.4E-06
	Biomethane	SATS	29	3.1E+13 ± 6.1E+12	2.1E-04 ± 2.7E-05
			3611	9.2E+12 ± 2.5E+12	4.8E-05 ± 3.8E-05
Engines	Biogas	VW Dairy	50	8.5E+13 ± 4.7E+12	9.5E-04 ± 6.5E-05
			500	7.5E+14 ± 7.4E+12	4.6E-04 ± 7.2E-05
		Keifer	50	4.3E+13 ± 3.6E+12	7.9E-04 ± 1.2E-04
			500	1.2E+14 ± 5.5E+12	2.7E-03 ± 8.6E-05

Uncertainty represents two times standard deviation

Source: University of California, Davis

Table 38: PN and PM Measured From Different Sources Using Natural Gas, Biogas, or Biomethane: Section 3

Section 3: Photo reactive chamber		*DF*	PN(#/kg-fuel)	PM(g/kg-fuel)
Automobile	commercial CNG (0h)	50	1.1E+03 ± 2.5E+03	2.0E-04 ± 4.4E-04
	commercial CNG(2h)	50	5.8E+04 ± 5.5E+03	1.1E-02 ± 1.1E-03
	SATS Biomethane (0h)	50	1.5E+03 ± 3.0E+03	1.8E-04 ± 4.0E-04
	SATS Biomethane (2h)	50	6.0E+04 ± 5.0E+03	8.7E-03 ± 8.5E-04
Water Heater	pipeline CNG (0h)	850	1.6E+01 ± 2.4E+01	6.9E-04 ± 1.9E-03
	pipeline CNG (3h)	850	2.4E+02 ± 9.2E+01	9.4E-03 ± 5.0E-03
	READ Biomethane (0h)	850	5.9E+00 ± 1.3E+01	1.7E-04 ± 4.2E-04
	READ Biomethane (3h)	850	3.1E+02 ± 1.1E+02	1.3E-02 ± 4.6E-03
	NH Dairy Biomethane (0h)	850	4.6E+00 ± 1.1E+01	5.3E-04 ± 1.7E-03
	NH Dairy Biomethane (3h)	850	9.2E+02 ± 2.0E+02	2.9E-02 ± 6.7E-03

Uncertainty represents two times standard deviation

Source: University of California, Davis

UFP Volatility

Numerous studies have shown that primary particles emitted from multiple sources, e.g. wood burning, diesel exhaust, and motor oil, are semivolatile. More than half of the primary particles mass measured under low dilution conditions (concentrated) can evaporate into the gas phase when the exhaust is further diluted in the atmosphere (Kuwayama et al., 2015; May et al., 2013a; May et al., 2013b, c; May et al., 2012). Therefore, it is important to estimate dilution-driven changes in gas-particle partitioning to update emission inventories and simulate UFPs from biogas and biomethane with a chemical transport model (May et al., 2013a; May et al., 2013b, c). Figure 59 shows the fuel-consumption-based PSDs measured with cooking stove, water heater, and engine-generator sources at higher and lower dilution levels, with *DF* varying from ~40 to ~8,000. The overall UFPs emission rates (ER_{PN} and ER_{PM}) are compared in Figure 60 and detailed in Table 35.

The observed change in PSDs in Figure 60(a-e) directly demonstrates that most of the UFPs emitted from the cooking stove and the water heater were semivolatile. Between 58% and 70% of the UPF number observed at the lower *DF* evaporated under the higher *DF*. Likewise, between 60% and 80% of the UPF mass evaporated under higher *DF*.

In contrast, UFP emissions from the high-emitting engine-generators were constant or even increased at the higher dilution factors, indicating that these particles are not semivolatile. Nucleation mode particles were historically considered to be liquid and semivolatile (Kittelson et al., 2006), but new transmission electron microscopy (TEM) measurements found residual nonvolatile materials in the nucleation mode particles generated by premixed hydrocarbon flames (Maricq, 2006; De Filippo and Maricq, 2008; Dobbins, 2007). The current measurements are consistent with the results from these previous studies, showing that a fraction of the UFPs produced by the combustion of natural gas/biomethane/biogas applications are solid and nonvolatile. These particles can contribute to ambient particle number concentrations even after extensive dilution in the atmosphere.

Despite the large differences caused by engine technology, all the engine-generators tested in the current study are clean relative to other potential combustion sources. For example, PM mass emitted from the engine-generator sources (~2×10^{-5} g MJ^{-1}) was 4-5 orders of magnitude lower than emissions from biomass burning (0.2-4 g MJ^{-1}), which is the next most likely source of renewable fuel. PM mass emitted from engine-generator sources was comparable to the lowest emission levels attributed to vehicles operated with gasoline or diesel (4-20×10^{-5} g MJ^{-1}).

Figure 59: Particle Size Distribution Under Lower and Higher Dilution Conditions

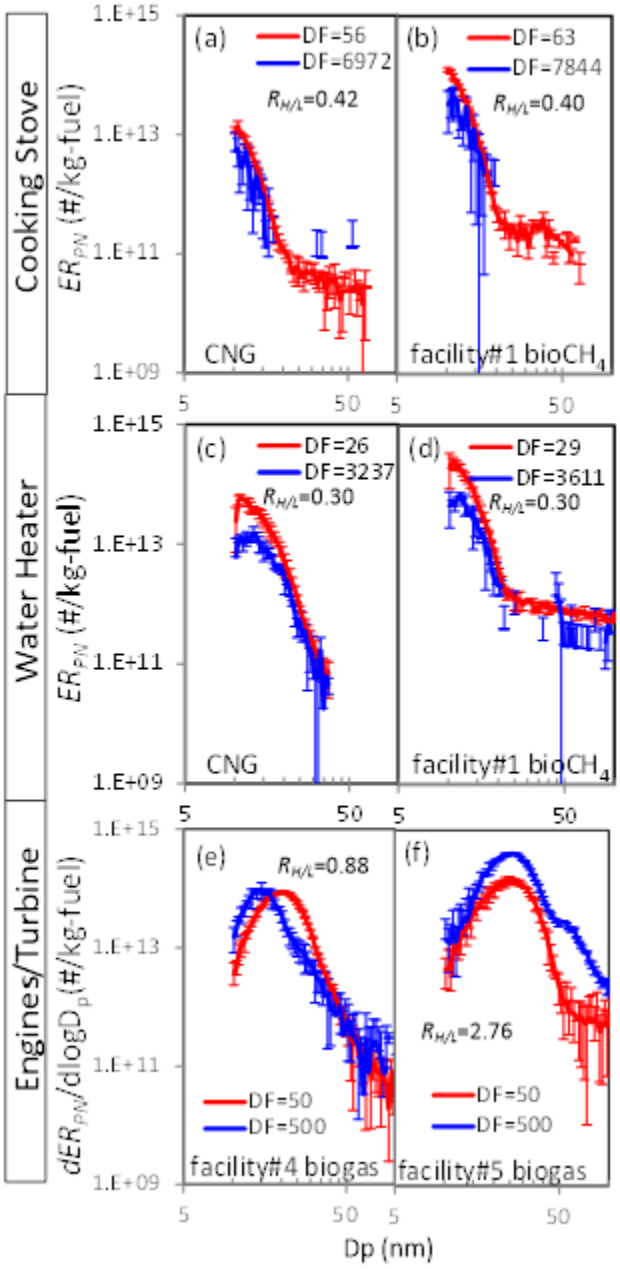

Data were corrected for background. Error bars represent two times standard deviation. Facility 1=SATS, facility 2=READ, facility 3=NH Dairy, facility 4=VW Dairy, facility 5=Kiefer.

Source: University of California, Davis

Figure 60: Particle Emission Rates Measured Under Lower and Higher Dilution Conditions

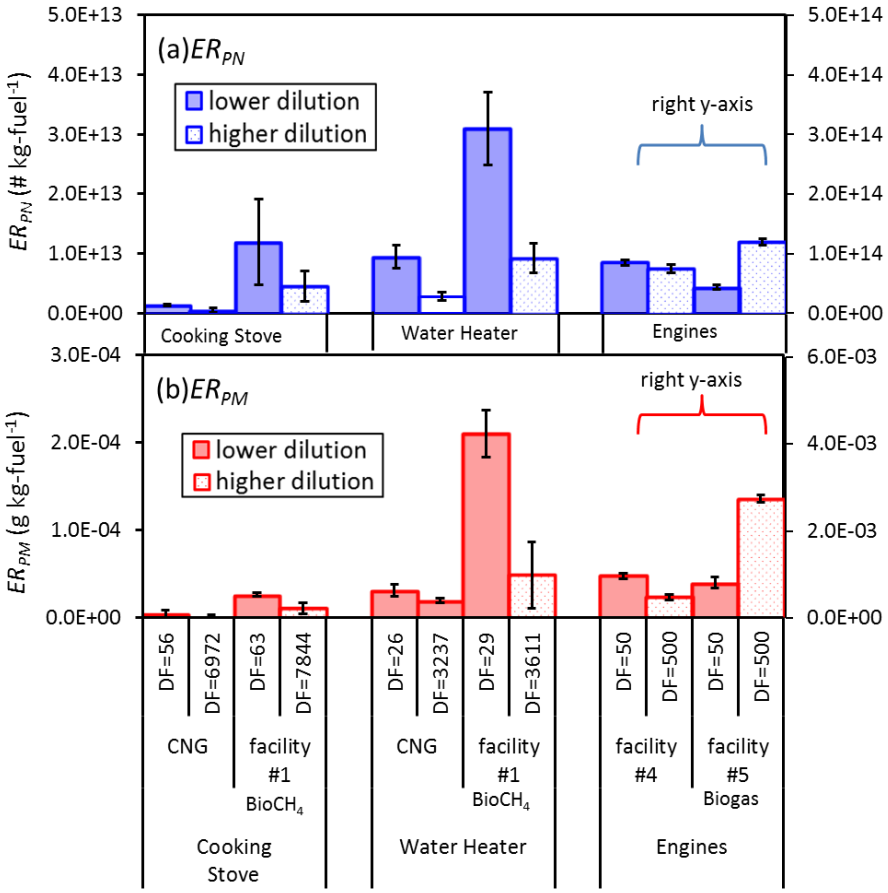

Data were corrected for background. Error bars represent two times standard deviation. Facility 1=SATS, facility 2=READ, facility 3=NH Dairy, facility 4=VW Dairy, facility 5=Kiefer. Source: University of California, Davis

UFP photochemical aging

Photochemical chambers have been widely used to study the evolution of primary exhaust (Bian et al., 2017). Figure 61 shows the development of UFP size distribution under UV radiation with VOC surrogate with and without the vehicle or water heater exhaust. The left panels of Figure 61 illustrate the fresh combustion PSD while the right panels of Figure 61 illustrate the PSD after 2 hrs of photochemical aging.

The strongest feature apparent in Figure 61 is the development of a large mode in the automobile exhaust distribution at 55 nm after 2 hrs of aging. This mode did not develop in separate tests that used only the background surrogate VOC and injected NO. The most likely source of the particle-phase material in this mode is the reaction of gas-phase semi-volatile motor oil that forms products with lower volatility that condenses onto the surface area of the primary particle emissions. It is noteworthy that the primary UFP mode at 10 nm is not influenced by this process, but the primary UFP mode at 31 nm appears to be strongly influenced by the condensation of the semi-volatile material. There were no significant differences in behavior due to the use of CNG vs. biomethane during these tests, further confirming that the condensing material was not associated with the combustion fuel.

The lower panels of Figure 61 illustrate that water heater exhaust does not significantly contribute to SOA formation after photochemical aging for 3 hrs in the Teflon reaction chamber. The PSD associated generated by the surrogate VOC plus injected NOx was similar to the aged PSD generated burning various types of CNG and biomethane. These findings suggest that biomethane combustion from home appliances will likely not make significant contributions to secondary organic aerosol formation.

Figure 61: Development of PSDs under UV Radiation with VOC Surrogate and VOC Surrogate Mixed with Vehicle or Water Heater Exhaust

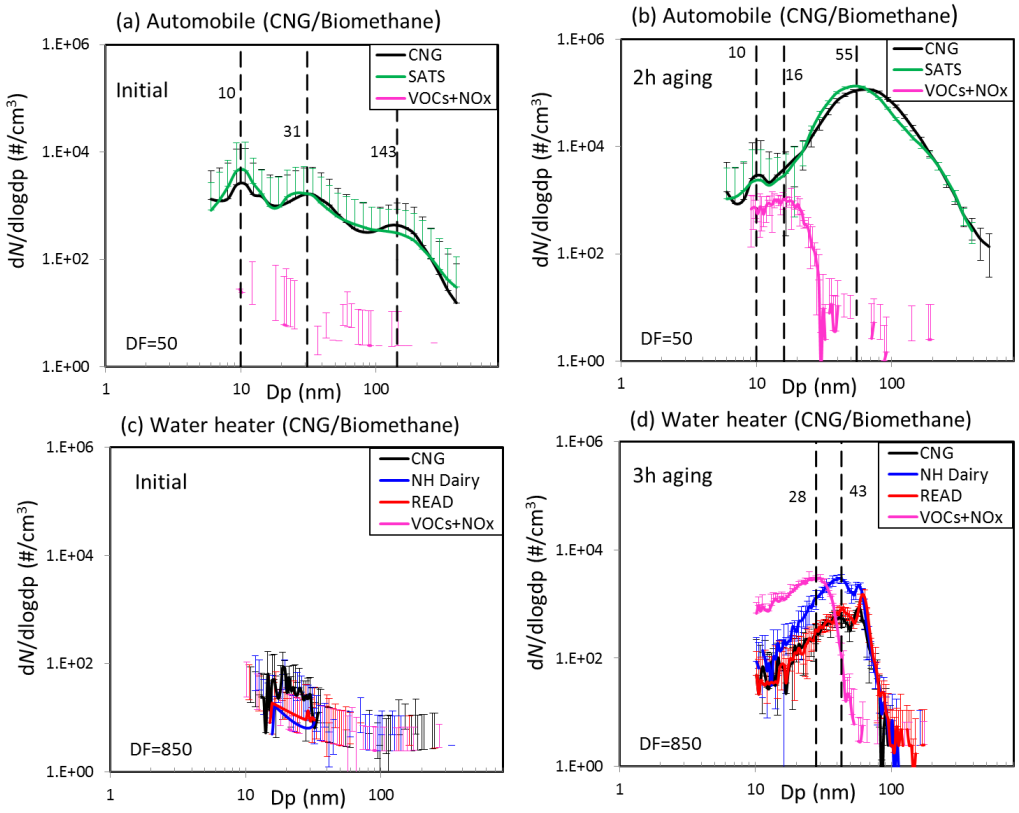

Source: University of California, Davis

Conclusions

A series of tests were conducted to investigate the impact of replacing natural gas with biogas and biomethane on ultrafine particle (UFP) emissions in California. Multiple application sectors were tested including motor vehicle, cooking stove, water heater, and engines for power generation. The results indicate that UFP emissions from petroleum natural gas and biomethane are very similar. Higher concentrations of impurities such as sulfur-containing compounds enhance UFP emissions but pre-treatment of biogas to remove these compounds can mitigate this effect in the downstream biomethane.

Measurements carried out over a range of dilution factors show that UFPs emitted from CNG/biomethane combustion in home appliances are semi-volatile causing them to partially evaporate when they are diluted with large amounts of clean air. In contrast, UFPs emitted from CNG/biomethane combustion in mobile sources and biogas combustion in stationary

power generation sources did not evaporate when diluted. UFPs emitted from these biogas and biomethane applications will contribute to regional UFP concentrations.

Tests conducted using photochemical smog chambers indicate that little secondary organic aerosol (SOA) is produced from the combustion exhaust of biogas and biomethane that is aged in a representative urban atmosphere. Mobile sources operating on CNG/biomethane did display significant SOA formation but this was caused by the semi-volatile motor oil used in the vehicle, not by the fuel.

CHAPTER 9:
Preliminary Modeling of Regional Biogas Scenarios

Introduction

Preliminary regional modeling simulations were conducted to predict the air quality impacts of various biogas and biomethane adoption strategies on air quality in California during the year 2054. This preliminary analysis focuses on the potential public health impacts attributable to wide scale utilization of landfill biogas in California. Landfill gas production in California is projected into the future (July 2054) under a Business as Usual (BAU) scenario and the air quality impacts are analyzed using Gaussian plume and Eulerian reactive chemical transport models, respectively. Ground level concentrations of nano-particles, PM2.5 mass, and PM2.5 nitrates, sulfates, elemental carbon (EC), and organic carbon (OC) are predicted with and without extensive adoption of biogas. Gas-phase pollutant concentrations for ozone, oxides of nitrogen, and ammonia are also predicted. This preliminary modelling study presents an initial review of the potential public health impacts associated with the increase in exposure due to exhaust from extensive biogas combustion.

Methods

Presently there are 652 operational landfills (2163 MW capacity) in the U.S. with 81 of these (380 MW capacity) in California. ENREF 17 Out of these 81 operational landfills, 53 have a capacity greater than 2.5 million tons yr^{-1} which subjects them to the US EPA regulations requiring open flaring or other utilization of LFG to prevent direct release to the atmosphere. The location of existing operational landfills generating wastes above the threshold limit are mapped as shown in Figure 62. Almost 75% of the operational landfills in California use LFG for electricity generation either through micro turbines or reciprocating engines when compared to other applications of LFG. In the present study, it is assumed that the 53 landfills with capacity greater than 2.5 million tons yr^{-1} will all utilize their LFG for electricity production.

Figure 62: Location of Operational Landfills in California 2016

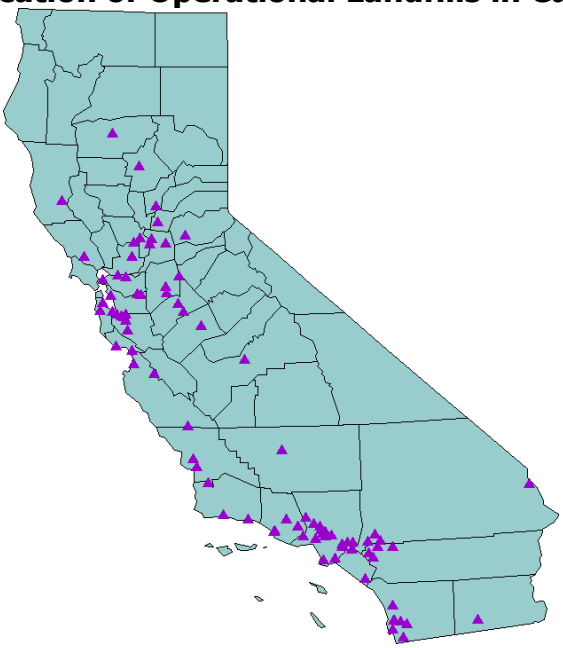

Source: University of California, Davis

Ozone and airborne particles with aerodynamic diameter < 2.5 μm ($PM_{2.5}$) are associated with multiple adverse health effects including cardio vascular mortality, decreased respiratory function, low birth weight and birth defects (Dockery, 2001;Langrish et al., 2012;Willers et al., 2013;Beelen et al., 2008;Laurent et al., 2013). Ozone and $PM_{2.5}$ may be released directly by LFG combustion or they may form through the atmospheric chemical reaction of LFG combustion emissions. H_2S in biogas is converted to SO_2 during the combustion process. SO_2 emitted from LFG combustion reacts to form sulfuric acid which condenses and contributes to $PM_{2.5}$ mass concentrations in the atmosphere. Volatile organic compounds (VOCs) contained in LFG combustion react with oxides of nitrogen (NOx) to produce ozone and particle-phase nitrate which once again increase $PM_{2.5}$ mass. In 2012, NOx emissions from bioelectricity production contributed about 2.1% of total state wide emissions (2162 tons day^{-1}). However, it is projected that by 2020, NOx emissions from bioelectricity production will increase to 10% of total state wide emissions assuming maximum technical potential of bioelectricity production is achieved. This increased level of emissions has the potential to increase ozone and $PM_{2.5}$ concentrations (Carreras-Sospedra et al., 2016).

LFG combustion also contains trace species that can potentially impact public health. As one example, LFG is known to contain siloxanes which produce silicon dioxide (SiO_2) nanoparticles when burned. The exact size of the SiO_2 nanoparticles in the exhaust depends on the flame temperature and air-fuel mixing ratio with typical values ranging from 40-70 nm in diameter (Berrin Tansel, 2014). Multiple studies have demonstrated that high concentrations of nanoparticles are toxic and therefore SiO_2 nanoparticles potentially pose a public health concern.

Sulfate formation

Hydrogen sulfide (H_2S) is the major sulfur compound present in LFG. H_2S oxidizes during combustion to form SO_2 as shown in Eqn (9-1).

$$2H2S + 3O2 \rightarrow 2H2O + 2SO2 \quad (9\text{-}1)$$

The SO_2 (S (IV)) formed from reaction (9-1) oxidizes to H_2SO_4 (S (VI)) in the atmosphere through any of three major pathways in the aqueous phase based on reaction with either O_3 or H_2O_2 or O_2 catalyzed by metals. Typical conversation rates from SO_2 to H_2SO_4 aerosol are 1-10% hr^{-1} depending on ambient conditions. It is assumed that all H_2S present in the LFG is oxidized to H_2SO_4 in the present study.

Siloxanes

Siloxanes are man-made organic compounds containing Si-O bonds that are widely used in personal care, cosmetic, electronic and industrial products(Raf Dewil a, 2006;McBean, 2008).

Figure 63: Siloxane Functional Group Present in Larger Molecule

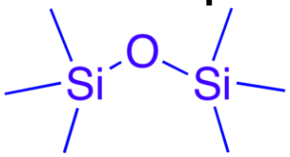

Source: University of California, Davis

Siloxanes are semi-volatile and generally present in LFG yielding undesirable products when they are burned. Siloxane combustion products include solid SiO_2 and other silicate particles that can foul engine equipment or cause nanotoxicity during exposure (Raf Dewil a, 2006;Berrin Tansel, 2014).

$$Siloxanes + O2 \rightarrow SiO2 + Silicates \quad (9\text{-}2)$$

Commonly used siloxanes found in landfills include octamethylcyclotetrasiloxane (4 SiO bonds, aka D4) and decamethylcyclopentasiloxane (5 SiO bonds, aka D5) (L.Pierce, 2005;Berrin Tansel, 2014). The combustion products of these compounds are given in Eqn (9-3) and (9-4). Hence in this report, emission analysis of siloxanes is limited to only these two compounds.

$$D4 + 16O2 \rightarrow 4SiO2 + 8CO2 + 12H2O \quad (9\text{-}3)$$

$$D5 + 20O2 \rightarrow 5SiO2 + 10CO2 + 15H2O \quad (9\text{-}4)$$

Gaussian Plume Modelling

Gaussian plume models predict the ensemble-average concentration field downwind of an emissions source accounting for dilution caused primarily by turbulent mixing. Ground level concentrations downwind of the pollutant release point are influenced by the emissions rate, wind speed, atmospheric stability, solar radiation, and degree of chemical reaction. Well known solutions to this problem are available for multiple geometries that include perfectly reflecting surfaces, perfectly absorbing surfaces, elevated inversion layers, etc.

The Gaussian plume equation for ground-level emissions associated with an elevated release with a temperature inversion and a reflecting surface is:

$$C = \frac{Q}{\pi u \sigma_z \sigma_y} \exp\left(-\frac{1y^2}{2{\sigma_y}^2}\right)\left\{\exp\left(-\frac{1(H)^2}{2{\sigma_z}^2}\right)\right\} \quad (9\text{-}5)$$ (David Cooper, 2002)

Where C= steady state concentration of pollutant at point (x, y, z) in µg m^{-3}

- Q = emission rate in μg s^{-1}
- $б_y$, $б_z$ = horizontal and vertical spread parameters respectively
- $б_y = ax^b$
- $б_z = cx^d + f$ where a, b, c and d are curve fit constants taken from table 20.2, Air Pollution Control, by C. David Cooper and F.C. Alley. (David Cooper, 2002)
- u = average wind speed at stack height in m s^{-1}
- y = horizontal distance from plume center line
- z = vertical distance from ground level
- H = effective stack height (physical stack height (h) + plume rise (Δh)).

In the present study, hypothetical Gaussian plume scenarios were explored to determine the maximum ground level concentrations downwind of LFG combustion sources.

Eulerian Chemical Reactive Modelling

Eulerian chemical reactive models predict pollutant concentrations across an entire region accounting for emissions, transport, deposition, and chemical reaction. These models solve a coupled set of partial differential equations with the form:

$$\frac{\partial C_i}{\partial t} + \nabla \cdot uC_i = \nabla K \nabla C_i + E_i - S_i + R_i^{gas}(C) + R_i^{part}(C) + R_i^{phase}(C) \quad (9\text{-}7)$$

where C_i is the concentration of gas or particle phase species i at a particular location as a function of time t, u is the wind vector, K is the turbulent eddy diffusivity, E_i is the emissions rate, S_i is the loss rate, R_i^{gas} is the change in concentration due to gas-phase reactions, R_i^{part} is the change in concentration due to particle-phase reactions and R_i^{phase} is the change in concentration due to phase change.

The Eulerian source oriented University of California, Davis Davis/California Institute of Technology (UCD/CIT) chemical transport model was used for regional calculations in the current study (see for example (J. Hu, 2015)). LFG emissions corresponding to Figure 62 were specified on a Lambert Conformal projection consistent with standard emissions inventories developed by the California Air Resources Board. The LFG emissions were used within the business as usual emissions scenario for the year 2050 developed from the CA-TIMES economic optimization model (Zapata et al., 2018). Meteorological information was obtained for the year 2054 by downscaling global predictions from the Community Earth System Model (CESM) to 4km resolution using the Weather Research & Forecasting (WRF) model. The year 2054 was chosen as the median meteorology year within the range 2045-2055. The UCD/CIT air quality model was then used to predict changes in pollutant concentrations in response to the LFG emissions.

Results

Gaussian Plume Modelling

Ground level concentration of pollutants (here H2SO4 & SiO2) for each atmospheric stability class (A to F) were calculated using equation (9-5) with varying downwind distance 'x'. Sample calculations for ground level H2SO4 & SiO2 concentrations for stability class F are shown in Table 39 and Table 41, respectively. Calculations assume a stack height (H) of 20 feet based

on the existing landfill data. The maximum pollutant concentration obtained in each stability class is listed with corresponding downwind distance (x) as shown in Table 40 and Table 42. Based on the zoning regulations in California, it is unlikely that any residence would be located closer than 500 feet to a LFG combustion plant. Hence we consider the pollutant concentration at a downwind distance (x) of 500 feet as the reference concentration to analyze the potential public health impact. Incorporating all the factors mentioned above, maximum ground level concentrations are determined under the worst case scenario.

Ground Level H_2SO_4 Concentrations

The concentration of H_2S present in the LFG is taken as 0.45 ppmv, which is the average concentration of H_2S in four LFG samples collected during a comparative analysis study by Gas Technology Institute (2009). To calculate the maximum G.L H_2SO_4 concentration, it is assumed that all the H_2S present in the LFG is oxidized to SO_2 and then subsequently completely oxidized to H_2SO_4 i.e.

0.45 ppmv of SO_2 →18.404 μmoles SO_2 m^{-3} exhaust gas (At 298 Kelvin Temperature and 1 atm)
18.404 μmoles m^{-3} SO_2 in exhaust gas → 18.404 μmoles m^{-3} H_2SO_4 in exhaust gas

18.404 μmoles m^{-3} H_2SO_4 in exhaust gas→1803.6 μg m^{-3} H_2SO_4 in exhaust gas.
The concentration of 1803.6 μg m^{-3} is the maximum H_2SO_4 concentration that can be formed at the exit stack on combustion of LFG with 0.45 ppmv of H_2S. This instantaneous conversion assumption provides a worst-case scenario to determine if more detailed calculations are warranted.

Emission rate (Q) of H_2SO_4 of 902 μg sec^{-1} is obtained with an assumed exhaust gas flow rate of 0.5 m^3 s^{-1}. Ground level concentrations of H_2SO_4 (C) incorporating calculated emission rate and the factors mentioned earlier are listed in Table 39 and Table 40.

Table 39: Ground Level Pollutant Concentrations of H_2SO_4 at Varying Horizontal Distances when Released from Stack Height (H) of 20 Feet for Stable Class 'F' and Wind Speed u= 1 m s^{-1}

x (ft)	σy (m)	σz (m)	C (μg m^{-3})
100	1.500	0.734	0.000
200	2.788	1.460	0.012
300	4.006	2.094	0.494
400	5.181	2.674	1.541
500	6.325	3.217	2.342
600	7.445	3.732	2.721
700	8.545	4.225	2.808
800	9.628	4.700	2.736
1000	11.754	5.607	2.412
1500	16.889	7.691	1.614
2000	21.843	9.599	1.119
3000	31.386	13.081	0.627

Source: University of California, Davis

Table 40: Maximum G.L H_2SO_4 Concentration for Various Stability Classes with Stack Height (H) of 20 Feet and Wind Speed u= 1 m s^{-1}.

Stability class	Wind speed ($m\ s^{-1}$)	C max ($\mu g\ m^{-3}$)	x (ft)	C (@500 ft)
F (night clear sky)	1	2.808	700	2.342
F (night clear sky)	2	1.404	700	1.171
E (night cloudy)	1	3.076	400	2.925
D (night cloudy)	3	0.981	300	0.745
C (slight solar radiation)	2	1.559	200	0.579
B (slight solar radiation)	1	4.043	100	0.588
A (strong solar radiation)	1	2.573	100	0.335

Highlighted data shows the worst case scenario.

Source: University of California, Davis

From Table 40 it can be seen that atmospheric stability class 'B' during day time with slight solar radiation favors maximum formation of H_2SO_4. The maximum ground level H_2SO_4 concentration of 4.04 $\mu g\ m^{-3}$ is formed assuming a stack height (H) of 20 feet and wind speed u= 1 m s^{-1}. This concentration is sufficient to merit concern about public health impacts. Further analysis of PM2.5 is done using Eulerian chemical reactive modelling which considers the transport and the chemistry time scales of pollutants in the atmosphere.

Ground Level SiO_2 Concentrations

The average concentrations of D4 and D5 siloxane compounds in four LFG samples collected during a comparative analysis study by Gas Technology Institute (2009) were measured to be 3.45 ppmv and 1.1 ppmv, respectively. To analyze the worst case scenario, SiO2 formed due to combustion of both D4 and D5 siloxanes are considered. The combustion engine was assumed to have a power of 1 MW burning $19.5x10^6$ scf of biogas per month ($6.63x10^6\ m^3$ of LFG per year) (Berrin Tansel, 2014). Assuming 10% deposition of siloxanes on engine parts, SiO_2 yields on combustion of D4 and D5 siloxanes are calculated as follows.

- SiO2 produced for 1 mole of D4 burned, From Eqn (3)
  - = 3.45 x 4 = 13.8 ppmv of SiO2
  - = 564.377 µmole m^{-3} x 60.08 µg $\mu mole^{-1}$ x $6.63x10^6\ m^3\ yr^{-1}$ x 1 /(365*24*60*60) yr s^{-1}
  - = 7128.6 µg s^{-1}
- Similarly, SiO2 produced for 1 mole of D5 burned = 2841.1 µg s^{-1} From Eqn (4)
- Total SiO2 produced on LFG combustion = 7128.6 + 2841.1 = 9969.7 µg s^{-1}
- Assuming 10% deposition in the combustion chamber, SiO2 emitted
  - = 0.9* 9969.7 = 8972.8 µg s^{-1}.

The ground level SiO_2 concentrations (C) incorporating the calculated emission rate Q = 8972.8 µg s^{-1} and the factors mentioned earlier are listed in Table 41 and Table 42.

Table 41: Ground Level Pollutant Concentrations of SiO_2 at Varying Horizontal Distances when Released from Stack Height (H) of 20 Feet for Stable Class 'F' and Wind Speed u= 1 m s^{-1}.

x (ft)	σy (m)	σz (m)	C (µg m^{-3})
100	1.500	0.734	0.000
200	2.788	1.460	0.116
300	4.006	2.094	4.917
400	5.181	2.674	15.328
500	6.325	3.217	23.304
600	7.445	3.732	27.077
700	8.545	4.225	27.940
800	9.628	4.700	27.219
1000	11.754	5.607	24.000
1500	16.889	7.691	16.061
2000	21.843	9.599	11.135
3000	31.386	13.081	6.241

Source: University of California, Davis

Table 42: Maximum Ground Level SiO_2 Concentration for Various Stability Classes with Stack Height (H) of 20 Feet and Wind Speed u= 1 m s^{-1}.

Stability class	Wind speed (m s^{-1})	C max (µg m^{-3})	x (ft)	C (@500 ft)
F (night clear sky)	1	27.94	700	23.304
F (night clear sky)	2	13.97	700	11.652
D (slight solar radiation)	3	9.764	300	7.408
E (night cloudy)	1	30.607	400	29.101
C (slight solar radiation)	2	15.514	200	5.759
B (slight solar radiation)	1	40.225	100	5.853
A (strong solar radiation)	1	25.597	100	3.333

Highlighted data shows the worst case scenario.

Source: University of California, Davis

The values shown in Table 42 predicts that maximum SiO_2 nanoparticle concentrations downwind of the LFG combustion site may reach 40.2 µg m^{-3} under atmospheric stability class 'B ' with same conditions as that of H_2SO_4 case. The maximum ground level SiO_2 concentration is far below the OSHA recommendations for worker exposure limits of nanoscale SiO_2 particles which is 300 µg m^{-3} (Bhangar et al., 2011), but the contribution to direct PM2.5 mass suggests that these particles could once again pose a public health risk. Further analysis of the regional effects will be discussed in the context of predictions from the UCD/CIT model.

Eulerian Regional Chemical Transport Modeling

Figure 64 through Figure 67 below show the predicted concentration fields associated with electricity production from LFG during the month of July in the year 2054. Figure 64a illustrates the Business as Usual distribution of PM2.5 mass with peak concentrations of almost 16 µg m^{-3} around major population centers in Los Angeles and the San Francisco Bay Area. Figure 64b shows that sulfate concentrations are a major component of PM2.5 mass, of almost 2.00 µg m^{-3} associated with this chemical component. Extensive adoption of LFG combustion for power generation increases PM2.5 mass concentrations by 1.3% and sulfate concentrations by 3.8% where additional emissions distribution of PM2.5 mass and sulfates compared to base case is seen in figure 9-3c and 9-3d respectively.

Figure 64: a) Business as Usual PM2.5 Mass, b) Businesss as Usual Sulfate, c) LFG additional PM2.5 Mass and d) LFG additional Sulfate

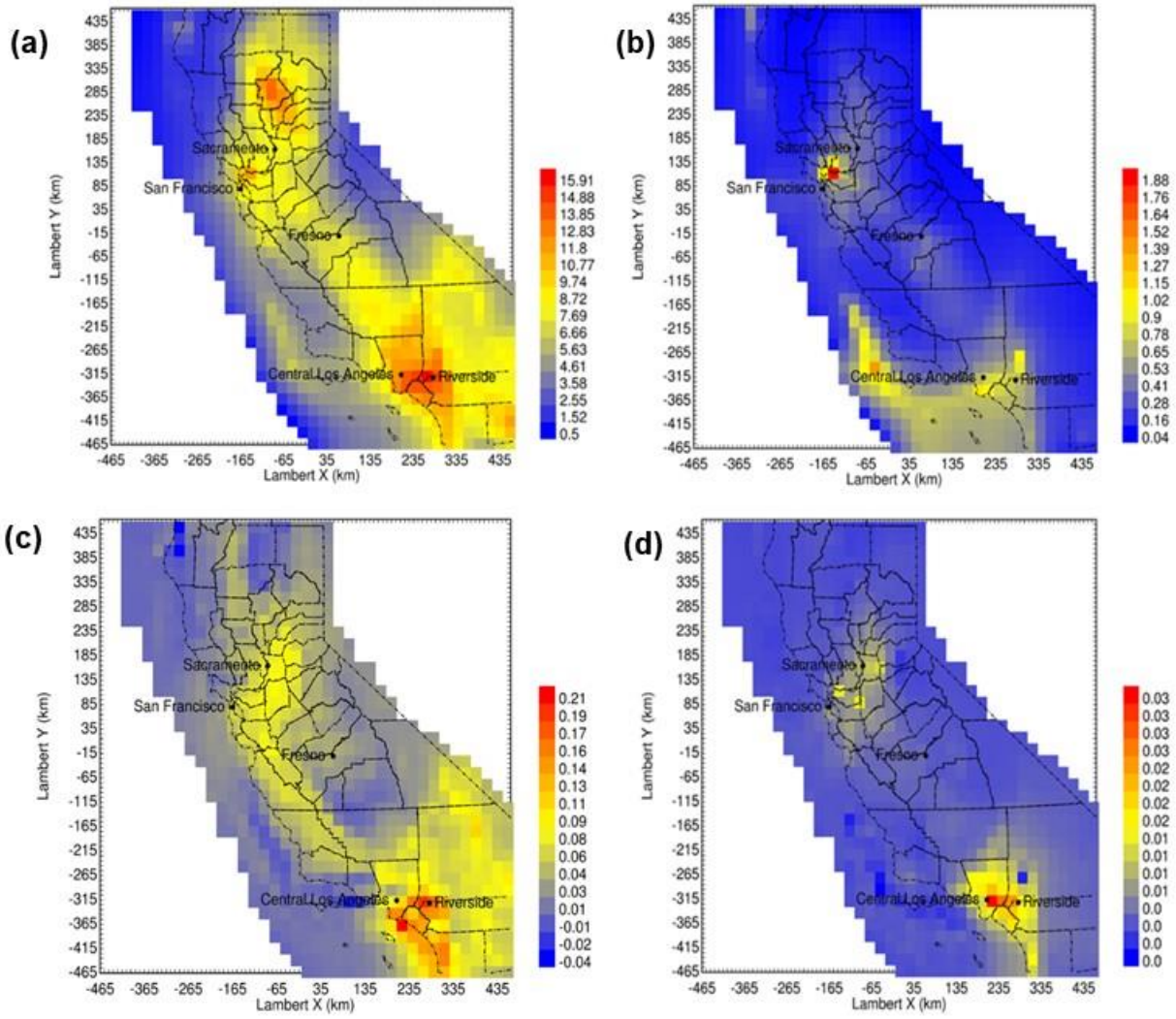

Source: University of California, Davis

Figure 65a and Figure 65b show the Business as Usual distribution of nitrate and ammonia concentrations with peak values of 1.33 μg m^{-3} and 0.89 μg m^{-3} respectively. Peak concentrations are mostly observed in densely populated areas like Los Angeles and San Francisco similar to that of PM2.5 mass and sulfates. Figure 65c depicts large increase in nitrate concentrations of about 9% compared to base case in Figure 65a and about 4.5% increase in ammonia concentrations as seen in Figure 65d.

Figure 65: a) Business as Usual Nitrates, b) Businesss as Usual Ammonia, c) LFG Additional Nitrates and d) LFG Additional Ammonia

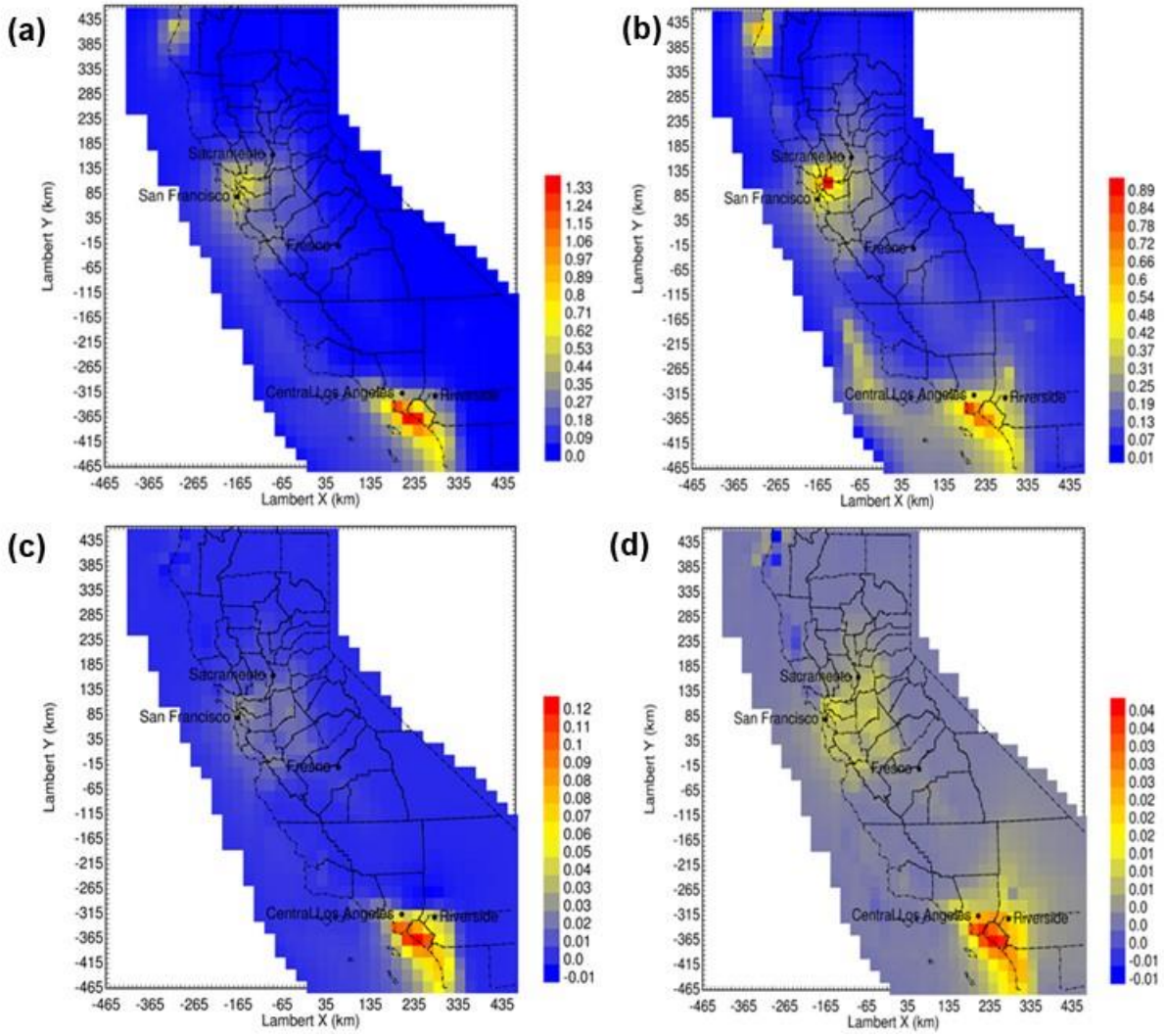

Source: University of California, Davis

Figure 66a illustrates the Business as Usual distribution of EC concentrations with peak value of 0.92 μg m^{-3}. Figure 65b shows that OC is also another major component of PM2.5 mass besides sulfates, with peak concentrations of 2.93 μg m^{-3}. From Figure 66c and Figure 66d, it can be seen that EC concentrations aren't much affected by large-scale adoption of LFG with about 0.7% increase in OC concentrations compared to base case emissions. Also it is observed that the primary and secondary components of PM2.5 follow nearly same spatial pattern (increased concentrations in regions like central LA and Riverside) when compared the effect of extensive LFG combustion to the base case scenario.

Figure 66: a) Business as Usual EC, b) Businesss as Usual OC, c) LFG additional EC and d) LFG additional OC

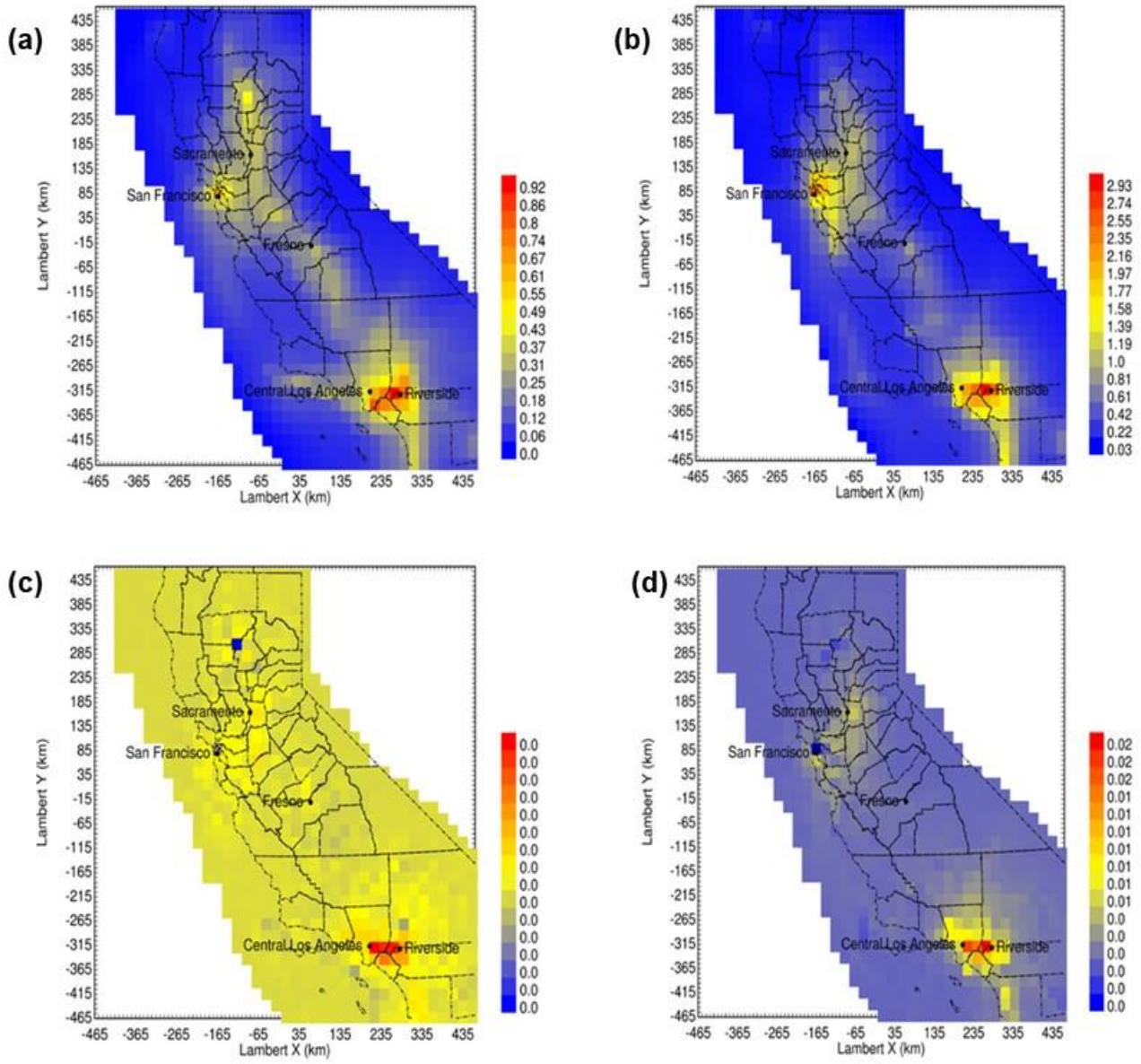

Source: University of California, Davis

Figure 67a shows the Business as Usual distribution of ozone concentrations with peak concentrations around 90ppb. Ozone concentration hasn't increased much (very low magnitude) due to extensive LFG combustion but higher concentrations are generally observed in eastern LA. This may be due to higher concentrations of NOx and VOC's released from huge number of automobiles in LA.

Figure 67: a) Business as Usual Ozone, b) LFG additional Ozone

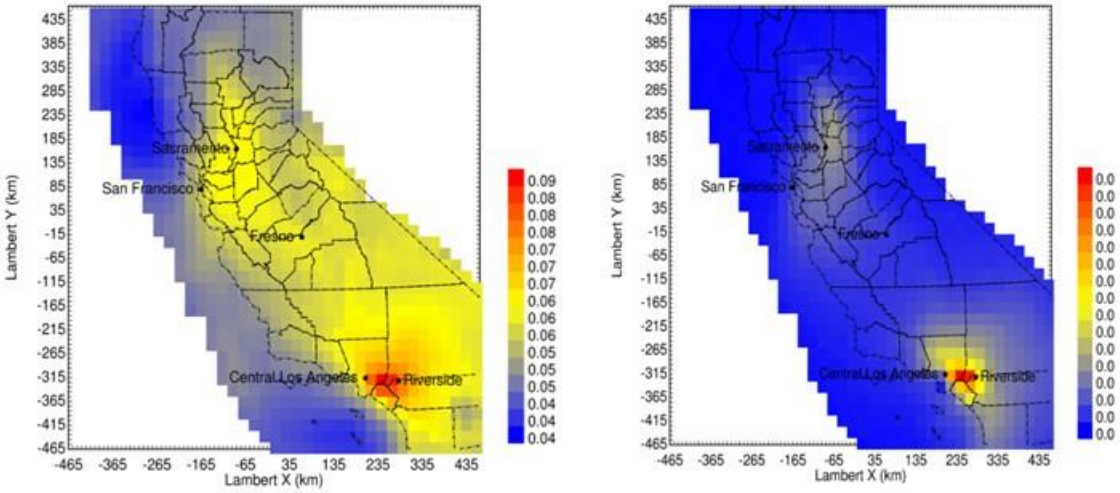

Source: University of California, Davis

Conclusions

The initial analysis of combustion emissions from extensive utilization of LFG in California predict a 1.3% increase in PM 2.5 concentrations with little effect on ozone concentrations. Increasing PM2.5 concentrations are mostly associated with an increase in sulfates and OC concentrations, particularly in densely populated regions like central LA. This clearly suggests that wide scale adoption of LFG may influence public health.

There is also an increased risk of nanotoxicity when exposed to the combustion exhaust due to the presence of siloxanes in LFG. However in depth analysis should be carried out by varying the siloxanes concentration from different sources to understand their toxicity effects and contribution to PM2.5 mass.

LFG utilization offsets traditional natural gas extraction, distribution, and combustion. The long-term climate benefits of LFG adoption are difficult to quantify and this analysis is beyond the scope of the current report. Never-the-less, these long-term climate benefits will partially offset the short term air quality impacts associated with LFG adoption. These trade-offs must be weighed during policy development.

Future Work

The current report performs an initial screening of potential air quality impacts associated with widespread adoption of LFG for power generation in California. There are several noteworthy limitations in the current analysis.

The calculations inherently assume that none of the LFG produced by landfills is currently used for power generation. In reality, the majority of this gas is already captured and burned meaning that the actual projection of future conditions may be closer to the LFG perturbation than the Business as Usual Base-case. In that case, the results of the current report can be interpreted as the air quality impact that we are already experiencing due to the combustion of LFG in California, and the Business as Usual Case can be viewed as a cleaner result that could be achieved if we remove the emissions of SO2 and SiO2 from these sources.

The resolution of the UCD/CIT model calculations in the current study was 24km which masks some of the highest concentrations around emissions sites due to numerical diffusion. The predicted concentration fields therefore represent a lower bound of exposure analysis in the regions immediately surrounding the emissions sources.

The siloxanes concentration considered in the Gaussian plume analysis are not represented in the grid model as the PM2.5 emission factor considered doesn't account for SiO_2 particles. Incorporating this might lead to further increase in the PM2.5 concentrations.

CHAPTER 10: CONCLUSIONS

Upgrading to Biomethane Using Membrane Separation

A small-scale membrane upgrading system with a capacity of 100 $Nm^3\ h^{-1}$ was tested at two food waste digesters and one dairy digester operating in California. The membrane removed a majority of the carbon dioxide and part of the oxygen from the biogas with performance matching expected targets. The average composition of upgraded biomethane satisfied the trace contaminant requirements for pipeline injection in California, mainly because the pre-cleaning steps upstream of the membranes removed these contaminants from the gas stream. Residual air in the biogas was not removed efficiently by the membrane separation system which prevented methane concentrations from reaching levels sufficient to meet the heating value requirements for pipeline injection. Dedicated upgrading plants could carefully eliminate air leakage to address this issue. Additionally or alternatively, propane can be mixed into the upgraded biomethane to achieve the target heating value.

An economic model developed for small scale biogas production facilities operating at optimal conditions predicts that capital costs for a typical plant exceed $2M and projects only become financially viable over a 15 year return period when natural gas prices exceed approximately $20 GJ^{-1}. Current market prices for petroleum natural gas are far below this level, so financial incentives would be required to make small-scale biogas projects viable in the near term.

Health Effects Assay Results

Three types of assays were used to quantify potential health effects of biogas, biomethane, and CNG combustion products in typical commercial, transportation, and residential applications. All assay results were first compared to test blank levels to ensure that measurements were above method detection limits in each test configuration. Assay results from biomethane were then compared to assay results from CNG to identify statistically significant differences.

The macrophage reactive oxygen species (ROS) assay measured the ROS generating capacity of exhaust particulate matter using rat macrophage cells. Mobile sources powered by CNG had higher macrophage ROS generation than mobile sources powered by biomethane. Macrophage ROS generation from consumer appliances operating on CNG and biomethane were similar at the 95% confidence level.

Cellular in vitro assays measure inflammatory and toxic potential using human macrophages in cell culture that can directly exhibit inflammatory responses. Cell biomarkers were monitored including Cytochrome P450 monooxygenase (CYP1A1: marker for PAHs), Interleukin 8 (IL-8: marker for inflammation), and Cyclooxygense (COX-2: a key enzyme for inflammation; up-regulated in cancer cells). CYP1A1 response was elevated above background levels in all mobile source tests, with comparable results for all fuels (including CNG). CYP1A1 and IL-8 were higher for READ biomethane than CNG in cooking stove tests. CYP1A1, IL-8, and COX-2

were higher in New Hope biomethane than CNG for water heater tests. CYP1A1 response was elevated in engine-generator tests operating on raw biogas at Kiefer Landfill.

Larger amounts of DNA damage were detected in samples exposed to biomethane combustion exhaust than natural gas combustion exhaust from mobile sources and home appliances. Pooled data from home appliances suggests that these results are statistically significant at the 95% confidence level for the SATS biomethane.

The Ames genotoxicity assay measures DNA alteration (aka mutations) in several strains of bacterium, positively identifying 50-90% of known human carcinogens. Elevated mutagenicity above background levels was detected in mobile source tests fueled by SATS biomethane. Elevated mutagenicity above background levels was also detected in cooking stove tests fueled by SATS and READ biomethane, and water heater tests fueled by New Hope biomethane. Mutagenicity was elevated in engine-generator tests operating on raw biogas at Kiefer Landfill.

Initial testing found that CNG combustion exhaust did not produce elevated mutagenicity above background levels. Repeated stove tests indicated elevated mutagenicity above background levels for CNG that is comparable to the biomethane results. This increased CNG mutagenicity in the repeated tests could not be explained by changes in the concentrations of target chemical compounds between the two rounds of testing. Increased mutagenicity was correlated with three DNPH-reactive non-target chemical compounds and an additional 7 compounds collected in impingers. Further analysis of non-target compounds may identify the cause of this increased mutagenicity, but these analyses are beyond the scope of the current study.

Photochemical reaction under typical summer conditions did not increase any toxicity measured by the health effects assays considered in the present analysis.

Microorganism Characterization

Exhaust gas samples from biogas, biomethane, and CNG combustion were monitored for microorganisms including bacteria, human viruses, and fungi. Cultivable heterotrophic and spore-forming bacteria were quantified with the most probable number (MPN) test. Cultivable fungi were tested using the plating method. Quantitative polymerase chain reaction (qPCR) analysis was used to estimate the densities of target genes. DNA sequencing of qPCR products was conducted for further confirmation.

The number of microorganisms found in vehicle combustion exhaust was similar when using biomethane and CNG as the fuel source. Similarly, no significant difference was found between the DNA concentration in vehicle combustion exhaust using either biomethane or CNG. These results suggest that there is no additional microbial risk associated with the use of biomethane as an alternative fuel source in motor vehicles.

Target pathogenic bacterial DNA was measured in the biomethane exhausts in the cooking stove test. Given that these organisms were not cultivable, the bacterial DNA may have originated from dead cells or represented extracellular DNA. Human adenovirus DNA concentrations of biomethane and CNG exhausts were similar and comparable to background levels. No target pathogenic DNA or cultivable microorganisms were found in biomethane exhausts in the water heater test. The results indicate that the likelihood of increased

microbial emissions in the indoor environment by using biomethane in home appliances compared to the use of natural gas is low.

Target pathogens were not detected in the on-site engine-generator exhaust tests. Based on the cultivation and molecular analysis results, the microbial risks of target pathogens from on-site engine/turbine generator usage appear low.

Target Chemical Analysis

The concentration of standard analytes including hydrocarbons and aldehydes was similar in combustion exhaust generated using petroleum natural gas and biomethane. Although some of the target compound concentrations were linearly correlated with bioassay activities on a per liter basis, it is not clear that they can completely explain the bioactivity differences observed between, in particular, CNG and biomethane samples.

Non-Target Chemical Analysis

Non-target chemical analysis is a useful tool for exploring the chemical composition of biomethane exhaust samples to identify features that are correlated with elevated toxicity in bioassays. Over 40 compounds were discovered that are correlated with toxic response in the current research effort. Some of these molecular formulas of interest have structural isomers that could be responsible for the observed bioactivity in a concentration dependent manner. Two examples of such compounds are C_2H_5NO (possible isomers include nitrosoethane or acetamide) and $C_{10}H_{10}O_2$ (possible isomers include 1-phenyl-1,3-butanedione). Both of these compounds were statistically significantly correlated with COX2 inflammatory markers in the engine-generator tests, and both have shown activity when tested in some batteries of screening bioassays.

Correlations between non-target analytes and the mutagenicity of appliance combustion samples have special significance in the current study given the results described in Chapter 4. The current analysis identified the non-target analyte $C_6H_3NO_4$ (dialdehyde) associated with increased mutagenicity in the original appliance tests and the non-target analyte C_2H_5NO associated with increased mutagenicity in the stove retests.

Ultrafine Particles

Ultrafine particles are toxic and most of the particulate matter released from natural gas combustion falls into the ultrafine size range. UFP emissions from commercial, residential, and mobile sources were compared when using biogas, biomethane, and CNG as a fuel source. UFP emissions from petroleum natural gas and biomethane were very similar. Higher concentrations of impurities such as sulfur-containing compounds enhance UFP emissions from biomethane, but pre-treatment of biogas to remove these compounds can mitigate this effect in the downstream combustion source.

The UFPs emitted from CNG/biomethane combustion in home appliances are semi-volatile, causing them to partially evaporate when the exhaust is diluted. In contrast, UFPs emitted from CNG/biomethane combustion in mobile sources and biogas combustion in stationary power generation sources did not evaporate when diluted.

Biomethane combustion exhaust produced little additional SOA relative to CNG combustion exhaust when both were tested in a photochemical smog chamber under atmospherically relevant conditions. The potential for biomethane to generate nucleation events that contribute to ambient ultrafine particle concentrations seems small.

Regional Modeling

Preliminary regional modeling simulations were conducted to analyze the potential air quality impacts attributable to wide scale use of landfill biogas in California. Gaussian plume models and Eulerian regional chemical transport models were used to evaluate the potential impacts of sulfur compounds and siloxanes in landfill biogas on concentrations of airborne particulate matter. The results suggest that extensive use of landfill gas would contribute to a 1.3% increase in PM 2.5 concentrations with little effect on ozone concentrations. Increasing PM2.5 concentrations are mostly associated with an increase in sulfates and OC concentrations, particularly in densely populated regions like central LA. Siloxane concentrations in the landfill gas can lead to significant concentrations of SiO_2 nanoparticles near the facility. Further research is needed to understand this nanoparticle toxicity effect and the potential contribution to PM2.5 mass.

Future Research

Further tests should be performed to study the mutagenicity of biomethane combustion products, fully identify the chemical or biological agents responsible for the increased mutagenicity, and suggest methods to remove these agents from the biomethane production stream.

Additional characterization should be performed on membrane separation systems to determine the fate of trace compounds important to air quality such as halogenated hydrocarbons, siloxanes, and sulfur. The composition of the permeate gas and liquid condensate from the membrane system should be analyzed to understand potential impacts of these major discharge streams.

Exhaust emissions from a natural-gas power plant should be characterized to provide a comparison point for the measurements made for biogas power plants.

High-throughput gene sequencing technologies such as amplicon sequencing should be used to gain insight into the microbial communities of biomethane and corresponding exhaust samples and enable further identification of other potential pathogenic species.

The results of the bioassays considered in the current study suggest that all petroleum natural gas and biomethane fuels combusted in a mobile source promote inflammatory responses. Future tests should verify that this outcome is driven by the reaction products of the motor oil in these tests, and consider whether synthetic and traditional motor oils have similar properties.

Scenarios of biogas and biomethane adoption should be created that are economically optimized. The regional air quality effects of each scenario should be analyzed, with further simulations conducted with chemical transport models.

LIST OF ACRONYMS

Term	Definition
AB	Assembly Bill
APB	acid producing bacteria
BLAST	Basic Logical Assignment Search Tool
CARB	California Air Resources Board
CEC	California Energy Commission
CFR	code of federal regulations
CNG	compressed natural gas
CPUC	California Public Utilities Commission
CSTR	continuous stirred tank reactor
CVS	constant volume sampling
DNA	deoxyribonucleic acid
FPD	flame photometric detector
GC	gas chromatography
GTI	Gas Technology Institute
H/C	hydrogen to carbon ratio
ICPMS	inductively coupled plasma mass spectrometry
IOB	iron oxidizing bacteria
LC	liquid chromatography
LOD	limit of detection
LOQ	limit of quantification
MPN	MPN – most probable number
MS	mass spectrometry
NM	no measurement
NQ	Not Quantifiable
OEHHA	office of environmental health hazard assessment
PAC	project advisory committee
PAH	polycyclic aromatic hydrocarbon

Term	Definition
PBS	phosphate buffered saline
PCB	polychlorinated biphenyl
PCR	polymerase chain reaction
POTWS	point of treatment water systems
ppbv	parts per billion by volume
qPCR	quantitative polymerase chain reaction

REFERENCES

California Global Warming Solutions Act, in, California, AB 32, 2006.

Pipeline Quality Biogas: Guidance Document for Dairy Waste, Wastewater Treatment Sludge and Landfill Conversion, in, edited by: Hazardous, U.S.DoTPa., and Administration, M. S., LaboratoryTesting and Analysis of Biogas 250, Gas Technology Institute, 121, 2009.

Abatzoglou, N., and Boivin, S.: A Review of Biogas Purification Processes, Biofuels, Bioproducts, Biorefining, 42-71, 2009.

Abdeldaim, G. M. K., Stralin, K., Olcen, P., Blomberg, J., and Herrmann, B.: Toward a quantitative DNA-based definition of pneumococcal pneumonia: a comparison of Streptococcus pneumoniae target genes, with special reference to the Spn9802 fragment, Diagnostic Microbiology and Infectious Disease, 60, 143-150, 10.1016/j.diagmicrobio.2007.08.010, 2008.

"Natural Gas": U.S. Energy Information Administration (EIA). https://www.eia.gov/naturalgas/, access: February 5, 2017, 2017.

AGA: Natural Gas Contract Measurement and Quality Clauses, American Gas Association Transmission Measurement Committee, Washington, DC, 2001.

Agency, U. S. E. P.: 40-CFR-Part-86-CONTROL OF EMISSIONS FROM NEW AND IN-USE HIGHWAY VEHICLES AND ENGINES, in: 40 CFR Part 86, 1995.

Agency, U. S. E. P.: 40-CFR-Part-1066-Vehicle-Testing-Procedures, in: 40 CFR Part 1066, 2014.

AHS: American housing survey for the United States: 2005, Available at: https://www.census.gov/prod/2006pubs/h150-05.pdf, 2005.

Beelen, R., Hoek, G., van den Brandt, P. A., Goldbohm, R. A., Fischer, P., Schouten, L. J., Armstrong, B., and Brunekreef, B.: Long-term exposure to traffic-related air pollution and lung cancer risk, Epidemiology, 19, 702-710, 2008.

Berrin Tansel, S. C. S.: Oxidation of siloxanes during biogas combustion and nanotoxicity of Si-based particles released to the atmosphere, Environmental Toxicology and Pharmacology, 37, 166-173, 2014.

Bhangar, S., Mullen, N. A., Hering, S. V., Kreisberg, N. M., and Nazaroff, W. W.: Ultrafine particle concentrations and exposures in seven residences in northern California, Indoor Air, 21, 132-144, 10.1111/j.1600-0668.2010.00689.x, 2011.

Bian, Q. J., Jathar, S. H., Kodros, J. K., Barsanti, K. C., Hatch, L. E., May, A. A., Kreidenweis, S. M., and Pierce, J. R.: Secondary organic aerosol formation in biomass-burning plumes: theoretical analysis of lab studies and ambient plumes, Atmos Chem Phys, 17, 5459-5475, 2017.

Black, N.: Kern Dairy Biogas Cluster's R-CNG Sustainable Freight Pilot Project, California Bioenergy LLC, 2015.

Brauner, E. V., Forchhammer, L., Moller, P., Simonsen, J., Glasius, M., Wahlin, P., Raaschou-Nielsen, O., and Loft, S.: Exposure to ultrafine particles from ambient air and oxidative stress-induced DNA damage, Environ Health Persp, 115, 1177-1182, 2007.

Brewer, E., Li, Y., Finken, B., Quartucy, G., Muzio, L., Baez, A., Garibay, M., and Jung, H. S.: PM2.5 and ultrafine particulate matter emissions from natural gas-fired turbine for power generation, Atmospheric Environment, 131, 141-149, 2016.

Carreras-Sospedra, M., Williams, R., and Dabdub, D.: Assessment of the emissions and air quality impacts of biomass and biogas use in California, Journal of the Air & Waste Management Association, 66, 134-150, 10.1080/10962247.2015.1087892, 2016.

Carter, W. P. L., Luo, D. M., Malkina, I. L., and Pierce, J. A.: Environmental Chamber Studies of Atmospheric Reactivities of Volatile Organic-Compounds Effects of Varying Rog Surrogate and Nox, Abstracts of Papers of the American Chemical Society, 209, 34-Envr, 1995.

Chen, P. S., and Li, C. S.: Quantification of airborne Mycobacterium tuberculosis in health care setting using real-time qPCR coupled to an air-sampling filter method, Aerosol Science and Technology, 39, 371-376, 10.1080/027868290945767, 2005.

Chen, X., Vinh-Thang, H., Ramirez, A. A., Rodrigue, D., and Kaliaguine, S.: Membrane gas separation technologies for biogas upgrading, Royal Society of Chemistry, 5, 24399-24448, 2015.

Coker, C.: Pipeline Injection of Biomethane in California, Biocycle 2018, San Diego CA, 2018.

Cooper, C. D., F.C. Alley: Air Pollution Control: A Design Approach, 3rd ed., Waveland Press, Long Grove, Illinois, 2002.

D'Anna, A.: Combustion-formed nanoparticles, P Combust Inst, 32, 593-613, 2009.

David Cooper, C. A., F.C: Air Pollution Control-A Design Approach, 3 ed., Waveland Press,Inc., Prospect Heights,IL, 2002.

De Filippo, A., and Maricq, M. M.: Diesel Nucleation Mode Particles: Semivolatile or Solid?, Environ Sci Technol, 42, 7957-7962, 2008.

Dennekamp, M., Howarth, S., Dick, C. A. J., Cherrie, J. W., Donaldson, K., and Seaton, A.: Ultrafine particles and nitrogen oxides generated by gas and electric cooking, Occup Environ Med, 58, 511-516, 2001.

Dobbins, R. A.: Hydrocarbon nanoparticles formed in flames and diesel engines, Aerosol Sci Tech, 41, 485-496, 2007.

Dockery, D. W.: Epidemiologic evidence of cardiovascular effects of particulate air pollution, Environ Health Persp, 109, 483-486, 2001.

Eishi, Y., Suga, M., Ishige, I., Kobayashi, D., Yamada, T., Takemura, T., Takizawa, T., Koike, M., Kudoh, S., Costabel, U., Guzman, J., Rizzato, G., Gambacorta, M., du Bois, R., Nicholson, A. G., Sharma, O. P., and Ando, M.: Quantitative analysis of mycobacterial and propionibacterial DNA in lymph nodes of Japanese and European patients with sarcoidosis, Journal of Clinical Microbiology, 40, 198-204, 10.1128/jcm.40.1.198-204.2002, 2002.

Elder, A., and Oberdorster, G.: Translocation and effects of ultrafine particles outside of the lung, Clinics in occupational and environmental medicine, 5, 785-796, 10.1016/j.coem.2006.07.003, 2006.

Fang, H., and Hedin, G.: Rapid screening and identification of methicillin-resistant Staphylococcus aureus from clinical samples by selective-broth and real-time PCR assay, Journal of Clinical Microbiology, 41, 2894-2899, 10.1128/jcm.41.7.2894-2899.2003, 2003.

Ghio, A. J., Carraway, M. S., and Madden, M. C.: COMPOSITION OF AIR POLLUTION PARTICLES AND OXIDATIVE STRESS IN CELLS, TISSUES, AND LIVING SYSTEMS, Journal of Toxicology and Environmental Health-Part B-Critical Reviews, 15, 1-21, 10.1080/10937404.2012.632359, 2012.

Giraudet, S., P. Le Cloirec. : Activated carbon filters for fitration-adsorption, in: Activated Carbon Fiber and Textiles, edited by: Chen, J. Y., Elsevier, 2017.

Glarborg, P.: Hidden interactions - Trace species governing combustion and emissions, P Combust Inst, 31, 77-98, 2007.

GTI: Guidance document for the introduction of dairy waste biomethane., Gas Technology Institute20614, 2009.

GTI: Guidance document for the introduction of landfill-derived renewable gas into natural gas pipelines, Gas Technology Institute20792, 2012.

GTI: Conduct a Nationwide Survey of Biogas Cleanup Technologies and Costs, Gas Technology InstituteContract #13432, 2014.

Gulder, O. L.: Influence of Sulfur-Dioxide on Soot Formation in Diffusion Flames, Combust Flame, 92, 410-418, 1993.

Hagen, M. E. P. A. M. J. J. O. J., Biomil AB, Anders Dahl: Adding Gas from Biomass to the Gas Grid, GasTec NV; Danish Gas Tech Center; Swedish Gas Center, 2001.

Haider, S., A. Lindbrathen, M.B. Hagg: Techno-economical evaluation of membrane based biogas upgrading system: a comparison between polymeric membrane and carbon membrane technology, Green Energy and Environment 2016.

Harasimowicz, M., Orluk, P., Zakrzewska-Trznadel, G., and Chmielewski, A.: Application of polyimide membranes for biogas purification and enrichment, Journal of Hazardous Materials, 144, 698-702, 2007.

Heim, A., Ebnet, C., Harste, G., and Pring-Akerblom, P.: Rapid and quantitative detection of human adenovirus DNA by real-time PCR, Journal of Medical Virology, 70, 228-239, 10.1002/jmv.10382, 2003.

Herner, J.: Chemical and biological assays employed by the California Air Resources Board (CARB). in, edited by: Kleeman, M., 2013.

Holtappels, K., V. Schroder, A. Pekalski, H. Schildberg: Limiting Oxygen Concentrations-Process Safety by Oxygen Monitoring, ICDERS, Irvine, CA, 2011.

Hueglin, C., Scherrer, L., and Burtscher, H.: An accurate, continuously adjustable dilution system (1:10 to 1:10(4)) for submicron aerosols, J Aerosol Sci, 28, 1049-1055, 1997.

J. Hu, H. Z., Q. Ying, S.-H. Chen, F. Vandenberghe and M. J. Kleeman: Long-term particulate matter modeling for health effect studies in California – Part 1: Model performance on temporal and spatial variations, Atmos Chem Phys, 15, 3445-3461, 10.5194/acp-15-3445-2015, 2015.

Jaffe, A., R. Dominguez-Fans, N. Parker, D. Scheitrum, J. Wilcock, M. Miller: Feasiblity of Renewable Natural Gas as a Large-Scale, Low Carbon Substitute, STEPS Program; Institure of Transportation Studies, UC Davis13-307, 2016.

Kado, N. Y., Guirguis, G. N., Flessel, C. P., Chan, R. C., Chang, K. I., and Wesolowski, J. J.: Mutagenicity of Find (less than 2.5-mu-m) Airborne Particles - Diurnal-Variation in Community Air Determined by a Salmonella Micro Preincubation (Microsuspension) Procedure, Environmental Mutagenesis, 8, 53-66, 10.1002/em.2860080106, 1986.

Kittelson, D. B., Watts, W. F., and Johnson, J. P.: On-road and laboratory evaluation of combustion aerosols - Part 1: Summary of diesel engine results, J Aerosol Sci, 37, 913-930, 2006.

Klippel, N., Kasper, M., and Bengtsson, K.: Gas turbines-sources or sinks for ambient air aerosol?, In: 6th ETH conference on Nanoparticle Measruement, Switzerland, Zurich, 2002.

Klippel, N., Wood, T., Pearce, B., Bengtsson, K., Kasper, M., and Mosimann, T.: On-line measurement of ultrafine particle emissions from gas turbines (Tachnical report ALSTOM Power), 2004.

Kosusko, M., Williams, R., Ely, C., and Martynowicz, T.: Evaluating the Air Quality, Climate & Economic Impacts of Biogas Management Technologies, U.S. Environmental Protection AgencyEPA 600/R-16/099, 2016.

Krich, K. D. A., J. Batmale, J. Benemann, B. Rutledge, D. Salour: Biomethane from Dairy Waste: A Sourcebook for the Production and Use of Renewable Natural Gas in California, Sustainable Conservation, 2005.

Kuwayama, T., Collier, S., Forestieri, S., Brady, J. M., Bertram, T. H., Cappa, C. D., Zhang, Q., and Kleeman, M. J.: Volatility of Primary Organic Aerosol Emitted from Light Duty Gasoline Vehicles, Environ Sci Technol, 49, 1569-1577, 2015.

L.Pierce, J.: Siloxane quantification,removal and impact on landfill gas utilization, 8th Annual LMOP conference and project expo, Baltimore,Maryland, 2005.

Langrish, J. P., Bosson, J., Unosson, J., Muala, A., Newby, D. E., Mills, N. L., Blomberg, A., and Sandström, T.: Cardiovascular effects of particulate air pollution exposure: time course and underlying mechanisms, Journal of Internal Medicine, 272, 224-239, 10.1111/j.1365-2796.2012.02566.x, 2012.

Laurent, O., Wu, J., Li, L., Chung, J., and Bartell, S.: Investigating the association between birth weight and complementary air pollution metrics: a cohort study, Environmental Health, 12, 1, 2013.

Lawton, S. A.: The Effect of Sulfur-Dioxide on Soot and Polycyclic Aromatic Hydrocarbon Formation in Premixed Ethylene Flames, Combust Flame, 75, 175-181, 1989.

Lin, W., T. Chung: Gas permeability, diffusivity, solubility, and aging characteristics of 6FDA-durene polyimide membranes, Journal of Membrane Science, 186, 183-193, 2000.

Long, C. M., Suh, H. H., Catalano, P. J., and Koutrakis, P.: Using time- and size-resolved particulate data to quantify indoor penetration and deposition behavior, Environ Sci Technol, 35, 2089-2099, 2001.

Makaruk, A., Miltner, M., and Harasek, M.: Membrane biogas upgrading processes for the production of natural gas substitute, Separation and Purification Technology, 74, 83-92, 2010.

Maricq, M. M., and Xu, N.: The effective density and fractal dimension of soot particles from premixed flames and motor vehicle exhaust, J. Aerosol Sci. , 35, 1251-1274, 2004.

Maricq, M. M.: A comparison of soot size and charge distributions from ethane, ethylene, acetylene, and benzene/ethylene premixed flames, Combust Flame, 144, 730-743, 2006.

Masiol, M., Hofer, A., Squizzato, S., Piazza, R., Rampazzo, G., and Pavoni, B.: Carcinogenic and mutagenic risk associated to airborne particle-phase polycyclic aromatic hydrocarbons: A source apportionment, Atmospheric Environment, 60, 375-382, 10.1016/j.atmosenv.2012.06.073, 2012.

May, A. A., Saleh, R., Hennigan, C. J., Donahue, N. M., and Robinson, A. L.: Volatility of Organic Molecular Markers Used for Source Apportionment Analysis: Measurements and Implications for Atmospheric Lifetime, Environ Sci Technol, 46, 12435-12444, 2012.

May, A. A., Levin, E. J. T., Hennigan, C. J., Riipinen, I., Lee, T., Collett, J. L., Jimenez, J. L., Kreidenweis, S. M., and Robinson, A. L.: Gas-particle partitioning of primary organic

aerosol emissions: 3. Biomass burning, J Geophys Res-Atmos, 118, 11327-11338, 2013a.

May, A. A., Presto, A. A., Hennigan, C. J., Nguyen, N. T., Gordon, T. D., and Robinson, A. L.: Gas-particle partitioning of primary organic aerosol emissions: (1) Gasoline vehicle exhaust, Atmospheric Environment, 77, 128-139, 2013b.

May, A. A., Presto, A. A., Hennigan, C. J., Nguyen, N. T., Gordon, T. D., and Robinson, A. L.: Gas-Particle Partitioning of Primary Organic Aerosol Emissions: (2) Diesel Vehicles, Environ Sci Technol, 47, 8288-8296, 2013c.

McBean, E. A.: Siloxanes in biogases from landfills and wastewater digesters, NRC Canada, 35, 431-436, 10.1016/j.enconman.2005.10.016, 2008.

McCann, J., Choi, E., Yamasaki, E., and Ames, B. N.: DETECTION OF CARCINOGENS AS MUTAGENS IN SALMONELLA MICROSOME TEST - ASSAY OF 300 CHEMICALS, Proceedings of the National Academy of Sciences of the United States of America, 72, 5135-5139, 10.1073/pnas.72.12.5135, 1975.

Milieutechniek, D.: The DMT Carborex® MS Biogas Upgrading System, 2014.

Minutolo, P., D'Anna, A., Commodo, M., Pagliara, R., Toniato, G., and Accordini, C.: Emission of Ultrafine Particles from Natural Gas Domestic Burners, Environ Eng Sci, 25, 1357-1363, 2008.

Minutolo, P., Sgro, L., Costagliola, M. A., Prati, M. V., Sirignano, M., and D'Anna, A.: Ultrafine particle emission from combustion devices burning natural gas, Chem Engineer Trans, 22, 239-244, 10.3303/Cet1022039, 2010.

Moletta-Denat, M., Bru-Adan, V., Delgenes, J.-P., Hamelin, J., Wery, N., and Godon, J.-J.: Selective microbial aerosolization in biogas demonstrated by quantitative PCR, Bioresource Technology, 101, 7252-7257, 10.1016/j.biortech.2010.04.035, 2010.

Monarca, S., Zanardini, A., Feretti, D., Falistocco, E., Antonelli, P., Resola, S., Moretti, M., Villarini, M., and Nardi, G.: Mutagenicity and clastogenicity of gas stove emissions in bacterial and plant tests, Environmental and Molecular Mutagenesis, 31, 402-408, 1998.

Nadkarni, M. A., Martin, F. E., Jacques, N. A., and Hunter, N.: Determination of bacterial load by real-time PCR using a broad-range (universal) probe and primers set, Microbiology-Sgm, 148, 257-266, 2002.

NFPA: Standard on Explosion Prevention Systems, in, 2014.

OEHHA, C.: Recommendations to the California Public Utilities Commission Regarding Health Protective Standards for the Injection of Biomethane into the Common Carrier Pipeline, 2013.

Olson, S.: RNG, Cellulosic Fuels and the Renewable Fuel Standard, in: Biocycle Magazine, 2, 30-32, 2017.

Ong, M., Williams, R., and Kaffka, S.: Comparative Assessment of Technology Options for Biogas Clean-Up California Biomass Collaborative, University of California, DavisContract Report to the California Energy Commission. Contract CEC-500-11-020, 2014.

Ostling, O., and Johanson, K. J.: Microelectrophoretic study of radiation induced DNA damage in individual mammalian cells, Biochem. Biophys. Res. Communications, 123, 291-298, 1984.

Ozgen, S., Becagli, S., Bernardoni, V., Caserini, S., Caruso, D., Corbella, L., Dell'Acqua, M., Fermo, P., Gonzalez, R., Lonati, G., Signorini, S., Tardivo, R., Tosi, E., Valli, G., Vecchi, R., and Marinovich, M.: Analysis of the chemical composition of ultrafine particles from two domestic solid biomass fired room heaters under simulated real-world use, Atmospheric Environment, 150, 87-97, 2017.

Patterson, T., Esteves, S., Dinsdale, R., and Guwy, A.: An evaluation of the policy and techno-economic factors affecting the potential for biogas upgrading for transport fuel use in the UK, Energy Policy, 39, 1806-1816, 2011.

Perry, R. a. G., D.: Perry's Chemical Engineers' Handbook, 8th ed., McGraw Hill, Chicago, 2008.

Raf Dewil a, L. A., Jan Baeyens Energy use of biogas hampered by the presence of siloxanes, Energy Conversion and Management, 47, 1711-1722, 10.1016/j.enconman.2005.10.016, 2006.

Rasi, S., Läntelä, J., and Rintala, J.: Trace compounds affecting biogas energy utilisation – A review, Energy Conversion and Management, 52, 3369-3375, http://dx.doi.org/10.1016/j.enconman.2011.07.005, 2011.

Rogge, W. F., Hildemann, L. M., Mazurek, M. A., Cass, G. R., and Simoneit, B. R. T.: Sources of Fine Organic Aerosol .5. Natural-Gas Home Appliances, Environ Sci Technol, 27, 2736-2744, 1993.

Ryckebosch, E., Drouillon, M., and Vervaeren, H.: Techniques for transformation of biogas to biomethane, Biomass and Bioenergy, 35, 1633-1645, http://dx.doi.org/10.1016/j.biombioe.2011.02.033, 2011.

Scholes, C., G. Chen, W. Tao, J. Bacus, C. Anderson, G. Stevens, S. Kentish: The effect of minor components on the gas separation performance of membranes for carbon capture, Energy Procedia, 681-687, 2011.

Scholes, C., S. Kentish, G. Stevens: The effect of condensable minor components on the gas separation performance of polymeric membranes for carbon dioxide capture, Energy Procedia, 1, 311-317, 2009.

Scholz, M., Melin, T., and Wessling, M.: Transforming biogas into biomethane using membrane technology, Renewable and Sustainable Energy Reviews, 17, 199-212, http://dx.doi.org/10.1016/j.rser.2012.08.009, 2013.

Shimekit, B., and Hilmi Mukhtar Natural Gas Purification Technologies - Major Advances for CO2 Separation and Future Directions, Advances in Natural Gas Technology, in: Advances in Natural Gas Technology, InTech, 2012.

Singh, N. P., McCoy, M. T., Tice, R. R., and Schneider, E. L.: A simple technique for quantitation of low levels of DNA damage in individual cells, Exp. Cell. Res., 175, 184-191, 1988.

Somers, C. M., Yauk, C. L., White, P. A., Parfett, C. L. J., and Quinn, J. S.: Air pollution induces heritable DNA mutations, Proceedings of the National Academy of Sciences of the United States of America, 99, 15904-15907, 10.1073/pnas.252499499, 2002.

Sun, Q., Li, H., Yan, J., Liu, L., Yu, Z., and Yu, X.: Selection of appropriate biogas upgrading technology-a review of biogas cleaning, upgrading and utilisation, Renewable and Sustainable Energy Reviews, 51, 521-532, http://dx.doi.org/10.1016/j.rser.2015.06.029, 2015.

Thran, P., Gromke, Ponitka, Seiffert, Baldwin, Kranzl, Schipfer, Matzenberger, Devriendt, Dumont, Dahl, Bochmann: Biomethane: Status and Factors Affecting Market Development and Trade, 2014.

TSI: ROTATING DISK THERMODILUTER 379020A, Available at: http://www.tsi.com/rotating-disk-thermodiluter-379020a/, 2018.

USEPA: Compendium of Methods for the Determination of Toxic Organic Chemicals in Ambient Air. In TO-11A: Determination of Formaldehyde in Ambient Air Using Adsorbent Cartridge Followed by High Performance Liquid Chromatography (HPLC), U.S. Environmental Protection Agency, 1999a.

USEPA: Compendium of Methods for the Determination of Toxic Organic Compounds in Ambient Air. TO-15: Determination of Volatile Organic Compounds (VOCs) in Air Collected in Specially-Prepared Canisters and Analyzed by Gas Chromatography/Mass Spectrometry (GC/MS), U.S. Environmental Protection Agency, 1999b.

Vaaraslahti, K., Virtanen, A., Ristimaki, J., and Keskinen, J.: Nucleation mode formation in heavy-duty diesel exhaust with and without a particulate filter, Environ Sci Technol, 38, 4884-4890, 2004.

Wagner, A. Y., Livbjerg, H., Kristensen, P. G., and Glarborg, P.: Particle Emissions from Domestic Gas Cookers, Combustion Science and Technology, 182, 1511-1527, 10.1080/00102202.2010.486015, 2010.

Wallace, L., Wang, F., Howard-Reed, C., and Persily, A.: Contribution of Gas and Electric Stoves to Residential Ultrafine Particle Concentrations between 2 and 64 nm: Size Distributions and Emission and Coagulation Rates, Environ Sci Technol, 42, 8641-8647, 2008.

Wallace, L. A., Emmerich, S. J., and Howard-Reed, C.: Source strengths of ultrafine and fine particles due to cooking with a gas stove, Environ Sci Technol, 38, 2304-2311, 2004.

Willers, S. M., Eriksson, C., Gidhagen, L., Nilsson, M. E., Pershagen, G., and Bellander, T.: Fine and coarse particulate air pollution in relation to respiratory health in Sweden, European Respiratory Journal, 42, 924-934, 2013.

Yáñez, M. A., Carrasco-Serrano, C., Barberá, V. M., and Catalán, V.: Quantitative detection of Legionella pneumophila in water samples by immunomagnetic purification and real-time PCR amplification of the dotA gene, Appl. Environ. Microbiol., 71, 3433-3441, 10.1128/AEM.71.7.3433-3441.2005, 2005.

Yang, L., Ge, X., Wan, C., Yu, F., and Li, Y.: Progress and perspectives in converting biogas to transportation fuels, Renewable and Sustainable Energy Reviews, 40, 1133-1152, 2014.

Yoon, S., Hu, S., Kado, N., Thiruvengadam, A., Collins, J., Gautam, M., Herner, J., and Ayala, A.: Chemical and toxicological properties of emissions from CNG transit buses equipped with three-way catalysts compared to lean-burn engines and oxidation catalyst technologies., Atmospheric Environment, 83, 220-228, 2013.

Zapata, C., Yang, C., Yeh, S., Ogden, J., and Kleeman, M.: Estimating Criteria Pollutant Emissions Using the California Regional Multisector Air Quality Emissions (CA-REMARQUE) Model v1.0, Geoscientific Model Development, 11, 1293-1320, 2018.

Zhang, X., B. Gao, A. Creamer, C. Cao, Y. Li: Adsorption of VOCs onto engineering carbon materials: a review, Journal of Hazardous Materials, 102-123, 2017.

Zheng, Z. Q., Durbin, T. D., Karavalakis, G., Johnson, K. C., Chaudhary, A., Cocker, D. R., Herner, J. D., Robertson, W. H., Huai, T., Ayala, A., Kittelson, D. B., and Jung, H. S.: Nature of Sub-23-nm Particles Downstream of the European Particle Measurement Programme (PMP)-Compliant System: A Real-Time Data Perspective, Aerosol Sci. Technol., 46, 886-896, 2012.

Zhou, G., Whong, W. Z., Ong, T., and Chen, B.: Development of a fungus-specific PCR assay for detecting low-level fungi in an indoor environment, Molecular and Cellular Probes, 14, 339-348, http://dx.doi.org/10.1006/mcpr.2000.0324, 2000.

APPENDIX A:
Target Compounds for Chemical Analysis

List of Target Compounds Measured

(1-Methylethyl) benzene
1,1,1,2-tetrachloroethane
1,1,1-trichloroethane
1,1,2,2-tetrachloroethane
1,1,2,3,4,4-hexachloro-1,3-Butadiene
1,1,2-trichloro-1,2,2-trifluoroethane
1,1,2-trichloroethane
1,1,3,3-Tetramethyldisiloxane
1,1-dichloroethane
1,1-dichloroethene
1,1-Dichloropropene
1,2,3-Trichlorobenzene
1,2,3-trichloropropane
1,2,4-trichlorobenzene
1,2,4-Trimethylbenzene
1,2-dibromo-3-chloropropane
1,2-dibromoethane
1,2-dichloro-1,1,2,2-tetrafluoroethane
1,2-Dichlorobenzene
1,2-Dichloroethane
1,2-dichloropropane
1,2-Dinitrobenzene
1,3,5-Trimethylbenzene
1,3-Butadiene
1,3-Dichlorobenzene
1,3-Dinitrobenzene
1,4-Dichlorobenzene
1,4-Dinitrobenzene
1-Methylnaphthalene
1-Propanethiol
2,2',3,4,4',5'-Hexachlorobiphenyl
2,2',4,4',5,5'-Hexachlorobiphenyl
2,2-dichloropropane
2,3,4,6-Tetrachlorophenol
2,3,5,6-Tetrachlorophenol
2,4,5-Trichlorophenol
2,4,6-Trichlorophenol
2,4-Dichlorophenol
2,4-Dimethylphenol
2,4-Dinitrotoluene
2,5-Dimethylthiophene
2,6-Dinitrotoluene
2-Butanone
2-Chloronaphthalene
2-Chlorophenol
2-Chlorotoluene
2-Ethylthiophene
2-methyl-2-Propanethiol
2-Methylnaphthalene
2-Methylthiophene
2-Nitroaniline
2-Nitrophenol
2-Propylthiophene
3-chloropropene
3-Nitroaniline
4-Bromophenyl Phenyl Ether
4-Chloro-3-Methyl Phenol

4-Chloroaniline
4-Chlorophenyl phenyl ether
4-Chlorotoluene
4-Ethyltoluene
Acenaphthene
Acenaphthylene
Acetaldehyde
Acetone
Acrolein
Anthracene
Azobenzene
Benz [a] anthracene
Benzaldehyde
Benzene
Benzo [b] fluoranthene
Benzo [k] fluoranthene
Benzo {a} pyrene
Benzothiophene
Benzyl Alcohol
Benzyl butyl phthalate
Bis(2-Chlorethoxy) Methane
Bis(2-Chloroethyl) Ether
Bis(2-Chloroisopropyl) ether
Bis(2-ethylhexyl) adipate
Bis(2-ethylhexyl) phthalate
bromobenzene
Bromochloroethane
bromochloromethane
bromodichloromethane
Bromoform
Bromomethane
Butyraldehyde
Carbazole
Carbon disulfide
Carbon Tetrachloride
Carbonyl sulfide
Chlorobenzene
Chloroethane
Chloroethene
Chloroform
Chrysene
cis-1,2-Dichloroethene
cis-1,3-dichloropropene
Crotonaldehyde
Decamethylcyclopentasiloxane (NM)
Decamethyltetrasiloxane
Decane
Dibenzofuran
dibromochloromethane
dibromomethane
Dichlorobiphenyl
Dichlorodifluoromethane
Diethyl phthalate
Diethyl sulfide
Dimethyl disulfide
Dimethyl naphthalene
Dimethyl phthalate
Dimethyl Sulfide
Di-n-butyl phthalate
Di-n-octyl phthalate
Diphenylamine
Di-tert-butyl sulfide
Dodecamethylcyclohexasiloxane
Dodecamethylpentasiloxane
Dodecane
Eicosane
Ethyl disulfide
Ethyl mercaptan
Ethylbenzene
Fluoranthene
Fluorene
Formaldehyde

Heptachlorobiphenyl
Heptane
Hexachlorobenzene
Hexachlorobutadiene
Hexachlorocyclopentadiene
Hexachloroethane
Hexadecane
Hexaldehyde
Hexamethyldisilane
Hexamethyldisiloxane
Isophorone
Isopropyl mercaptan
Isopropylbenzene
m,p-Cresol
m,p-Xylene
Methacrolein
Methyl benzothiophene
Methyl mercaptan
Methyl naphthalene
Methylene chloride
Methylethyl sulfide
Naphthalene
n-butylbenzene
n-Hexane
Nitrobenzene
N-Nitroso-di-N-propylamine
Nonane (NM)
n-Propylbenzene
O-Cresol
Octacosane
Octadecane
Octamethylcyclotetrasiloxane (NM)
Octamethyltrisiloxane
Octane
o-Xylene
Pentamethyldisiloxane
Phenanthrene
Phenol
Phenol
p-Isopropyltoluene
Propionaldehyde
p-Xylene
Pyrene
Pyridine
s-Butylbenzene
Styrene
tert-butylbenzene
Tetrachlorobiphenyl
Tetrachloroethene
Tetracosane
Tetradecane
Thiofuran
Tolualdehyde
Toluene
Trans-1,2-dichloroethene
trans-1,3-dichloropropene
Trichlorobiphenyl
Trichloroethene
Trichlorofluoromethane
Undecane
Valeraldehyde